The Optimisation of Radiation Dose in Paediatric Radiology

Claire-Louise Chapple

NEWCASTLE UNIVERSITY LIBRARY
098 26560 6
MED Thesis L6425

Thesis submitted for the degree of PhD
at the Faculty of Medicine
University of Newcastle upon Tyne

December 1998

Abstract

The importance of monitoring, and where possible reducing, the level of radiation dose from diagnostic X-ray examinations has been recognised for many years and is becoming of increasing concern. Dose reduction is of particular concern in paediatric radiology, and there are specific problems associated with the monitoring and comparison of radiation doses to children.

Any optimisation study relies on a framework of good dosimetry. Two techniques have been developed to improve the collection of patient dose data: the automation of survey techniques to increase the quantity of data collected; and a method of correcting for patient size which reduces one source of variability in the data. An optimisation strategy has been developed, consisting of theoretical simulations, experimental verification and clinical implementation.

Monte Carlo techniques were used for the theoretical study, which investigated the effect of beam filtration on radiation dose and image quality for a wide range of parameters, specifically for a neonatal size phantom. Simulations included both radiography of bone in soft tissue and fluoroscopy of iodine and barium based contrast media. The results were assessed in terms of the beam spectra and the absorption and transmission characteristics of the phantom and image receptor. Experimental measurements of dose and contrast were made for a simple slab phantom corresponding to that simulated, and results showed good agreement with those predicted. A further set of experimental measurements were carried out using anthropomorphic phantoms in a clinical setting, which demonstrated how the theoretical predictions translated to clinical practice. A clinical trial of the use of a 0.1mm copper filter for fluoroscopic examinations of infants was performed, and the filter shown to give substantial dose reduction with no significant loss in image quality. Some general recommendations on dose quantities and the application of optimisation strategies to paediatric radiology have been made.

Acknowledgements

Many people have helped me in the completion of this work, particularly in the latter stages. First and foremost of these, I would like to thank my supervisor Dr Keith Faulkner for his encouragement throughout, without which I would never have reached this stage, and his comments on this manuscript. I would also like to thank Professor Keith Boddy, Professor Brian Diffey and Dr Roger Harrison for their support. Many other colleagues have contributed in various ways, through discussions and general bonhomie, so many thanks to Dawn Broadhead, Jill Hetherington, John Kotre, Andrew Lecomber, Nick Marshall, David Rawlings and Kevin Robson.

This project would not have been possible without the close cooperation of Liz Hunter, senior paediatric radiographer at the RVI, and I am very grateful to her for practical assistance, advice and many helpful discussions. I would also like to thank Dr Dick Lee and other staff at the RVI for participating in the clinical trial, and radiographers throughout the region for their contribution to the data collection.

Thanks must also go to Roger Marsh and Diane Cobbledick for installing and maintaining the dose monitoring equipment, besides providing computing advice when needed, and to Alan Nicklin for cutting the slab phantoms and insets used in the experimental work.

Finally, thank you to family and friends who have supported me throughout, particularly my parents and sister Olivia and, most importantly, my husband John for his patience, his diligent proof-reading, and for not allowing me to give up!

The work was partially supported by a grant from the National Health Service Locally Organised Research Committee of the Northern Regional Health Authority, and the District Research Committee of Newcastle Health Authority.

For Dominic and Nicholas...

'What does *Crustimoney Proseedcake* mean?' said Pooh. 'For I am a Bear of Very Little Brain, and long words Bother me.'
'It means the Thing to Do.'
'As long as it means that, I don't mind,' said Pooh humbly. '

A.A.Milne

Contents

Chapter 1

Introduction

Diagnostic X-rays have been in use for over a hundred years and whereas their usefulness has never been in question, there is a growing awareness of the associated radiation risks both in the scientific and lay communities. Diagnostic radiology accounts for ninety-five percent of the UK population dose from man-made radiation, a total of approximately twenty thousand man sieverts (Hughes and O'Riordan, 1993). The importance of monitoring, and where possible reducing, the level of radiation doses from diagnostic X-ray examinations has been recognised for many years, and is becoming of increasing concern. Recent years have seen initiatives from the Commission of the European Communities (EUR 16260, 1996; EUR 16261, 1996), the World Health Organisation (WHO 689, 1986; WHO 757, 1987) and, in the UK, the National Radiation Protection Board (IPSM, 1992) dealing specifically with this issue.

Radiation dose from diagnostic X-ray examinations has been the subject of much investigation over the years. Early work often focussed specifically on either gonadal dose from a variety of X-ray examinations (Clayton *et al*, 1957; Johns and Wilson, 1958) or on obstetric radiography (Bewley *et al*, 1957). This reflected the chief concerns at that time, which were the genetically significant dose and foetal doses, as such doses affected individuals who were not directly benefiting from the radiographic examination. Since then, analysis of the available risk data has shown genetic effects to be less significant at low doses than first thought (ICRP 60, 1990) and advances in ultrasound have rendered obstetric radiography less common. The main risk arising from low radiation doses, such as those from diagnostic radiology, is now taken to be that of carcinogenesis (ICRP 60, 1990) and the principle of keeping medical irradiation *As Low As Reasonably Achievable* applies. As a results of this, the clinical benefit to the patient of a diagnostic X-ray examination does not diminish the importance of monitoring and where possible reducing their dose.

The first large scale dose survey to be carried out in Britain was that of the Adrian committee (1959, 1960, 1966) and this concluded that the benefit to the patient of carrying out radiological examination outweighed both the risk of cancer induction and the slight genetic risk. It was also shown that if the radiography standards in all hospitals were raised to those of the best 25%, the genetically significant dose would be reduced by a factor of 7. This raised the significant problem of large fluctuations in radiation dose for what is nominally the same examination, which was then highlighted in a number of national surveys including Australia (Morris, 1983), the USA (Johnson and Goetz, 1986) and England (Shrimpton *et al*, 1986) besides regional surveys in Britain (Harrison *et al*, 1983). Differences in both radiological practices and patient doses were also identified between countries (Contento *et al*, 1988).

The legislative framework for radiation protection of the patient was established in the Ionising Radiations Regulations (1988) (POPUMET), and guidelines have been drawn up by both the National Radiological Protection Board (NRPB, 1990) and the Royal College of Radiographers (CoR, 1990). In addition, a combined working party from the NRPB, CoR and Institute of Physical Sciences in Medicine (IPSM) has drawn up a National Protocol for patient dose measurement in diagnostic radiology (IPSM, 1992), to encourage both the continued collection of patient dosimetry data and a uniform manner of collection.

Over recent years, the advent of new technology, such as carbon fibre tabletops, rare-earth screens and sophisticated digital equipment has helped to decrease doses from individual examinations, as has increasing awareness of the radiation detriment to the patient (Rainbow and Cockshott, 1989). This is well illustrated by comparison of the results from the most recent British surveys (Shrimpton *et al*, 1986; Hart *et al*, 1996) in which patient doses per examination were shown to have fallen by around 30% for most examinations. This reduction, however, is offset by the increasing numbers of radiological examinations and particularly the more widespread use of X-ray computed tomography, so that the population dose from diagnostic radiology has not fallen in the same way, and is expected to increase over the next decades. The most recent national survey also demonstrates that variation in

performance between hospitals is still substantial, indicating continuing scope for patient dose reduction.

1.1 Paediatric radiology

Dose reduction is of particular concern in paediatric radiology for a number of reasons. Firstly, and most importantly, there is a greater chance for expression of radiation induced effects for children than for the adult population. Children are usually considered to be at greater risk for certain types of cancer (Stather *et al*, 1988), although there is not general agreement (Muirhead *et al*, 1993), mainly due to the uncertainty in the risk data which arises from the fact that for the main data source - that from the Japanese atomic bomb survivors - people irradiated as children have not yet lived long enough for all possible radiation effects to be observed. There is even greater uncertainty over genetic risk factors, as it will take considerable time before any radiation induced effects can be traced through the genetic pool. This represents an additional potential hazard from irradiation of a paediatric population. For neonates, especially those born prematurely, the most appropriate risk factors are almost certainly those used for foetal irradiation, which are higher than those for the general population, although uncertainties are again large. Another factor to consider is that some examinations are carried out with greater frequency for children. In particular, premature or sick neonates may receive a large number of X-ray examinations during the first few months of life, as their condition is monitored, and this can sometimes continue throughout early childhood. Finally, children will often be uncooperative during X-ray examination, thus requiring repeat or longer exposures.

There are particular problems associated with monitoring radiation doses to children. As doses are generally significantly lower than for adults, sometimes comparable with background fluctuations, greater sensitivity is required in equipment used to record accurately dose parameters such as entrance skin dose or dose-area product. This may require purchase of specialised equipment, or development of specific techniques for making measurements (Broadhead *et al*, 1997). There are also sparse data available for converting such parameters to quantities more directly related to risk, such as energy imparted or effective dose. Factors

for deriving energy imparted are limited to the work of Persliden and Sandborg (1993) and a general method for estimation of dose distributions using depth dose curves (Almen and Nilsson, 1996). Conversion factors for some organ doses have been published (Rosenstein *et al*, 1979; Zankl *et al*, 1989) and also coefficients for estimating effective dose (Hart *et al*, 1996). Such factors exist only for specifically defined patient sizes and examination types, and extrapolation to different situations needs to be carried out with care. While this is true of all such data, it is particularly important for children whose small size means that critical organs will often be close to the edge of the radiation field, which increases the difficulty in applying normalised organ dose data when the examination geometry differs from that modelled.

Comparisons of paediatric dose data are also problematic, due to the wide range of patient sizes involved. The term 'paediatric' applies to a wide range of patients, from a premature neonate, who may weigh as little as a few kg, to a young adult of 16 who may be fully grown, with a continuous spectrum of sizes in between. This size variability creates problems in both the actual dosimetry such as the application of organ dose data, as described above, and in the analysis of data, as a simple dose quantity measured for different sized patients cannot meaningfully be compared. Although many authors have highlighted the problems arising from paediatric size variations (Maillie *et al*, 1981; Lindskoug, 1997; Almen *et al*, 1995), and several have studied the effect (Martin *et al*, 1995; Wraith *et al*, 1996), there is still no consensus on the best method for addressing the problem, or even the most suitable age or size banding to use. The most commonly adopted approach at present is to group paediatric dose data in bands according to patient age, with suitable bands defined by the CEC (1992). However, there are two problems with this approach. Firstly, the size of a patient cannot be reliably linked to his age as, although mean or typical size parameters are well publicised, there is considerable variation around these figures. Secondly, even if a given age band represented a given band of patient sizes the variation within the band would still be large. The use of smaller age or size bands, with correspondingly less variability, automatically decreases the amount of data in each group, thus increasing other statistical

uncertainties. This issue of size is one of the most fundamental problems in paediatric dosimetry, and is addressed in this work.

Although many surveys have been performed of radiation dose to patients undergoing diagnostic radiology, very little of this data relates to paediatric radiology. For instance, the 1985 National Survey of doses to patients in Britain reports a total of around four thousand dose measurements, of which just over one hundred are for children (Shrimpton *et al*, 1986). In the more recent survey, only around 500 of the 52 thousand measurements received by the national collation centre were for children (Hart *et al*, 1996). This lack of data results chiefly from the problems described above, and the development of techniques for collecting paediatric dose data and the establishment of a paediatric dose database are essential components of the work presented here. A review of published paediatric dose data, and the methodologies used is given in Chapter 3.

1.2 Optimisation

The recommended system for dose limitation for persons undergoing medical exposure is based on the principles of justification and optimisation (ICRP 60, 1990) *ie* an exposure must be clinically necessary and the radiation dose should be as low as reasonably achievable (ALARA). It is important, however, that any radiation risk is balanced against the clinical benefit to the patient of performing the examination. Variations in patient dose resulting from changes in technique cannot be viewed in isolation, as the associated change in image quality must also be considered. An examination performed with minimal radiation dose is of no value if it is diagnostically unacceptable and a repeat exposure is required. The indexes used to assess image quality must be selected with care, and the required information content for the procedure taken into consideration. Not all examinations require the same level of image quality *eg* the detection of an intussusception (a fairly gross intestinal malformation) in a small child can be performed with much lower image quality than that required for a skeletal survey performed to exclude the possibility of non-accidental injury. The dose quantity used for comparison must also be chosen carefully. In addition to being easily and reproducibly measurable, the doses described should be related to the radiation risk to the patient. It is

essential that the development and implementation of an optimisation strategy must be based on a framework of good dosimetry (in both quality and quantity), in order to establish the need for such optimisation and to demonstrate its benefits.

Suggested optimal techniques for paediatric patients have been documented by the CEC (1996) but are fairly general in nature, being designed to apply to "..*normal basic radiographs which could address any clinical indication*" with little scientific work referenced to justify the recommendations. The recommendations are made for a limited number of patient ages and the examination categories include only plain film radiography with the exception of micturating cysturethrography which is carried out under fluoroscopic control. As the practice of paediatric radiology encompasses a wide range of variable parameters: patient age and size; examination type; clinical indications; available equipment; individual radiologist preferences *etc*, the concept of patient and examination specific optimisation is an important consideration. While general recommendations may be a useful starting point for a departmental optimisation strategy, an understanding of the underlying science and the effect of variations in the recommended technique parameters is required to be able to apply them successfully to a particular situation.

1.2.1 Filtration

Many potential methods of dose reduction have been investigated over the years, including the use of new technology such as carbon fibre tables and rare earth screens (Herman *et al*, 1987; Burton *et al*, 1988; Faulkner *et al*, 1989), careful use of protective devices (Faulkner *et al*, 1989; Kenny and Hill, 1992) and the selection of technique factors. All these are important aspects of the optimisation process, as are the technical practices of both radiographers and radiologists. One specific method of reducing dose is the shaping of the X-ray beam spectrum through the use of additional or replacement filter material (Jennings, 1988; Carrier and Beique, 1992; Sandborg *et al*, 1994). The use of so called 'k-edge' filters has been of particular debate, as these have been thought to shape the beam spectrum in an optimal manner. Investigations into the effectiveness of such filters have been carried out in

a number of ways, as described fully in Chapter 4, and opinion is divided on the efficacy of the technique.

This study involved the assessment of beam filtration as an optimisation tool for several reasons:

- Unlike some other parameters, such as the use of rare-earth screens, which are proven and generally accepted as dose reducing, there is no consensus on what constitutes 'optimal' filtration.
- Changes in filtration can generally be implemented relatively easily on a clinical basis, compared to the purchase of new 'dose saving' equipment.
- Filtration may also, in principle, be changed on an examination by examination basis, and so constitutes a potential method of patient and examination specific optimisation.

1.2.2 Optimisation methodologies

A variety of techniques has been used to perform optimisation studies. Generally, they may be classed as theoretical, experimental or clinical techniques, and each has advantages and disadvantages. Theoretical studies may be analytical in nature, with a situation modelled mathematically from the underlying physics of the problem, usually employing simplifying assumptions (Koedooder and Venema, 1986; Jennings, 1988). Such an approach may be straightforward to carry out, but the necessary simplification of the theory *eg* neglect of scatter, may bias the results or lead to the neglect of interesting effects. The other common theoretical technique employed is that of Monte Carlo simulation, where the random trajectories and interactions of particles ('histories') are monitored individually, by sampling the probability distributions of possible events. The cumulation of a large number of such histories is used to determine quantities of interest (Shrimpton *et al*, 1988; Sandborg, 1994). Such simulations can be used to characterise radiation behaviour on an interaction by interaction basis, thus generating a more realistic representation and therefore more accurate results than a simple mathematical model. However, such code is complex to use, and may take considerable time to 'run' simulations to the required degree of accuracy.

Experimental measurements may be carried out using simplified phantoms, such as slab or water phantoms to represent the patient (Regano and Sutton, 1992), or by using anthropomorphic phantoms. The latter should give a good anatomical representation of the human body, but may not always show the correct attenuation properties for the desired beam spectra, as they are often designed for a use in a wide range of radiation work. Clinical studies use measurements made on actual patients to assess an optimisation technique, and so should always be the end point of an optimisation study, but for ethical reasons such measurements can only be used to confirm predictions of improved performance.

Theoretical studies usually have the advantage of allowing variation of a wide range of parameters and may be very accurate, within the limitations of any assumptions that are made. Experimental work will involve measurement uncertainties, will often be more restrictive in scope, but should yield a more realistic picture of what is actually happening, and take account of local factors such as limitations in equipment. Clinical studies will be even more representative of actual practice, but often involve only subjective assessment of image quality, and are likely to be affected by statistical uncertainties. Ideally, assessment of an optimisation strategy should include each type of methodology.

1.3 Summary of background

In summary, although the collection and study of patient dosimetry data has become an active field, there is still a paucity of high quality paediatric dose data, and no suitable method for taking individual patient size into account when monitoring doses. General methods of optimisation and dose reduction have often been developed with the adult population in mind, and are not always directly transferable to a paediatric population. The concept of patient and examination specific optimisation needs to be more fully explored, particularly in relation to paediatric radiology. Consideration of the dose and image quality indexes used in optimisation studies has not always been sufficient and, finally, no such study should be considered complete until it has reached the stage of successful clinical implementation.

1.4 Purpose of work

The aims of this work were as follows:-

(1) to devise a method of collecting and utilising paediatric dose data, to perform a large scale survey of doses in a number of hospitals.

(2) to address the question of accounting for patient size.

(3) to collect data for fluoroscopic examinations on children, from departments across the north of England, to study the dose levels and factors affecting them.

(4) to consider the principles of optimisation as applied to paediatric radiology, and look at the use of different dose and image quality indices.

(5) to look specifically at optimisation of beam spectra, using different filter materials; firstly employing Monte Carlo techniques in order to allow variation of a wide range of parameters, followed by a more selective study using phantoms to verify the theoretical results and form a link to clinical practice.

(6) to implement results using a clinical trial to assess the practicalities of any suggested modification to current X-ray technique.

Although the development of the data collection and optimisation strategy was designed to apply to all paediatric age-ranges, the main focus for the simulations was neonatal radiology. This age-group is the extreme example for most of the considerations that have been outlined in the first section, with respect to both risk and dosimetric problems. It also represents the subset of the population furthest from the 'reference man' for which the majority of radiation protection work has been carried out. The application of the methods to older age groups was considered, and tested by a set of preliminary Monte Carlo simulations.

1.5 Outline of thesis

Chapter 2 contains a discussion of the different methods used to describe patient dose, including their advantages and disadvantages and their applicability to this work. Chapter 3 discusses the problems associated with the large scale collection of paediatric dose data, along with a brief review of work published to date. A method of automating dose data collection is described and a technique for correcting collected data to a number of standard patient sizes is developed, in order to facilitate comparisons of the data. The results of a

survey of paediatric doses from fluoroscopic examinations around the north of England are also presented. Chapter 4 contains a consideration of the different factors that must be considered in the optimisation of dose and image quality, and the choice of quantities to be used in studying these parameters. A discussion of radiation filters and their effects is also given here, along with a review of published work in this area. Chapter 5 describes the principles of Monte Carlo simulation and the development of the code used in this work, and the results of the Monte Carlo simulations are described in chapter 6. Chapter 7 describes the phantoms and methodology used for the experimental study, and chapter 8 the results of the experimental optimisation study. The clinical implementation of the ensuing results is described in chapter 9. The application of the work to other age groups, and examination categories is considered in chapter 10, along with suggestions for further work, and the conclusions from the work are given in chapter 11. The full set of results from the dose survey is presented in Appendix A, and Appendix B contains a full listing of the user code written for the Monte Carlo simulations. A description of the Mortran programming language used in the Monte Carlo code is given in Appendix C and Appendix D contains the forms used in the clinical trial.

Chapter 2

Radiation Dose Assessment

2.1 Introduction

The development and application of any optimisation strategy relies on a framework of good dosimetry. The reasons for this are, firstly, to establish where potential for optimisation lies and, secondly, to be able to assess the effect of any changes made. Radiation dose to a patient may be described in several different ways, including both measurable and calculated quantities. The most common dose descriptors are entrance skin dose, effective dose, dose area product and energy imparted. In this chapter each of these will be discussed, along with their associated measurement and calculation methods. The usefulness of each of these quantities has been assessed in terms of their ease of measurement; their comparability when used in differing circumstances; and their relationship to the radiation risk to the patient. Their specific application to paediatric dosimetry has also been addressed. A section is also included to discuss the concept of radiation risk and data pertaining to it.

2.2 Radiation risk

Radiation dose to an individual is only important in so much as it carries with it an associated risk. Radiation risks may be divided into those that are stochastic in nature *ie* the probability of occurrence increases with the dose received, and those that are non-stochastic or deterministic, where a minimum dose must be received before the effect is exhibited. In diagnostic radiology it is rare for patient doses to exceed those for which deterministic effects may be shown, except for some high dose interventional procedures, so it is the stochastic risks that are generally of concern. The chief of these is the risk of cancer induction. Possible genetic effects may also have to be considered.

There are several sources of data from which radiation risk estimates have been assessed. The most important of these is the follow up of the Japanese atomic bomb survivors. There is a

large amount of uncertainty in the extrapolation of the risk data, particularly down to low doses, but it is generally accepted that there is no threshold dose for the risk of cancer induction (ICRP, 1991). Risk data for paediatrics is even less well established, as sufficient time has not yet elapsed for all possible late effects to be observed. It is suggested though that the relative probability of cancer induction in the various organs is different for the paediatric population than for the adult population (ICRP, 1991). Changes in the way existing data is analysed, and acquisition of further data may both alter current perceptions of risk in the future. All risk data must therefore be used with caution, and uncertainties assumed to be a factor of at least 2.

2.3 Entrance skin dose

Entrance skin dose (ESD), usually expressed in mGy, is the maximum dose at a point on the surface of the patient, where the X-ray beam enters the body. It is a very simple quantity to both measure and calculate. Measurement can be carried out using a thermoluminescent dosimeter (TLD), or by derivation from a dose area product measurement (see Section 2.5 below) when the entrance field size is known or measured. It can be calculated from the technique factors used for the examination and knowledge or assumption of the tube output, using the following equation.

$$ESD = OUTPUT \times \frac{kV^2}{80^2} \times mAs \times \frac{1}{FSD^2} \times BSF$$

where *OUTPUT* is defined in terms of absorbed dose per unit mAs, at 80kV, 1m from the tube focus. *FSD* is the focus-skin distance, *kV* the generating tube potential, and *mAs* the product of tube current and exposure time. *BSF* is the back scatter factor, values of which are tabulated for different beam qualities, field sizes, and patient thicknesses. The formula uses the assumption that output is proprtional to the square of the generating tube potential, as is commonly held, but this is not always valid so for greater accuracy the output should be measured at each kV of interest. ESD has the advantage of being commonly used in a wide range of circumstances, and is the recommended quantity for patient dose assessment for simple examinations in adults, for the establishment of reference doses (IPSM, 1992).

There are, however, disadvantages to using entrance skin dose as a measure of patient dose. Firstly, for complex fluoroscopic examinations there will not be a single entrance point for the X-ray beam, so that the measurement will be highly dependent on the exact location chosen, and will not adequately represent the entire examination. In addition to this, the quantity is not directly related to radiation risk, unless being used to assess the probability of skin erythema occurring in high dose interventional procedures. Although useful for comparing doses from similar procedures, if very different energy spectra are used in two irradiations, measurement of surface dose alone may be a very poor indicator of the change in overall patient dose.

2.4 Effective dose

Effective dose cannot be measured directly, but is a derived quantity that can be related to radiation risk. It is calculated from a weighted sum of organ doses, and was introduced by the International Commission on Radiological Protection (ICRP, 1991) as a means of assessing the risk to occupationally exposed persons, receiving non-uniform exposure. The tissue weighting factors are derived from radiation risk data as applicable to adult workers, and are given in table 2.1. The unit used for effective dose is mSv.

Tissue	Weighting Factor
gonads	0.20
red bone marrow	0.12
colon	0.12
lung	0.12
stomach	0.12
bladder	0.05
breasts	0.05
liver	0.05
oesophagus	0.05
thyroid	0.05
skin	0.01
bone surface	0.01
remainder	0.05

Table 2.1 : Tissue weighting factors (the *remainder* comprises adrenals, brain, upper large inestine, small intestine, kidney, muscle, pancreas, spleen, thymus & uterus)

Although this quantity is commonly used for assessing the risk from diagnostic X-ray

exposure, there are recognised problems in its application as the patient population is considerably different from the adult worker population, and the paediatric patient population is different again. There is very little justification for assuming that relative tissue sensitivities are the same in children as for adults. The calculation of effective dose requires the use of published organ dose data. Such data are normally quoted in relation to entrance surface dose, or occasionally relative dose area product, and may be derived from Monte Carlo calculations (Hart *et al*, 1996) or from TLD measurements in an anthropomorphic phantom (Broadhead, 1998). Normalised organ dose factors are highly dependent on beam quality used and on the size and shape of the patient. They also apply only for the specific beam size and position for which they were derived. Appropriate data may not be available for the particular conditions of interest, especially for paediatric patients. Uncertainties in calculations of effective dose are considerable, due to the combination of uncertainties in assessment of the different organ doses, the radiation risk data used, and the extrapolation to different populations of people. These uncertainties make comparisons of effective dose between centres difficult.

2.5 Dose area product

Dose area product (DAP) is defined as the dose integrated over the beam area

$$DAP = \int D\ (x,y)\ dx\ dy$$

It is measurable directly, using a dedicated ionisation chamber attached to the X-ray tube. DAP is independent of distance from the tube, and may be taken to be equivalent to the product of the entrance surface dose (without backscatter) and the entrance field size. It is normally measured in terms of mGy cm^2. Occasionally air kerma area product may be specified instead, when the DAP meter has been calibrated in terms of dose in air rather than dose in soft tissue. DAP is the recommended quantity for assessment of dose from complex X-ray examinations (IPSM, 1992). It is easy to compare results from such measurements, provided that the instruments used have been calibrated in a similar manner, and it is the only

reliable way of making dose assessments when the field of view is constantly changing throughout an examination.

The drawbacks of the method are the initial cost of the DAP meter used to make the measurements and, for paediatrics in particular, the possibility that the beam area might extend outside the patient thus giving an inaccurate reflection of dose. Occasional practical difficulties may arise if, for instance, a department uses wedges for beam shaping that cannot be fitted easily in conjunction with the ionisation chamber. Factors are available to convert DAP measurements to risk estimates, under specific conditions (Le Heron, 1992), and also to values of effective dose (Hart *et al*, 1996). These are subject to the same problems and uncertainties as those described above for conversion from ESD to effective dose.

2.6 Energy imparted

The term 'energy imparted' refers to the total amount of energy absorbed by the patient's body during the X-ray examination, measured in mJ. It may be derived from measurements of DAP by using published conversion factors (Carlsson *et al*, 1984; Persliden & Sandborg, 1993). Data has also been published relating energy imparted to entrance dose for neonates (Chapple *et al*, 1994) When investigating the use of different beam spectra, comparison of energy imparted will give a better assessment of changes in patient dose than will a comparison of entrance surface dose alone, as it includes information about dose absorption throughout the body instead of just at the surface. It does not, however, make any allowance for individual organ radiosensitivities.

An assessment of radiation risk may be made from energy imparted by calculating an equivalent effective dose, assuming the energy to have been absorbed uniformly by all radiosensitive organs in the body. For many anatomically specific examinations this approximation results in large uncertainties in the ensuing risk estimate, but its usefulness increases as the proportion of irradiated tissue to unirradiated tissue increases, as the approximation to whole body exposure improves. For fluoroscopic examinations of small children this condition is often well satisfied, as organs are all close together (for an infant,

the total length of the trunk may only be 30-40 cm long) and energy imparted may be the most appropriate way of assessing such doses. Energy imparted is not, however, in widespread current use - probably because of the almost universal acceptance of effective dose as a reliable risk estimator for patient dosimetry, in spite of the limitations discussed earlier.

2.7 Summary

The most easily measured dose quantities for assessment of patient dose are entrance surface dose and dose area product. From these, factors are available for calculating the risk related quantities effective dose and energy imparted. Although the former of these gives a well defined risk estimate, with consideration of the dose to and radiosensitivity of different organs, there are significant uncertainties in its general application. The most appropriate quantity to use in a given situation will depend on the reasons for carrying out the measurement (*eg* for specific comparative purposes; to determine the radiation risk for a specific patient; or as part of a routine dose survey) and the conditions under which it is made, including factors such as patient age and examination type. The correct choice of dose quantity may have a significant effect on the quality of the dosimetry data obtained.

Chapter 3

Paediatric Dose Data

3.1 Introduction

The collection and analysis of patient dose data is a prerequisite for any optimisation study. The dosimetry techniques used must allow comparisons with other data, and the inherent variability in patient dose requires that large amounts of data need to be collected. This is necessary in order to draw significant conclusions about differences between groups and the effect on dose of the various parameters involved. Whereas this is true of all patient dosimetry, it is of particular importance in paediatric dosimetry (patients aged 0-16 years) as patient size variability is so much greater than for the adult population. This issue of size is crucial to the assessment of paediatric dose data.

A number of authors have contributed to the existing information on paediatric X-ray doses over recent years, and their work is reviewed in this chapter in conjunction with some of the problems arising in paediatric dosimetry and recommended dosimetry methods. As part of this work, two techniques have been developed in order to improve both the quality and quantity of paediatric dose data, namely patient size correction and the automation of data collection to make large data sets available, and each is described in detail. The results of a survey of doses to paediatric patients, carried out using these techniques, are then described.

3.2 Published data

3.2.1 Dosimetric techniques

The National Protocol for patient dose measurements makes recommendations on the type and frequency of dose assessments that should be performed in X-ray departments (IPSM, 1992). Recommendations on sample size and criteria are also made, although there are no specific recommendations for paediatric dosimetry. The document states that the currently preferred dose measurement techniques are direct measurement using TLD for single

radiographs, and dose area product measurement using a calibrated dose area product (DAP) meter for complete examinations. A summary of the most recently published paediatric dose data, excluding that presented exclusively for neonates, is given in Table 3.1.

TLDs have been used by a number of groups for the measurement of entrance surface dose on paediatric patrients (Smith *et al*, 1979; Almen and Mattsson, 1995; Martin *et al*, 1994; Persliden *et al*, 1996). For simple X-ray examinations, the low doses involved for young children give these measurements a high level of uncertainty. Entrance surface doses (ESD) may be as low as around 0.05 mGy for a neonatal chest X-ray (Smith *et al*, 1979), and may only be around 2 mGy for a pelvic radiograph on an older child in the 6-15 age group (Almen *et al*, 1995). The most usual form of TLD used for such measurements, chips or pellets of lithium fluoride or lithium borate, have a minimum detection limit of around 0.1 mGy (Broadhead, 1997) and the uncertainty due to background fluctuations may be as much as 20% at low doses. There are also practical problems with using TLD for neonatal examinations, as described by Martin *et al* (1994) who found TLD unsatisfactory in the neonatal nursery because their placement interfered with infection control procedures, and also because they produced artifacts on the image.

ESD values have also been calculated for dose assessment purposes, either from technique factors (McDonald *et al*, 1996; Kyriou *et al*, 1996) or from DAP measurements (Ruiz *et al*, 1991). The latter requires assessment of field size, which is not always straightforward. Calculation of ESD for paediatrics has been reported to agree with TLD measurement (Kyriou *et al*, 1996), although the spread in the ratios of measured and calculated results was large with standard errors of up to 65%. Insufficient details were given to be able to fully assess the data in this paper. Care has to be taken that appropriate back scatter factors are used in calculations, and these will vary according to patient thickness, field size and tube voltage. Values suitable for paediatric radiography have been tabulated, but they are fewer data available than for adults and not all radiographic situations are covered.

Author	Examinations	Age banding	Dosimetry methods	Total no patients	No / group
Gustafsson & Mortensson (1983)	chest	1-6 mths 4mth-6.5yrs 2.5-11 yrs	meas. DAP & ESD, calc. energy imparted	38	5 - 20
Cleveland *et al* (1991)	voiding cystourethrogram	0-1 yrs 1-5 yrs 5-7 yrs	phantom meas, calc ESD & mid plane dose	47	9 - 20
Ruiz *et al* (1991)	abdomen, hip & pelvis, skull, spine, chest	1 mth-1 yr 1-5 yrs 5-10 yrs 10-14 yrs	ESD calc. from meas. DAP	492	not reported
Karlsson *et al* (1994)	diagnosis & hydrostatic reduction of interssusception	none	meas. DAP	45	-
Martin *et al* (1994)	chest, pelvis, abdomen, skull, MCU, ba meal	infant 1-5 yrs 6-10 yrs 11-15 yrs 6-15 yrs	calc & meas ESD meas DAP	522	4 - 99
Gonzalez *et al* (1994)	micturating cystourethrogram	1 mth -1 yr 1-5 yrs 5-10 yrs 10-14 yrs	meas. DAP	48	1 - 13
Almen *et al* (1995)	pelvis, IVU, MCU	0-1 yr 2-5 yrs 6-15 yrs	meas. DAP & ESD, calc. organ doses & energy imparted	95	2 - 18
Kyriou *et al* (1996)	chest, skull, abdomen, hip, spine, sinus, knee, ankle, wrist, ba meal ba enema, ivu	1 mth-1 yr 1-5 yrs 5-10 yrs 10-14 yrs	meas. DAP, calc ESD	1342 ESD 1123 DAP	1 - 151
McDonald *et al* (1996)	pelvis, chest, abdomen, spine, skull	1 mth-1 yr 1-5 yrs 5-10 yrs 10-14 yrs	meas. DAP, calc. ESD	392	5 - 25
Persliden *et al* (1996)	small intestinal biopsy	none	meas. ESD	257	-

Table 3.1 : Summary of published paediatric dose surveys

DAP measurements have been used in a number of surveys, both for fluoroscopy (Karlsson *et al*, 1994; Martin *et al*, 1994; Gonzalez *et al*, 1994; Almen *et al*, 1995; Kyriou *et al*, 1996)

and radiogaphy (Gustaffsson and Mortensson, 1983; Ruiz *et al*, 1991; Martin *et al*, 1994; Kyriou *et al*, 1994; McDonald *et al*, 1996). DAP values from paediatric examinations may be as low as 50 mGy cm^{-2} for a simple cystogram, or down to around 5 mGy cm^{-2} for a radiographic exposure. Many DAP meters have low dose sensitivity of around 10 mGy cm^{-2}, which would obviously be insufficient for the above cases, although some have special paediatric settings which can give a sensitivity of 0.1 mGy cm^{-2}, as was used by Martin *et al*(1994). One method of improving the accuracy of both DAP and ESD measurements is to integrate the dose over a number of exposures on different patients, but this also has the effect of reducing the sample number, and losing information on individual patients.

Values of ESD and DAP have been used to derive values of energy imparted (Gustaffsson and Mortensson, 1983; Almen *et al*, 1995; Chapple *et al*, 1994) and effective dose (Almen *et al*, 1995). The latter needs to be applied with great caution to paediatric patients, as was pointed out by Almen *et al* in their conclusions. They, however, based this advice solely on the unreliability for paediatrics of the risk data used for the determination of organ weighting factors. No mention was made of the uncertainties in effective dose values arising from varying beam size and position, which make comparisons difficult.

3.2.2 Grouping of data

As there are many factors influencing individual patient dose, a reasonable sample size is required to make the data meaningful. In addition to variations in dose due to different X-ray equipment, factors such as patient size, compliance, clinical indications and complications will all influence the resultant dose. Technique factors, such as tube kilovoltage, and individual radiologist/radiographer technique, such as the degree of coning and different projections used will also have an effect. In the light of this, although the National Protocol for Patient Dose Measurements recommends a minimum sample size of 10 per category of patient (IPSM, 1992), the uncertainty in mean dose from a sample of this size may still make comparison with other data difficult. The survey carried out as part of this work, in comparison, used sample numbers of up to 200 for each combination of age group, examination type and X-ray room.

One of the chief problems in paediatric dosimetry is the wide range of size from neonates up to young adults of sixteen years of age. The CEC have defined a number of standard age bands into which categories dose estimates should be split. These are 0-1 month (neonates), 1 month - 1 year (infants), 1-5 years, 5-10 years and 10-16 years (CEC, 1993). While some authors have used these divisions for collating their data (Ruiz *et al*, 1991; Martin *et al*, 1994; Gonzalez *et al*, 1994; Kyriou *et al*, 1996; McDonald *et al*, 1996) others have chosen different age ranges (Gustafsson and Mortensson, 1983; Cleveland *et al*, 1991; Chapple *et al*, 1992 & 1993; Almen *et al*, 1995) and others have not grouped data at all (Karlsson *et al*, 1994; Persliden *et al*, 1996). Some confusion is still apparent as to the boundary between the different age groups recommended by the CEC *eg* whether a child between his 5th and 6th birthdays belongs in the 1-5 group or the group above *etc*. This makes comparisons between centres rather confusing although, in fact, the high variability in size for children of any particular age makes such slight differences in age grouping immaterial. This illustrates how the basic premise of grouping dose data according to age rather than a body size parameter is fundamentally flawed. This point has been recognised by others (Almen *et al*, 1995).

While the use of a grouping system for presenting paediatric dosimetry results is desirable, it inevitably decreases the patient numbers in each category. Unless the number of patients in a single group is sufficient for their size to be approximately normally distributed *ie* so that their mean size is representative of the whole group, the data may still give distorted comparisons with those of other centres. Sample numbers in the published data vary enormously. The studies presenting data for all patient ages together (Karlsson *et al*, 1994; Persliden *et al*, 1996) report the results of several hundred measurements, which would be a good sample size were it not for the wide age and size ranges involved. The 1985 national dose survey presented data for 9 paediatric examinations, with between 1 and 20 patients in each sample (Shrimpton *et al*, 1986), but no grouping of the data according to either size or age was used. The data presented by Ruiz *et al* (1991) includes only the total number of measurements made (492) and sample numbers in the 20 individual data groups are not reported, which makes assessment of or comparisons with their data difficult. Most of the other age banded data is presented in variable group sizes, with the most extreme example

being the work of Kyriou *et al* where patient numbers range from 1 to 151. Several other authors have presented data for sample sizes of less than 5 (Martin *et al*, 1994; Gonzalez *et al*, 1994; Almen *et al*, 1995), which can have very limited use, due to the high statistical uncertainties. Very little data exists for age grouped data with sample sizes greater than 20, excepting some of the initial results from the survey reported here (Chapple *et al*, 1992, 1993). It is noteworthy that in the 1995 national survey of patient doses (Hart *et al*, 1996) it is mentioned that for paediatrics 402 ESD measurements and 135 DAP measurements were received, but the results are not reported as the amount of data was considered insufficient.

3.2.3 Examination categories

The majority of recently reported work has centred on radiographic examinations (Ruiz *et al*, 1991; Martin *et al*, 1994; Kyriou *et al*, 1996; McDonald *et al*, 1996), including skull, chest, abdomen, hip, pelvis and spine radiographs. Several studies have also been reported of doses from cystourethrograms - probably the most frequent fluoroscopic examination in early childhood (Cleveland *et al*, 1991; Martin *et al*, 1994; Gonzalez *et al*, 1994; Almen *et al*, 1995). Other data from fluoroscopic procedures is limited to a small amount of barium study data (Martin *et al*, 1994; Kyriou *et al*, 1996) and results from two specific interventional procedures, namely the diagnosis and hydrostatic reduction of interssusception (Karlsson *et al*, 1994) and small intestinal biopsies (Persliden *et al*, 1996). Some work has also been carried out for paediatric patients undergoing cardiac catheterization (Wu *et al*, 1991; Schueler *et al*, 1994) and initial results from the survey carried out as part of this work have been published, for a range of examinations (Chapple *et al*, 1993). As fluoroscopic procedures generally result in considerably larger patient doses than simple radiographic procedures, this paucity of data represents a significant gap in the literature.

3.2.4 Analysis of data

Many of the paediatric dose surveys that have been performed had a further objective apart from contributing to the accumulation of dose data. The most common of these were to compare techniques at two or more centres (Gonzalez *et al*, 1995; Kyriou *et al*, 1996) or to investigate how patient dose is affected by changes in technique such as removal of the grid

(McDonald *et al*, 1996) and the use of digital instead of fluoroscopic spot films (Cleveland *et al*, 1991). Potential dose savings from optimisation of techniques were assessed by Gonzalez *et al* (1995) but the projected 85% reduction in DAP was not verified clinically. The potential risk from paediatric chest radiography was assessed by Gustafsson and Mortensson (1983), who concluded that the greatest risk was that for possible future breast cancer, for girls past infancy. Other studies have investigated relationships between patient size and dose (Martin *et al*, 1994; Karlsson *et al*, 1994; McDonald *et al*, 1996) and this issue is explored in a later section.

3.2.5 Neonatal data

The measurement of radiation dose to neonates is an even more specialised subject than paediatric dosimetry in general. This is partly due to the fact that neonatal radiography is normally carried out in a special care baby unit or nursery, using mobile equipment, so necessitates separate dose survey arrangements. As neonates represent the extreme end of the size range for paediatrics *ie* that furthest from adults, many of the dosimetry problems that have been referred to above are exaggerated for examinations of this age group, particularly those concerning sensitivity of the dose measurement device.

A relatively large body of data exists for neonatal radiation doses, compared to paediatrics in general. Much of this data consists of TLD measurements of entrance skin dose on patients (Smith *et al*, 1979; Smathers *et al*, 1984; Werner *et al*, 1986; Herman *et al*, 1987;) in spite of the practical problems and high uncertainties associated with such measurements on neonates. Others have calculated values of entrance dose (Robinson and Dellagrammaticas, 1982; Fletcher *et al*, 1986; Faulkner *et al*, 1989; Wraith *et al*, 1995; Chapple *et al*, 1994), or used phantom measurements to assess the dose (Wesenberg, 1977; Burton *et al*, 1987). Other dose quantities such as DAP, selected organ doses or energy imparted have also been calculated in some cases (Robinson and Dellagrammaticas, 1982; Faulkner *et al*, 1989; Wraith *et al*, 1995; Chapple *et al*, 1994). Dose reduction methods have been usefully outlined by Faulkner *et al* (1989). There is virtually no data in the public domain concerning dose to neonates from fluoroscopy. Although such procedures are far more rare than plain

radiography, the higher dose associated with them means that assessment of such doses is an important area of study.

3.2.6 Conclusions from literature review

Altogether, the amount of paediatric dose data collected is small compared to that existing for the adult population, and there are difficulties in comparing data from different centres. Even when centres have used the same age divisions, the range of patient sizes within the band, and the relatively small numbers of dose assessments made usually preclude meaningful comparison. For the same reason, development of reference doses for paediatrics has also been slow and difficult to apply.

3.3 Automation of dose survey

As shown above, many of the problems encountered in paediatric dosimetry may be eased by increasing the number of dose assessments made, as this improves the statistical analysis of the data. However, the practical problems associated with this have to be addressed. Even if only twenty dose measurements are to be made for each age group and examination type, and the survey is limited to five common procedures, this will still necessitate five hundred measurements in one room. If data is to be recorded on paper, this will result in time consuming work for the radiographic staff and the ensuing analysis will require laborious entry of data into a suitable software package. This is likely to produce a number of data transfer errors, and makes routine surveys unfeasible. The collection of a large quantity of paediatric dose information, on a routine basis, is thus facilitated by the automation of dose survey techniques. One important advantage of this approach is that data is collected in a uniform manner.

3.3.1 Design of survey

The priority in designing the dosimetry data collection system was its acceptibility to radiographic staff. This was important in order to be able to implement the initiative on a routine basis. For this reason, development was carried out with the close cooperation of a number of radiographers. This allowed practical problems to be addressed at an early stage.

It also enabled the system to meet the needs of the individual X-ray departments, for instance providing an instant dose indicator for each patient, in addition to the requirements of the physicists wishing to analyze the data. The other requirements of the system were that it record all information pertaining to full analysis of the data, and that the data be easily exported for analysis.

The data collection system was designed for use in a regional survey of doses from fluoroscopic procedures, monitored with DAP meters. The automation was carried out by using computers to collect, store and analyse the dosimetric data. DAP meters were installed in X-ray rooms at hospitals throughout the north of England. Each DAP meter was connected to a laptop computer, on which data could be collected and stored. Data was then transferred at regular intervals to a central computer database for analysis. The data collected consisted of dose area product for the examination, read directly from the DAP meter, and data input by the radiographer, consisting of the following:

patient name
sex
age
height
weight
examination type
radiologist
screening time
kVp
number of radiographs
number of 100mm/DSI films

The only hardware requirements for running the software were

- any PC or laptop, 386 or above
- serial communication link to DAP meter
- floppy disk drive
- minimum disk space 1 MByte

The connections between DAP meter control box, ionisation chamber and the computer were wired by technologists from the electronics department and, in most cases, this was a straightforward operation using existing cable trunking.

3.3.2 Data collection software

The data collection software was written in BORLAND PASCAL and the impact on the radiographer minimised by using a series of prompts and menus, *via* a simple in-house graphical user interface. Height and weight information could be entered in either metric or imperial units, and age either directly or indirectly as a date of birth from which age was calculated. The software was configurable for each department, in that the most frequently used radiologist names and examination types were stored in a customised menu. An option was developed whereby most of the patient information could be entered prior to the session. On arrival of each patient this previously entered data could be retrieved, leaving only height and weight to be entered. This minimised the time spent at the computer between patients, and ensured that the performance of the examination was not compromised by the data collection. The software was designed to reset the DAP meter automatically and take a reading from it when the end of the examination had been signalled by a keystroke. The examination details and any comments pertaining to it were then entered. Screening time, as recorded on the X-ray console, was entered manually *via* a user prompt, as screening times read from the DAP meter were found to be inaccurate for intermittent fluoroscopy. Calibration factors for the DAP meter were stored in a department specific data file and applied to the DAP readings. The total calibrated DAP value for each examination was displayed at the end of the procedure. All data recorded during an examination was appended in an ASCII format file, stored on the hard drive.

The data collection system has been in use for over three years in over twenty X-ray departments. Removable disks are sent to each department at three monthly intervals in order to transfer data to the central computer in the Medical Physics department. This procedure is normally carried out by a designated radiographer at each site. This central computer is used to store and analyse the data. Reports are produced for each department detailing the DAP values for the quarter according to examination type and radiologist, as agreed between Medical Physics and the local department.

3.3.3 Impact of automated system

The system was designed for routine use in a busy X-ray department by staff who were not necessarily familiar with the use of computers. After initial training and familiarisation, it was generally found to be straight-forward and easy to use. A designated member of staff at each site was given additional training to deal with any minor problems, update the list of radiologists as required, and download and return the data on receipt of the disk. The automated approach has financial implications in that a PC or laptop computer is required in addition to the DAP meter used for the dose measurements. The sum involved, however is small compared to the costs of installing a new X-ray facility. The automated system enables continuous collection of dosimetry data for all patients undergoing fluoroscopic examination in a room where it is installed.

3.4 Size correction

The importance of accounting for variations in patient size when analysing paediatric dose data has already been stressed in the earlier sections of this chapter. The objectives of any approach dealing with this issue are:

- to enable comparisons of data between centres
- to enable the determination and application of reference dose levels for paediatrics
- to enable an assessment of radiation risk to be made for any specific patient.

The first two of these points essentially relate to **removing** the size component from actual dose measurements to obtain 'typical' values, and the last point relates to **including** a size component in the extrapolation of 'typical' dose/risk factors to a particular patient, who may be of a different size. The ways in which size affects dose, and some of the work previously carried out in this area are discussed below. The derivation of a technique for routinely correcting data for patient size is then described, and an analysis carried out of its effect on sample dose data.

3.4.1 Affect of patient size on dose

The size of a patient affects the radiation dose received in a number of ways. The chief of these is the increase in technique factors required for a larger patient. In addition to this, a

greater proportion of beam energy will be absorbed than for a smaller patient and a larger field size may be required. Several authors have addressed the question of patient size (Maillie *et al*, 1981; Lindskoug, 1992; Martin *et al*, 1995; Wraith *et al*, 1996; Almen *et al*, 1995), including the problems in determining an individual patient's dose (Maillie *et al*, 1981) and the assessment of 'typical' data for a given set of patients (Lindskoug, 1992). Recommendations have been made that exposure-area product measurements be interpreted in terms of the beam quality used for the examination (Maillie *et al*, 1981). The issue of organ dose data for a continuous range of phantom sizes has also tackled in a number of ways. These include an algorithm for determining organ position according to age and sex for paediatrics, using growth curves (Francois *et al*, 1988), and the use of voxel phantoms for studying the variation of paediatric organ doses with patient diameter (Veit and Zankl, 1993). The latter work showed that organ doses increased with patient diameter, especially for organs on the beam entrance side of the patient, as might be expected. Organ dose data has recently become available for a defined range of paediatric sizes, examinations and beam qualities (Hart *et al*, 1996). This covers a much wider range of applications than previously available (Rosenstein *et al*, 1979), but no guidance is given on extrapolating between sizes.

Dose data in the form of DAP or ESD measurements have been plotted as functions of quantities such as age (Kyriou *et al*, 1996) and weight (Karlsson *et al*, 1994; Wraith *et al*, 1995) but the reported correlation is variable, with the correlation between DAP and age reported as mainly affected by use of a grid for the older patients (Kyriou *et al*, 1996). DAP is reported as being proportional to neonatal weight in one study (Wraith *et al*, 1995), but no correlation was observed in another study involving a wider range of ages (Karlsson *et al*, 1994).

To facilitate the comparison and checking of radiation dose estimates, the ICRP (1975) defined the concept of 'Reference Man' as a *well defined reference individual for estimation of radiation dose in health physics*. This concept was then adapted by Lindskoug (1992) in his work on dose data reduction. He introduced the parameter equivalent cylindrical diameter, which is derived from a person's height and weight, by assuming them to be a cylinder with the density of water (1 g cm^{-2}), as illustrated in Figure 3.1, and equating density to mass

divided by volume. Height and weight are measured in cm and g respectively to give the correct form of the equation.

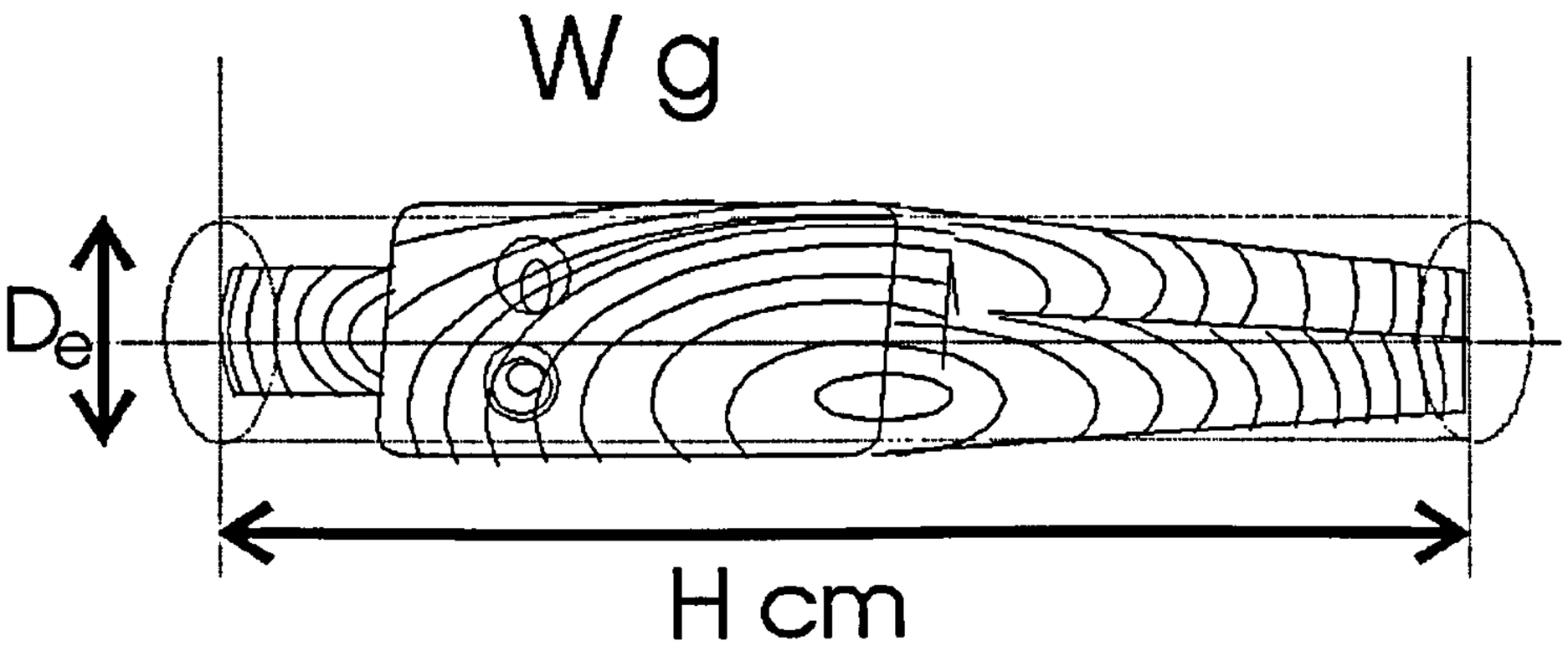

Figure 3.1 : Body Equivalent Cylinder

$$\textit{Equivalent diameter} \quad d_e = 2\sqrt{\frac{W}{\pi H}} \qquad (3.1)$$

This parameter *equivalent diameter* was used in preference to quantities such as weight or body thickness as the outer dimension of the trunk does not include any information about density and the weight takes no account of body shape. The formula described above takes some account of both body shape and composition. Additionally, for fluoroscopic examinations, multiple projections are normally used so that a single body thickness measurement would not be appropriate. The total energy imparted during an examination was shown to correlate well with equivalent cylindrical diameter of the patient (Lindskoug, 1991), and the equivalent diameter of Reference Man was used to standardize the data using a simple coordinate transform. Lindskoug also showed that the energy imparted to children during trunk examinations increased logarithmically with equivalent diameter, in a similar manner to that for adults. He used this to derive appropriate exposure parameters for paediatric examinations, according to the height and weight of the patients. Martin *et al* (1994) have also investigated the relationship between dosimetric quantities and equivalent cylindrical diameter for children, and showed good correlation of entrance dose with this parameter for simple radiographic examinations. For complex examinations, energy imparted showed some correlation with equivalent cylindrical diameter for barium meal examinations,

but not for cystogram examinations. This was explained by the large amount of scatter in dose-area product due to differences in individual examinations, and also a general decrease in screening time with age for the latter examination which compensated for increasing size. For the radiographic exposures, simple exponential correction factors were derived from retrospective analysis of the data to enable comparisons to be made between children of different ages.

3.4.2 Isolation of size dependence

The work described above illustrates the usefulness of the concept of equivalent cylindrical diameter, and its potential for enabling comparison between dose data for individual patients, including children. The methods previously used, however, require retrospective analysis of an existing data set, and isolation of the size dependence is difficult due to the many other criteria affecting variation in dose, such as complexity of the examination and the technique used. An independent method of determining dose variation due to patient size would be more generally applicable.

Separation of the size dependent component of dose variability may be made by considering how dose at the exit side of a phantom may be expressed as a function of the dose at the entrance side. Both point dose and DAP will be considered as the dose quantity of interest. A pictorial representation is given in Figure 3.2, where d is the soft tissue thickness and FSD the focus skin distance. D and D' represent the dose quantity of interest.

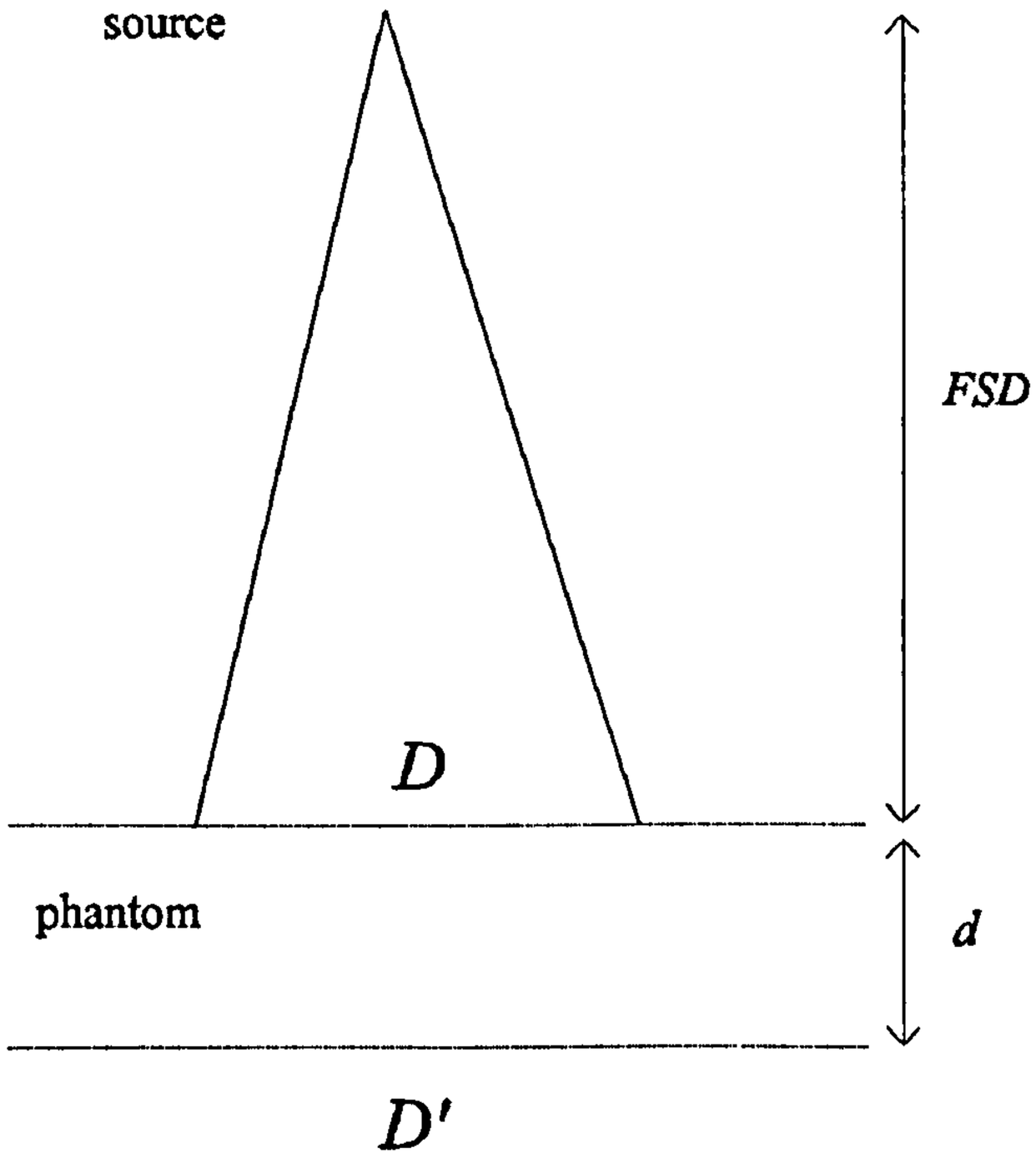

Figure 3.2 : Parameters used in derivation of equations

The attenuation through the phantom may most simply be expressed by

$$D' = D\, e^{-\mu_{eff} d} \qquad (3.2)$$

where μ_{eff} is the effective attenuation coefficient for the phantom. This would then give

$$\ln D = \mu_{eff} d + \ln D' \qquad (3.3)$$

ie a simple exponential relationship between dose and size, which is an intuitive approximation, and has been validated and used in previous work (Martin *et al*, 1994). However, equation **3.2** neglects several effects, which should be mentioned. These may be summarized as follows:

- When applying equation **3.2** to point doses, a term should be included to allow for the reduction in D' due to the inverse square law effect. This would give

$$D' = D\, e^{-\mu_{eff} d}\, \frac{FSD^2}{(FSD + d)^2} \qquad (3.4)$$

and

$$\ln D = \mu_{eff} d + 2 \ln \left(\frac{FSD + d}{FSD}\right) + \ln D' \quad (3.5)$$

This additional factor is automatically included when using DAP as the dose quantity of interest, as the change in area includes the inverse square effect.

- Equation **3.2** only strictly applies to narrow beam conditions *ie* when the effect of scatter is neglected. An additional factor B is required in the expression to account for the increase in D' arising from photons scattered inside the phantom. B is a complex variable and will depend on the beam energy, beam area, phantom thickness d and the distance between phantom and image receptor. Inclusion of this factor in the expression for variation of DAP would give

$$\ln DAP = \mu_{eff} d + \ln D' - \ln B \quad (3.6)$$

- The above analysis assumes that examinations are carried out under conditions of equal dose at the exit of the phantom whereas, in fact, the correct criteria would be equal film density or intensifier light output. Each of these will depend on the energy absorption in the image receptor which will vary to some extent with the energy of the beam entering it. This in turn will depend on the original beam quality and the phantom thickness.

An exact evaluation of the interdependence of these parameters is beyond the scope of this work, but it should be noted that as the phantom thickness increases the generating potential will also be increased, leading to a decrease in μ_{eff}, and an increase in B.

As a first approximation, the simple exponential form of the equation can be applied to DAP measurements on patients to give

$$\ln DAP = kd_e + c \quad (3.7)$$

where d_e is the effective equivalent diameter, k a scaling factor and c is a size independant term. From this one may derive that the dose-area product equivalent to a standard sized patient is given by

$$DAP_{ref} = DAP_{meas} \times \frac{e^{kd_{e(ref)}}}{e^{kd_{e(meas)}}} \qquad (3.8)$$

where *meas* refers to measured values and *ref* those for a standard sized patient. From this, one may define a size correction factor

$$F = e^{k(d_{e(ref)} - d_{e(meas)})} \qquad (3.9)$$

$d_{e(ref)}$ is the equivalent diameter of the reference size patient to which data is being corrected, and $d_{e(meas)}$ is the equivalent diameter of the patient.

3.4.3 Experimental determination of equation parameters

The factor k, which is equivalent to the effective attenuation coefficient through the phantom, can be determined experimentally. This was done by carrying out fluoroscopic exposures of different thicknesses of tissue equivalent phantom material (RMI, Wisconsin, USA) under automatic exposure control. Dose-area product values, normalised to 1 minute screening time, were recorded for each thickness. The field size was kept constant so that the observed changes in DAP were due solely to the changes in exposure factors, as determined by the automatic exposure control (AEC) device required for imaging different phantom thicknesses. A plot of ln DAP against phantom thickness yielded a straight line graph, the gradient of which was the factor k. Figure 3.3 shows such plots for a number of X-ray sets around the region. Values of k ranged from 0.13 to 0.18 cm^{-1} (median 0.14 cm^{-1}) for the different rooms in which measurements were made, all with correlation coefficients greater than 0.997. For the purposes of the regionwide survey, a single value of 0.14 was selected for ease of calculations. Individually determined values of k could be used for each X-ray set for greater accuracy.

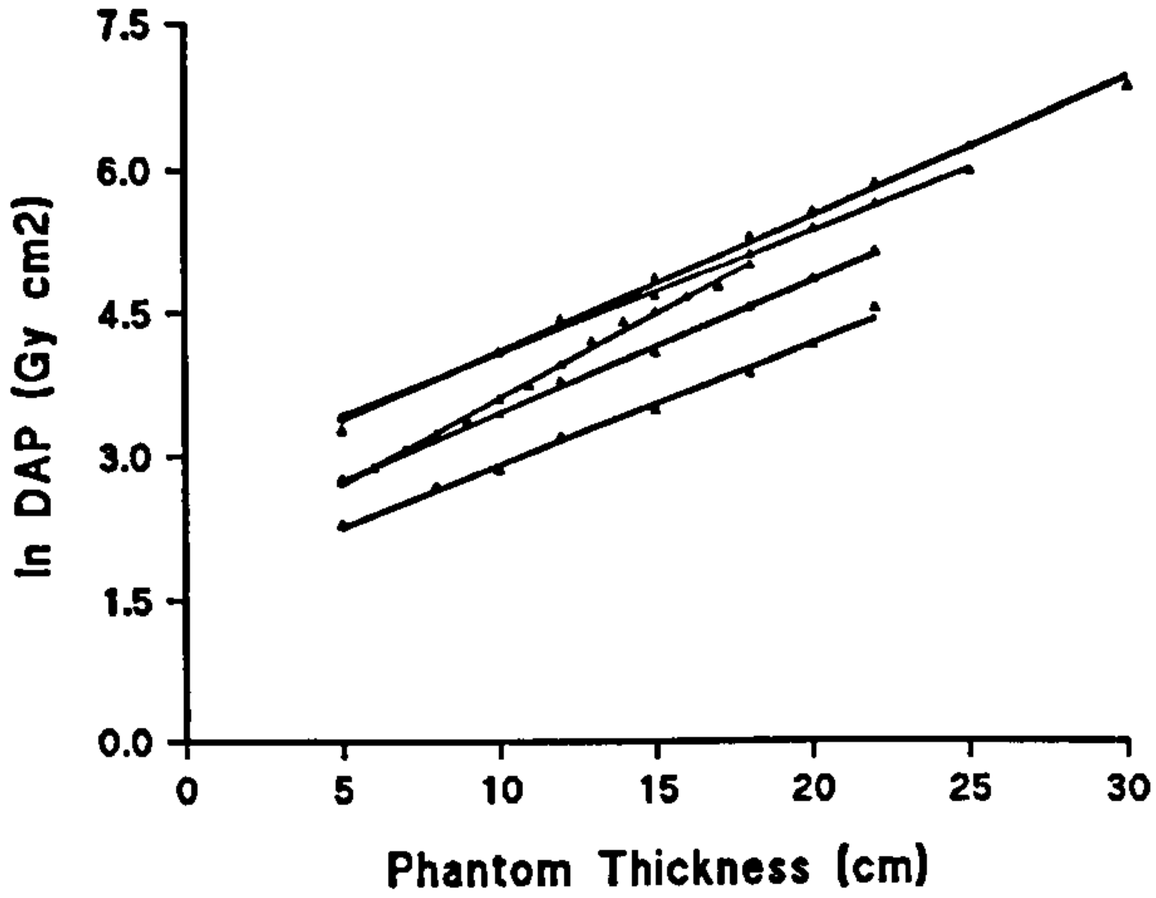

Figure 3.3 : Determination of k for five different x-ray sets

Several points should be made about the form of this graph. Firstly, the curves all exhibit excellent linear regression fits to the data. Although this conforms well to the simplified theory, it is not the behaviour expected as the AEC devices increase tube voltage with increasing phantom thickness, and this should reduce the effective attenuation coefficient and hence the slope of the graph. This would result in a flattening of the curves as phantom thickness increases. Although the magnitude of the effect may be small, and partially compensated for by the other effects described, it is suprising that such linearity is obtained.

The similarity of the slopes of the curves indicates that the effective attenuation coefficient over the range of thicknesses used is fairly invariant between the sets investigated. This might be expected if similar kV values are selected by the AEC devices, as tube filtration does not vary much between the rooms. The shift between the curves relative to the y-axis of the graphs is related to the different AEC settings for the brightness required (different values of D' in equation **3.2**).

It can be seen from this analysis that the scaling factor is essentially a property of the AEC device on the set, which determines the kV and mA combination used, along with the tube filtration. When exposures are being performed under manual control the analysis will still be valid, if it is assumed that the radiographer selects technique factors in a similar manner

to the AEC. If the factors selected are very different (for instance the same factors for both a 6 year old and a twelve year old) the effect of the patient size will deviate from that deduced above.

3.4.4 Application to paediatric dosimetry data

This method of size correction may easily be applied to paediatric dose data, by using age bands for grouping the data. A standard height and weight is defined for each age band, as given in Table 3.2. These data are taken from that used for the CRISTY anthropomorphic paediatric phantoms (Cristy, 1980). The resultant equivalent diameter, in each case, is used in equation **3.9** for correcting the dose-area products of all children in that age band. The Cristy model is widely accepted and has been used in many applications (Hart *et al*, 1996). The heights and weights given in Table 3.2 agree closely with those found from child growth charts based on United Kingdom cross-sectional reference data (Cole, 1994, Freeman *et al*, 1995, Chinn *et al*, 1996). This latter data is given in Table 3.3 in the form of centiles. The centile values also give an idea of the spread in height/weight data for the different age-groups, and are further evidence for the inappropriateness of using age bands for grouping data. Any change to the reference size being used may be made by a simple substitution of $d_{e(ref)}$ in equation **3.9**.

Age Band	Reference Age	Reference Height (cm)	Reference Weight (kg)	Equivalent Diameter (cm)
neonate	0	51.5	3.51	9.32
infant	1	75.0	9.36	12.61
1-5 yrs	5	109.0	19.1	14.94
6-10 yrs	10	138.6	32.1	17.17
11-16 yrs	16	164.0	54.5	20.57

Table 3.2 Reference Paediatric Sizes

Age	height (cm)			weight (kg)		
	2nd centile	50th centile	98th centile	2nd centile	50th centile	98th centile
birth	46.5	50.5	54.5	2.6	3.3	4.3
1 yr	69.2	75.0	80.5	7.9	9.9	12.1
5 yrs	101.0	109.3	118.0	14.7	18.5	24.1
10 yrs	126.0	138.5	151.5	23.3	33.0	48.0
16 yrs	154.0	168.8	181.8	43.3	60.0	82.8

Table 3.3 : Height/weight data from local child growth charts

The correction factors derived in this way account for the effect of patient size on the exposure factors required for the examination, but make no allowance for changes in field-size, which will also affect DAP. However the size of internal organs, which govern the required field size, are not as variable as the outer dimensions and composition of the trunk. The relationship between organ size and d_e will be complex and depend on age, the organ concerned and, in some circumstances, any existing pathology. Although there will be significant differences in field size between examinations of an infant and an adolescent, within an age band field-size variations will be a relatively minor effect.

3.4.5 Analysis of the effect of size correction on data

To assess the use of the size correction factors that have been developed, the technique was applied to DAP data from paediatric cystograms that were monitored as part of the dose survey described earlier, to study its effect on the dispersion of the data. The unavoidable problem in this approach is that for real data the variation arising from different patient sizes may be masked by the other sources of variation in the data. One of these other sources of variation was removed to some extent by dividing the DAP values by screening time. The effect of the manipulation of the data is shown in Figures 3.4 and 3.5. These show the spread of dose-area product data, normalised to unit screening time, for cystogram examinations for two age bands both with and without size correction. Data for which height and weight information is unavailable, or obviously entered incorrectly, has been omitted from the analysis.

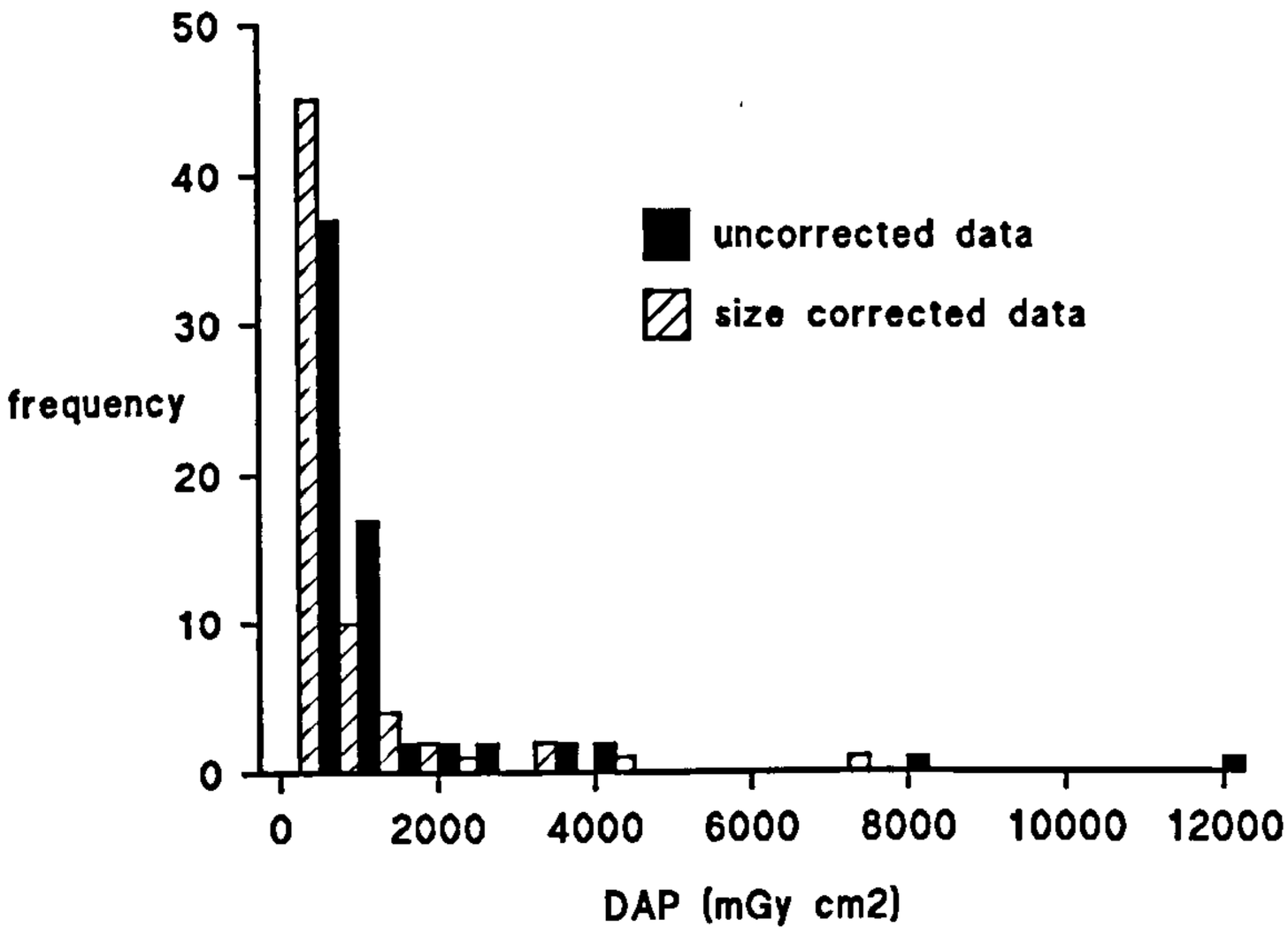

Figure 3.4 : DAP data, normalised to unit screening time, for cystograms (neonates)

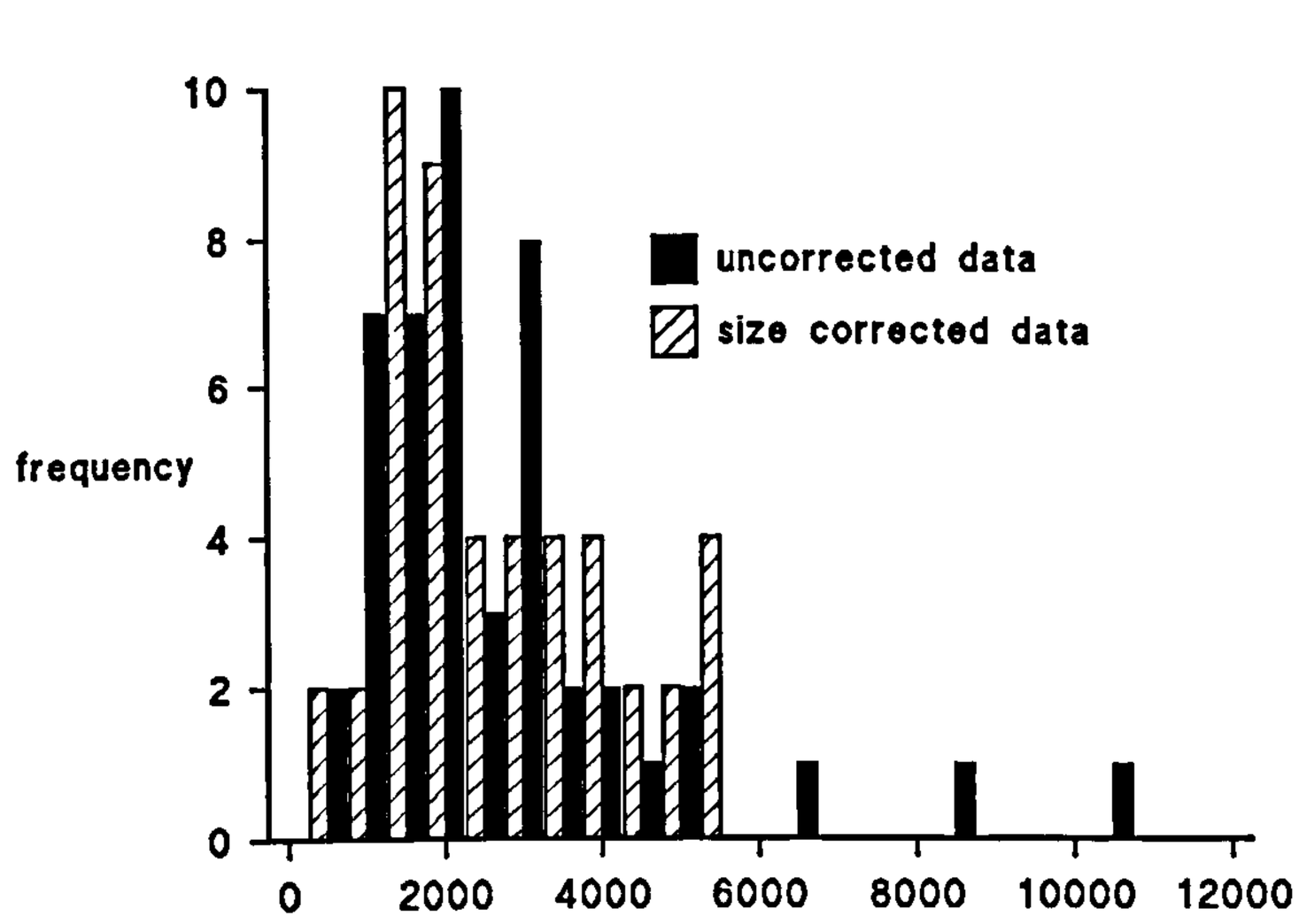

Figure 3.5 : DAP data, normalised to unit screening time, for cystograms (11-16 yrs)

The dispersion of the data is characterised in Tables 3.4 and 3.5. The former gives standard deviation as a percentage of the mean DAP value and the latter gives the interquartile range, defined as the difference between the upper and lower quartile values of the data.

Age Band	Stand. Dev. of DAP normalized to Unit Screening Time		No in sample
	Uncorrected Data	Size Corrected Data	
neonates	184%	167%	66
infants	173%	155%	252
1-5 years	89%	89%	266
6-10 years	66%	63%	173
11-16 years	81%	57%	47

Table 3.4 Effect of size correction on DAP distribution (standard deviation)

Age Band	Interquartile range of DAP normalized to Unit Screening Time		No in sample
	Uncorrected Data	Size Corrected Data	
neonates	665 mGy cm^2	506 mGy cm^2	66
infants	513 "	492 "	252
1-5 years	755 "	734 "	266
6-10 years	835 "	893 "	173
11-16 years	1816 "	2296 "	47

Table 3.5: Effect of size correction on DAP distribution (interquartile range)

Standard deviation is a quantity that is most usefully used to describe a normal data distribution, whereas patient dose data typically forms a positively skewed distribution with a long, high dose, tail. It may, however, be defined numerically for any distribution and gives an efficient measure of dispersion of the data, as all data points are used. It is particularly useful in this context as the comparison is between the same data set before and after a numerical transformation, rather than between two different data sets. The interquartile range is not affected by outliers to the distribution, but gives the range of variability which is sufficient to contain fifty percent of the population.

Tables 3.4 and 3.5 show that for the 11-16 year age group the standard deviation of the data is considerably reduced by application of size correction factors, though the interquartile range increases. This is a relatively small data set compared to the other groups (47 patients) with probably the greatest range of patient sizes. The extreme normalised DAP values are mostly due to patients at each end of the size range, and these are taken closer to the centre of the distribution during the size correction analysis. Variations throughout the mid-range of DAP values will be influenced by technique differences as well as size. For the neonate age group the reduction in interquartile range is more marked, with a smaller decrease in standard deviation. Size variations within this group are smaller and less likely to be the cause of extremes of DAP value. The middle age-groups demonstrate small reductions in standard deviation after size correction and, apart from the 6-10 year group decrease in interquartile range also. The older age group may have greater variability in clinical indication. Overall, the technique can be seen to reduce variability in paediatric DAP data, even for these samples which contain data from a number of different hospitals with modification made only for screening time.

For interest, it is possible to correct data for the different reference ages to that for a reference adult size (equivalent diameter 22.8 cm). The results of this are shown in Table 3.6 for barium meal and enema studies where for each age group the mean size corrected DAP, as found in the study, is listed along with the same value corrected to reference adult size. The mean adult doses for these examinations, for the same region are 9 and 21 Gy cm^2 respectively. It can be seen that even with corrections made for patient size there are still differences in DAP between the different age groups. The effect of variations in field-size with age should produce a small increase of DAP with age, but other factors such as patient compliance will also affect the results, and may be related to patient age. Compliance, for example, is generally at its worse for the 1-5 year group, as the children are not small enough to be easily held and not old enough to cooperate. The clinical reasons for performing an examination and the type of diagnosis required may also vary for different age-groups, and influence the dose given. All this is evidence that size correction should not be applied over broader age groupings than those used currently. It also supports the view that children are not just 'small adults' and cannot be treated as such for dosimetry purposes.

Age Band	DAP for Barium Meal (Gycm^2)		DAP for Barium Enema (Gycm^2)	
	ref. child size	ref. adult size	ref. child size	ref. adult size
neonates	1.2	8.7	1.2	8.9
infants	1.0	4.4	4.6	20.1
1-5 years	1.4	4.7	4.5	14.6
6-10 years	2.5	5.9	8.3	19.5
11-16 years	4.9	6.8	10.8	15.0

Table 3.6 : Paediatric DAP data with conversion to reference adult size

3.5 Survey results

The automated dose survey has been carried out for 3 years in hospitals around the north of England. The data collected has been subdivided into agebands and the size correction factors described above applied. A total of 3859 paediatric measurements had been collected at the time of analysis. Large variations were observed between hospitals, as shown by Figure 3.6.

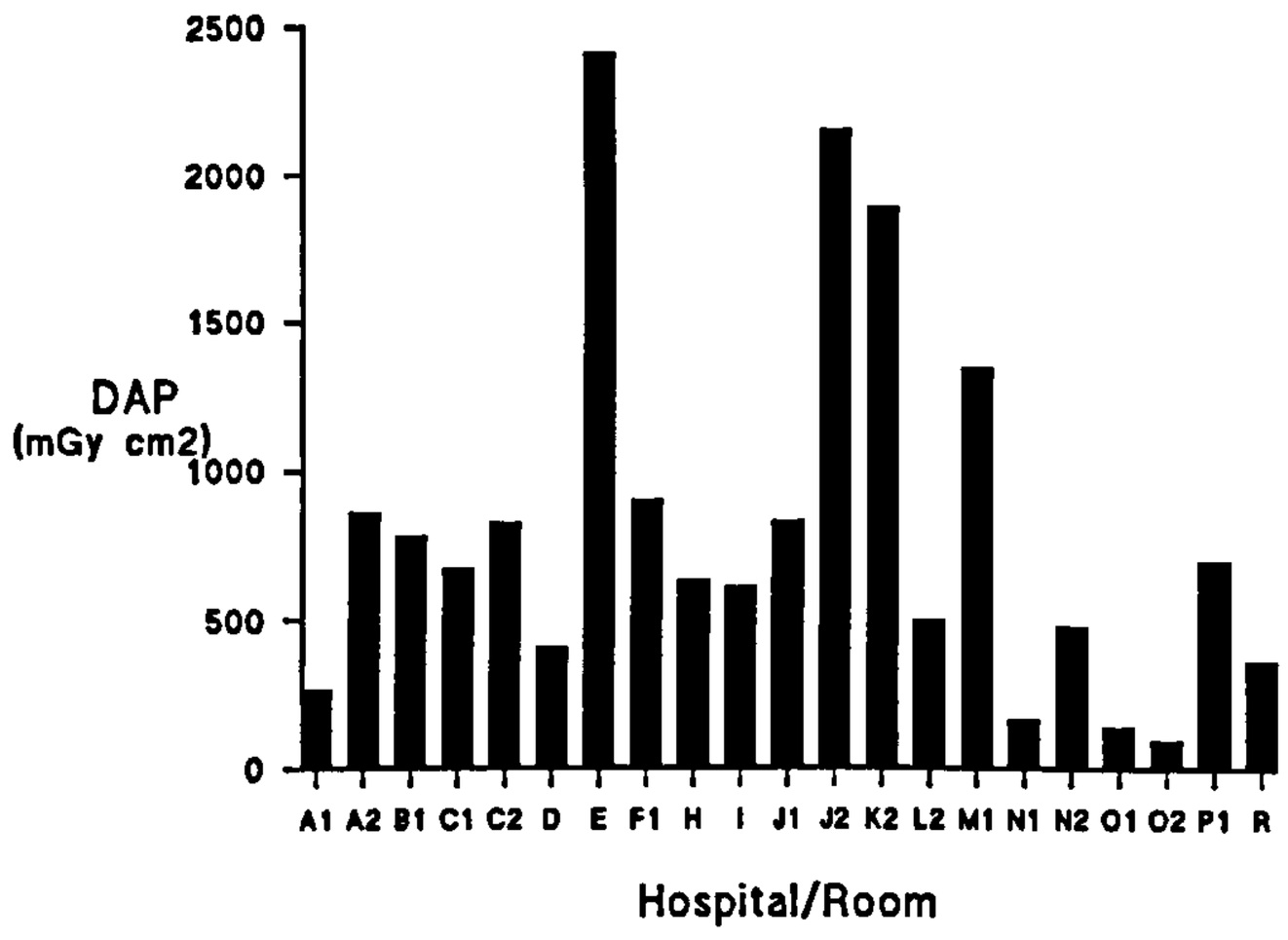

Figure 3.6 : Dose variation between hospitals for infant cystograms

Mean size-corrected doses across the region for the different examinations are given in Tables 3.7 - 3.11. Each hospital is represented by a letter, with different numbers for each room in

that hospital. One of the main factors influencing dose is the type of equipment in each room. The majority of rooms have digital X-ray sets but rooms A2, E, G, J2, K2 and M1 have older non-digital equipment and it is apparent that these give consistently higher doses, throughout the range of ages and examination types. The other factors having a major impact on dose are the screening time and the number of radiographs taken. Common practice at most hospitals is to take a minimal number of radiographs, if any. Room O1 has fairly consistently low doses. This room uses dedicated paediatric techniques, with low radiation dosage an active priority. Full details of the technique factors and other data collected during the survey are given in Appendix A.

For the neonatal examinations (Table 3.7), many of the higher doses are mirrored by higher screening times, in particular for the cystograms in M1 and A2, barium swallows in M1, F1 and K2 and the barium enema in F1. The high dose for barium meals in room G is probably related to the 13 radiographs taken. The majority of rooms use only a single radiograph or none at all.

For infants (Table 3.8), the extremely low barium swallow dose at Q1 corresponds to a minimal screening time (6 s). This may, in fact have been an incomplete examination. The high dose at K1 for the same examination is also markedly due to the screening time.

In the 1-5 year old data (Table 3.9), the highest screening times for cystograms are found at A2, F1, H, K2 and M1. These are also the rooms with the highest doses. A long screening time is also found for barium swallows at K1. The extremely high barium meal dose at room G is due to a combination of 8 radiographs, 10 spot films and a long screening time. Similarly, the high enema doses at A2 and Q1 involved 4 and 2 radiographs respectively. The low dose at N2 for barium meal and swallow corresponds to a short screening time.

For the 6-10 year old children (Table 3.10), room A2 gives by far the highest cystogram dose, with a long screening time. The high dose enema examinations are all from rooms utilising multiple radiographs. Screening time appears to be the main contributor to the barium meal and swallow dose in A2.

For the highest age group (Table 3.11), high doses are again linked to either screening time (cystograms in A2 and M1, barium swallows in H and K1, barium follow through in K2) or number of radiographs (10 for A2 enemas, 8 for G enemas, and 5 for L2 enemas).

It should be noted that much of the data presented, in all age groups consists of only a single examination for a given room. Such data cannot be assumed to be representative of routine practice. However, some trends may be indicated, as illustrated above and results from different rooms combined to give local reference dose levels for the different examinations. Third quartile values of dose area product have been produced in this way and are given in Table 3.12 for the three most common examinations. Routine dosimetry results are reported back to both radiologists and radiographic staff at each department to enable further investigation of doses or potential changes in technique where appropriate. Potential for dose reduction is indicated where results are consistently high. This may be achieved in some cases by purchase of new equipment but also by review of technique, in particular in relation to the use of radiographic films for diagnosis.

3.5 Summary of chapter

A review has been given of data published in the field of paediatric dosimetry, with particular respect to the dosimetric techniques employed, the grouping of the data and the sample sizes. The amount of data available is small compared to that for the adult population, particularly for fluoroscopic examinations, and there are problems in comparing data and deriving reference dose levels due to the large variability in patient size. Two techniques for improving the collection of paediatric dose data have been presented: the automation of survey techniques and a method of correcting for patient size. These techniques have been applied to a region wide survey of paediatric doses, and the results of the survey have been described.

Hospital ID	Mean Size Corrected Dose Area Product (mGy cm^2) and (Number in Sample)					
	Cystogram	Ba Swal.	Ba Meal	Ba Enema	Ba Fol.Thr.	Ba Meal&Swal
A2	1164 (9)		1995 (1)			
B1	530 (2)	478 (5)	4474 (5)		1469 (1)	
C1	928 (3)	437 (5)	800 (1)			526 (3)
C2	341 (2)	1070 (5)				1198 (3)
D	144 (1)	188 (2)	491 (3)			
E	1042 (2)	702 (1)	850 (1)			
F1		723 (1)	927 (5)	8116 (1)	1015 (3)	292 (1)
G			10011(1)			
H		649 (4)	189 (1)			667 (2)
I	251 (23)	1251 (1)	655 (9)			
J1	118 (2)		3149 (1)			
K1		583 (1)				
K2	1272 (2)	1226(13)	3490 (1)		1225 (1)	761 (4)
L2	430 (86)	589 (11)	1095(29)	1787 (1)		491 (23)
M1	1573 (17)	2094 (5)	2136(16)	893 (1)		1551 (1)
N1			205 (2)	123 (2)		
N2	40 (1)	317 (3)	253 (7)			
O1	72 (14)	133 (1)	234(16)	96 (2)		
O2	60 (18)	76 (1)	125(10)			
P1	485 (9)	432 (2)	798 (1)		636 (1)	
R	334 (3)	219 (2)	297 (3)			

Table 3.7 : Dose area product data for neonates

Hospital ID	Mean Size Corrected Dose Area Product (mGy cm^2) and (No in sample)				
	Cystogram	Ba Swal.	Ba Meal	Ba Enema	Ba Meal&Swal
A1	254 (6)				464 (1)
A2	815 (11)		223 (1)		2699 (1)
B1	746 (12)	1113(16)	1360 (11)		750 (2)
C1	661 (8)	763 (6)	1740 (5)		613 (2)
C2	785 (9)	1705(11)	819 (2)		1027(5)
D	388 (3)	957(11)	466 (4)	874 (1)	427 (1)
E	2416 (1)		2088 (1)	4342 (1)	
F1	852 (15)	496 (3)	708 (9)	2275 (2)	719 (3)
H	622 (4)	2296(15)	1184 (3)	4793 (1)	
I	583 (67)	1284 (6)	1438 (26)	14937 (7)	1494 (4)
J1	787 (9)	798 (2)	955 (1)		661 (1)
J2	2041 (4)		296 (1)		
K1		59245(2)	1488 (3)		1495 (8)
K2	1841 (3)	1792 (14)			
L2	526 (203)	918 (20)	878 (81)	1156 (14)	682 (43)
M1	1260 (5)	3479 (11)	2142 (12)	3197 (3)	1710 (4)
N1	165 (4)			561 (1)	
N2	472 (12)	500 (12)	845 (3)		
O1	133 (57)	168 (7)	371 (16)	171 (2)	268 (3)
O2	92 (58)	193 (1)	184 (12)		
P1	667 (52)	856(30)	1297 (1)		
Q1		18 (1)	1415 (1)		
Q2		240 (1)			
R	356 (12)		511 (4)		196 (1)
S				5029 (1)	

Table 3.8 : Dose area product data for infants

Hospital ID	Mean Size Corrected Dose Area Product (mGy cm^2) and (No in Sample)					
	Cystogram	Ba Swal.	Ba Meal	Ba Enema	Ba Fol.Thr.	Ba Meal&Swal
A1	142 (1)					
A2	3452 (2)	1867 (1)	1678 (4)	24456 (1)		
B1	943 (20)	1357 (3)	1116 (7)			2749 (1)
B2				6877 (1)		
C1	1543 (4)	118 (1)	1256 (3)	3235 (1)		2565 (1)
C2	962 (7)	2107 (5)		3500 (3)	2133 (1)	2896 (3)
D	1013 (8)	500 (1)	760 (2)			
E			1632 (2)	5880 (2)		
F1	1770 (18)	570 (4)	1040 (5)	1611 (3)	1440 (1)	
F2				371 (1)		
G			36867(1)			
H	1521 (5)	4838 (4)	1863 (3)	1427 (1)	804 (1)	3267 (4)
I	1177 (50)	3175 (3)	2132(17)	4178 (6)	1310(22)	2401 (3)
J1	1718 (6)	698 (1)		6409 (1)		1056 (1)
J2	1145 (1)					1158 (1)
K1		4893 (1)				
K2	1671 (19)	1367 (7)	4112 (1)			2024 (2)
L2	1138(204)	1733(32)	1560(64)	2707 (12)	510 (2)	1351 (49)
M1	3723 (10)	4814 (4)	2447 (5)	3151 (3)		
N1	536 (7)				217 (1)	
N2	411 (21)	283 (7)	537 (8)	8013 (3)	3261 (1)	215 (1)
O1	310 (34)	359 (1)	607 (25)	203 (1)	215 (3)	2146 (3)
O2	216 (27)	458 (5)	310 (26)			
P1	1148 (38)	1162(11)	2047 (6)	3056 (1)	2449(13)	1382 (4)
Q1				21233 (1)		
R	555 (11)		1015(5)			
S		294 (1)				

Table 3.9 : Dose Area Product data for 1-5 yr olds

Hospital ID	Mean Size Corrected Dose Area Product and (No in Sample)					
	Cystogram	Ba Swal.	Ba Meal	Ba Enema	Ba Fol.Thr.	Ba Meal&Swal
A2	14492 (1)		5465 (1)			9266 (1)
B1	1653 (3)	2519 (2)	2105 (4)			
C1	3304 (1)	1706 (2)	5617 (1)	5767 (2)	1199 (1)	
C2	3172 (3)	4434 (5)		3193 (2)	3318 (4)	3242 (9)
D	1469 (3)	1377 (2)				
E			7604 (2)			
F1	3122 (13)	789 (1)	1402 (1)	12397(2)	1271 (1)	
G				25531(4)		
H	998 (4)	2310 (2)	2961 (3)		2734 (1)	2974 (3)
I	1859 (32)	2016 (2)	3059(16)	3779 (1)	3168(13)	4164 (4)
J1	1483 (1)	1472 (1)		1358 (1)		
J2	986 (1)					
K2	1844 (9)	2501 (3)	9236 (1)	3388 (1)		3231 (3)
L2	1758(103)	1389(14)	2413(31)	6088 (7)	667 (2)	2180 (14)
M1	2885 (6)	10773(3)	5760 (1)	14734(2)		5152 (1)
N1	5368 (6)	1625 (1)				
N2	1026 (13)	4240 (7)	1423(13)		434 (1)	
O1	516 (15)		1439(13)	1559 (5)	1168 (4)	
O2	378 (16)		592 (6)			
P1	2351 (15)	1601 (8)	4953 (7)	5031 (3)	1528(11)	4633 (1)
Q1		733 (1)	3130 (1)			
R	604 (7)		722 (7)			1393 (1)
S					3157 (1)	
U			5220 (1)			

Table 3.10 : Dose area product data for 6-10 yr olds

Hospital ID	Examination Type					
	Cystogram	Ba Swal.	Ba Meal	Ba Enema	Ba Fol.Thr.	Ba Meal&Swal
A1					149 (1)	2146 (1)
A2	20487 (2)		2419 (1)	16070(1)	1145 (1)	
B1	841 (1)	2883 (2)				2215 (1)
B2						
C1	599 (1)	2395 (1)	3786 (2)			2045 (1)
C2	4234 (1)	6381 (2)	8542 (3)		3273(11)	
D		4725 (1)	5204 (3)			2294 (1)
E			12584(1)			
F1	3272 (3)		1937 (2)	7560(5)	2163 (2)	
G		1568 (1)		12956(2)		
H		6406 (6)	4554 (2)			8917 (2)
I	3476 (12)	2772 (4)	7137(14)	8446(4)	3625(21)	5871 (2)
J1					8286 (1)	
K1		6212 (3)	5078 (1)			
K2	8619 (1)	6506 (3)	12314(1)		20043(1)	24126 (2)
L1	1655 (1)					
L2	4253 (46)	3548(12)	5167(36)	15828(7)	6979 (3)	3980 (16)
M1	10332 (1)	3977 (2)	10644(1)	22289(1)	3230 (1)	6626 (3)
N1			3911 (2)			
N2	243 (1)	759 (5)	2930(11)	6252(2)	3778 (2)	1806 (2)
O1	1640 (1)	1031 (2)	1508 (4)	1574(3)	5053 (4)	359 (3)
O2	5071 (7)	1088 (7)	1467 (4)	1235(1)	1457 (4)	
P1	5071 (7)	5418 (7)	4750 (5)	16174(3)	4455 (4)	6198 (1)
Q1		4943 (3)	6823 (4)			
R	2246 (4)	1716 (1)	1701 (7)			2081 (1)
S		3480 (1)			4623 (3)	

Table 3.11 : Dose area product data for 11-16 yr olds

Age Band	Dose Area Product (mGy cm^2)		
	Cystogram	Barium Meal	Barium Swallow
neonates	431.2	1082.1	1190.6
infants	672.6	1561.3	1713.7
1-5 years	1373.2	2073.5	2448.6
6-10 years	2043.8	3290.0	-
11-16 years	4826.7	5819.9	-

Table 3.12 : Third quartile dose area product values for frequent examinations

Chapter 4

Optimisation of Dose and Image Quality

4.1 Introduction

One of the fundamental problems in diagnostic radiology is the conflicting requirements for good image quality and low patient dose. Optimisation, in this respect, is the process of balancing the different technique factors for a given examination in order to achieve maximum patient benefit *ie* a successful diagnosis with minimal radiation dose. The principles governing this process and the techniques used are reviewed here. The specific use of beam filtration as an optimisation technique is discussed in depth, followed by a description of the optimisation strategy to be used in this work.

4.2 Principles and techniques of optimisation

To achieve good image quality, the photon energies in the X-ray beam must be such as to maximise the differential absorption between the various body tissues that are being examined - usually bone and soft tissue, or soft tissue and an artificially introduced contrast medium such as barium or iodine. This differential absorption generally decreases with increasing photon energy and thus a lower generating tube voltage (kV) is beneficial to contrast, and hence image quality. However, to minimise the radiation dose to the patient requires a reduction in the number of photons absorbed. As low energy photons are preferentially absorbed, this is achieved by increasing the mean photon energy of the X-ray spectrum by increasing the tube potential. This results in a favouring of high tube potential on the grounds of dose. The product of tube current and exposure time (mAs) must be selected in order to achieve an acceptable film density and dose increases with mAs.

An X-ray beam contains a spectrum of energies from zero up to the generating tube potential. The relative proportions of photons of different energies is often referred to as the 'shape' of the X-ray beam, and this will depend on the tube potential used and the X-ray

absorption characteristics of any media through which the beam has passed. The use of a beam filter, usually aluminium (Al), removes the lowest energy photons from the beam, which are absorbed in the patient and contribute to dose but little to image formation. The current regulatory requirement for diagnostic X-ray sets is for a minimum total filtration equivalent to 2.5 mm Al - including both the inherent filtration of the tube housing and light beam diaphragm and any additional filtration. The European guidelines on quality criteria for diagnostic radiographic images in paediatrics (Kohn *et al*, 1996) recommend additional filtration of up to 1mm Al plus 0.1-0.2 mm Cu, in addition to inherent filtration of 2.0 mm Al, although no scientific evidence is referenced to support this recommendation.

In practice, the selection of all the relevant technique parameters is usually carried out according to individual department protocol, with reference to prescribed guidelines such as those documented by the European Commission for both adults and children (EUR 16260 and EUR 16261, 1996). The problems in selecting technique factors are compounded when radiographing children, due to the wide variations in size, and also the need to minimise exposure time to limit the, often inevitable, patient movement. For paediatrics, the type of radiographic equipment used plays a crucial role in the optimisation process. Some generators are not capable of producing the short exposure times needed, and an undesirable drop in generating tube potential may be required to prevent overexposure of the film. Ideally all paediatric radiography would be carried out on powerful machines producing a radiation waveform that is almost rectangular, with minimal ripple. This is because, for short paediatric exposures, any pre and post peak voltage times are likely to be a significant proportion of the total exposure time, and thus have a noticeable effect on the mean beam energy for the exposure. Automatic exposure control devices, unless specifically designed for paediatric use, are often inappropriate for X-raying children due to their inability to compensate for varying body sizes and proportions. This is due to the large size and fixed position of the ionisation chambers used in the devices. Ideally, a small mobile detector is required, that can be positioned with regard to the area of interest. Unfortunately, financial constraints result in many X-ray departments being unable to use dedicated paediatric equipment, or upgrade equipment to the recommended specification.

A full discussion of the different principles associated with good imaging performance is given in the European guidelines on quality criteria for diagnostic radiographic images in paediatrics (EUR 16261). This document aims to produce a list of quality criteria that characterise the level of acceptability of normal basic radiographs which could address any clinical indication. The influence of patient age, and functional differences between adults and children - such as heart rate, ability to control inspiration *etc* - are recognised. The general principles, such as use of low attenuation materials in table-tops and cassettes and the importance of accurate positioning, beam limitation and shielding, are outlined clearly and apply to all paediatric radiography. Examples of good radiographic technique are then given for different radiographic examinations, along with diagnostic requirements for image criteria and patient dose criteria. Although comprehensive, the recommended techniques are stated to have 'evolved from the results of European trials' rather than having any firm scientific basis. The image criteria specify important anatomical structures that should be visible on a radiograph to aid accurate diagnosis and three degrees of visibility are defined and used. Although some of the criteria specified reflect the performance of the imaging system and the technique factors employed, others reflect the positioning and compliance of the patient. The latter group are not descriptive of image quality in the usual sense of the word, and would be better considered separately. The selection of image criteria for a given examination are those deemed necessary to produce an image of standard quality, and are intended to ensure that pathological details are not missed. Although it is stated that lower levels of image quality may be acceptible for certain clinical indications, this is not discussed at length and this is a definite weakness in the document. Discussion with a small number of paediatric radiographers revealed that the quality criteria were felt to be rather too general for their use to be readily applicable. The criteria used for radiation dose to the patient is the reference entrance surface dose for the examination. These values are derived from results of a European trial, but values given are for a five year old patient only, which limits their usefulness. It should also be noted that the dosimetric results are based on only a single measurement for each examination category at each hospital involved in the trial, and for several examination types no data is presented at all. The dose criteria are thus virtually unusable for most applications.

The optimisation of image quality and patient exposure in paediatric diagnostic imaging has also been discussed by Fendel *et al* (1989). This paper defines radiological effective quality as a function of the product of effective (*ie* that needed and not more than that needed) information and the reciprocal of patient dose. This parameter thus increases with increasing information content and with decreasing dose, both of which are desirable features. The results of a survey at 35 institutions are presented, comparing dose and image quality coefficient - defined in terms of optical density, resolution and low image contrast - for different paediatric examinations. Results are analysed in terms of technique factors and equipment used. Although use of such a coefficient simplifies comparisons between centres and procedures, the image quality parameters used take no consideration of the level of image quality required for an examination and thus do not represent the 'effective information' described earlier. There is no justification for combining the different parameters in any specific format to give an 'optimised' result, and presentation of data in such a way may not accurately reflect the true situation.

A number of optimised techniques have been proposed for specific examinations, where the degree of image quality required can be specified more exactly. Joseph *et al* (1976) described a technique utilising selective filtration, high kilovoltage and fine focal spot magnification for the study of upper airway obstruction in infants and small children. The filter used comprised tin, copper and aluminium and effectively increased the air contrast with respect to the bone contrast. A high kilovoltage filtered beam technique has also been proposed for demonstrating bronchial situs in children (Furlonger, 1982). This also utilises a copper/tin filter, inserted into the collimator, and is reported to reduce patient exposure in addition to providing satisfactory images without repeat exposures.

Further advances in optimisation of patient dose and image quality are unlikely unless consideration is taken of the particular requirements of different X-ray examinations, in terms of diagnostic endpoint, image quality and any specific dose concerns, *eg* if one particular radiosensitive organ is being irradiated. The required end point of any examination needs to be well defined, especially when image quality need not be improved beyond a

certain level. Once the required information content is reached, improving the quality of the image will only increase the detriment to the patient in terms of radiation dose. A second important consideration is that variations in technique and their influence on both patient dose and image quality need to be assessed on a scientific basis, rather than from an ad hoc or historically based approach. Assumptions made in the past, particularly concerning the capabilities of equipment, should always be justified in the light of current knowledge and technology. Finally, any recommendations or suggestions for optimisation must always take into consideration the practicalities of their application. Even a well designed, scientifically based optimisation strategy with proven benefits will fail if implementation is not feasible in the majority of departments.

4.3 Choice of quantities to be optimised

4.3.1 Dose descriptors

A full discussion of the different quantities used to describe patient dose has already been given in Chapter 2. The computer simulations presented in this work use values of both entrance surface dose and total energy imparted to compare the dose effectiveness of different techniques. These quantities are straightforward to model, allow comparison with the work of others and, together, give a reliable indication of the dosimetric effects of irradiations performed using different techniques. The dose quantities measured during experimental work were chosen to mirror these as far as possible, and consisted of entrance surface dose, mid-body dose and individual organ doses.

4.3.2 Image quality descriptors

The quality of an image may be assessed in many different ways, and is a complex subject as it is affected not only by characteristics of the image but also the viewer's visual response system. Image quality indexes describing physical performance of a system include contrast, unsharpness and noise, and each of these may be specified and measured by a number of means. The effect of the observer may be included by physical and physiological assessment of images. Subjective quality criteria, such as those recommended by the CEC (1996) may also be used. The choice of image quality parameter to be used in a comparative study is

influenced chiefly by the techniques under investigation and their effect, but also by the ease of measurement or calculation of the parameter in a reproducible fashion.

In film-screen radiography, radiographic contrast is defined as the difference in optical density between two adjacent areas of film

$$C_{radiog} = D_1 - D_2$$

This is dependant on both the inherent contrast of the film as described by γ, the gradient of the characteristic curve, and the radiation or primary contrast. Radiation contrast has been defined in a number of ways, most commonly in terms of photon contrast or kerma contrast

$$C_{photon} = \frac{N_1 - N_2}{N_2} \qquad C_{kerma} = \frac{K_1 - K_2}{K_2}$$

where N_1 and N_2 are the photon fluences through the contrast area and the background respectively and K_1 and K_2 are the air kerma values due to the photon fluences N_1 and N_2. Other variables that give a measure of the signal may also be used in this definition and the appropriate choice will depend on the situation to which it is being applied. As an image receptor responds proportionally to the energy imparted to it, one variable which is particularly useful is the energy absorbed in the receptor, per unit area, behind (E_1) and outside (E_2) the region of interest.

$$C_{abs\ en} = \frac{E_1 - E_2}{E_2}$$

This parameter has been used by others as a measure of contrast (Koedooder, 1985; Sandborg, 1989) and also in derivation of signal to noise ratios (Sandborg *et al*, 1989). The energy absorption contrast thus includes detector response and is related to air kerma contrast through the absorption coefficients of the screen phosphor, which will depend on the energy spectra of the beam.

Radiation contrast may be related to radiographic contrast through the phosphor and film

responses. The relationship between the speed of a screen/film system and the energy absorption in the screen has been investigated by a number of authors. Venema (1976) showed that the speed of seven rare earth screens, relative to that of calcium tungstate screens, has the same energy dependence as did their relative X-ray absorption. Vyborny *et al* (1977) demonstrated that the effects of the screen phosphor absorption edge on system speed are of great importance in determining the overall response, while the effect of the film is negligible by comparison. The same authors later investigated six typical systems and concluded that their speeds act in a manner similar to that which would be predicted if only the energy absorption properties of their screens were considered, except for energies below 30 keV where the screen conversion efficiency drops and, to a small extent, around the K absorption edge of non calcium tungstate screens (Vyborny *et al*, 1980; Vyborny, 1977) also showed that radiographic contrasts in film-screen systems can be predicted using a single characteristic curve for a particular system, with photographic density expressed as a function of X-ray energy absorbed in the screens rather than of relative exposure. This sensitometric relationship between absorbed X-ray energy and film density was verified by Chan and Doi (1983).

Radiation contrast is very much affected by the energy of the X-ray beam, as it fundamentally relies on the difference in attenuation coefficients between the tissue or medium of interest and the surrounding area. It also depends on the thickness of the contrast region. Photon, kerma or absorbed energy contrasts may all be fairly easily determined from a Monte Carlo simulation, and radiographic contrast may be derived from measurements of film density. Different definitions of contrast would be expected to give different numerical results for the same irradiation conditions, but comparative measurements to illustrate the effect of a change in parameter should give broadly similar results. Radiation contrast defined in terms of energy absorption in the phosphor will give the closest approximation to radiographic contrast.

Unsharpness of a radiological image may be geometric unsharpness, arising from the focal spot of the X-ray tube, movement unsharpness, or unsharpness arising from the image

receptor. None of these are directly affected by the technique factor selected or energy of the beam, although a longer exposure time may increase the likelihood of patient movement, especially for paediatrics. Image unsharpness is often described in terms of the modulation transfer function (MTF), a concept based on Fourier analysis. This may be explained simply by considering that at any stage in the imaging process all information may be expressed in terms of a spectrum of spatial frequencies. For an exact image, all frequencies would have to be reproduced with one hundred percent efficiency. However, each separate component of the imaging chain will modify this spatial frequency spectrum by the component's MTF. An MTF of 1 results in precise transmission of that frequency and, in general, the MTF decreases with increasing spatial frequency as the high frequency information in an image (fine detail) is more likely to be degraded. The MTF of the entire system is given by the product of the individual component MTFs. MTF is generally used to describe the imaging characteristics of a chain of system components itself, and is dependant on the equipment used and not by changes in beam spectrum. Image unsharpness may be assessed in practice by measuring the resolution obtainable from a system, using a suitable test object.

Noise can degrade an image irrespective of its contrast and resolution. Noise may arise from statistical fluctuations in the number of X-ray photons detected per unit area - known as quantum noise - or from the receptor itself - radiographic noise. Noise can be expressed in terms of its Wiener spectrum or as a signal to noise ratio. The Wiener spectrum is obtained by taking the Fourier transform of the noise and plotting its square against frequency, to give the power spectrum. It will contain information on all components of noise and its measurement is complex. The signal to noise ratio (SNR) may be defined according to the theory of Rose (1948), in which an observer is thought to compare a signal with a region of background equivalent in area to the object. From this, the SNR may be given by

$$SNR = \frac{(N_2 - N_1)at}{(N_1 at)^{1/2}}$$

where a is the area of the object, t the integration time of the image receptor and N_2 and N_1 the photon fluences through and beside the object. It may be seen from this that SNR is

closely related to photon contrast. If two images of an object have the same contrast, they will only differ in SNR if the number of photons reaching the detector per unit area is significantly different. In practice, noise is usually only a limiting factor for image detection when very fast intensifying screens are used, radiographs are enlarged, or in digital radiology over a small area. For the same image receptor and display system, noise will only be affected by the number of photons reaching the receptor. Under conditions of equal background film density, in a comparative study such as this, the noise variation should be small; and ratios of SNR are unlikely to yield any more information than ratios of contrast, as defined earlier. Calculations of SNR will only be of use in an optimisation study if the parameters being varied have an effect on the image noise *eg* when comparing different types of equipment.

For the simulations presented here, energy absorption contrast was selected as the image quality parameter to be optimised against dose since, of all the parameters, contrast will be affected most by changes in the input energy spectrum, which is the major variable in the study. Energy absorption contrast in the detector was used in preference to other contrast definitions as it takes account of phosphor response, is easily calculated using Monte Carlo techniques and, for film-screen radiography, can be related to the radiographic contrast observed on the film. For the experimental work, radiographic contrasts were derived from measurements of film density behind and beside the area of reduced transmission.

4.4 Beam filters

X-ray beam filters are used to change the shape of the energy spectrum emitted from the tube in order to improve performance. This occurs as all materials will selectively attenuate different photon energies. The way in which they do this will depend on the atomic number of the filter material. Low atomic materials, such as carbon, may be classed as general attenuators, with the most uniform attenuation across a beam spectrum. This occurs as their chief mode of attenuation is by Compton scattering which is independant of photon energy. As atomic number increases, photo-electric absorption becomes the dominant feature over the diagnostic energy range. When this occurs, the absorption coefficient will decrease with

increasing photon energy, except when an absorption edge occurs in the energy range of interest, when the absorption coefficient increases sharply. When such a K-edge is not present, and photo-electric absorption is dominant the material acts as a high-energy pass filter, removing chiefly low energy photons from the beam. Materials with atomic number ranging from 25 to 35 fulfil these criteria most effectively. For materials with slightly lower atomic number, such as aluminium both photo-electric absorption and Compton scattering are present, making them less efficient high energy pass filters. When a K-edge occurs within the emitted spectrum the material acts as a bandpass filter, selectively removing both low energy photons and those with energies above the K-edge of the filter material. It has been proposed that such filters can both reduce patient dose and maintain or improve image contrast. To illustrate the characteristics of the different filter types, Figure 4.1 shows how the reciprocal of the mass attenuation coefficient varies with energy for carbon (Z = 6), aluminium (Z = 13), copper (Z = 29) and erbium (Z = 68). Plotting the reciprocal of μ means the graphs give an illustration of the transmission of the filters.

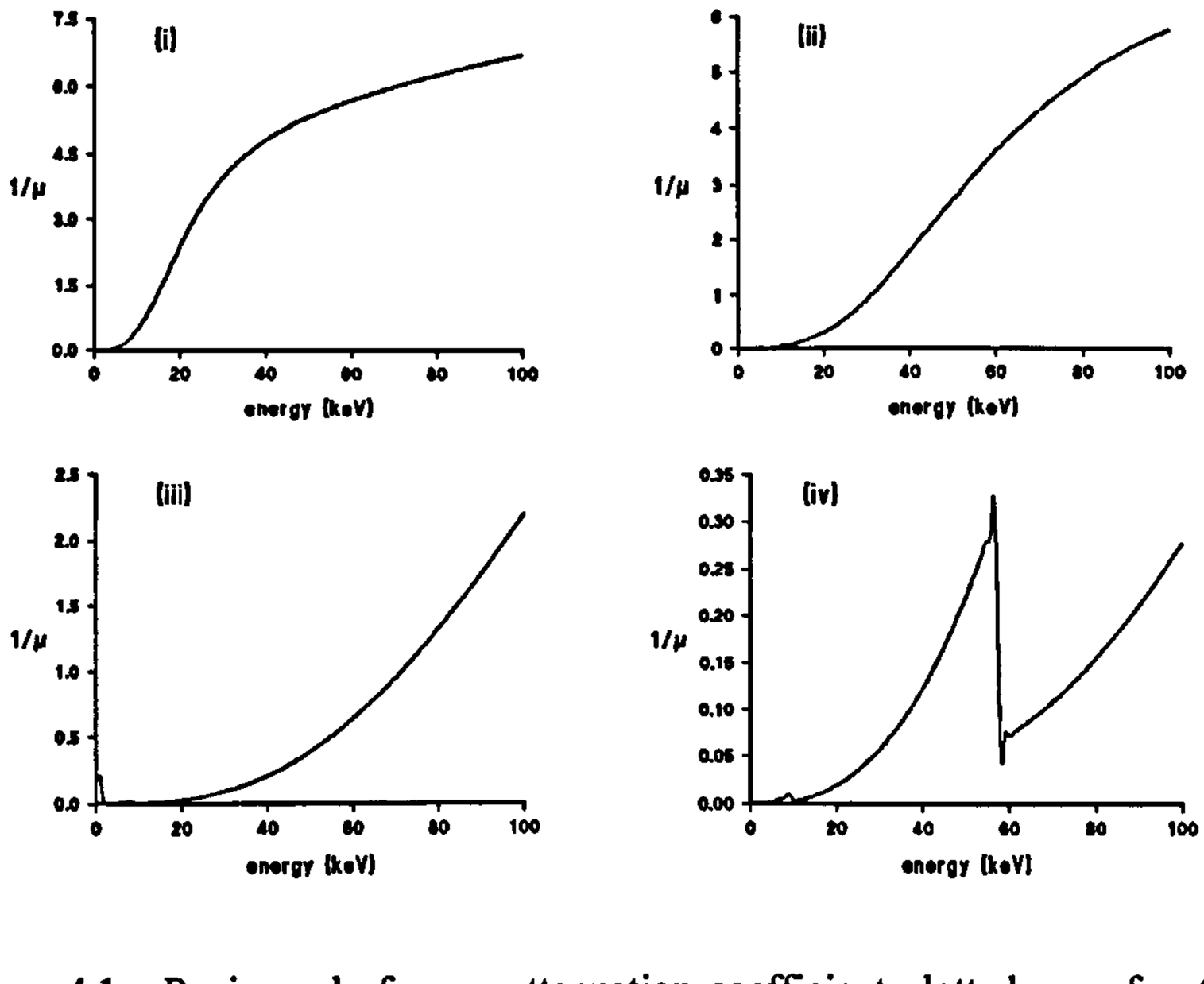

Figure 4.1 : Reciprocal of mass attenuation coefficient plotted as a function of energy for (i) carbon; (ii) aluminium; (iii) copper; (iv) erbium

4.4.1 Previous work

Many authors have addressed the issue of filtration in diagnostic radiology, but there is still no consensus of opinion on the suitability of K-edge filters for dose reduction. This is mainly due to the wide range of both methodology and endpoint employed in the various studies. The methodologies used may generally be classified as theoretical, often utilising computer programming to 'rank' filters according to defined performance criteria; experimental where laboratory measurements are carried out with phantoms to determine how parameters change according to beam filtration; or clinical where a filter is installed in an X-ray room and its effect on patient dose and image quality assessed. Each of these three techniques has its merits and drawbacks, and these are discussed below.

Early work on the use of K-edge filtration was based on the intuitive premise that the beam shaping properties of such band pass filters would be beneficial to X-ray imaging (Atkins *et al*, 1970; Villigran *et al*, 1978; Fleay *et al*, 1980). The filters studied were selected on the basis of a subjective consideration of the spectra obtainable and the absorption characterisitics of the contrast media. While this is a reasonable starting point, it results in a fairly arbitrary choice as the K-edge energy does not vary rapidly for elements of similar atomic number, and the reason for selecting one over its neighbours is unclear. The experimental measurements made were limited in nature as only a small range of parameters was investigated in each case. The quantity used to assess dose reduction, in all the above work, was entrance exposure which gives a poor indication of risk to the patient. In addition, the parameter used to assess image contrast has not always been clearly defined (Atkins *et al*, 1970; Fleay *et al*, 1980). The recommended filters were gadolinium (Atkins *et al*, 1970) and holmium (Villigran *et al*, 1978) for iodine studies and erbium or samarium for paediatric examinations (Fleay *et al*, 1980).

A number of clinical trials of specific filters have been carried out including the use of gadolinium in paediatric radiology (Johnson and Burgess, 1981), the use of yttrium (Wang *et al*, 1984) and several evaluations of erbium filters (Wesenberg *et al*, 1987; Levett, 1990; Cranage *et al*, 1992). Each of these demonstrated dose reduction with acceptable contrast.

The results of such trials are important as they involve results from actual patients who should always be the end point of any optimisation study. The subjective assessment of image quality also takes account of the fact that the most significant criteria in such a comparison is whether or not the resultant images are of acceptable diagnostic quality. However, a number of points must be made about the limitations of such purely clinical trials:

- All the above papers refer only to reduction in entrance skin exposure and include no assessment of any absorbed dose quantity, which would almost certainly be affected far less by the introduction of extra filtration.
- As only one filter is assessed in each case, there is no reason to suppose that use of a different filter might not achieve equally good, or improved, results.
- The results obtained strictly only apply to the conditions involved in the trial. Use of the filter under other conditions (patient thicknesses, tube potentials, examination types *etc*) may not give comparable results.

Two main types of theoretical assessment of filtration have been carried out. The first of these is a consideration of the spectra themselves, and methods for comparing or matching spectra passing through different filter materials (Shrimpton *et al*, 1988; Jennings, 1988; Carrier and Béïque, 1992; Nickloff *et al*, 1993). A theoretical study of the influence of filtration and tube potential on dose (Shrimpton *et al*, 1988) concluded that the best dose reduction could be achieved using a high kV technique and that effective dose was affected much less than entrance dose by additional filtration. The concept of precise spectral matching for different filter materials has been explored theoretically (Jennings, 1988; Nickloff, 1993) with similar spectra obtained for different filter materials, depending on their thicknesses. Relative efficiencies (*ie* transmissions) of the different filters were then used to compare their performance and that for aluminium (the most usual filter material) was shown to be low. An alternative comparison of filters, matching those that gave the same ratio of entrance exposure to energy absorbed in the detector, demonstrated similar results (Carrier and Béïque, 1992). However, it was not possible to achieve spectral matching for K edge filter materials, and unpredictable behaviour was observed regarding efficiency, contrast and

dose for such filters (Carrier and Béïque, 1992), illustrating that the presence of a K-edge discontinuity cannot be easily fitted into a simple theoretical model.

The second type of theoretical study appearing in the literature is the comprehensive computer based investigation, which aims to cover a wide range of filter materials and irradiation conditions, in order to determine the advantages, if any, of one type of material over another (Koedooder and Venema, 1985; Gagne *et al*, 1992; Sandborg, 1994). These were carried out using computer models incorporating attenuation through a phantom, absorption in an image receptor and calculation of dose and image quality parameters. The conclusions of the studies are similar in that beam hardening filters, such as copper, are reported to be at least as good as, if not better, than K-edge filters in most circumstances. The advantage of these studies lies mainly in the large number of parameter variations that are covered, but a number of flaws may be identified:

- In order to make absolute comparisons of different filter materials, the studies have all incorporated constraints to the system under investigation. *Equal energy absorption in the energy receptor* (or background density on a film) was a universal requirement, and most have enforced *equal contrast* (Koedooder and Venema, 1986; Gagne *et al*, 1993) and some *equal tube load* (Sandborg *et al*, 1994). Although such methodology does allow an absolute ranking of filters it is not necessarily a reflection of clinical practice. Clinical use of a filter would certainly require that the images obtained were still **approximately** the same background density, and that images were still of **diagnostic quality,** but *equal* is not always the most relevant term for an X-ray reporting room. The complexity of spectral behaviour - influenced by filter, kV, patient tissues and thicknesses *etc* - means that slight fluctuations in one parameter, *eg* contrast, might be accompanied by relatively large changes in another parameter *eg* dose. Constraining system parameters may thus result in some interesting effects being missed, or poor understanding of the underlying behaviour.
- Although many filter types have been studied, and a number of image receptors and contrast media, fewer data are available for paediatric than for adult thicknesses even although that which has been presented shows more potential for the use of K-edge

filtration (Gagne *et al*, 1993).

- Experimental verification of the theoretically determined results is, in general, sparse and insufficiently detailed (Koedooder *et al*, 1985), and for some studies no such verification has been carried out at all (Gagne, 1993). There has also generally been no extrapolation to the clinical environment.

A smaller number of purely experimental studies have been carried out (Regano and Sutton, 1992; Heggie, 1992; Hansson *et al*, 1997). The first of these used heavy metal salt solutions as filters with bone/soft tissue contrast, and took the approach of matching a range of phantom thicknesses and tube potentials to a given filter, from a consideration of the K-edge. The results give some insight into the effect of the K-edge and tube potential on the different parameters, but the method of calculating absorbed energy contains large uncertainties. Heggie (1992) studied the use of a number of filters in Automatic Brightness Controlled (ABC) Fluoroscopy and Digital Subtraction Angiography (DSA), using phantoms and test objects. The results are highly dependent on the operation of the ABC algorithm. The study reported by Hansson *et al* (1997) contains high quality data but again is for one highly specific examination, with only one filter tested. It is also worth noting that the examination in question (double contrast enemas) is not one that is performed on paediatrics in this region.

To summarise, those authors who advocate the use of K-edge filtration have in general focussed on the dose reductions achievable, and assessed the associated effect on contrast subjectively, often looking only for 'acceptable' contrast. In many cases only the impact on entrance dose has been assessed. This is a serious flaw as it has been shown to be very different to the impact on integral dose, which is the more important quantity. Direct comparison with beam hardening filters, such as copper, have not usually been made. Those who reject the superiority of K-edge filters over more conventional materials have usually done so on the basis of a more theoretical study in which various constraints are put on the system, such as equal contrast or tube loading. Although this may seem to be a logical way forward, in practice the concept of 'acceptable' contrast may be more in keeping with the

principles of dose limitation than that of 'equal' contrast. More importantly, tube loading will now often not be a major factor to be taken into consideration, particularly for paediatric examinations where exposures are small. A filter that may be appropriate for a particular examination, and perhaps a particular range of patient sizes, may not necessarily be appropriate for general use. Optimisation of beam spectra should ideally be applied on an examination and patient specific basis. This then raises the important consideration of the practicality of using a given filter, if it is not suitable for permanent installation on a piece of equipment.

4.5 Methodology for optimisation study

4.5.1 Aims

Three stages were identified in the development of an optimisation strategy:

(1) A theoretical analysis of the behaviour of a wide range of filters with variation of different parameters, and interpretation of the results.

(2) Experimental verification of the theoretical results, and assessment of the influence of practical and clinical constraints.

(3) Clinical implementation of results

The theoretical analysis was necessary in order to carry out as complete a study as possible, and to avoid prejudicing results by artificially constraining the system *eg* by forcing equality of tube load or contrast. Experimental validation was essential not only to ensure that the results were correct, but also so that practical considerations could be accounted for. The clinical implementation, and assessment, of an optimised technique had to be the final objective of any such study, as the increased benefit to the patient is the motivation for performing it.

The specific aims of the theoretical study, which was carried out using Monte Carlo techniques as described in the next chapter, may be listed as follows:-

- For each simulation, to calculate both the entrance surface dose and the total energy imparted to the patient, plus the absorbed energy contrast and total absorbed energy in the screen.

- To study a wide range of filter materials and thicknesses, in order to explore the characteristics of different filter materials without imposing numerous constraints.
- To consider a number of different contrast scenarios, *eg* bone in soft tissue; barium/iodine in soft tissue; lung in soft tissue.
- To use a simulation geometry that could be reproduced experimentally, in order to verify the results.
- To carry out simulations for a range of paediatric patient sizes.

The reasoning behind the choice of dose and image descriptors has been discussed above. It could be expected that optimal beam spectra might depend crucially on the patient thickness and also on the tissues and contrast media being imaged, so the effect of these factors needed to be studied as far as possible. As neonates comprise the extreme of the size range - differing the most from adults, for whom the majority of filtration work has been carried out - this age group was the focus of the initial set of simulations. The criteria of experimental reproducibility was essential in order to validate the Monte Carlo results obtained.

4.5.2 Geometry

The geometry used for the simulation is shown in Figure 4.2.

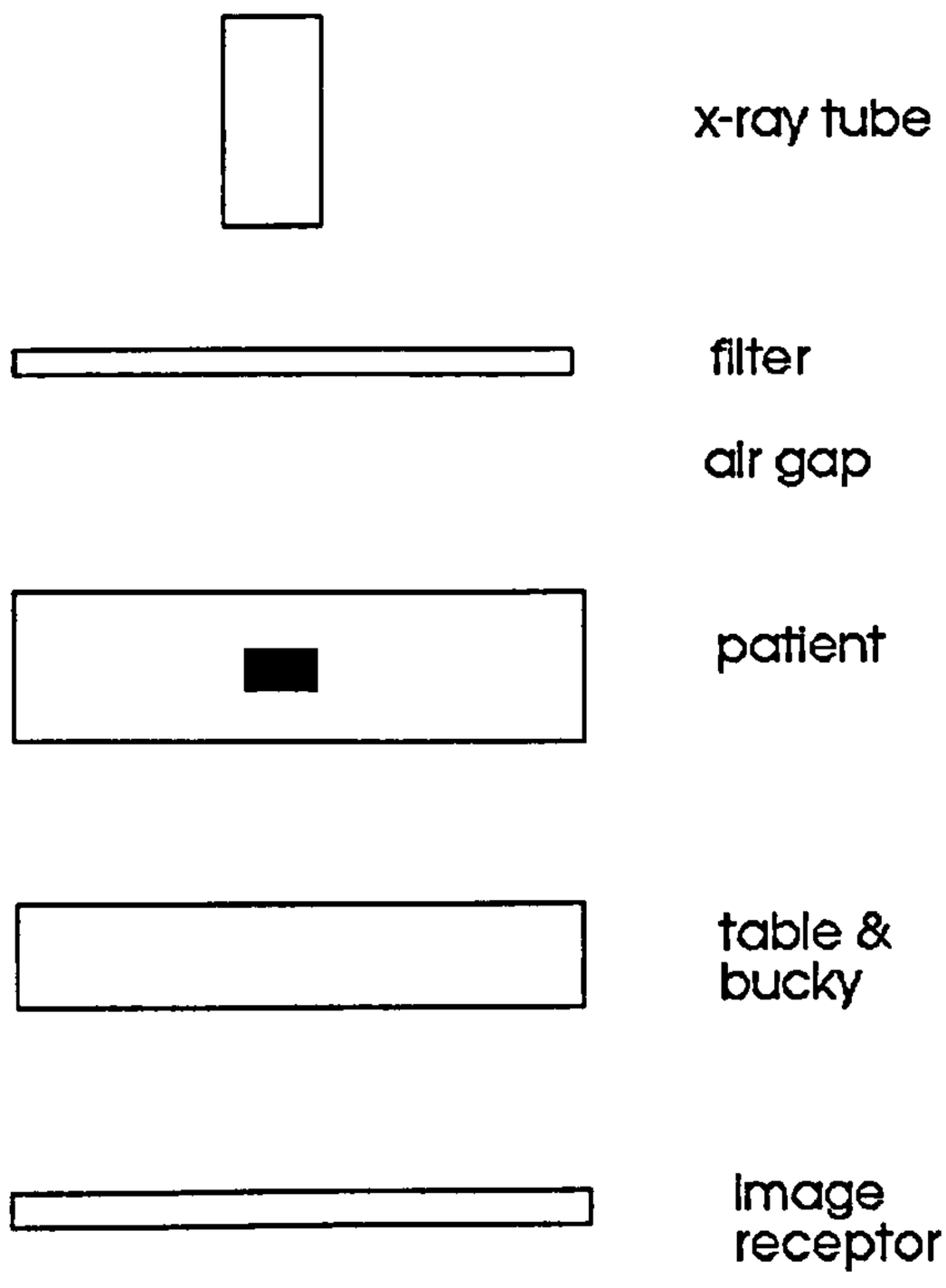

Figure 4.2 : Geometry for Simulation

An X-ray beam is incident normally on a thin filter, with the patient phantom a fixed distance beyond. The phantom is represented by a defined thickness of uniform tissue, containing a small disc of contrasting material at its centre. Below the patient is an optional thickness of table top (which is not required when simulating irradiation of an infant lying directly on a film cassette) followed by the image receptor, which may be an intensifying screen, as used with film, or a phosphor used directly in fluoroscopy. The incident spectrum is prefiltered with aluminium, and produces a circular field of variable size.

4.5.3 Range of variables to be tested

The filter materials included in the computer study are listed in Table 4.1 together with the range of thicknesses used. The choice of filter thickness was made initially from study of previous work, using a range of thicknesses similar to those recommended by others. For most materials, this meant multiples of 0.05 mm thicknesses, although filters of samarium

and tin have commonly been used in smaller thicknesses (Jangland and Axelsson, 1990; Gagne *et al*, 1994) Early results were then used to assess where extension of the range of simulations would be useful, leading to simulations incorporating slightly greater thicknesses of tin and samarium and intermediate thicknesses of both copper and dysprosium, to give more closely spaced data points for these graphs on subsequent analysis.

Filter Material	Thicknesses (mm)
Aluminium	0.5, 1.0, 1.5, 2.0, 2.5, 3.0, 3.5, 4.0
Dysprosium	0.050, 0.075, 0.100, 0.125, 0.150, 0.175, 0.200, 0.225, 0.250
Erbium	0.05, 0.10, 0.15, 0.20
Copper	0.050, 0.075, 0.100, 0.125, 0.150, 0.175, 0.200
Gadolinium	0.05, 0.10, 0.15, 0.20
Holmium	0.05, 0.10, 0.15
Samarium	0.04, 0.05, 0.08, 0.10, 0.15, 0.20
Tin	0.04, 0.05, 0.10, 0.15
Terbium	0.05, 0.10, 0.15, 0.20, 0.25
Ytterbium	0.05, 0.10, 0.15, 0.20

Table 4.1 : Filters used in simulation

The thickness of tissue being irradiated could be varied to represent patients of different ages. Initially all simulations were carried out for 5 cm tissue, to represent a neonate. This thickness is less than that of a 'standard' newborn, as the babies receiving most radiographic examination are those born prematurely, as they tend to have a range of clinical problems. The chosen thickness thus corresponds to a typical patient size in a special care baby unit. Consideration was later given to how the techniques might be applied to other age groups. Appropriate tube voltages were selected for the study. For the neonates, the reference voltage was 60 kV and simulations were carried out at 55, 60 and 70 kV to investigate the effect of varying tube voltage. When considering thicker phantoms, the reference voltage was 70 kV. The reference voltages were determined from routine practices in the department where the clinical trial was carried out.

The composition of the irradiated tissue was either soft tissue or lung, with contrasting inset of bone, lung, iodine or barium, enabling a range of radiographic conditions to be simulated. The tissue compositions were taken from White *et al* (1977) who describes a number of epoxy resin systems for use in constructing simple phantoms. He showed that the composition of a child may be simulated by the same resin as for an adult. The materials used chosen for use here were MS20 was for soft tissue, LN10 for lung, and SB5 for bone. The relative compositions and densities of these materials are given in Table 4.2. The method by which these materials were incorporated into the Monte Carlo simulation are described in Chapter 5, and blocks of the material were obtained for the experimental measurements.

Material Name	Composition (% by weight of each element)								Density
	H	C	N	O	Mg	Cl	Ca	Si	(g cm^{-3})
MS20 (muscle)	8.1	58.4	1.8	18.6	13.0	0.1			1.00
LN10 (lung)	8.4	60.5	1.7	17.3	11.2	0.1		0.8	0.288
SB5 (bone)	2.6	30.6	1.0	38.9		0.1	26.8		1.87

Table 4.2 : Tissue equivalent materials used in simulation

Compositions were obtained of a number of commercially available intensifying screens, but the majority of work was carried out for two screens - Agfa Gevaert Curix Ortho Regular screens (Gd_2O_2S, phosphor thickness 60 mg cm^{-2}) and Agfa Gevaert MR200 screens (LaOBr, phosphor thickness 43 mg cm^{-2}) - and for a CsI fluoroscopic phosphor. The majority of rare earth screens contain either gadolinium or lanthanum, and the screens simulated correspond to those available for experimental work and that used locally. The appropriate thickness of phosphor to be used in the simulation was determined from the mass thickness and the density of the material.

4.6 Summary of chapter

This chapter has presented a discussion on the general principles and techniques of

optimisation in diagnostic radiology, with particular reference to paediatrics. A summary of different image quality parameters has been given, along with an explanation of the choice of both dose and image quality descriptors used for this work. The subject of beam filtration in relation to the optimisation of dose with image quality has been explored in depth and the published work in this area reviewed. In particular, the merits and drawbacks of the different types of optimisation studies performed have been outlined. Finally, the strategy employed for the optimisation study carried out in this work has been described.

Chapter 5

Development and testing of Monte Carlo Code

5.1 Introduction

The theoretical investigation of the effect of beam filtration on paediatric dose optimisation was carried out using Monte Carlo techniques. This chapter contains a general description of these techniques and details of the specific code, EGS4, used for the simulations. Modifications made to the code for the purpose of this work, and the development of the user-written interface are also described, along with full details of the input parameters and the format of the results obtained. A discussion of the variance reduction techniques employed and the accuracy of the code are included at the end of the chapter. A complete listing of the usercode that was written to run the simulations is given in Appendix B.

5.2 Monte Carlo techniques

Monte Carlo techniques are so named because they use the laws of chance to carry out sampling of an event, or sequence of events. Monte Carlo techniques of radiation transport, in particular, comprise the simulation of the random trajectories of individual particles. This is carried out using machine-generated random numbers to sample from the probability distributions governing the physical processes involved. A single particle history thus comprises the simulation of the movement and interactions of that particle and all particles arising from it until they have all either left the regions of interest or their energy has dropped below a cut-off value. The number of histories simulated affects both the statistical significance of the results and the execution time of the code.

Monte Carlo techniques of radiation transport have been in use for over forty years, and many codes have been developed, including the EGS4 (Electron Gamma Shower) code

(Nelson *et al*, 1985). The initial use of such code was confined to the realms of high energy physics, but applications in the field of medical physics were found and the code has been extended and improved to allow simulation of low energy interactions. Another code that was available was the ETRAN code, (Berger and Seltzer, 1968). This code treats low energy processes in greater detail than the earlier versions of EGS4, as it was originally designed for the energy regime below a few MeV whereas EGS was originally a high-energy physics code, designed for energies up to the GeV range. Thus, ETRAN includes treatment of fluorescence, sampling of the angular distribution of photoelectrons and the use of the Elwert correction factor to modify bremsstrahlung cross-sections. It does not, however, include coherent scattering which is an option in the EGS4 code. Other effects accounted for in ETRAN are the atomic binding effect on atomic electrons, and energy loss straggling. The chief disadvantage of ETRAN is its lack of flexibility. It is designed as complete codes, allowing the user to select one of a wide variety of geometries and elect a variety of outputs in each region. While this makes the code easy to use, it restricts the user's options and ability to extract information. The code has not generally been in widespread use, but was used extensively in testing EGS4. The remaining code of note that has been in general use is the MCNP code (Thompson, 1979) which consists of continuous-energy coupled neutron-photon transport, with an arbitrary configuration of materials using generalised geometry.

5.2.1 Use of Monte Carlo techniques in medical physics

Over the last twenty years there has been an increasing use of Monte Carlo techniques in the field of medical physics, mainly in the fields of nuclear medicine, radiotherapy, diagnostic radiology and radiation protection. A full review of this work has been given by Andreo (1991). Microscopic Monte Carlo techniques have also been used in the study of electron microscopy, radiation track structure and microdosimetry.

In the field of diagnostic radiology, the energy response of detectors used in the measurement of X-ray spectra has been investigated by Chen et al (1980), and Yamaguchi (1983) has investigated the influence of a tungsten absorption edge filter on X-ray spectra. Several authors have studied scatter fractions and scatter to primary ratios, using

monoenergetic photon pencil beams on a parallelpiped or slab water phantom (Neitzel *et al*, 1985), and Chan and Doi (1984) looked at the spatial distribution of energy deposition from pencil beams in water slabs. Monte Carlo techniques have been used extensively by Sandborg, Persliden and their colleagues for a number of diagnostic radiology problems, including studies of grid performance (Sandborg *et al*, 1994), performance of contrast agents (Sandborg *et al*, 1995), calculation of dose and image quality parameters (Sandborg *et al*, 1993) and the derivation of factors for calculating energy imparted to a patient (Persliden and Alm-Carlsson, 1984). Work has also been carried out in the area of mammography, such as the derivation of conversion factors for mean glandular breast dose from air kerma (Dance, 1990). More recent work includes the calculation of dose conversion factors for posterior-anterior chest radiography (Schultz *et al*, 1994), using the MCNP package, and simulation of the upper gastrointestinal fluoroscopic examination for the calculation of absorbed dose to tissue (Stern *et al*, 1995). Monte Carlo techniques have also been used to determine the upper limiting values of back scatter factors for low energy X-ray beams (Patrocinio *et al*, 1996) . Applications in radiation protection include the use of mathematical anthropomorphic phantoms for the calculation of internal exposures and organ doses from external beams (Drexler *et al*, 1984). There are also calculations using the ICRU sphere (Grosswendt, 1988) and radiation shielding problems such the retrospective analysis of shield design in a diagnostic X-ray room (Metzger, 1993) using the MCNP code.

5.2.2 Choice of Monte Carlo code

The EGS4 code was chosen for use in this work as it has many advantages to its use, the chief of which is its extreme flexibility. The geometries may be defined by the user, using any combination of planes, spheres and cylinders and any materials may be specified, in the form of elements, compounds and mixtures. The code is also easily modified and extended to suit the user's requirements. The use of EGS4 is widespread, and this has enabled the code to be tested under a variety of conditions. This code was also already available for use within the department. The EGS4 code may be run on a VAX system, PC DOS system or a unix operated system. The PC version was used in this instance, and the code run initially on a 386 Compaq with 4 Mbytes memory, later on a 486 Opus with 16 Mbytes memory.

5.3 EGS4 code

The EGS (Electron Gamma Shower) code was first introduced in 1978 and is a general purpose package for the Monte Carlo simulation of the coupled transport of electrons and photons in an arbitrary geometry. The radiation transport of electrons or photons can be simulated in any element, compound or mixture and both photons and charged particles are transported in random rather than discrete steps. The dynamic range of charged particle kinetic energy goes from a few tens of keV up to a few thousand GeV, and for photons the dynamic range lies between 1 keV and several thousand GeV. The code has been used in many medical applications, including both radiotherapy and diagnostic radiology problems. EGS4 has been used to calculate the shielding requirements for constant potential diagnostic X-ray beams, by simulating their transmission through lead, concrete, gypsum, wallboard, steel and plate glass (Simpkin, 1989). Simpkin and Mackie (1990) have also used the EGS system to compute β dose-kernels for monoenergetic electrons and β emitters. In radiotherapy, McCall *et al* (1978) calculated spectra from a number of high energy X-ray targets and flattening filters, using EGS.

5.3.1 Structure of code

The EGS4 package consists of a number of subroutines, which carry out the radiation transport, and these are held together by a flexible user interface which sets up parameters specific to the problem in hand and calls the transport subroutines. The properties of the original particles - type of particle, charge, initial position, direction and energy - are defined in this interface, as is the number of particles whose histories are to be tracked. All particles are tracked individually, by determining the distance that the particle will travel, the type of interaction undergone and the position, energy and direction of the original particle and all new particles arising from the interaction. As new particles are created, their properties are stored in a 'stack' structure *ie* tracking always continues with the most recently created particle, until it is either totally absorbed or leaves the region of interest, when the next

particle on the stack is selected. When the entire history is complete, the next incident particle history is initiated.

An accompanying preprocessor package, PEGS, is used to provide interaction data for the simulations, and this is described in section 5.3.2 below. The programming language used throughout EGS4 and PEGS4, including the usercode, is MORTRAN3; a structured language implemented as a set of macros which are used by the macro processor to translate the language into FORTRAN. A summary of the main features of the MORTRAN3 language is given in Appendix C. The macro facility is an important feature of EGS4 as macros may be defined in the usercode, and used to control or overide various functions in the EGS transport code. A macro definition takes the form

REPLACE {*pattern*} WITH {*replacement*}

where *pattern* is any string of text, including variables if required and *replacement* is the desired new text. This definition has the effect of searching all the ensuing code for the *pattern* and replacing it with the *replacement* text. This allows the user to make changes to the supplied code without having to edit it permanently.

The geometry of the simulation is defined by a subroutine named HOWFAR, which must be written by the user. Standard code is available for defining planes, cylindrical surfaces and spheres, from which many different three dimensional geometries may be constructed. A further user-written subroutine (named AUSGAB) is called under a set of very well defined and selectable conditions (*eg* at the end of every photon and electron step) and is used to keep track of the parameters of interest, and to extract the required information.

The relationship between the different parts of the EGS and user codes is shown in Figure 5.1, where the shaded regions indicate the parts of the code written by the user. Arrows indicate the direction of data flow: PEGS provides input to EGS4 *via* a group of data sets containing interaction data; all sections of the user-written code provide input to EGS, and may also request output *eg* an absorbed energy value at the end of a simulation or a running total of the number of particle histories simulated *etc.*

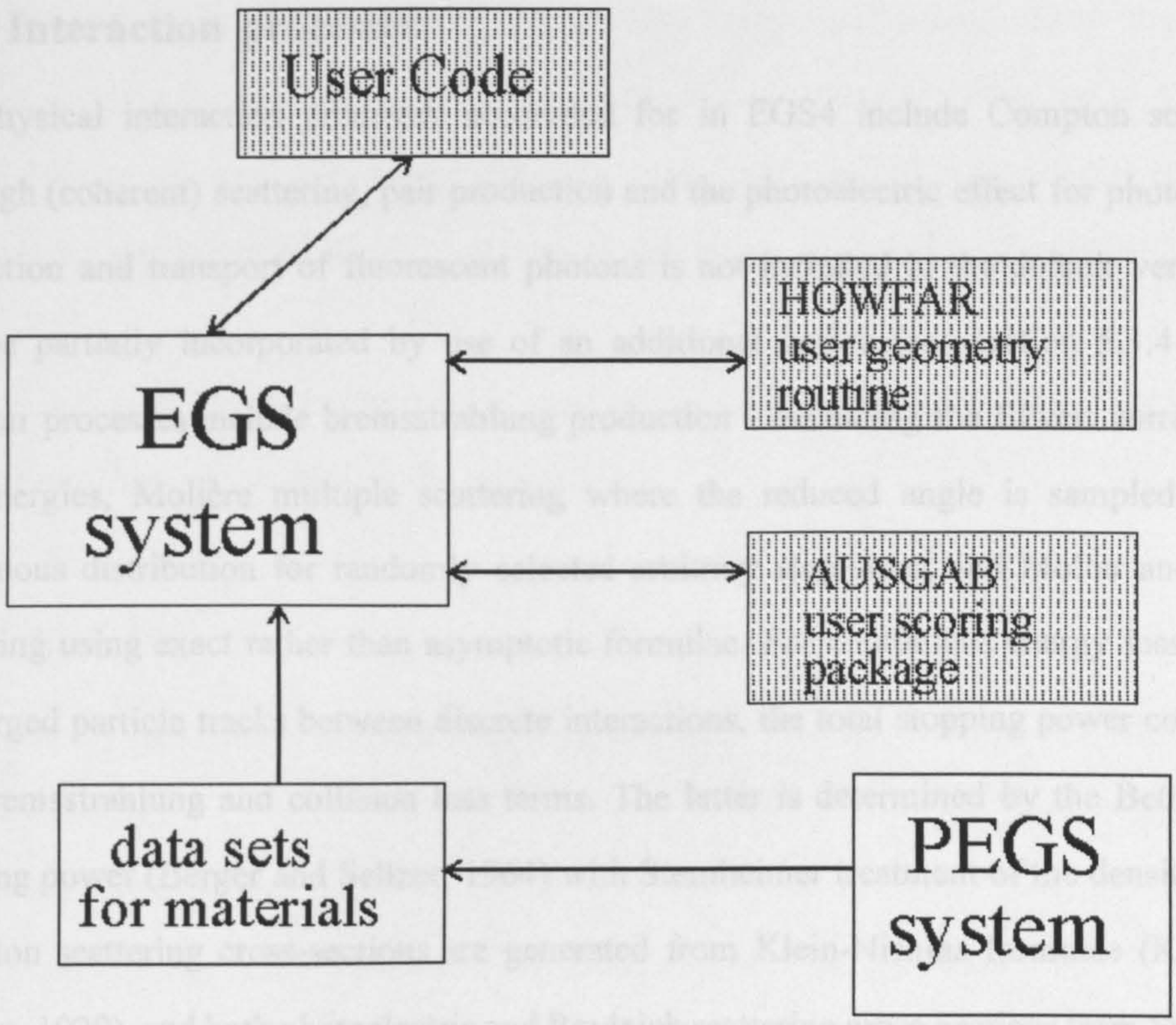

Figure 5.1 EGS Code Structure

5.3.2 Preprocessor for EGS4

The radiation transport simulation requires the appropriate data on the various interaction cross-sections employed, specific to the media being traversed, and the energy range of the particles tracked. An accompanying preprocessor program (PEGS4) is used to create cross-section data files, suitable for use by EGS4, for materials specified by the user, across a specified energy range. PEGS4 works by constructing piecewise-linear fits over a large number of energy intervals of the cross-section and branching ratio data. This means that a linear fit is performed with a given number of subintervals, and the number of subintervals is doubled until the fit satisfies all tolerances. Data can be produced for elements, compounds and mixtures of elements, as specified in a user-written input file of defined format. In general, PEGS4 need only be used once to obtain the media data files required by EGS4 for a given simulation.

5.3.3 Interaction processes

The physical interaction processes accounted for in EGS4 include Compton scattering, Rayleigh (coherent) scattering, pair production and the photoelectric effect for photons. The production and transport of fluorescent photons is not included in the default version but may be partially incorporated by use of an additional option (see section 5.3.4 below). Electron processes include bremsstrahlung production - excluding the Elwert correction at low energies, Molière multiple scattering where the reduced angle is sampled from a continuous distribution for randomly selected arbitrary step sizes, and Moller and Bhaba scattering using exact rather than asymptotic formulae. For continuous energy loss applied to charged particle tracks between discrete interactions, the total stopping power consists of soft bremsstrahlung and collision loss terms. The latter is determined by the Bethe-Bloch stopping power (Berger and Seltzer, 1964) with Sternheimer treatment of the density effect. Compton scattering cross-sections are generated from Klein-Nishina formulae (Klein and Nishina, 1929), and both photoelectric and Rayleigh scattering cross-sections from Storm and Israel (1970). The formulae used for bremsstrahlung are those described by Koch and Motz (1959), and cross-sections for Moller and Bhabha scattering are given by Messel and Crawford (1970). K-edge fluorescent yields are from Lederer *et al*, with cross-sections and energies from Storm and Israel (1970).

5.3.4 Options and enhancements to EGS4

In addition to the basic EGS4 code, there are a number of options that may be included. One of the more recent enhancements to the code is the PRESTA algorithm (parameter reduced electron step transport algorithm) for electron transport. This allows electron step sizes to be reduced in the vicinity of an interface, so that the majority of electron paths take place as if in an infinite medium. This algorithm was not incorporated into the current code as it was not available when the software was first obtained and used and in low energy photon beams, such as those simulated, the estimation of quantities such as absorbed dose is relatively insensitive to the electron transport part of the calculation (Rogers and Bielajew, 1990).

The EGS4 code includes optional subroutines which may be used to track the production and paths of K-edge fluorescence particles in elements with atomic number up to 100. This applicability to elements only is restrictive for many purposes and the treatment of K-edge fluorescence was extended for the purposes of this work, as described in section 5.6.1.

The simulation of Rayleigh scattering is also optional, and may be selected or deselected for each geometrical region used in the simulation.

5.4 User input

A number of parameters must be specified as input to each of EGS4 and PEGS4. For PEGS4 these are:

- definition of materials
- energy range over which cross-sectional data is to be generated
- whether or not Rayleigh scattering cross-sections are required.

These input parameters are listed in a data file of defined format, and typical PEGS input is shown in Figure 5.2 for an element (aluminium) and a mixture (tissue equivalent material MS20). Cross-section data was generated from 0 to 100 keV and Rayleigh scattering data was generated for all media.

```
select material that is an element

set Rayleigh scattering on
specify data set identifier as 'AL'
set atomic symbol to be 'AL'
set energy ranges for electrons & photons
do piecewise linear fit to data
```

(i)

```
select material that is a mixture
set no of elements to 6,density to 1g/cm3
specify relative atomic amounts by weight
set Rayleigh scattering on
specify data set identifier as 'MS20'
set atomic symbols to be H C N O MG CL
set energy ranges for electrons & photons
do piecewise linear fit to data
```

(ii)

Figure 5.2 : Examples of PEGS input files for (i) Aluminium & (ii) MS20

The input required for EGS4 includes:

- the random generator used (default or user-defined)

- cut-off energies for tracking particles
- selection or deselection for Rayleigh scattering in each region
- number of particle histories to be simulated

Additional information is required to detail the geometry, media types and result parameters for the problem in hand, and these aspects are dealt with more fully in later sections of this chapter.

The cut-off energy for tracking particles was selected to be 1 keV for photons and 0.7 MeV for electrons. Rayleigh scattering was switched on for all regions. The default random number generator was used for the simulation. This is a multiplicative congruential random number generator (MCRNG), of the form

$$I_{n+1} = (aI_n + c) \ modulus \ 2^k$$

where a = 663608941 and k = 32. As there is no theoretical method for predicting the optimum MCRNG parameters, they must be determined and evaluated experimentally and this MCRNG has been shown to be fast with good spectral qualities and a cycle length of approximately 10^9 (Ehrman, 1981). It is coded in-line which considerably improves the speed of the simulation as the alternative call to a subroutine takes significantly more time (Rogers and Bielajew, 1990).

The number of histories run for each simulation varied from 1 million to 4 million, depending on the stage of development and the precise materials being used. Particle splitting was used as a means of variance reduction, and this is described in detail later in this chapter.

5.5 Development of usercode

The basic EGS4 usercode uses a monoenergetic, uni-directional beam of particles from a point source. Code was written to enable simulation of a diverging beam containing a spectrum of energies, representative of diagnostic X-ray procedure.

5.5.1 Diverging beam

A macro was written to enable use of a divergent input beam. When used, a beam angle is specified, resulting in a circular radiation field of variable radius. The macro determines the direction of the incident particle by using random numbers to select the initial directional cosines of the particle over the required range. This macro is then called before the initiation of each new particle trajectory. The macro was tested by running a simulation which tested the positions of particles generated using the macro, on intersection with a plane at a distance of 80cm, and checked for uniform distribution. For a run of 100 000 histories, the standard deviation of the number of particles within each of one hundred equally sized squares was 4 percent of the mean. An outline of the macro is given in Figure 5.3, where UIN, VIN and WIN are the initial direction cosines of the incident particle.

```
select random numbers RANDIR1 and RANDIR2
use RANDIR1 to select COSTHE over allowed range
determine SINTHE from COSTHE
use RANDIR2 to select PHI (0-2pi)
find cos(PHI) and sin(PHI)
set UIN, VIN and WIN
(UIN = SINTHE × COSPHI, VIN = SINTHE × SINPHI, WIN = COSTHE)
```

Figure 5.3 : Form of macro used to produce a diverging beam.

5.5.2 Energy spectrum

The project required simulation of diagnostic X-ray spectra, and this necessitated using particles of variable initial energy. The spectral data used were generated using a program developed from the Birch-Marshall spectra generation program (Birch & Marshall, 1978). These spectra were developed according to a semi-empirical model, and were shown by the authors to give very good agreement with measured spectra. Their spectra have been widely used, and form the basis of the Hospital Physicists' Association handbook of spectral data (Birch *et al*, 1979). Other spectra have been published since the start of this work (Tucker *et al*, 1991) which have been demonstrated to give close agreement with measurement, and discrepancies with the Birch and Marshall model. Bissonnette and Scheiner (1991) carried

out a comparison of the two models and found that although the Tucker model had some advantages, the differences between the spectra were not very significant.

Code was written to select the initial energy of a particle according to the probability distribution of the appropriate beam spectra. The beam spectra data is stored in a separate data file and, as part of the initialisation procedure, the data from this file is read into an array (IRAWDATA), which then contains the number of photons at each energy, in 1 kV steps. A second array (ISUMDATA) is then set up to contain cumulative totals of photons at each energy

$$ISUMDATA(I) = ISUMDATA(I-1)+IRAWDATA(I).$$

and this array is then normalised to give the array SPECTRUM. A macro is then used to select the input energy by comparing a random number with this array. An outline of this macro is given in Figure 5.4. This macro is then called to determine the initial energy of each new particle in the simulation.

```
select random number RANDX
compare RANDX with each element of SPECTRUM
  until RANDX > SPECTRUM(IENERGY)
set input energy to IENERGY/1000
  (gives energy in MeV)
```

Figure 5.4 : Form of macro used to produce a spectrum of input energies

This macro was tested by running simulations in which particles were generated using the macro, and the initial energies selected were recorded. The distribution of these energies was then compared to the original Birch-Marshall spectra, and for 100 000 histories the mean difference between photon numbers at each energy was 2.8%.

5.6 Modifications made to EGS4

5.6.1 Simulation of K-edge fluorescence in compounds and mixtures

The optional subroutines included in EGS4 which may be used to track the production and paths of K-edge fluorescence particles are only valid for elements. They consist of an independent subroutine which sets up the branching ratios and fluorescent photon energies,

and a modified version of the subroutine controlling photoelectric interactions. A flag (IEDGFL) is used for each medium, which is set to the appropriate atomic number, or to zero to disable K-edge fluorescence. When a photoelectric event is selected during tracking of a photon history this flag is checked and, if the flag is non-zero and the photon energy is above the binding energy of the element, a random number is used to determine whether interaction occurs with the K-edge electron and whether fluorescence or the Auger process occurs. Any fluorescence photon created is added to the particle stack and treated as a new particle.

The planned simulations, however, involved the use of compound screen phosphor materials in which K-edge fluorescence was likely to be an important feature, as contrast and background were determined from energy absorption in the phosphor. The code was thus extended to account for K-edge fluorescence in mixtures and compounds. The extension to the code involved making IEDGFL a two dimensional array, to allow for up to three elements in each media. Subroutine PHOTO was further amended to include an initial step of determining with which type of atom within the media the photon is to interact, and then proceding with that element as in the default K-edge treatment. Determination of the atom with which interaction was to occur was according to its proportion by weight. The modifications required are outlined in Figure 5.5.

```
define EDGFL to be three dimensional array
set ATPROP to be proportions by weight of each
  type of atom in compund
set CUMPROP to be cumulative proportions of
  above
IN PHOTO compare random number RAND to CUMPROP to
determine which atom has been hit
check IEDGFL to see whether fluorescence occurs
```

Figure 5.5 : Outline of code used to track K-edge fluorescence in compounds

5.6.2 Testing of K-edge fluorescence

The treatment of K-edge fluorescence was tested by carrying out simulations of X-ray absorption in phosphor materials and comparing the results with published data. A summary of the results obtained is given in table 5.1, and good agreement was observed between the Monte Carlo results obtained here and those given elsewhere (Venema, 1979; Marshall *et al*, 1996).

Energy	Phosphor	Percentage energy absorption	
		Monte Carlo	Published data
80 kVp	Gd_2O_2S	41.1	37.7*
80 kVp	LaOBr	41.7	41.5*
100 kVp	Gd_2O_2S	5.5	5.7†

Table 5.1 : Comparison of energy absorption in phosphors with results of Venema* and Marshall†

5.6.3 Modifications to PEGS code

As a further test of the K-edge fluorescence code, simulations were also carried out of the absorption of monoenergetic X-rays by phosphor materials at a series of energies, in 1 keV steps around the K-edge. These results were used to check that the K-edge was being determined accurately, as the K-edge is marked by a sharp rise in absorption. The initial results revealed an inadequate resolution of photoelectric cross-section at the K-edge. This was due to the way in which the PEGS code interpolated between a limited number of points when determining cross-section data. The PEGS code was modified so that the energy of the highest K-edge in the media was forced to be an interval boundary, and the cross-sections immediately each side of this boundary were used for the interpolation of the intervals on either side. This effectively split the data fitting procedure into two parts, one above and one below the K-edge, and yielded good resolution of the cross-section data, as demonstrated by the Figures in Table 5.2 which shows the percentage absorption of monochromatic X-rays of different energies in a gadolinium filter (k edge 50.229 keV).

Energy (keV)	Absorption
49.0	25.9%
50.0	24.9%
50.1	24.8%
50.2	24.7%
50.3	80.2%
51.0	78.9%
52.0	77.0%

Table 5.2 : Absorption of monochromatic x-rays in gadolinium, using modified EGS code

5.6.4 Changes in Precision

During initial test simulations it was apparent that calculations of contrast were being adversely affected by the precision to which numbers used in the calculation were being stored. The precision of variable EDEP, which is used throughout the program to store the amount of particle energy that is about to be deposited, was increased to DOUBLE_PRECISION, by means of a macro called in the user program. This could then account for smaller differences in energy deposition in different parts of the screen.

5.7 Definition of Geometry

The geometry defined in the usercode is shown in Figure 5.6. This assumes a point radiation source at coordinates (0,0), with radiation incident along the z-axis. Six infinite planes, perpendicular to the z-axis, are defined (depicted with numbered triangles), and one cylindrical surface, to give the ten regions shown (depicted with numbered circles). Region 2 represents a filter, of variable thickness (TFILT) and composition and regions 1, 3 and 7 are air at standard temperature and pressure. The patient is represented by a slab of tissue, comprising regions 4, 8 and 9, enclosing region 10, a cylinder of contrast material of variable radius (RCONT). The thickness of tissue (TBODY) and depth (DCONT) and thickness (TCONT) of contrast are variable, as are the compositions of the two regions. Region 5 represents the table on which the patient is lying, and may be set to zero thickness

(TGAP) if the patient is in direct contact with a film cassette. Region 6 represents the screen phosphor of a film cassette or intensifying screen, of thickness TPHOS.

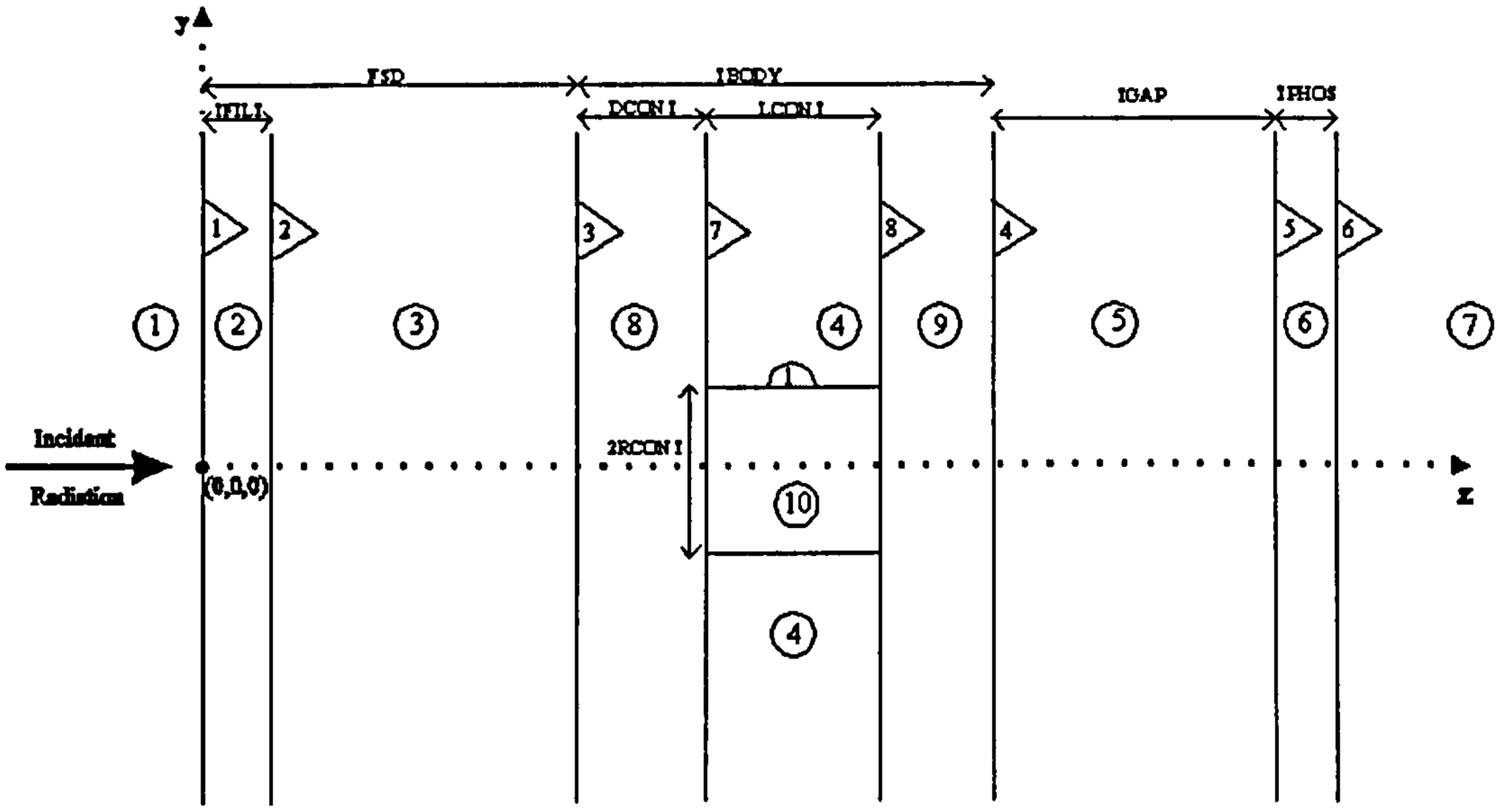

Figure 5.6 : Geometry used in simulation; as defined by subroutine HOWFAR

This simple geometry was chosen for ease of development, reproducibility under laboratory conditions and for a reasonable speed of simulations. As the study was designed to make comparative rather than absolute measurements of dose in the various regions, the possible effect on the results of a non-anthropomorphic model was outweighed by the large number of simulations that could be carried out. The biggest deviation from a true patient geometry was the use of semi-infinite planes throughout, which means that the loss of scattered radiation from the sides of the patient is neglected. However, for a small field-size toward the centre of the patient, this is a small effect and for the comparative measurements carried out in this work, the approximation should not significantly affect results. The single geometry illustrated was used throughout the study and, by varying the distances between planes and the composition of the different regions, a wide range of simulations could be carried out.

5.7.1 Simulation input

For each simulation carried out, the specific values of the geometry parameters were specified by means of an input data file. The format of this file is given in Figure 5.7, where the distances as defined in Figure 5.6.

```
random number seed
beam angle
filter, tissue, contrast, phosphor, gap
Z values for filter fluorescence
Z values for contrast fluorescence
Z values for phosphor fluorescence
particle splitting parameter
TFILT, FSD, TBODY, TGAP, TPHOS, TCONT, RCONT, DCONT
number of histories
```

Figure 5.7 : Format of input file for Monte Carlo simulation

the 3rd line of the input file contains the definitions of media type in the different regions, and the 'fluorescence' lines contain the atomic numbers of up to 3 constituent elements for which K-edge fluorescence is to be simulated in the stated media. The 'particle splitting parameter' is for variance reduction, and will be described later, in section 5.9.

5.8 Extraction of results

A number of parameters were required from the simulation, in order to study optimisation of patient dose and image contrast. The energy imparted to the patient corresponded to the energy absorbed in the whole of regions 4, 8 and 9. An assessment of entrance surface dose was made from the energy absorbed in region 8, within a depth of 1 cm from the body surface, and a radius of 1 cm from the central axis. Calculation of contrast and background density was made from the energy absorbed in region 6 at different spatial coordinates. All these quantities were easily calculated by summing any particle energies deposited in the appropriate region. All of the above parameters were recorded for each simulation, along with the input parameters. The code used for keeping track of the required parameters, as found in the AUSGAB subroutine, is outlined in Figure 5.8, where variable *EDEP* contains

the value of the current particle energy that is about to be deposited as part of the interactin process.

```
implement whenever energy EDEP is about to be
  deposited
if in region defining patient, increment absorbed
  energy by EDEP
if within 1cm of patient surface & inside 1cm
  radius disk, increment entrance dose by EDEP
if in screen & behind contrast area, increment E_cont
  by EDEP
if in screen & within background area, increment E_bak
  by EDEP
```

Figure 5.8 Code used for defining scoring quantities

5.9 Variance reduction

One of the fundamental problems in the use of Monte Carlo techniques is that of balancing the need for statistical accuracy (*ie* using a large number of particles to calculate a result) with reasonably short processing times. Variance reduction is the name applied to a variety of techniques that are used to improve the statistical accuracy of Monte Carlo simulations while minimising the increase in simulation time. Techniques available include, among others, exponential transformation of photon path length, which can be used to increase information in the build-up region, enhanced cross-sections to make the probability of an interaction more favourable, range rejection of electrons, where the tracking of an electron stops once its residual range is smaller than the distance to the nearest boundary, and particle splitting. These methods are described fully by Rogers and Bielajew (1990) and Nelson *et al* (1985). For this work, the method of particle splitting was employed.

Particle splitting is useful in regions where only a small number of particles are incident, or where important parameters are being scored. The technique involves turning single particles into multiple particles with identical properties but reduced *weight*. For example, a photon with *weight* 1 might be split into ten identical photons each with *weight* 0.1. The weighting

factor of a particle is then taken into account when scoring parameters such as the energy absorbed in a region, so that numerical results are not biased. The increased number of particles improves the statistical accuracy of quantities to which they contribute, as variance of a quantity is inversely proportional to the number of particles used to score the quantity. As the particle splitting is only carried out for specific regions, the increase in simulation time is far less than it would be if the total number of histories had been increased by the same factor.

For this series of simulations, particle splitting was carried out in region 10 (the small area of contrast) and region 6 (the screen). This ensured that the accuracy of parameters scored in these areas was comparable to that in other regions.

5.10 Accuracy of Code

There are many factors influencing the accuracy of the results obtained from a particular Monte Carlo simulation. These are uncertainties arising from the data used, systematic errors and statistical uncertainties.

All results are limited by the quality of cross-sectional data used by the code. For the simulations performed during this study, electron cross-sections have far less impact than the photon cross-sections, because of the low energy range employed, so their accuracy is not discussed here. For photon interactions, the uncertainty in total cross-section ranges from 2-3% where Compton interactions are dominant to 3-5% when photoelectric interactions dominate (Storm and Israel, 1970, Hubbell, 1982). The latter is for lower photon energies, upto around 30 keV for carbon, greater for higher atomic number elements. The way in which these uncertainties affect the final results can be complex and cannot be quantified exactly.

Systematic errors may arise from programming errors, that may still occur in spite of the extensive checking that codes such as EGS4 have received, modelling inaccuracies such as approximations in electron transport algorithms, or truncation errors resulting from the finite

precision with which the computer represents real numbers. Systematic errors need to be identified and removed or reduced as far as possible. One way in which this has been done for this study was the increase in variable precision described earlier (section 5.6.4). The possibility (albeit slight) of undiagnosed systematic errors is one reason for carrying out experimental verification of any particular usercode, to supplement the range of benchmark tests available.

Statistical uncertainties in Monte Carlo results are commonly obtained by calculating the best estimate of the variance of the mean of a quantity, by carrying out a number of independant runs, each with the same number of histories. If N runs are performed to estimate quantity x, and a normal distribution is assumed, this estimator s^2 of the true variance σ^2 is given by

$$s^2 = \frac{1}{N\,(N\,-1)} \sum_{i=1}^{N} (x_i - \langle x \rangle)^2 \qquad (5.1)$$

If it is also assumed that individual run estimates are drawn from a normal distribution then, in the limit of a large number of histories (n), the quantity $n\sigma^2$ is constant. Thus the estimated uncertainty in a calculation is roughly proportional to the inverse of the square root of the number of histories used.

$$\sigma \propto \frac{1}{\sqrt{(n)}} \qquad (5.2)$$

This can be used to assess the precision of a result from a series of runs taken with fewer histories. For the work carried out here, statistical uncertainty was calculated for each quantity of interest using 10 independant runs of 50,000 histories each. These were than used to assess the statistical uncertainty in the results obtained from the longer simulations used for the study.

5.11 Summary of chapter

The principles and brief history of Monte Carlo techniques were introduced in this chapter, along with a summary of some of the codes available. The reasons for using EGS4 were

outlined, and the structure and implementation of this code fully described, including the input required. Modifications made to the code for the purpose of this work, namely the extension of K-edge fluorescence treatment, increased precision of variables and the improved resolution of cross-section data at energies around a K-edge, have also been explained. The development of usercode to simulate a divergent beam with a spectrum of energies has been described, along with the simulation geometry and the method for obtaining the required results. The variance reduction techniques used and factors influencing the accuray of the results have been presented at the end of the chapter.

Chapter 6

Results from Monte Carlo Simulation

The first section in this chapter presents the numerical uncertainties for the calculated quantities obtained from the simulations. The results from the simulations carried out are then presented in detail, according to the flow diagram in Figure 6.1.

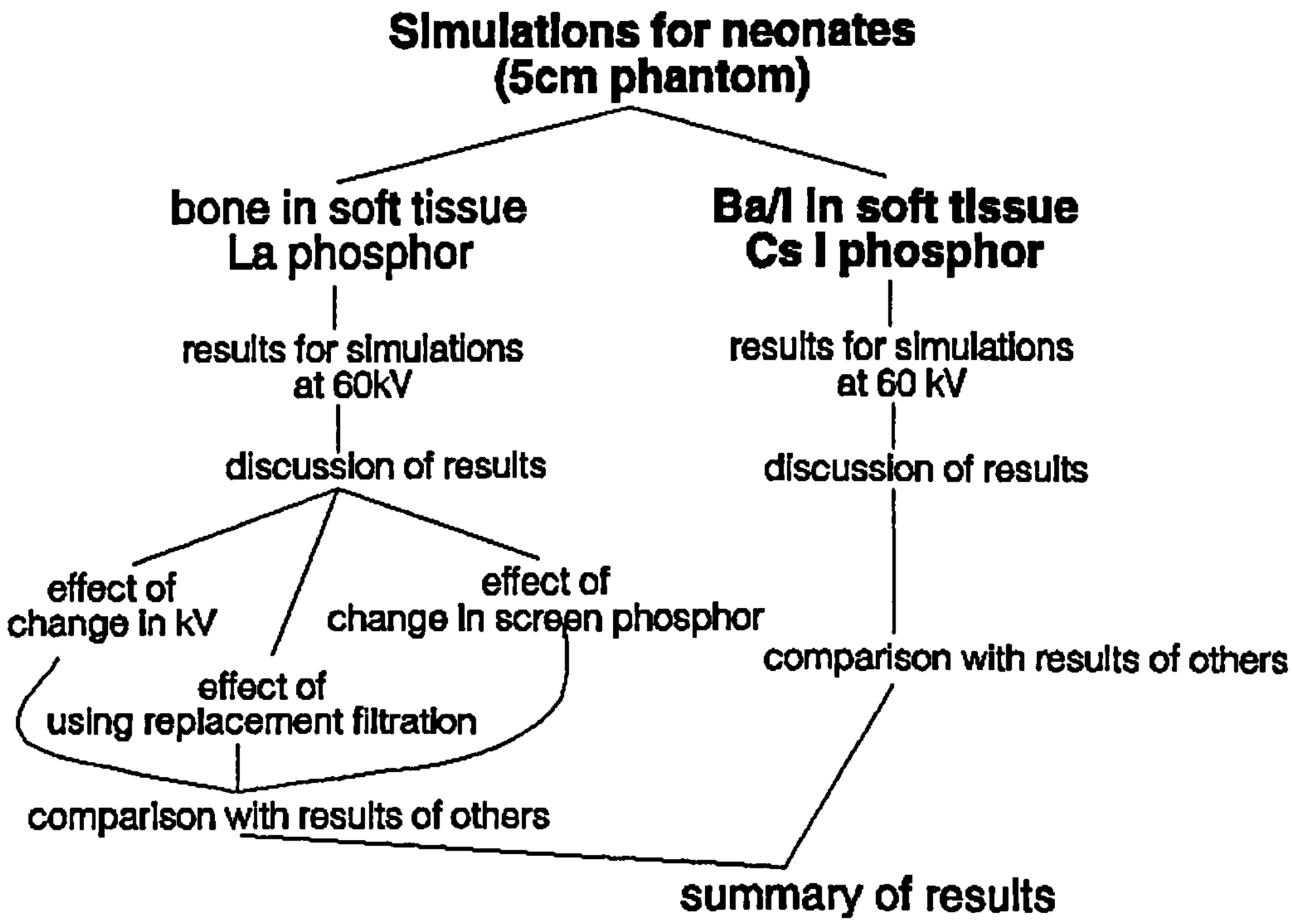

Figure 6.1 : Outline of chapter

All the results presented in this chapter are for a 5 cm phantom (a neonate) and for 2 categories of examination; radiography of bone in soft tissue and fluoroscopic examination involving iodine or barium based contrast media. The radius of the contrast cylinder was 1cm and all simulations were carried out with a FSD of 80 cm and no air gap *ie* direct contact between slab phantom and phosphor. The radiography of bone in soft tissue is considered first, and results presented for simulations carried out at 60 kV. These results are then

discussed in terms of the beam spectra used and the absorption and transmission characteristics of the various media simulated. The effect of a number of modifications in the simulation model are then presented and discussed; changes in tube voltage, the use of partial replacement filters instead of additional filters and changes in the screen phosphor used as the image receptor. The results from this category of simulations are then compared to results available from published literature. For the fluoroscopy simulations, results are presented for a number of mass thicknesses of contrast media, for beams generated at 60 kV and using a caesium iodide (CsI) phosphor. These results are also discussed in the light of the beam spectra produced by the various filters, and the absorption characteristics of the contrast media and image receptor. Results obtained from published literature are again used to compare those obtained here, and the chapter concludes with a summary of all the results that have been presented.

6.1 Calculation of uncertainties

Random uncertainties have been derived as described in Chapter 5, section 5.10 for each type of simulation carried out. Values of the uncertainties were calculated for each quantity of interest *ie* entrance dose, absorbed dose and contrast, though values for absorbed dose are small compared with the other two, due to the relatively high number of photons contributing to its measurement, even with the variation reduction techniques employed. Details of the batched runs used to calculate the standard error of the mean are summarised in Table 6.1 below, where the variance *s* is determined from equation 5.1.

simulation set	number batches (N)	number histories / batch (n)	estimator of variance s (for n histories)				backg'd value
			abs.en	ent.dose	contrast	backg'd	
radiography	10	50 000	0.14%	4.4%	3.3%	0.15%	405
fluoroscopy	10	10 000	0.22%	8.2%	6.1%	0.66%	43

Table 6.1 : Derivation of uncertainties in calculations

For the actual simulations, the standard errors of the mean of each dose quantity were calculated from the relative number of particle histories involved in the sample and the actual

simulations, according to equation 5.2. The figures in Table 6.1 were calculated for reference beam conditions, and so simulations involving additional filtration would be expected to have greater uncertainty than that predicted from consideration of the number of histories, as the filter reduces the number of photons contributing to the calculated quantities. Similar derivation of uncertainties for the most beam hardening filter simulated (0.2 mm erbium) gave uncertainties a factor of 2 higher than those given in Table 6.1, but this was compensated for by increasing the number of histories for the higher beam filtrations. For contrast, the uncertainties could be more accurately expressed by applying equation 5.2 to the number of photons reaching the image receptor, which is related to the energy absorption in the 'background' area of the phosphor. The uncertainties in ratios of dose and contrast were determined from summing the individual uncertainties in quadrature. The uncertainties derived for the different category of simulations performed are listed in Table 6.2 below, within 95% confidence limits (*ie* two standard errors of the mean). In this table, the contrast uncertainties are given in terms of the calculated background, as described above, along with values calculated for the minimum and maximum background values obtained in each of the two sections of the study.

	uncertainty for 10^6 histories		uncertainty in contrast		
	abs.energy	ent.dose	general	minimum	maximum
radiography	± 0.06%	± 2.0%	± 132% / √bkgd	± 0.9% (bkgd 20 000)	± 2.4% (bkgd 3000)
fluoroscopy	± 0.04%	± 1.6%	± 80% / √bkgd	± 0.9% (bkgd 8000)	± 2.5% (bkgd 2000)

Table 6.2 : Values of uncertainties used in calculations

6.2 Radiographs of bone in soft tissue

The first series of simulations was carried out for a 1cm thick bone detail in 5cm soft tissue, to simulate plain film radiography of a premature neonate, using a lanthanum based screen similar to those commonly in use on the local special care baby unit. Figure 6.2 shows the variation of contrast, entrance surface dose and total energy absorbed in the patient with

increasing tube load (corresponding to different filter thicknesses) for aluminium filtration. Graphs are shown for generating tube potentials of both 60 and 70 kV. For these plots, the total filtration ranged from 1.5 mm to 6 mm aluminium. Tube load can be defined as the product of tube current, exposure time, and generating potential. In this figure, however, all data has been normalised to that for a total filtration of 3 mm aluminium at the tube potential used *ie* in Figure 6.2(i) a tube load of 1.0 corresponds to 3 mm Al at 60 kV and in Figure 6.2(ii) a tube load of 1.0 corresponds to 3 mm Al at 70 kV. The tube load is then effectively proportional to mAs, which is related to the number of input photons used in the simulation. Measurements of entrance surface dose have been left in terms of energy absorbed in the appropriate region, rather than converting to conventional units as the values are for comparative purposes only. The error bars shown in the graphs represent ± two standard errors, calculated as described above. Those for values of absorbed energy are of the same magnitude as the data points themselves. The lines drawn on this and all subsequent graphs should be viewed as trend indicators, enabling multiple graphs to be viewed. They are not accurate curve fits to the data and, in some cases, it would be possible to draw slightly different shaped curves with equal validity.

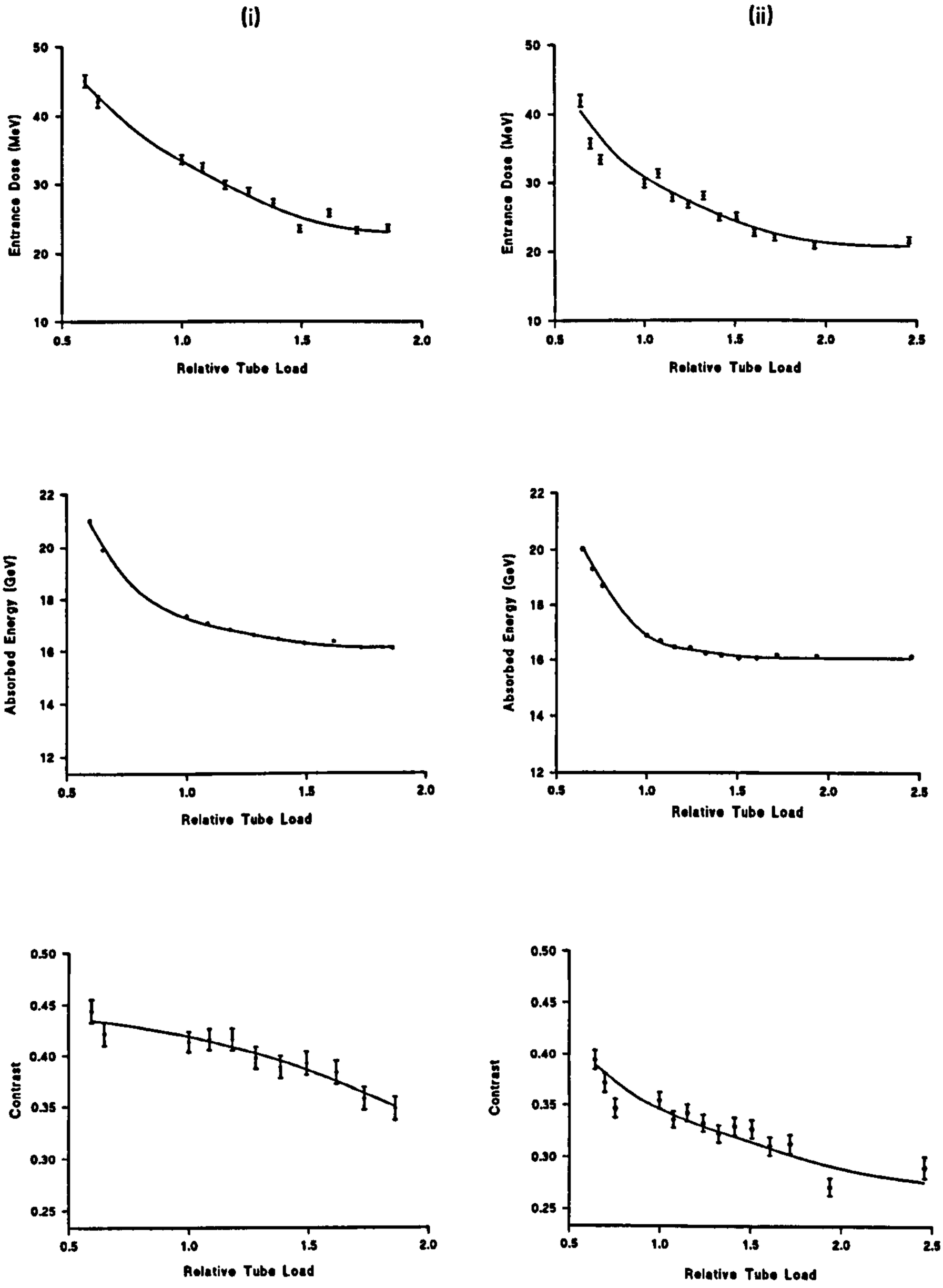

Figure 6.2 : Trends in dose and contrast for different thicknesses of aluminium filtration (i) at 60 kVp and (ii) at 70 kVp

It can be seen from the graphs that, as expected, each dose quantity decreases with increasing tube load, for both generating potentials. However, while entrance surface dose drops fairly steadily as the amount of filtration is increased, the corresponding plots for absorbed energy

show an initial sharp decrease followed by a flattening of the curves, above a tube load of around 1.0. This effect is more marked at the higher tube potential, and suggests that increasing the amount of aluminium filtration beyond 3 mm is an inefficient method of patient dose reduction. Numerically, at 70 kV the absorbed energy for a tube load of 1.5 is 95% of that at tube load of 1.0, whereas the entrance surface dose is 84% of that at tube load 1.0. At 60 kV, the figures are 94% and 70% respectively. From this it can be seen that filtration affects entrance dose more dramatically than absorbed energy, and that the reduction in absorbed energy is similar for the two tube voltages. The dose values illustrated for different values of tube voltage have been normalised to different background densities, each corresponding to that obtained for 3mm aluminium at the relevant tube voltage, so should not be directly compared. The plots of contrast against tube load show a gradual decrease with increasing amounts of filtration, and at 70 kV the contrast values are all significantly lower than at 60 kV as the beam energy is higher.

Similar curves were plotted for the other filters under investigation, in order to compare their behaviour. For ease of comparison, data for the different filters is displayed on the same graph, omitting the individual data points and error bars for clarity. Initially, three different filter thicknesses were simulated for each material, but additional simulations of intermediate thickneses were then performed for a selection of filter materials for which initial results were of particular interest, so that the number of data points used to generate each curve ranged from four to ten depending on the filter material. The data points correspond to the filter thicknesses listed in Table 4.1.

6.2.1 Dose variation for different filter materials

Figure 6.3 shows entrance surface dose and absorbed energy data for ten filters, including aluminium, using a generating potential of 60 kV. Reference conditions were taken to be 3 mm aluminium at 60 kV, and all other filters were used in conjunction with 3mm aluminium. This baseline filtration was chosen as it is representative of the total filtration found on X-ray sets around the local region.

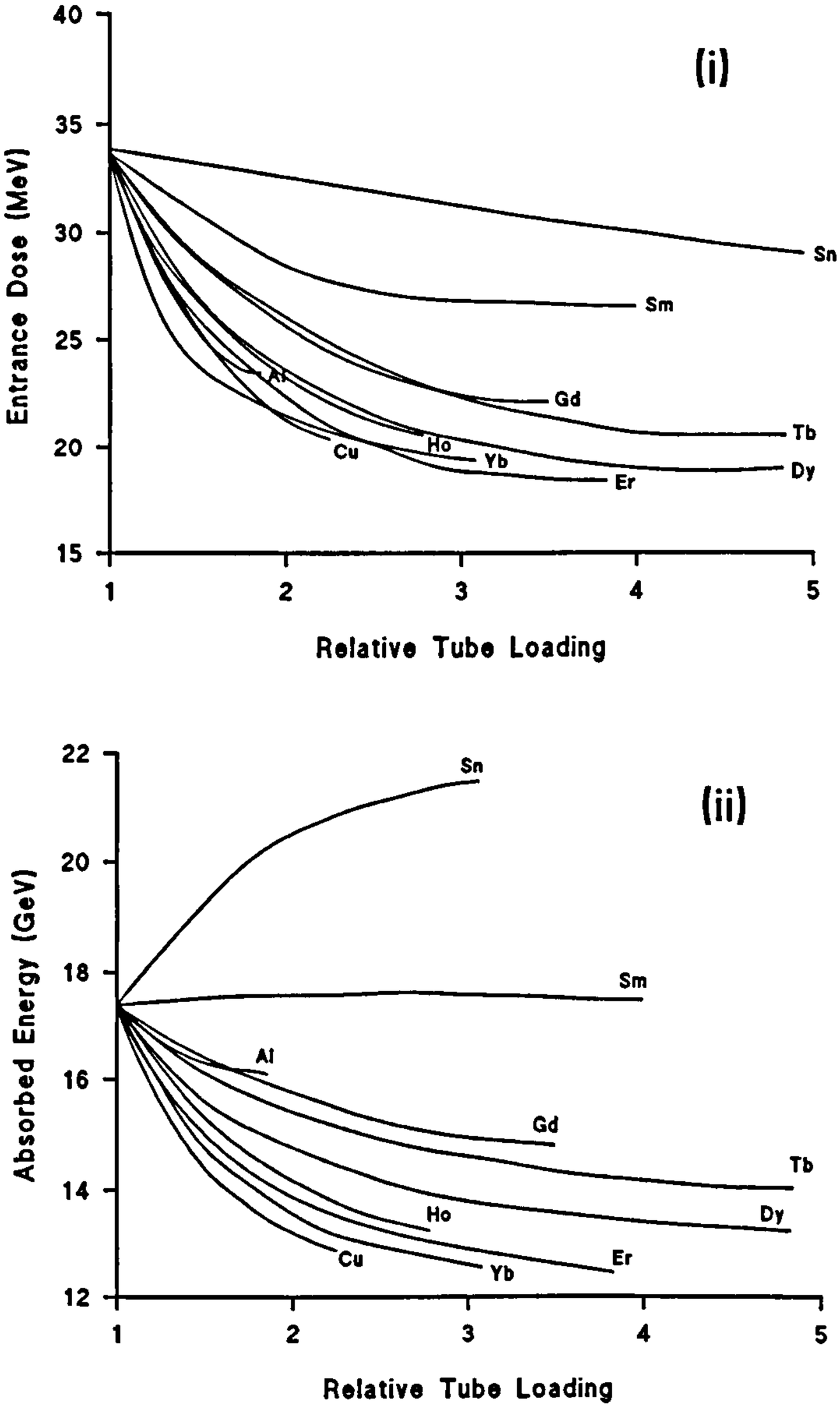

Figure 6.3 : Trends in (i) entrance surface dose and (ii) absorbed energy with increasing tube load for different filter materials at 60 kV

Several features are apparent from the above graphs. The first of these is the behaviour of the absorbed energy curve for the tin filter. Unlike the other curves displayed, this shows an increase in dose with filtration, up to 124% at a tube load of 3. The corresponding curve for samarium is almost flat, and all other filter materials show a gradual decrease in absorbed energy with tube load. The rate of dose reduction (described by the gradient of the curves) is dependant on the atomic number (Z) of the filter. Copper gives the greatest rate of dose reduction (absorbed dose is 83% of the reference level at a tube load of 1.5 and 76% at tube

load of 2), and aluminum one of the poorest (around 94% reference level at a tube load of 1.5) - an interesting result considering that it is the most widely used filter material for diagnostic X-ray sets. The curves for entrance dose reduction show less variation with atomic number, and a decrease is seen with increasing tube load for all filter materials, albeit a slight one for tin and samarium. The apparent crossing of some of the curves shown in Figure 6.3 is likely to arise from the magnitude of the uncertainties in the points plotted. Entrance dose reduction is of the order of 35% at a tube load of 2 for the majority of filter materials (*ie* entrance dose with additional filtration is 65% reference level). The Z-dependance of the dose reduction is depicted in Figure 6.4 where absorbed energy has been plotted as a function of Z for tube loadings of 1.5 and 2. The dashed lines in these plots join data points for which intermediate values cannot be deduced from the graph. A useful extension to this work would be obtain similar results for filter materials such as yttrium (Z=39) and niobium (Z=41) to characterise this part of the graph. The form of this graph will be considered in section 6.2.3.

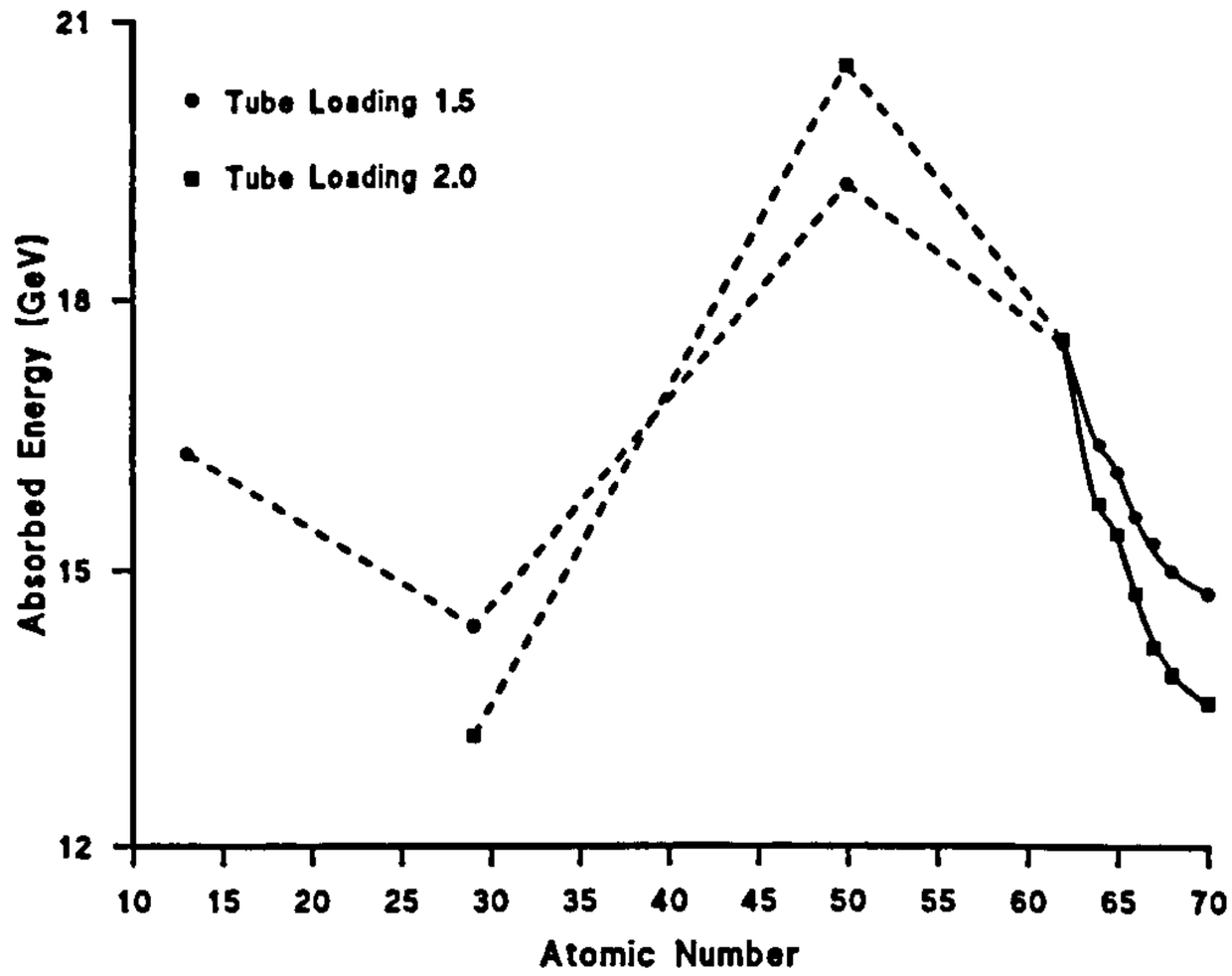

Figure 6.4 : Z-dependance of the calculated absorbed energy at fixed tube load (60 kV)

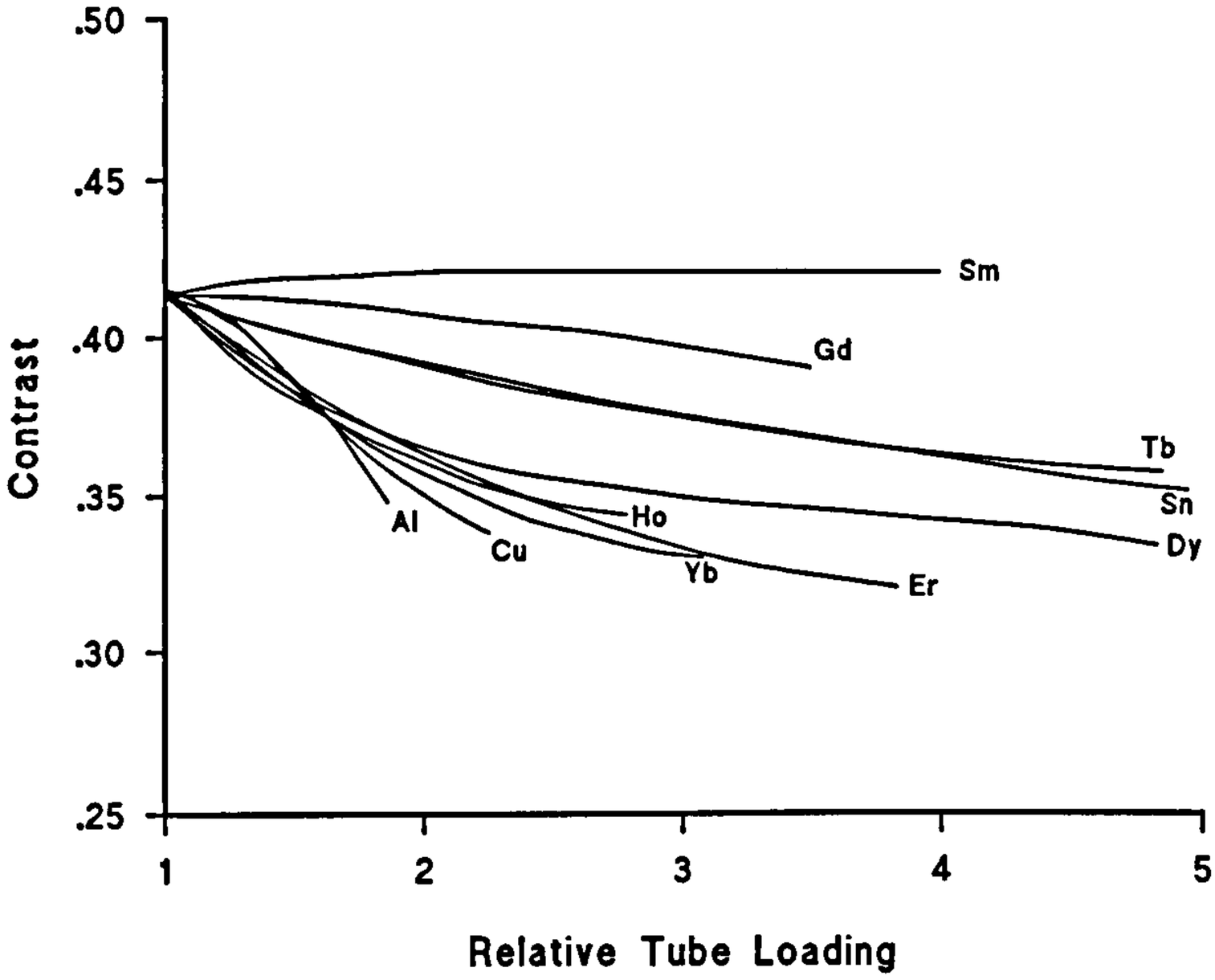

Figure 6.5 : Trends in calculated contrast with increasing tube load for different filter materials (60 kV)

6.2.2 Contrast variation for different filter materials

Curves were also plotted showing the variation of contrast with tube load, as shown in Figure 6.5.

In most respects these curves show similar trends to those for the dose variation illustrated in Figure 6.3; filters exhibiting a rapid rate of dose reduction with tube load also show a rapid reduction in contrast, as might be expected as the beam energy affects both dose and contrast in the same way with higher photon energies giving lower doses and lower contrast. The contrast reduction is of the order of 15% for copper, and 6% for terbium, at a tube load of 2.0. However, tin shows a reduction in contrast in addition to its poor dose performance, confirming it as a bad choice of filter material, and the curve for aluminium drops off steeply after a tube load of around 1.5. A full discussion of these effects is given in the next section. For small tube loads, most of the curves lie close together, within ±9% of the mean value at a tube load of 2 with most curves flattening off after this point. The crossing of some of the curves is again due to the magnitude of the uncertainties in the values. It should be noted that

the similarity of the contrast curves suggests that a choice of filter may be based primarily on its dose reduction properties. The Z dependance of the calculated contrasts is illustrated in Figure 6.6 for tube loads of 1.5 and 2.

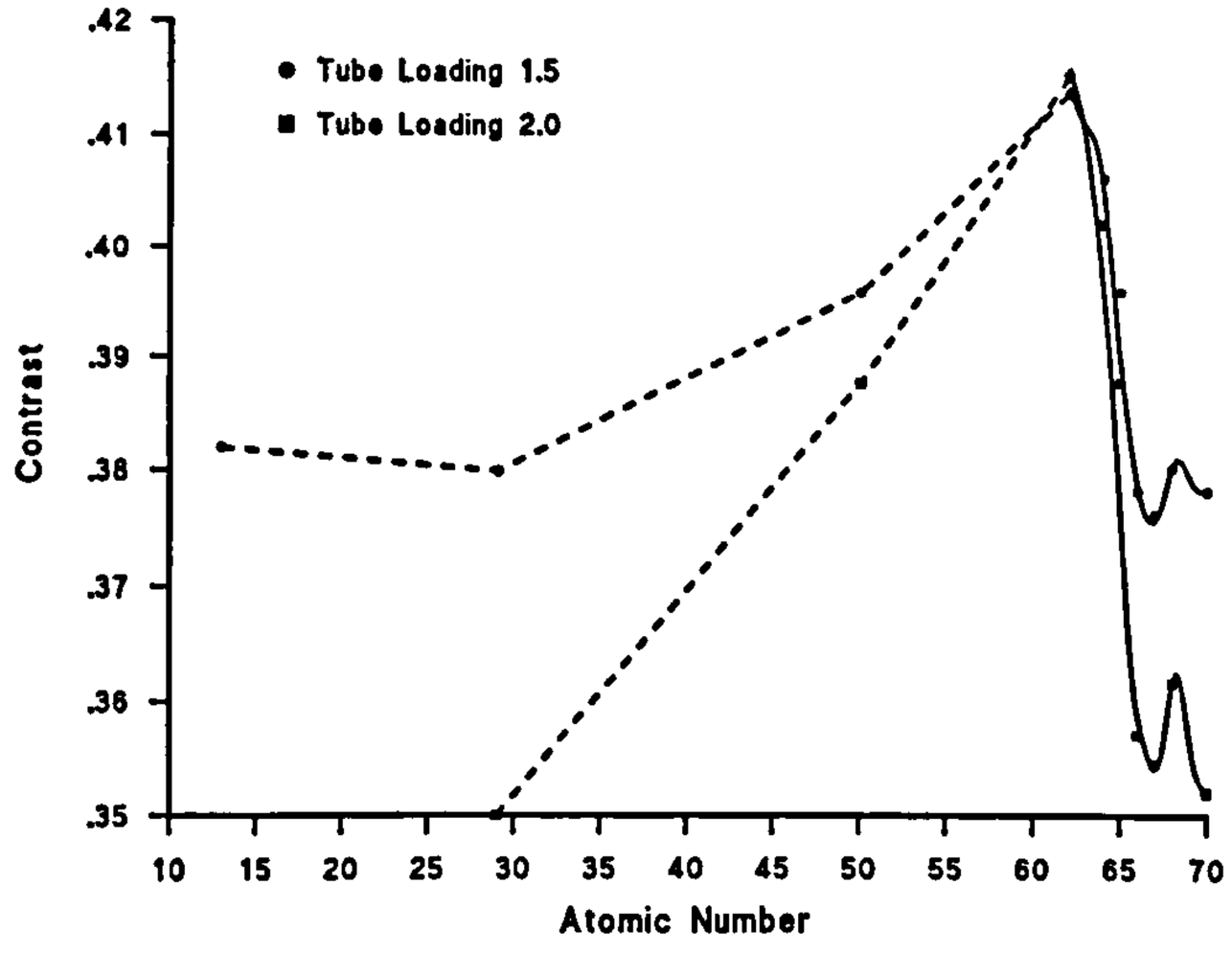

Figure 6.6 : Z-dependance of contrast at fixed tube load (60 kV)

A slight rise in contrast is apparent from the graph for Z = 68 (erbium) but this is only of the order of 2% and, as can be seen from Figure 6.5, the curves all lie close together at this point.

6.2.3 Discussion of results

Much of the performance predicted by the simulations can be explained by considering the spectra of the beams incident on the patient phantom for the different filtration conditions, and the absorption and transmission characteristics of the materials in the beam. All absorption and transmission spectra illustrated in this section have been produced using software based on Birch Marshall data, as described previously in Chapter 5, section 5.5.2. The absorbed spectra for a 60 kVp beam, filtered by 3 mm aluminium (*ie* the reference spectrum), passing through a 5 cm patient phantom is given in Figure 6.7. This is representative of energy absorption in the patient and shows a peak at around 28 kV. Beam

spectra produced by various additional filters are shown in Figure 6.8. The poor performance of tin as a filter material is readily explained by its transmission spectrum (Figure 6.8vi), which is dominated by its K absorption edge at 29.2 keV. This coincides with the absorption peak in the phantom and so a large proportion of the tin filtered beam will contribute to the absorbed energy in the patient. Increasing thicknesses of tin give an increasingly large K-edge peak and thus, for the same background energy absorption, the absorbed dose to the patient increases with increasing tin filtration.

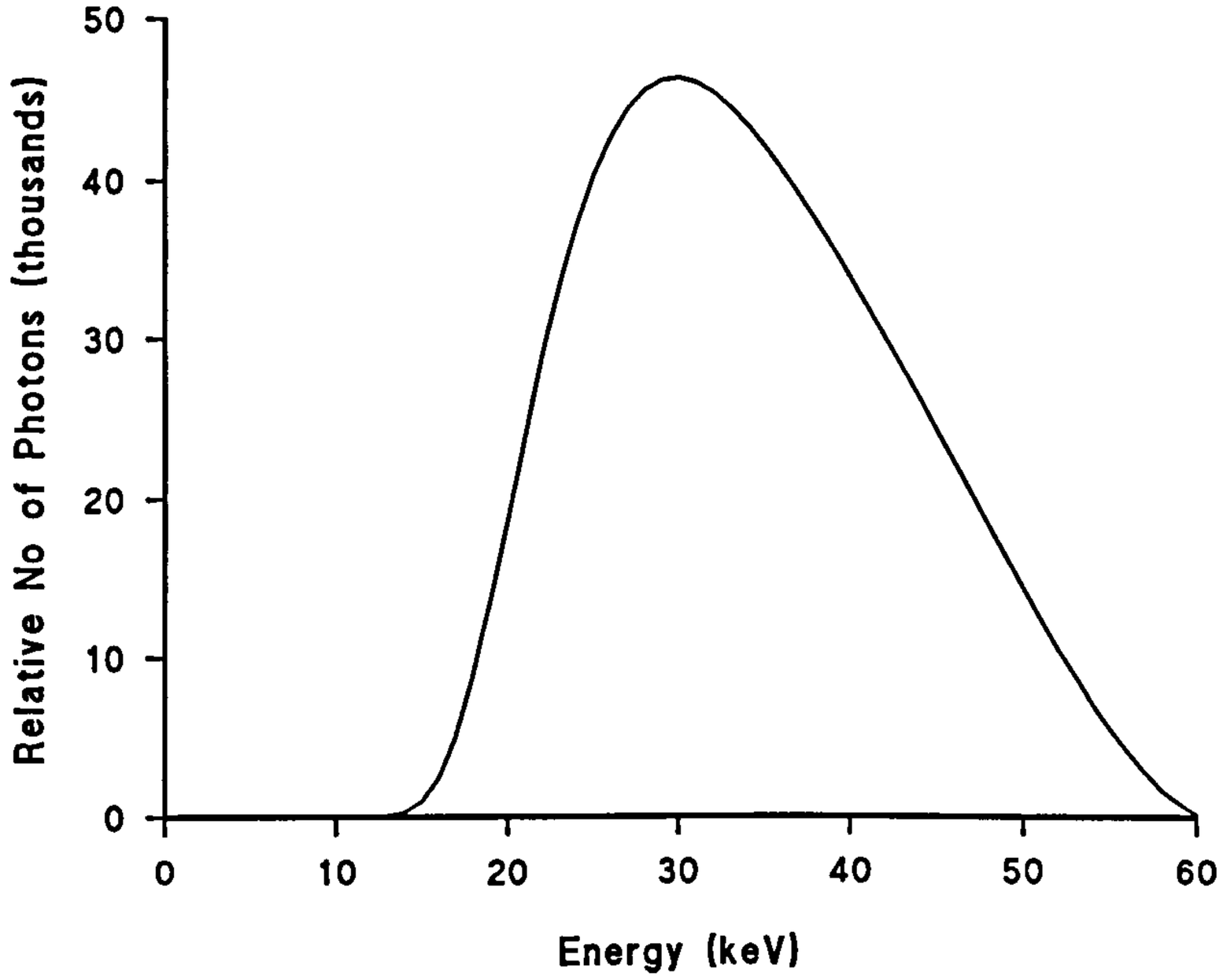

Figure 6.7 : Energy absorption in 5cm patient phantom for 60 kV beam filtered by 3 mm Al

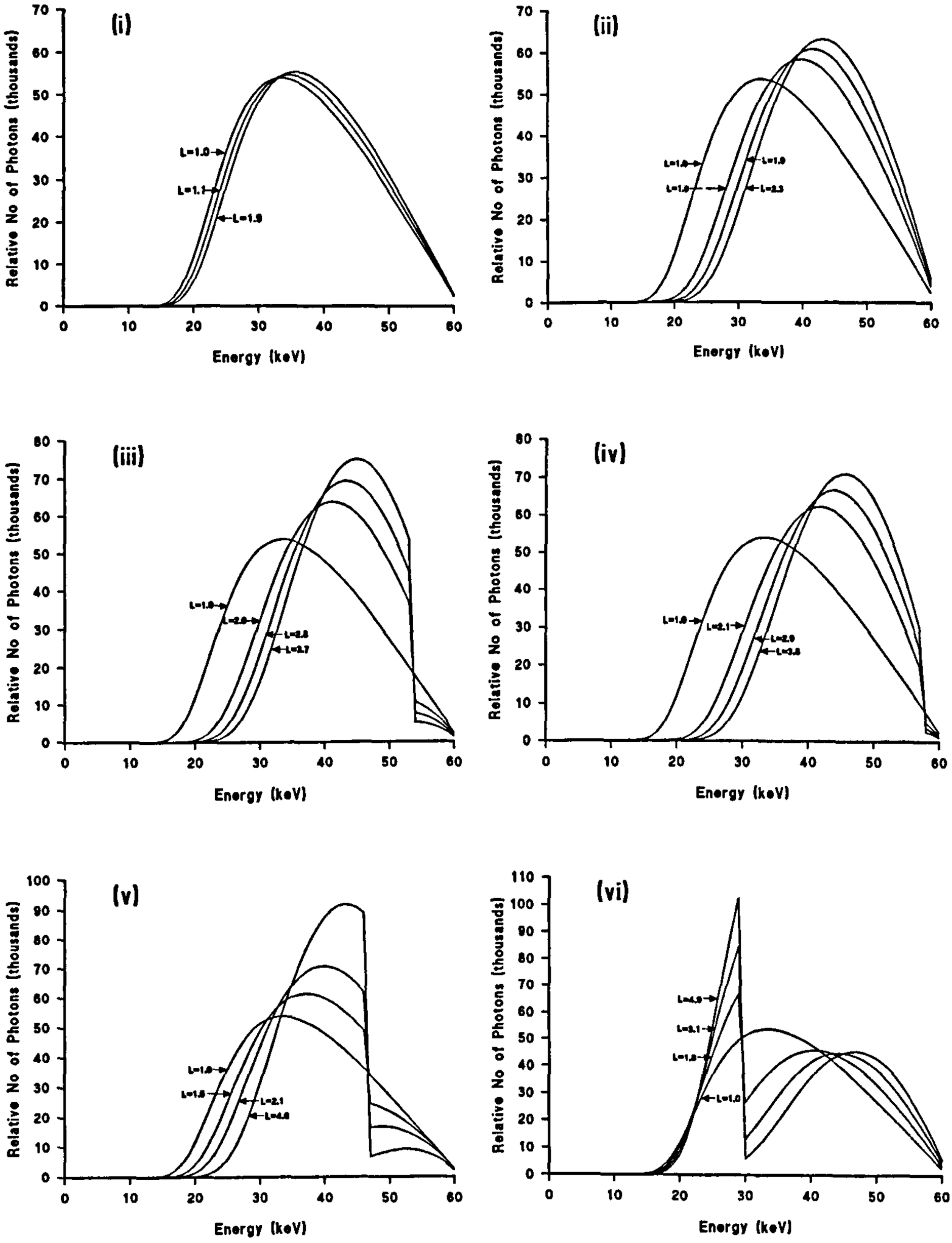

Figure 6.8 : Beam spectra, relative tube load L, for 60 kVp with added filtration of (i) aluminium (ii) copper (iii) dysprosium (iv) erbium (v) samarium and (vi) tin : reference spectra (tube load = 1) 3mm Al

For the materials with Z from 62 to 70 the transmitted spectra peak at progressively increasing energy, as the K-edge energy increases, which results in a higher mean photon

energy as given in Table 6.3. The effect of photon energy on dose has already been discussed in general terms (section 4.2) and the theory of lower dose with higher energy is followed for the mean beam energies observed here. This results in progressively greater dose reduction, for equal tube load, as the mean photon energy increases and this has the effect of reducing dose under conditions of equal background density. Table 6.3 lists mean spectral energies for all the filters illustrated in Figure 6.8, together with tube loads. The transmission curves for copper (Figure 6.8ii) show a broader spectrum, as the K-edge energy is not high enough to influence the shape of the beam, and as the highest energy photons are attenuated less, the mean energy of the spectrum is higher than that for the K-edge filters, at the same tube load, making it a particularly good filter for dose reduction.

Filter (all + 3mm Al)	Mean Photon energy(keV)	Relative Tube Load
no added filtration	37.06	1.0
0.5mm Al	37.76	1.1
1.0mm Al	38.39	1.2
0.1mm Cu	40.84	1.5
0.15mm Cu	42.09	1.9
0.2mm Cu	43.11	2.3
0.05mm Sn	37.80	1.8
0.1mm Sn	38.35	3.1
0.15mm Sn	38.74	4.9
0.05mm Sm	38.08	1.5
0.1mm Sm	38.71	2.1
0.2mm Sm	39.55	4.0
0.1mm Dy	40.97	2.0
0.15mm Dy	42.11	2.8
0.2mm Dy	43.01	3.7
0.1mm Er	42.08	2.1
0.15mm Er	43.52	2.9
0.2mm Er	44.65	3.8

Table 6.3 : Mean photon energy and tube load for 60 kV beam, with various filtration

The graph of contrast variation for the different beam spectra (Figure 6.5) may be understood from a consideration of the transmission spectra through the different parts of the phantom as these determine the calculated contrast values. The terms that will be used in this method of analysis are explained in Figure 6.9, which shows an 'input' spectrum incident on a phantom containing a contrast detail. The photon spectrum transmitted through the uniform phantom only is termed the 'background spectrum', and produces the background energy absorption in the image receptor. The signal transmitted through the contrast detail and phantom is termed the 'contrast spectrum', and contributes to the absorption in the phosphor behind the area of contrast. The difference between these two spectra (*ie* for each photon energy the number of photons in the background spectrum minus the number of photons in the contrast spectrum) is termed the 'signal spectrum'. This signal spectrum gives an indication of which photon energies in the input beam contribute most to the signal in the detector *ie* the difference in energy absorption behind and beside the area of contrast. This concept has been used previously to describe the imaging performance of various beam filters (Gagne *et al*, 1994) and these terms will be used to analyse results throughout this chapter.

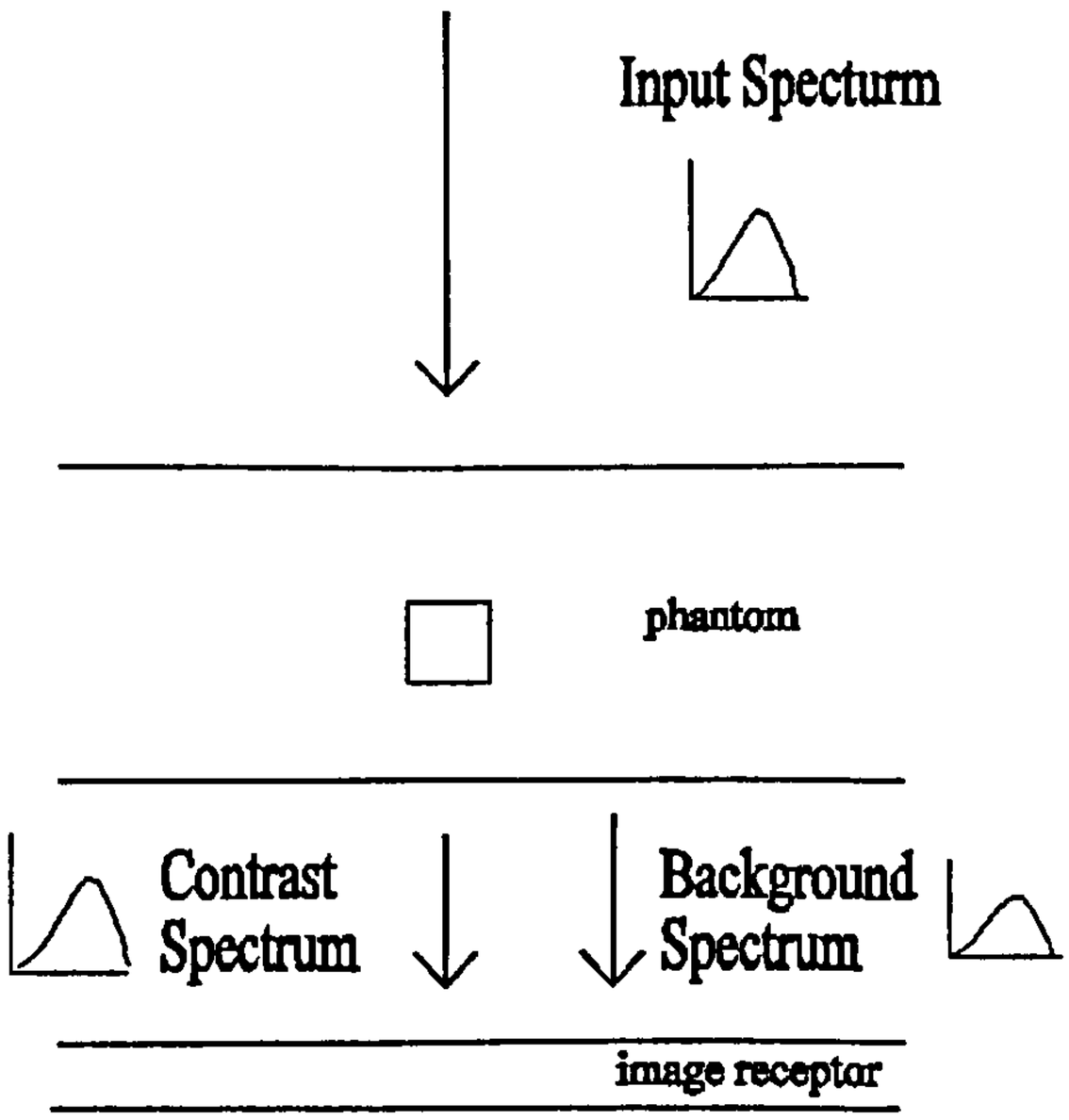

Figure 6.9 : Explanation of terms used for spectral analysis of results

Figure 6.10 illustrates this concept with the formation of the signal spectrum corresponding to 1 cm bone in 5 cm soft tissue. The spectra shown have been calculated for

- 60 kV, 3 mm Al beam filtered by 5 cm perspex (background spectrum)
- 60 kV, 3 mm Al beam filtered by 5 cm perspex + 0.27 cm calcium (contrast spectrum)
- The difference between the above two (signal spectrum)

The perspex was used to represent the soft tissue, and the calcium to represent the bone, with he thickness derived from the bone composition given by White (1991).

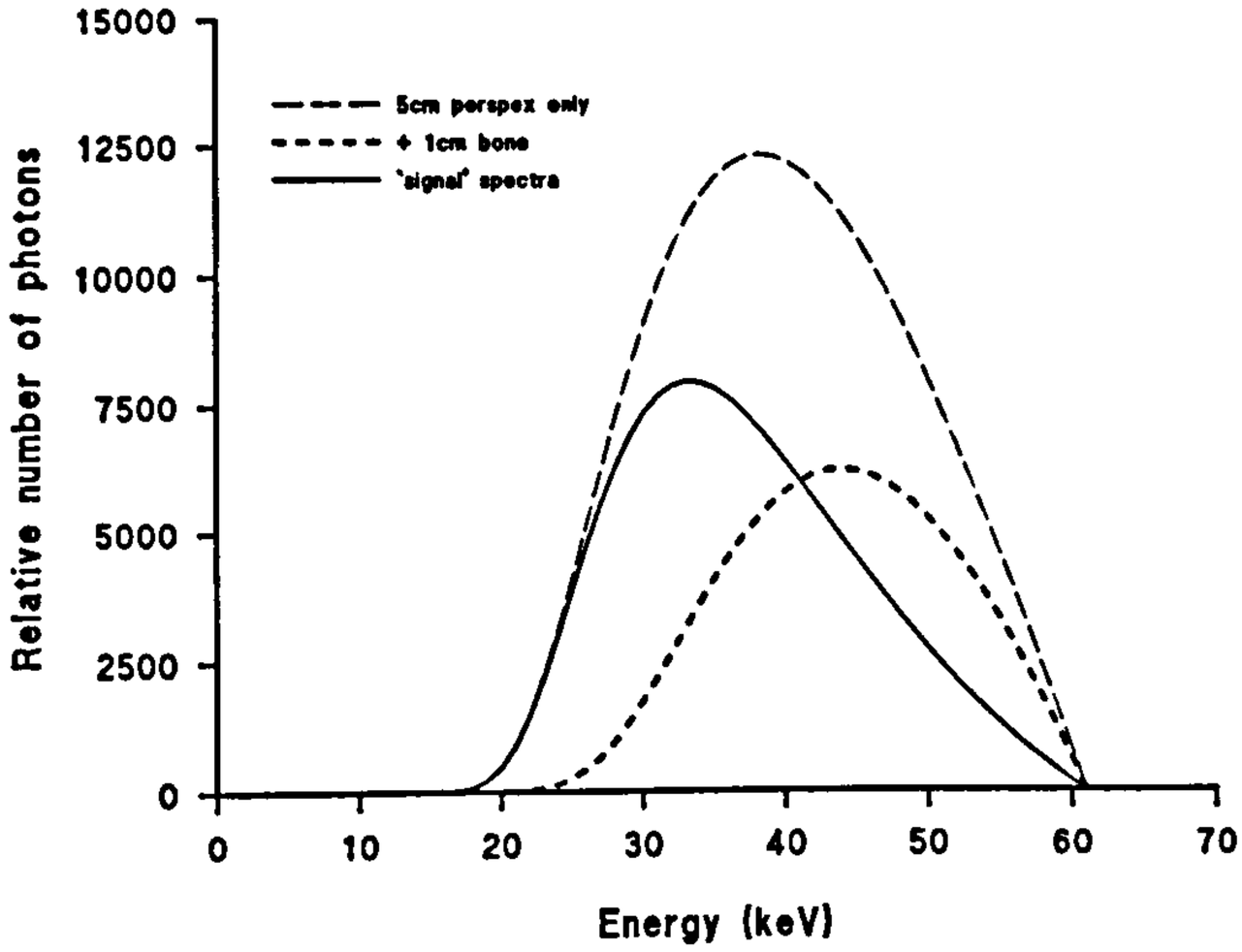

Figure 6.10 : Formation of contrast signal spectra for bone in soft tissue

The graph illustrates how the low energy part of the incident spectrum contributes to the resulting image contrast, with the signal peaking at around 33 keV. At higher photon energies, the difference in attenuation behind and beside the bone gets progressively less. At energies below the signal peak the number of photons transmitted through the phantom decreases rapidly so, although there is a large difference in attenuation coefficients for bone and soft tissue at these energies, they do not contribute much to the calculation of contrast.

Figures 6.8 and 6.10 can be used to explain the observed contrast variation for the different filters. In general, increasing filtration shifts the beam spectra to higher energies, away from the signal spectum peak exhibited in Figure 6.10, and results in a loss of contrast. Although the tin filtered spectra peak just below 30 keV (Figure 6.8vi), they drop sharply just above 30 keV and the combined effect is to reduce contrast for increasing tin filtration. The spectra

produced by filtration with samarium show a broad peak around 40 keV, with a reduction in the number of high energy photons (Figure 6.8v), which enables contrast to be maintained with increasing filter thicknesses. For the other K-edge filters, contrast is reduced with increasing filter thickness, as the attenuation of the highest energy photons is outweighed by the concurrent attenuations at the lower photon energies which contribute most to contrast. The often proposed beneficial effect of the higher K-edge filters on contrast is thus negligible for the phantom thickness and tube potential used here.

6.2.4 Variation in generating tube potential

The trends in dose and contrast for different filters (Figures 6.3 and 6.5) show that filter materials may be broadly classified into 2 groups, according to their dose/contrast characteristics.

(1) Those which displayed good dose reduction but a degradation of contrast (this includes the majority of filters)

(2) Filters showing little contrast degradation but also little dose reduction

For the filter materials in the first of these groups, simulations were carried out at 55 kV, as the lower energy could be expected to enhance contrast. The purpose of the simulations was to investigate whether an improved balance between dose reduction and contrast could be achieved. The results of simulations at 55 kV for these filter materials are shown in figure 6.11 for both absorbed energy and contrast. All results have been normalised to reference conditions of 3mm aluminium at 60 kV, and the absorbed dose and contrast for the reference conditions have been indicated on the graphs for comparison. The scales on the y-axis match those used earlier.

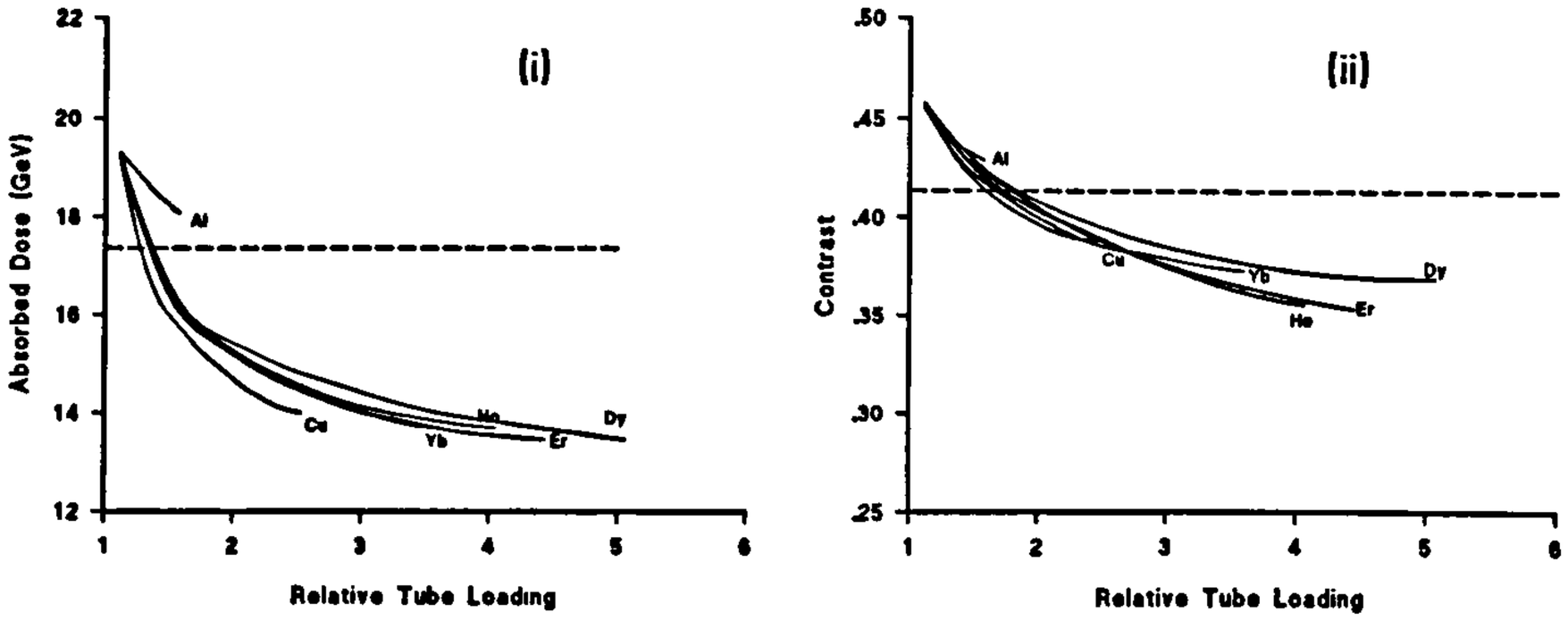

Figure 6.11 : Trends in (i) absorbed energy and (ii) contrast at 55 kV for various filter materials. The dose and contrast values for reference conditions of 3mm Al at 60 kV are indicated.

As anticipated, all the curves in Figure 6.11 are shifted up, toward higher dose and higher contrast. However, whereas the dose curves cross the reference line at a tube load of around 1.3, the corresponding contrast curves cross at a tube load of around 1.65. Between these values of tube load, contrast values are above reference levels and dose values below reference levels, which suggests that for these modest tube loads, at the reduced tube potential, dose reduction may be achieved with no loss in contrast. Although the dose reductions attainable for numerically equal contrasts are small (around 10% for copper), the dose curves exhibit a steeper gradient than those for contrast, so acceptance of a slight loss in contrast could result in much greater dose reduction (for copper a 18% dose reduction with 6% contrast reduction). The full implications of this point are discussed in detail in relation to the clinical implementation of results (Chapter 9). It can be concluded, however, that careful choice of tube voltage can be used in conjunction with thin additional filtration for dose reduction in neonatal radiography, provided that the required increase in tube load (effectively mAs) can be accommodated.

A further feature of Figure 6.11 is that the curves for the K-edge filters lie close together, with copper showing slightly better dose reduction than the K-edge filters and aluminium

very poor dose reduction. As 55 kV is below the K-edge energy of the filter materials shown on the graph, none of the materials are able to act as a band pass filter and they produce very similar spectra, as shown in Figure 6.12.

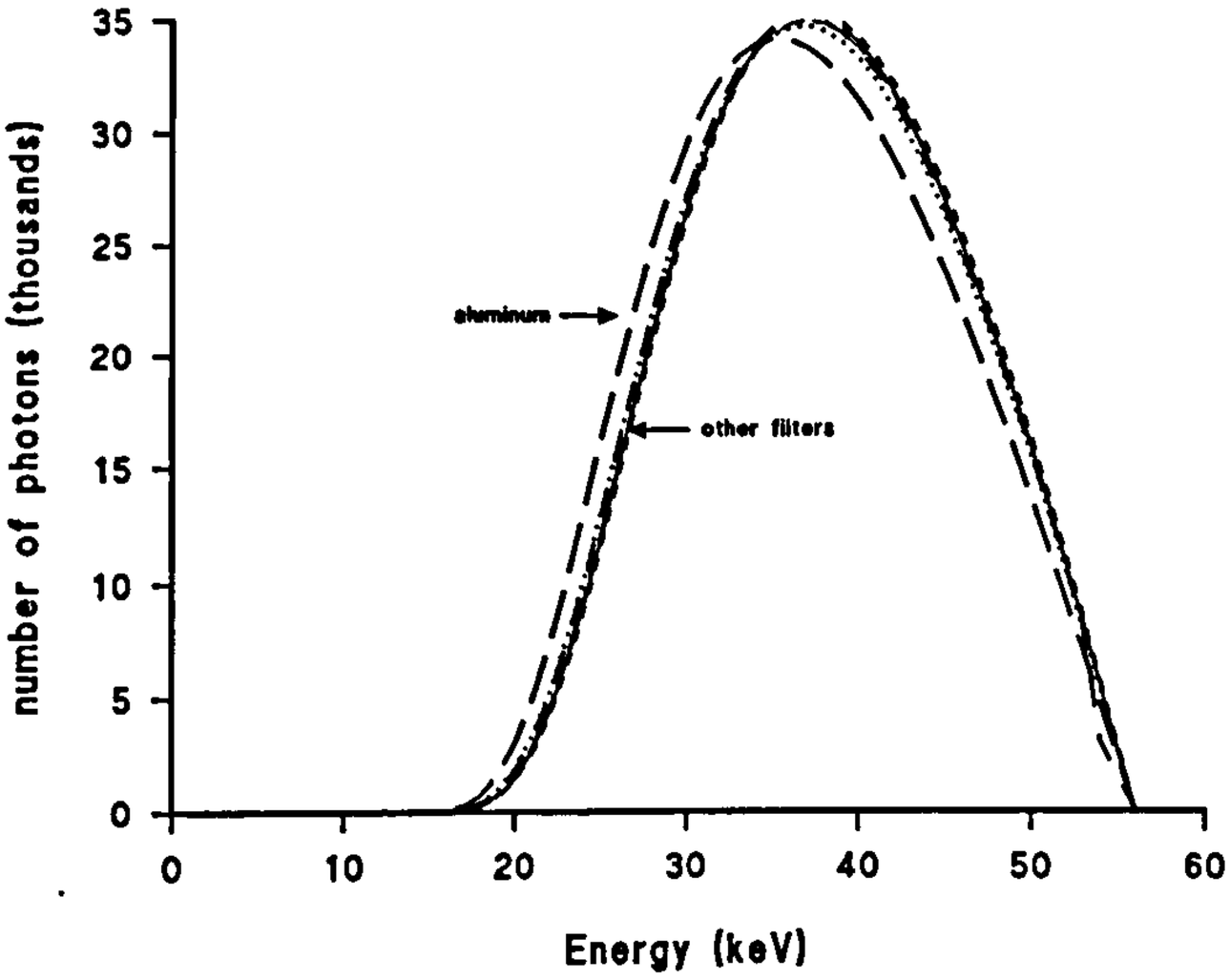

Figure 6.12 : Calculated spectra generated at 55 kV for different filter materials, at a tube load of 1.5

It is interesting to note that aluminium appears to give a much higher absorbed dose than the other materials, in spite of having a very similar beam spectra. This is due to the predominance of Compton scattering over photoelectric absorption in the aluminium filter. The spectra illustrated in Figure 6.12 represent narrow beam attenuation, and includes only photons that have passed straight through the filter. The Monte Carlo code, however, also accounts for absorption in the phantom of photons that were scattered in the filter. This has the effect of increasing the calculated absorbed energy values for the aluminium filter, relative to calculations made using a simple attenuation model which neglects scatter, as shown in Figure 6.13.

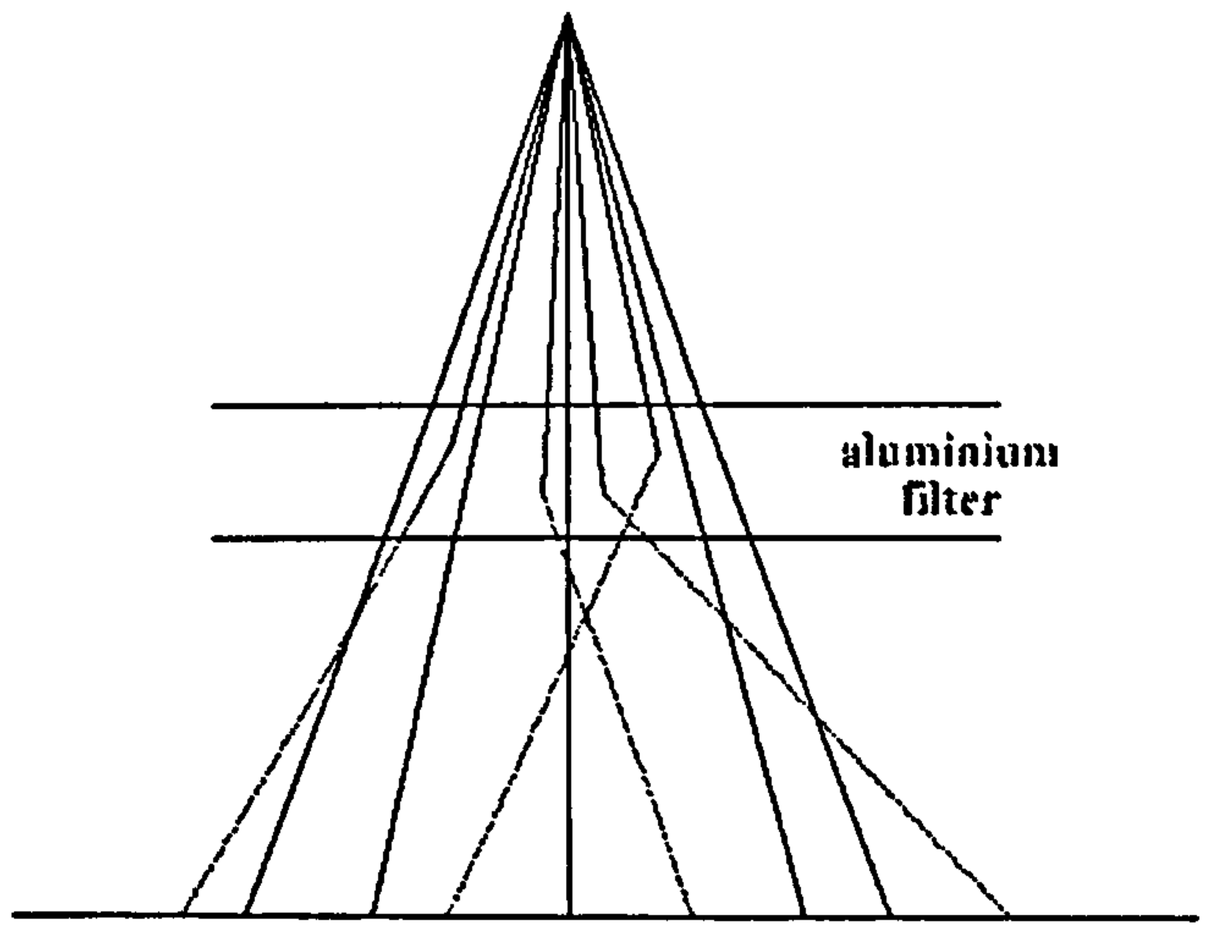

Figure 6.13 : Effect of Compton scatter in aluminium filter

This effect increases with filter thickness, as the amount of scatter produced increases with the thickness of the scattering material, as the number of Compton interactions increases. If the additional aluminium filtration is built into the X-ray tube, then this scattered dose to the patient would be reduced in clinical practice, due to the collimators which would remove any components of scatter not travelling within the beam direction. However, if an aluminium filter is added by the radiographic staff for selected examinations the dose increase due to the scatter, indicated by the results presented in Figure 6.11, will be genuine. Its magnitude will be slightly overestimated by the Monte Carlo simulation as this used a semi-infinite slab to simulate the patient, rather than one of finite dimensions. Further simulations to check the magnitude of this effect showed that, for 5 mm aluminium filtration, absorbed energy was reduced by 9% when all photons leaving the filter at a divergence greater than that of the beam were rejected. For the other filter materials under investigation, the chief mode of interaction is photoelectric absorption, so the effect of scatter in the filter is not apparent.

For filters in the second group (those giving good contrast but poor dose performance) simulations were carried out at 70 kV, as the higher tube voltage could be expected to reduce

doses. Figure 6.14 shows these results for samarium, gadolinium and tin. The results have again been normalised to those at 60 kV, 3 mm Al filtration, and the contrast and absorbed dose for these reference conditions are again indicated on the graphs for comparison.

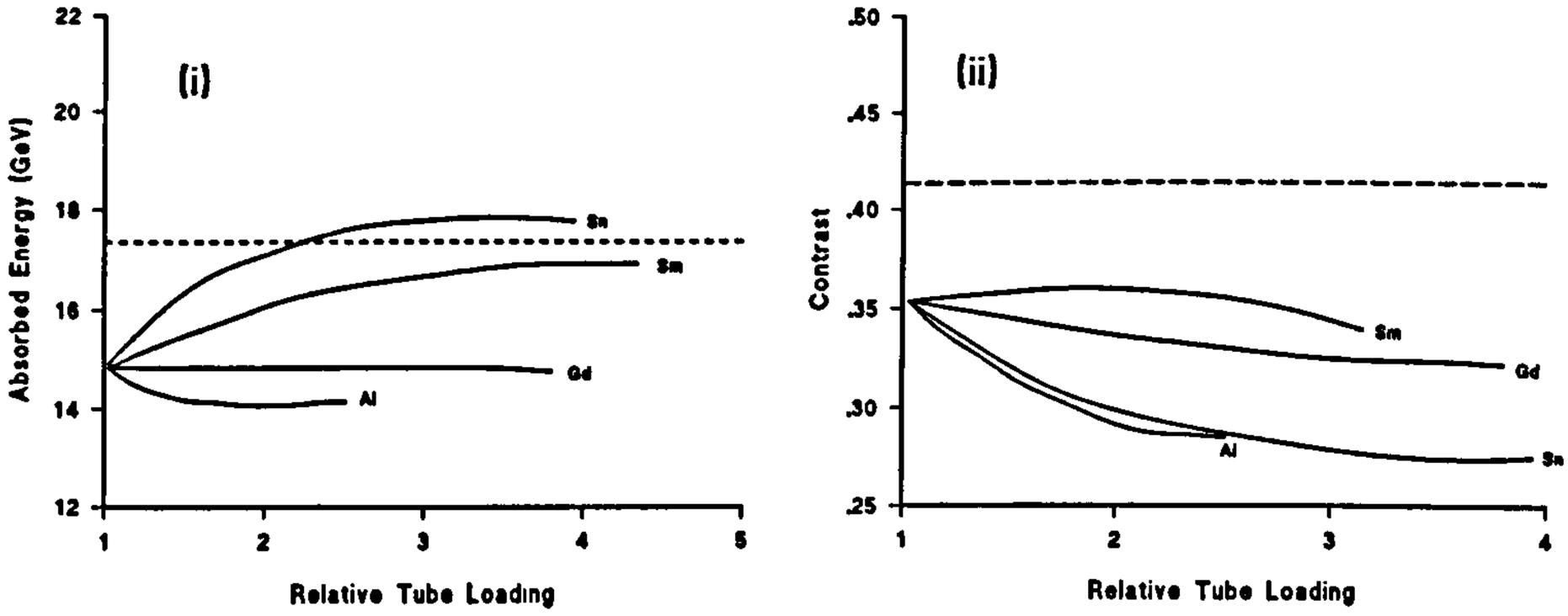

Figure 6.14 : Trends in (i) absorbed dose and (ii) contrast at 70 kV

It is apparent from Figure 6.14 that although doses have been reduced, the trends for both samarium and tin are for increasing dose with increasing filter thickness, and almost constant dose for gadolinium. Contrast has also been considerably reduced (around 15%). There is thus no benefit to using any additional filtration under these conditions. Although raising the tube voltage by a smaller amount, *eg* to 65 kV, may improve the results, the magnitude of the dose reduction is not as great as for the previous set of results at 55 kV.

6.2.5 Results for replacement filtration

Simulations were also carried out for the different filters in conjunction with 1.5 mm rather than 3 mm aluminium *ie* partially replacing the existing filtration on a set rather than adding

to it. These results are sumarised below in Figure 6.15, where results have been normalised to 3 mm Al for comparison.

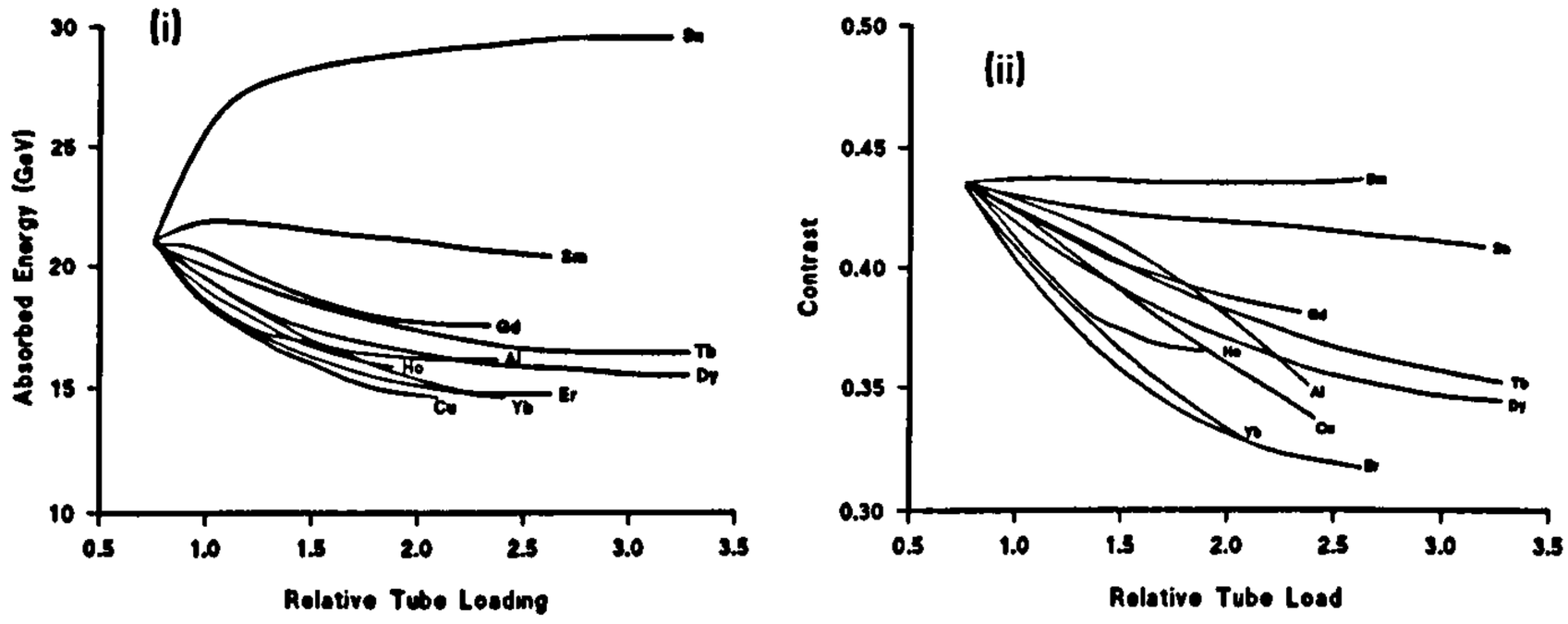

Figure 6.15 : Trends in (i) absorbed energy and (ii) contrast for filtration added to 1.5 mm Al (60 kV)

These curves are mostly similar in shape to those presented previously in Figures 6.3 and 6.5, although the following points can be noted:

- The increase in absorbed dose with increasing thickness of tin filtration is much greater than that observed previously.
- The absorbed dose curve for samarium initially shows a slight increase.
- For the other filters there is similar dose reduction at the same tube load, compared to adding the filter to 3 mm Al.
- For the contrast curves, tin shows better contrast performance than when used in conjunction with 3 mm Al, as do aluminium and copper to a lesser extent.

To understand these effects, Figure 6.16 shows the beam spectra produced by a number of filters in conjunction with 1.5 mm Al (*ie* replacement filters). Additional spectra are plotted for comparison, including that for the same filter thickness with 3 mm Al and that for the additional filter with the most similar tube load.

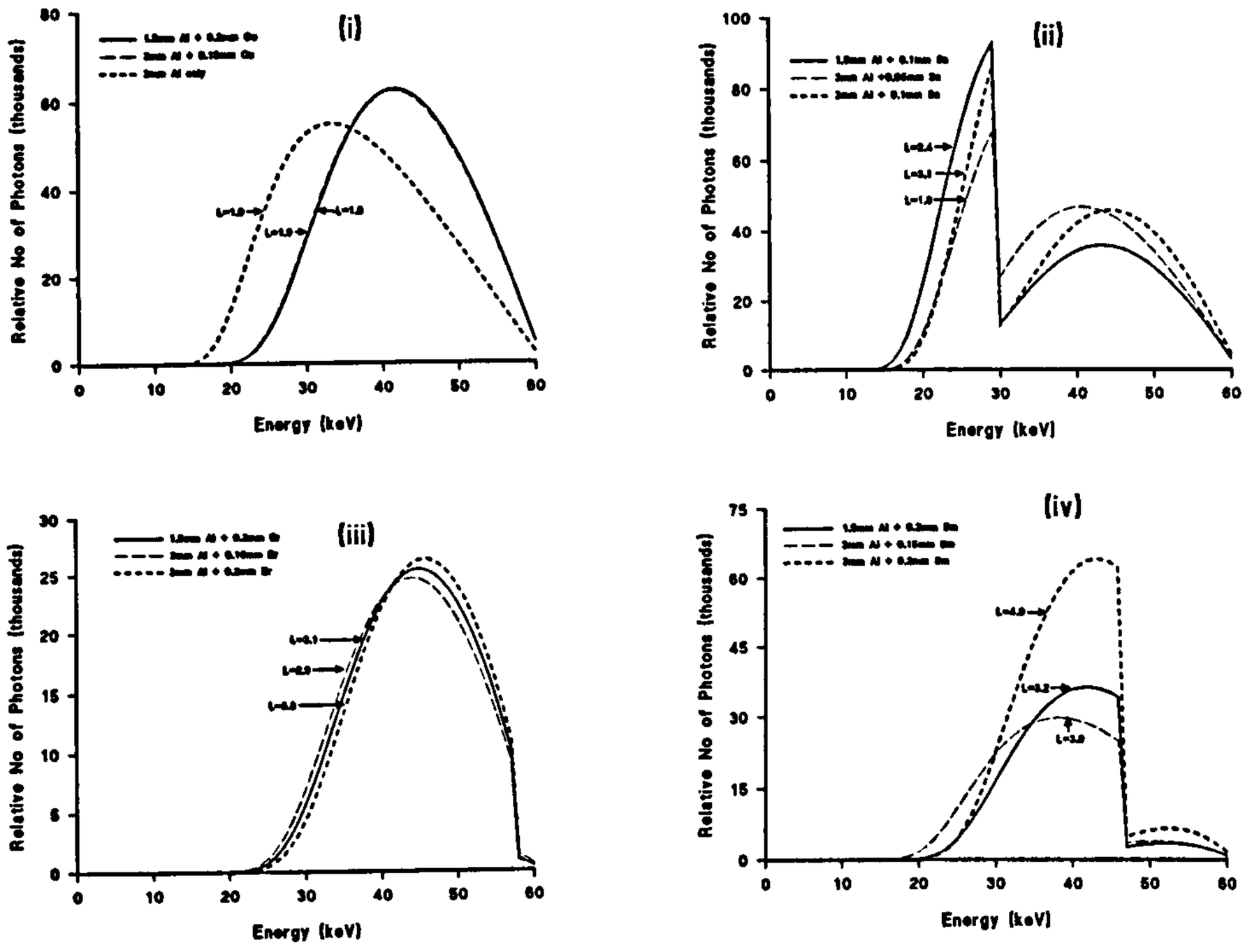

Figure 6.16 : Spectra for 60 kV beam filtered by 1.5 mm Al and (i) copper (ii) tin (iii) erbium and (iv) samarium

Figure 6.16 shows that for copper, which does not have a K-edge within the useful part of the spectrum, the replacement and additional filters resulting in the same tube load give almost identical beam spectra. Those for erbium, with its K-edge just below the maximum tube potential, are also very similar. For tin, however, the low energy peak is both broader and taller for the replacement filter than for the additional filters shown, as these low energies are well attenuated by the 'extra' 1.5 mm aluminium in the additional filter compared to the replacement one. This difference in spectral shape accounts for both the increased doses and reduced contrast loss observed for the replacement tin filtration in Figure 6.15 above. For samarium, the shift in spectra toward higher energies corresponds to the increase in tube load, although the spectral changes are relatively large for a small difference in tube load, compared to those for copper and erbium.

The results indicate that there is no advantage to the optimisation process in this approach and in clinical application there would be practical difficulties for existing X-ray units, as the required changes to existing filtration would probably need to be carried out by

manufacturers. Greater thicknesses of the chosen filter material would be required to give the same tube load and dose reduction properties as the equivalent additional filter, and this would have financial implications for the department. For these reasons, the use of replacement filtration was not investigated further in this work.

6.2.6 Results for a different intensifying screen

To investigate the effect of the image receptor on the results obtained, simulations were carried out with the lanthanum screen replaced with a gadolinium one. These results are displayed in Figure 6.17. The results may be assessed in terms of the absorption characteristics of the two screens, as shown in Figure 6.18.

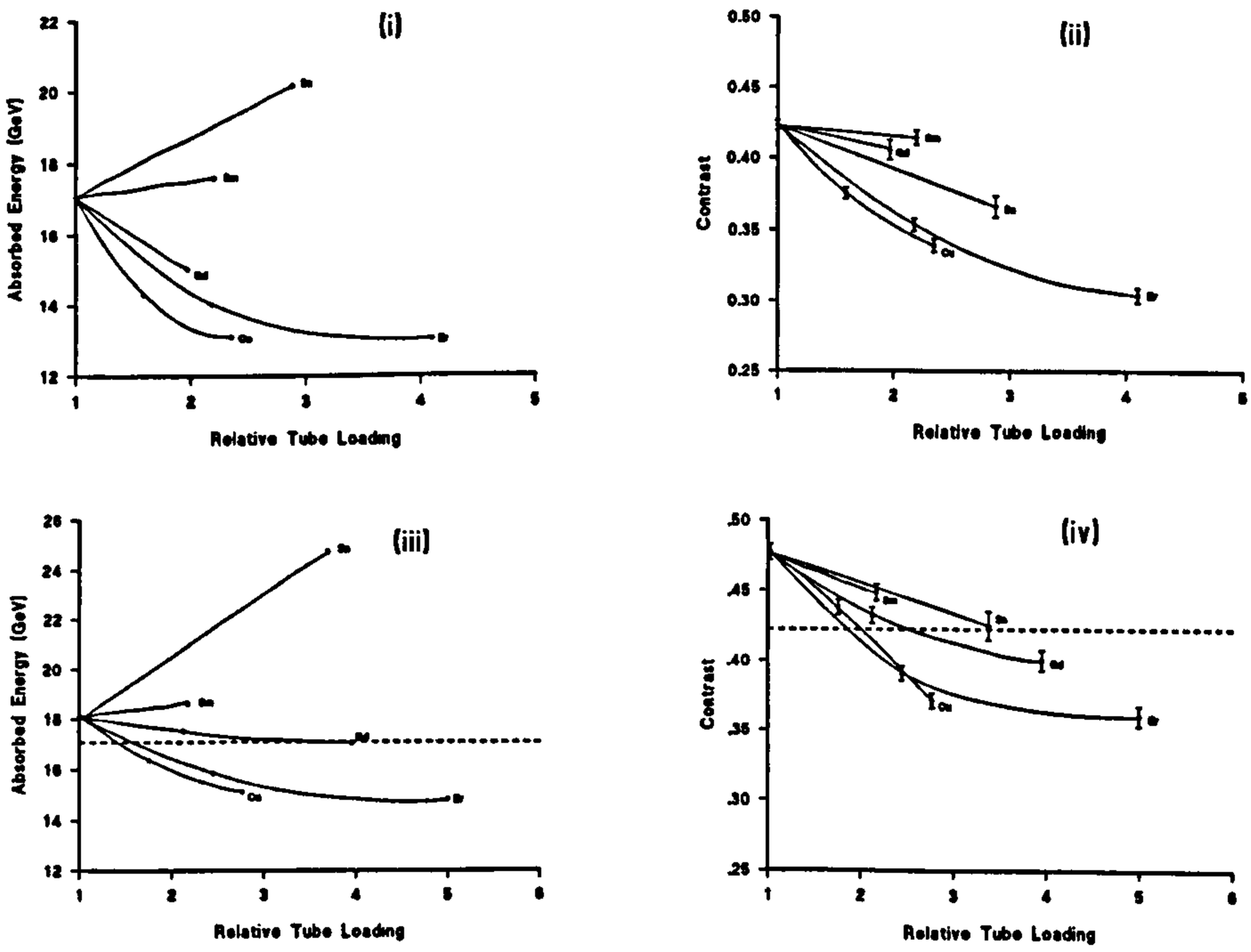

Figure 6.17 : Variation of (i) absorbed energy @ 60 kV (ii) contrast @ 60 kV (iii) absorbed energy @ 55 kV and (iv) contrast @ 55 kV for gadolinium screens

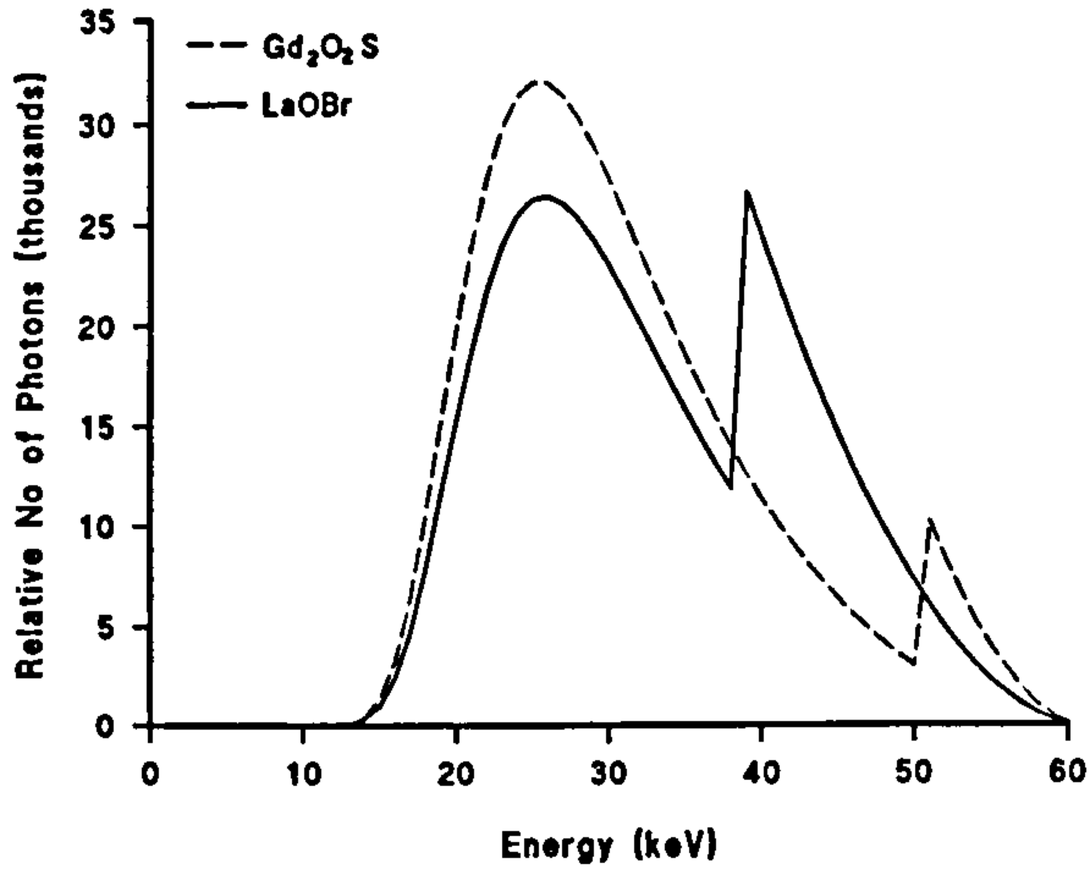

Figure 6.18 : Absorption characteristics of LaOBr and GdO_2S intensifying screens

The curves given in Figure 6.17 show very little difference from those for the lanthanum screens (Figures 6.3, 6.5 and 6.11). The variation in absorbed energy for samarium shows a slight increase with tube load whereas the corresponding curve for the lanthanum screen was almost flat. This could be due to the absence of the second absorption peak in the lanthanum screen (40-50 kV) which overlaps the peak in the samarium filtered beam spectra. The increase in detector absorption with increased tube load compensates for the increased absorption in the patient, so that absorbed dose at constant background absorption remains constant. Contrast variation is similar for both screens as their absorption in the 'signal' region of the spectrum (20-40 kV) is alike. The implication is that the results obtained for lanthanum based screens can be broadly applied to other rare-earth screens.

6.2.7 Comparison with previous work

Some of the results reported here may be compared with those presented by Koedooder (1986) from a wide-ranging theoretical study. Koedooder found an increase in absorbed dose with tube load for added tin filtration, as has been observed in this work, but also indicated that aluminium, copper and the higher K-edge filters all have a very similar effect on dose with increasing tube load, contrary to the results observed here. However the different methodologies used are largely responsible for this, in particular the calculation of results for

equal contrast, and thus at varying tube potentials. Koedooder's work was also carried out for greater phantom thicknesses, and correspondingly higher tube voltages than the simulations performed here. Scattered radiation was also neglected, which would result in overestimates of values of absorbed energy. The results that may be most easily compared (due to the small change in tube voltage) are those for 0.12 mm erbium at 69 kV, with reference conditions of 3 mm aluminium at 70 kV, for which the entrance dose ratio was 0.59 and the integral dose ratio 0.83, with a tube load of 2.0. The results presented here for 0.1 mm erbium relative to 3 mm aluminium (both at 60 kV) were a tube load of 2.1, entrance dose ratio of 0.73 and absorbed energy ratio of 0.82. These values are in good agreement with those of Koedooder considering the differences in methodologies. The greater similarity between ratios of entrance and absorbed dose found here are due to the smaller phantom size as, for constant entrance dose, the dose at a point inside the phantom for a heavily filtered beam relative to a less filtered beam increases with depth.

The results of Sandborg (1994) are more similar to those reported here in that copper was shown to exhibit the greatest dose reduction effects and a contrast increase with tube load was observed with the samarium filter, in addition to the absorbed dose increase with additional tin filtration. Table 6.4 gives some of Sandborg's results, obtained at constant tube potential (70 kV), compared to some of those presented here. Filter thicknesses were not identical and, for the copper filter, measurements were made at a different tube voltage, besides applying to a different phantom size. The results for copper are in excellent agreement, indicating that the use of a lower tube voltage combined with a thinner filter gives similar dose reduction in a small phantom to that obtained for a larger one at higher tube voltage and greater filter thickness. Results for the tin and samarium filters are also in reasonably good agreement, considering the different calculation parameters.

Results of Sandborg (1994), 20cm phantom				Results from this work, 5cm phantom			
Filter	Abs. dose ratio	Ent. dose ratio	Contrast ratio	Filter	Abs. dose ratio	Ent. dose ratio	Contrast ratio
0.27mm Cu	0.76	0.57	0.93	0.20mm Cu (60 kV)	0.73	0.58	0.83
0.08mm Sn	1.66	1.09	0.93	0.05mm Sn (70kV)	1.21	1.00	0.89
0.08mm Sm	1.50	1.29	1.11	0.10mm Sm (70kV)	1.10	1.00	1.01

Table 6.4 : Comparison of results with those of Sandborg (1994)

The results may also be compared to those reported for specific filters in clinical use. Cranage (1992) reports an entrance surface dose reduction of 50% with use of a 0.1mm erbium filter replacing 1 mm aluminium on the X-ray set. Effective dose reduction ranged from 17 - 64% depending on the examination. Technique factors used with the erbium in place were unchanged tube voltage and doubled mAs (*ie* a relative tube load of 2). Measurements were carried out for adult patient examinations, and the reported dose reductions are greater than the most similar results obtained in this work which were an entrance surface dose reduction of 27% and absorbed energy reduction of 18%. Several factors will contribute to this difference in dose, including the smaller size of patient being simulated in this study, compared to the adult data used by Cranage, and the corresponding lower tube voltage. In addition to this, the clinical measurements were made using subjective assessment of the mAs value required for radiographs comparable with those obtained without the erbium, and the tube load of 2.0 is slightly less than that calculated here for the same erbium thickness.

Levett (1990) reported entrance dose reduction of 34% after a clinical trial of use of a 0.1 mm erbium filter for paediatric examinations at 66 kVp, again with unchange tube voltage and a tube load of 2.0. This is in excellent agreement with the corresponding value of 27% demonstrated here. If results are extrapolated to a tube load of 2.1, as was found in this work, the dose reduction would be 31% which is in even closer agreement. Although

Levett's results were obtained for paediatrics, the average size was greater than the 5 cm phantom used here, and the tube voltage was slightly higher.

The above comparisons show that the results from the Monte Carlo simulations carried out as a part of this work are in broad agreement with the published literature. This is in spite of the difficulties in making direct comparisons of the data, due to the many variations in simulation and experimental set-up, and also in presentation of the data.

6.3 Fluoroscopy using iodine or barium contrast agent

The preceeding sections have dealt with the simulation of bone in soft tissue, corresponding to simple radiographs. Another important category of patient examination is that of fluoroscopic studies involving an artificially based contrast media, based on either barium or iodine. A second set of simulations was thus carried out for a contrasting disk of either barium or iodine in 5 cm soft tissue. The image receptor was 0.014 cm thick caesium iodide, corresponding to a typical image intensifier phosphor, and 2 cm perspex was used between the patient and the phosphor to represent the couch. Four different specifications of contrast media were used: 4930 mg cm^{-2} and 100 mg cm^{-2} iodine, 3500 mg cm^{-2} and 70 mg cm^{-2} barium. The simulation procedure followed was similar to that for the radiographic simulations with all calculations carried out at 60 kV. The results have been normalised to reference conditions of 60 kV and 3 mm Al filtration.

6.3.1 Dosimetry results

Figures 6.19 and 6.20 show the variation in dose parameters for both iodine and barium contrast media, for the different filter materials. The results presented here are for 4.9 g cm^{-2} iodine and 3.5 g cm^{-2} barium, but the dosimetry results are not discernably affected by the mass thickness of contrast used, as the composition of the small volume of contrast makes negligible difference to the amount of energy absorbed in the surrounding tissue, or at the phantom surface. The dosimetry results can also be seen to be similar for iodine and barium (Figures 6.19 and 6.20), for the same reason.

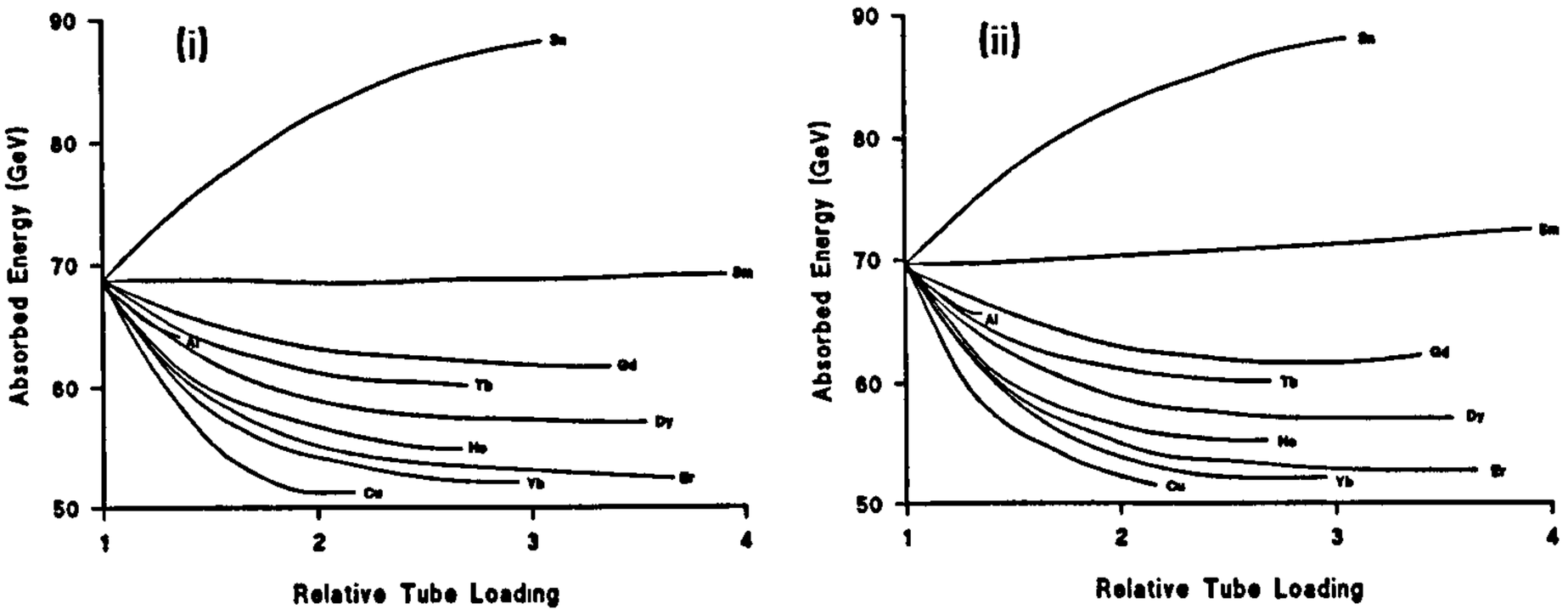

Figure 6.19 : Variation of absorbed energy with tube load for (i) iodine and (ii) barium contrast in soft tissue (60 kV, CsI detector)

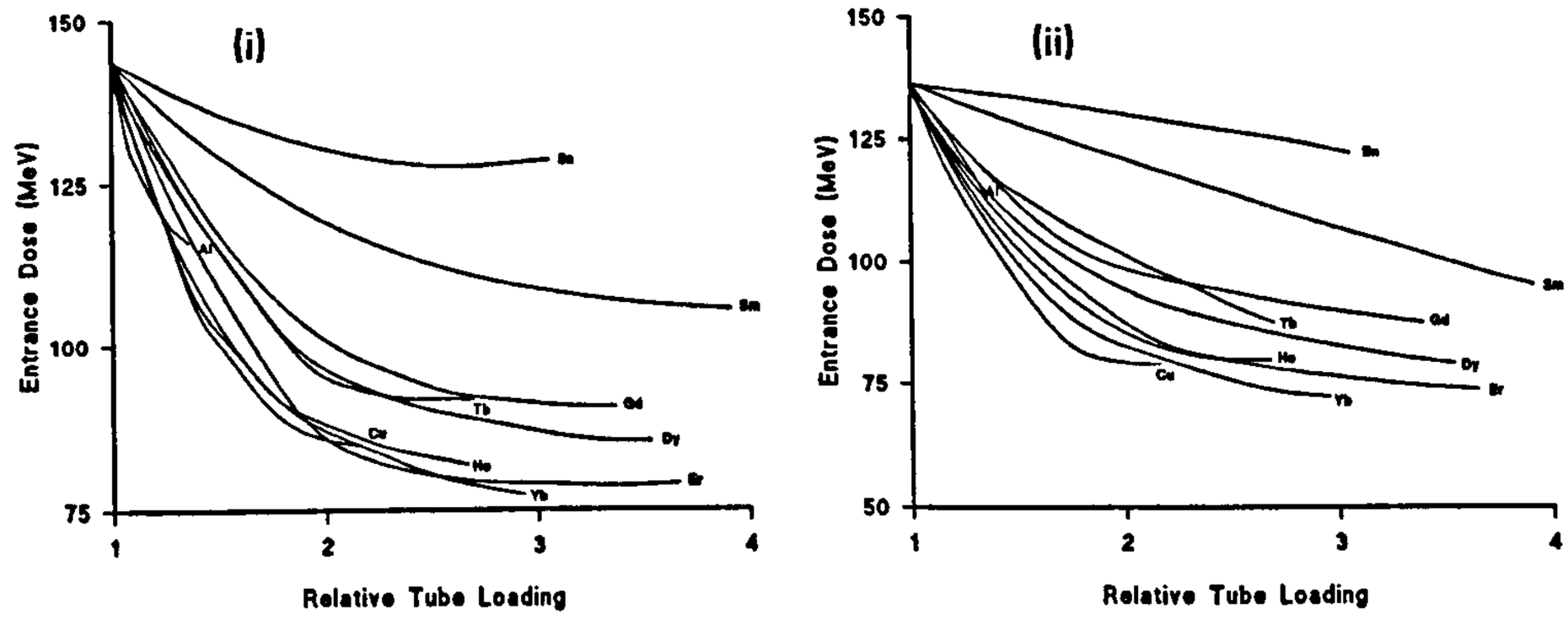

Figure 6.20 : Variation of entrance dose with tube load for (i) iodine and (ii) barium contrast in soft tissue (60 kV, CsI detector).

The curves are very similar in shape to those previously presented for bone in soft tissue (Figures 6.3, 6.5). Copper filtration exhibits the best rate of dose reduction, and tin is again a particularly poor choice of filter. Most of the comments previously made (section 6.2.3), pertaining to the effect of the different filtered spectra on patient dose apply also to the results observed here. The only altered parameter that will affect the dose is the image receptor. The absorption of the CsI phosphor, compared to the gadolinium and lanthanum screens is illustrated in Figure 6.21.

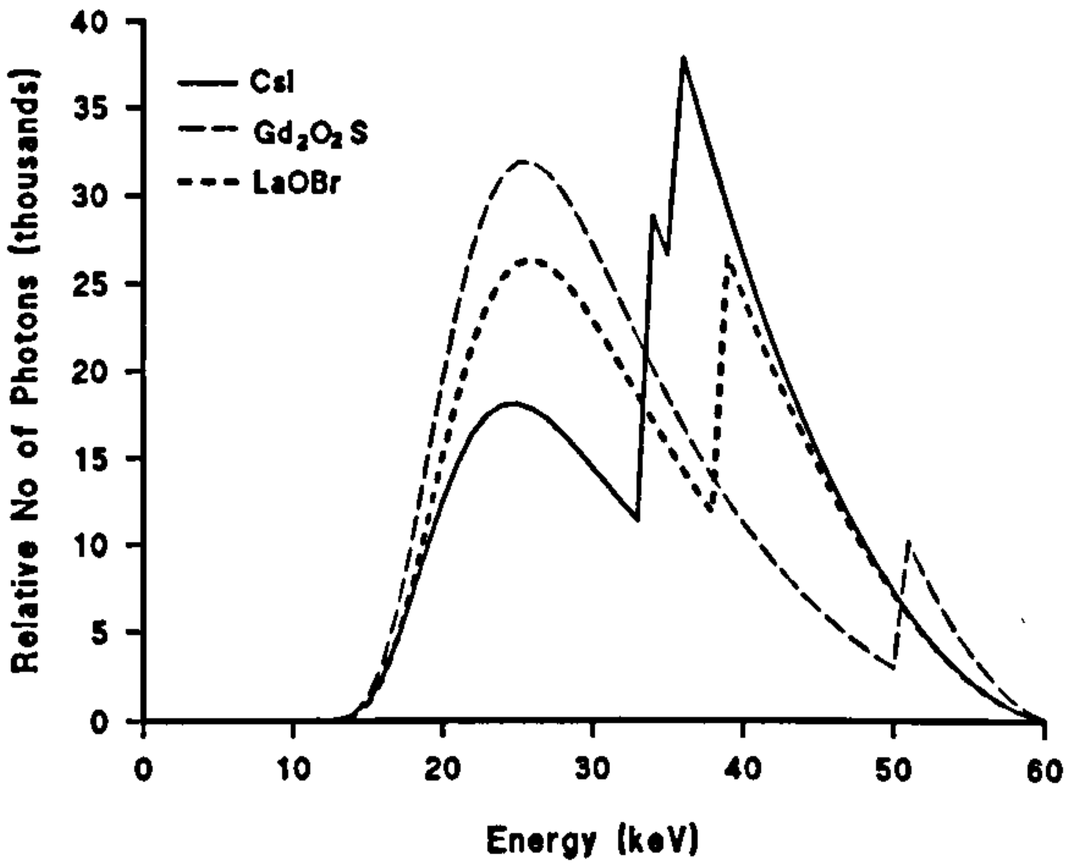

Figure 6.21 : Calculated absorption of caesium iodide phosphor compared with film screen materials

Although the absorption spectra for the caesium iodide detector peaks at a different energy from the two screens simulated previously, this does not greatly affect the trends in absorbed dose and entrance dose, except for filters with a K-edge close to one of those found in the screens.

6.3.2 Contrast results

Figure 6.22 shows the variation in image contrast for the different mass thicknesses of iodine and barium simulated.

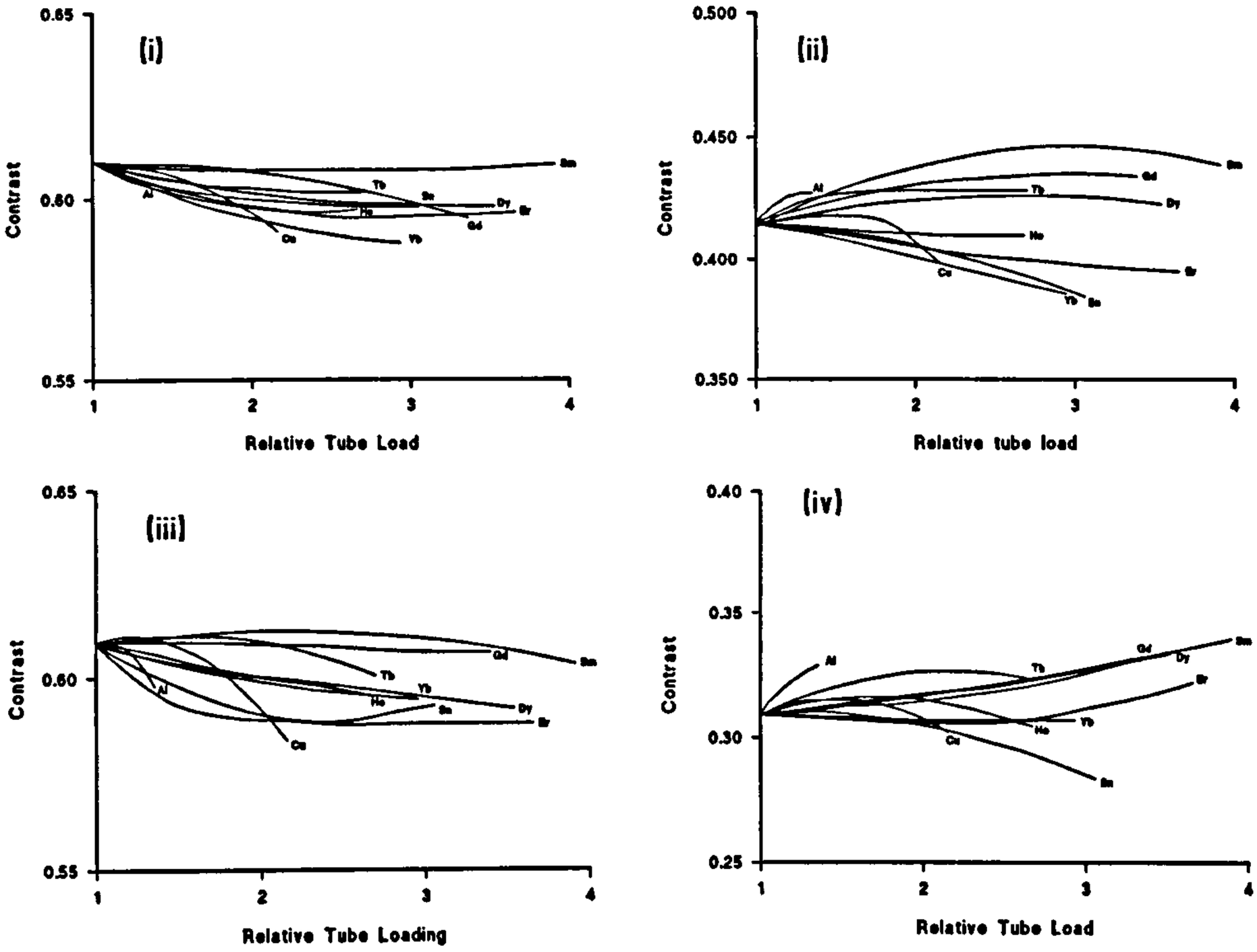

Figure 6.22 : Variation in contrast with tube load for (i) 4.9 g cm^{-2} iodine (ii) 100 mg cm^{-2} iodine (iii) 3.5 g cm^{-2} barium and (iv) 70 mg cm^{-2} barium in soft tissue (60 kV, CsI detector)

The first point to note from this set of graphs is the relatively small amount of contrast variation compared to that apparent in the bone/soft tissue graphs, given in Figure 6.5 (a spread of around 0.05 on the y-axis, compared to 0.1 for the radiography simulations). For the larger mass thicknesses of contrast (i and iii) the curves are almost flat, with contrast effectively independent of the filtration employed. This occurs due to the high X-ray absorption in the contrast media, which results in virtually no radiation passing directly through the area of contrast detail. Conversely this means that almost all the radiation passing through the phantom will contribute to the contrast, which then becomes independent of the shape of the beam spectrum and hence the filtration used. This will be the case for any study involving high levels of contrast.

For the lower contrast graphs, a more complex pattern emerges. Contrast is seen to improve with increasing tube load for aluminium and samarium and, to some extent, for gadolinium, terbium and dysprosium. The curve for copper is almost flat initially followed by a drop in contrast, and for the remaining filters a gradual decrease is seen with tube load. The shape

of the curves may be interpreted by looking at the absorption characteristics of iodine and barium, as illustrated in Figure 6.23 which shows the transmission of a 60 kVp beam through iodine and barium in conjunction with the 5cm phantom.

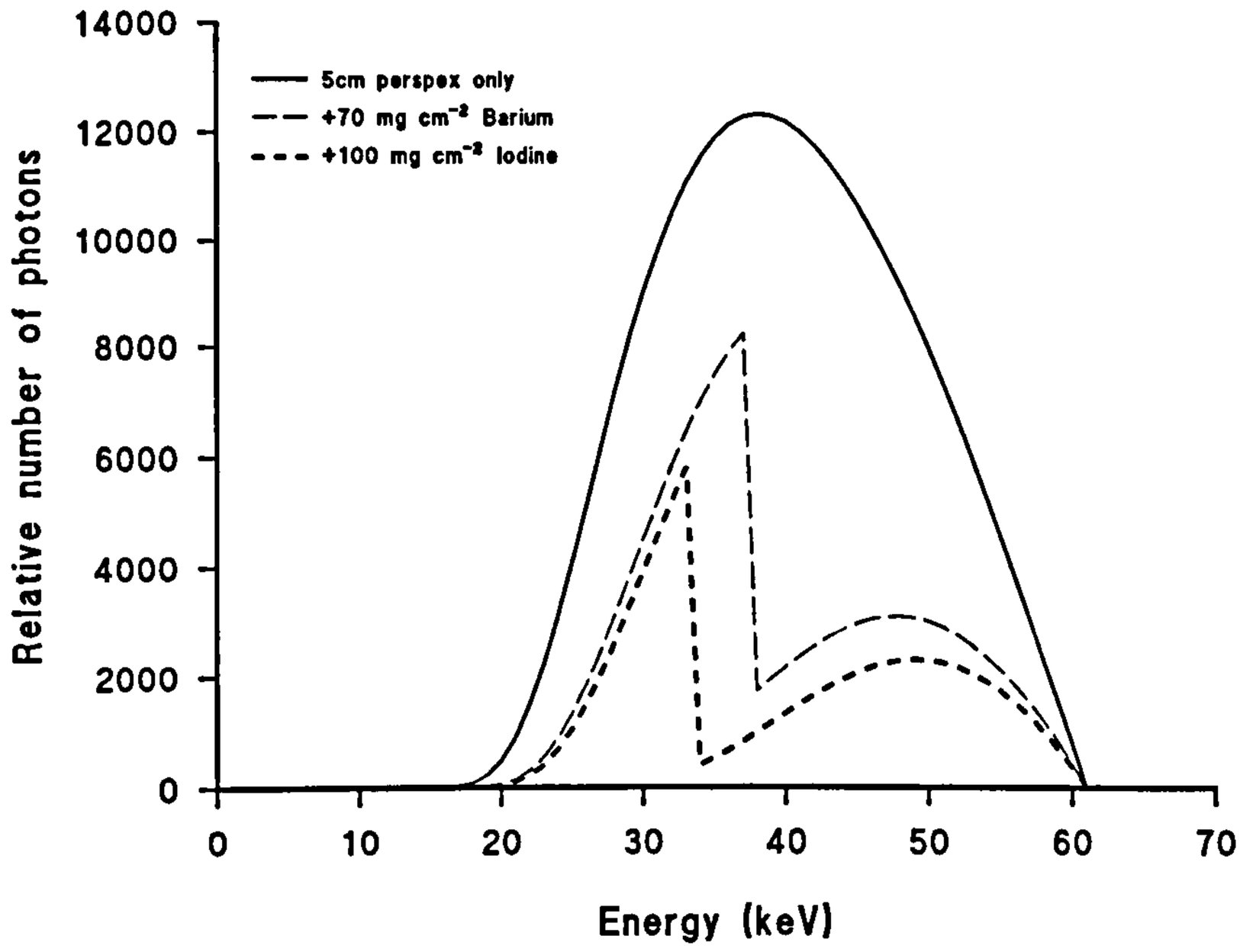

Figure 6.23 : Transmission of reference beam (60 kV, 3 mm Al filtration) through phantom and contrast media

From the above curves, the effective signal spectrum may be deduced for each contrast detail, as described in section 6.2.3, by subtracting its transmission curve (*ie* the contrast spectrum) from the backgound spectrum. Figure 6.24 shows the signal spectra derived in this way for 70 mg cm^{-2} barium and 100 mg cm^{-2} iodine.

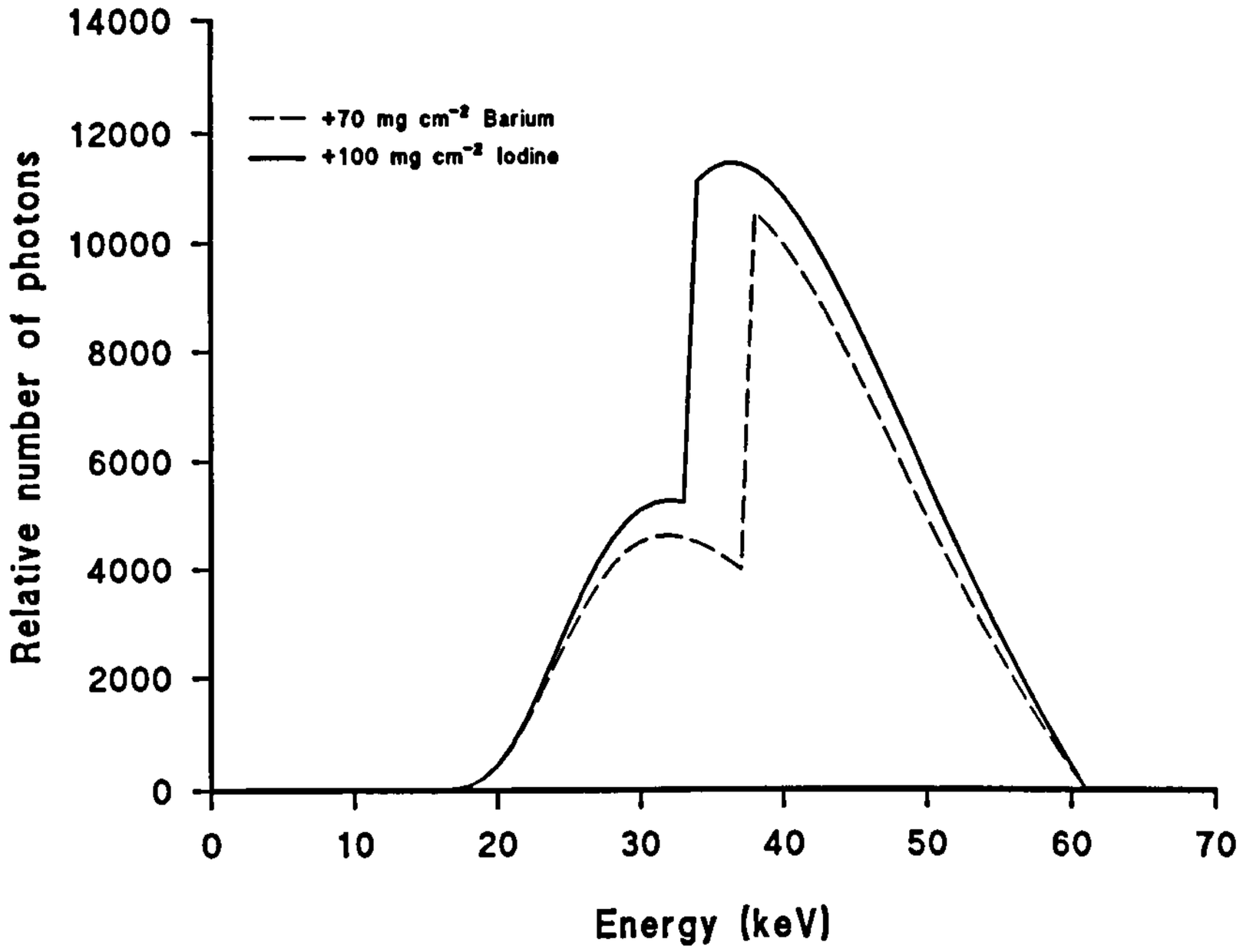

Figure 6.24 : Effective 'signal' spectra for iodine and barium in a 5cm phantom

These spectra show that for iodine and barium contrast media, the most useful part of the input beam spectrum is toward the middle of the range of beam energies, above the K-edge of the media, rather than at the low energy end of the spectrum. This means that the image contrast obtained from different filtered spectra will depend on the proportion of the resultant beam with energies within this range *eg* an incident spectrum which peaks at around 40 keV would give much better barium contrast than one that peaks below 30 keV and drops off rapidly at high energies. The use of this concept is illustrated for iodine in Figure 6.25 which shows the signal spectrum for 100 mg cm^{-2} iodine superimposed on some of the filtered beam spectra displayed earlier in Figure 6.8. The reference beam (60 kV, 3 mm Al) is also displayed on each graph. Contrast can be expected to depend on the amount of overlap between the input and signal spectra.

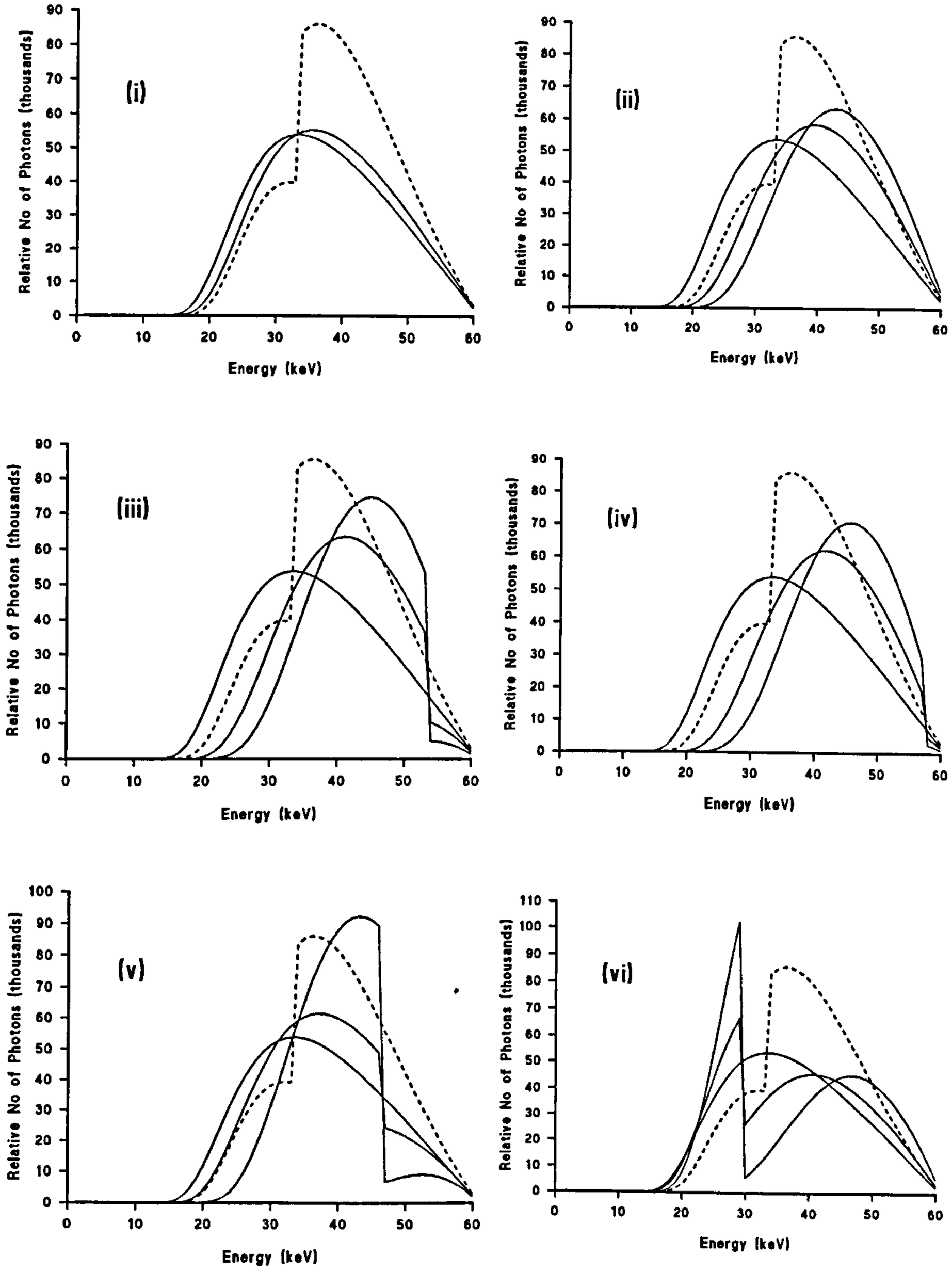

Figure 6.25 : Signal spectra for iodine (shown in dotted line) with filtered beam spectra for (i) aluminium (ii) copper (iii) dysprosium (iv) erbium (v) samarium (vi) tin. The reference beam (60 kV, no added filtration) is also given in each case.

The first graph in Figure 6.25 shows how increasing amounts of aluminium filtration cause the beam spectrum to shift towards that of the iodine signal spectrum, to give the increasing contrast observed in Figure 6.22. This is also the case for small amounts of copper filtration

(Figure 6.25ii), but as the amount of copper increases the peak shifts beyond that of the iodine signal, so that contrast starts to fall again. This effect can also be seen in the dysprosium graph. For erbium, the beam hardening effect is greater and even the thinnest filter simulated shifts the beam spectrum beyond that which is optimal for contrast. Additional samarium filtration gives a good contrast response as the beam spectra peak sharply in the same region as the iodine peak (Figure 6.25v), and this is more pronounced for increasing filter thicknesses. The low energy peak in the tin filtered spectra, however, gives rise to poor contrast performance, as there is little overlap between the input and signal spectra (Figure 6.25vi).

Similar arguments apply to the barium contrast studies but, as the barium signal peaks at a higher energy, the K-edge filters give improved contrast over a greater range of thicknesses, and samarium is no longer the optimal filter with respect to contrast.

6.3.3 Implication of results for optimisation

The above analysis shows how the potential for optimisation of dose and image quality with beam filtration is greater for contrast media studies than with simple radiography. For the phantom thickness and tube voltage studied here, small amounts of added filtration can be used to give reduced skin and whole body doses while maintaining image contrast. The presence of the K-edge in both iodine and barium means that it is not necessary to reduce the tube generating potential in order to prevent contrast degradation, which in turn increases the dose reduction achievable.

The results show that copper filtration exhibits the greatest dose reduction for equal tube load and, although it does not give the best contrast performance, for small amounts of copper contrast is maintained or slightly improved. This would make it the filter of choice when aiming to reduce the radiation dose to infants from fluoroscopy with iodine or barium contrast media. If, however, it is necessary to improve contrast for a particular examination *eg* when looking for a small fistula, then the use of a samarium or gadolinium filter may be preferable, as this would improve contrast without increasing the dose to the patient.

As the results, particularly those relating to contrast, are highly dependant on the tube potential and on the phantom thickness, care must be exercised in extrapolating to larger sizes. However, these results and the spectral analysis can be used to assess the most promising areas for further simulation. This application to other age-groups is discussed more fully in Chapter 10.

6.3.4 Comparison with the work of others

Several authors have presented work concerning the use of additional filtration in paediatric fluoroscopy. Nagel (1989) recommended gadolinium for iodine examinations in small patients, reporting a 7% increase in contrast and 5% reduction in integral dose compared to copper, for 0.3mm copper equivalent filtration at 70 kV. This result was based on a theoretical analysis and the contrast change compares very well with the result obtained here; a contrast increase of 9% for a 0.2mm gadolinium filter compared to a 0.2mm copper filter. The energy imparted, however, increased by 17% for gadolinium compared to copper in this work, but the discrepancy is not surprising considering the differences in tube potential and filter thicknesses.

Heggie (1992) also compared different filter materials for fluoroscopy, over a range of patient thicknesses, and demonstrated aluminum and copper to give the best dose reduction. For a 5cm phantom he reported relative dose rates of 0.58 for 0.2mm added copper at 68 kV and 0.74 for 0.1mm gadolinium at 70 kV, with contrasts of 0.81 and 0.86 respectively. These figures are compared to the situation with no added filtration at 63 kV. These values may be compared to those obtained here at 60 kV, namely relative entrance doses of 0.60 for copper and 0.80 for gadolinium, and relative contrasts of 0.96 and 1.05 respectively. These results are in good agreement as the increased tube voltage used by Heggie would be expected to improve dose reduction and reduce contrast.

The work reported by Gagne (1994) focusses on the variation of imaging performance per dose (SNR^2/D), and this also recommends copper as the best general purpose filter, with gadolinium giving improved performance for small patient thicknesses. The image quality

performances are partially analysed in terms of effective signal spectra, as has been done here, and this highlights the importance of patient thickness in optimisation of iodine contrast. For a 30 cm phantom the effective signal spectra for 100 mg cm^{-2} iodine has been calculated according to the method used throughout this work, and is as illustrated in Figure 6.26.

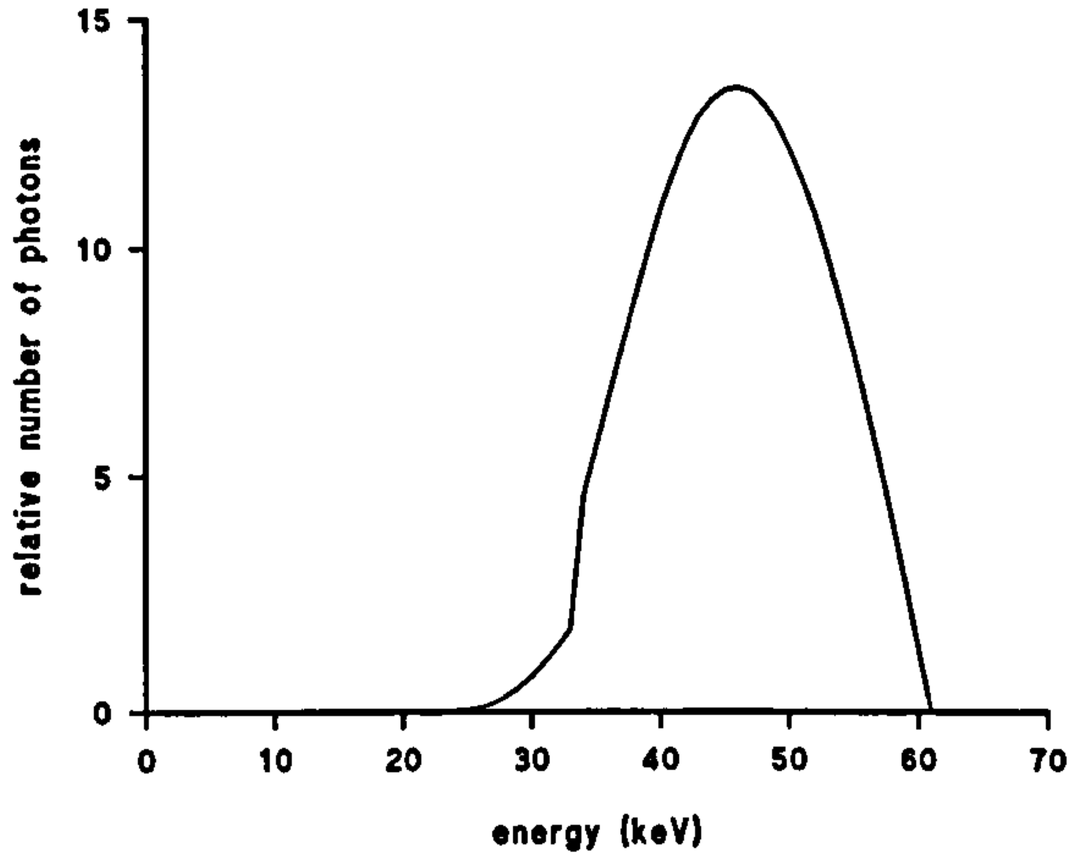

Figure 6.30 : Signal spectra for 100 mg cm^{-2} iodine in 30 cm tissue

This spectra appears the same as that given by Gagne (1994), and differs from that given earlier for 5cm tissue (Figure 6.24) as the lower energy peak has disappeared. In effect, the greater absorption in the thicker patient masks the K-edge of the iodine contrast media. This explains why the enhanced performance exhibited by filters such as gadolinium or samarium for small patient thicknesses disappears for larger patients. It is difficult to compare results directly to thos of Gagne, as the latter are mostly presented in terms of SNR^2/D rather than in separate dose and image quality parameters. However for a 10cm phantom, with barium contrast, the values of integral dose and contrast, relative to the reference system are 0.64 and 0.97 respectively. The most closely corresponding conditions found here gave corresponding results of 0.88 and 0.77, but these were for a thinner phantom, a thinner contrast detail, varying tube potentials and a slightly different reference spectrum.

6.4 Summary of Monte Carlo results

A large number of Monte Carlo simulations have been performed for a neonatal phantom, to calculate entrance dose, absorbed energy and contrast for various combinations of filter, generating tube potential, contrast media and image receptor. Results have been presented in terms of variation in each parameter with tube load, and analysed in terms of absorption and transmission spectra through the various media.

For radiographic examinations, it was shown that increasing the amount of aluminum filtration beyond 3mm was an inefficient method of dose reduction. Copper gave the best dose reduction performance, out of the materials included in the study, with tin a particularly poor filter. For the rare earth filter materials, dose reduction increased with atomic number. In all cases, the reduction in absorbed energy was less than that for entrance dose.

The reduction in absorbed dose and entrance dose was accompanied in each case by a reduction in contrast. However, by lowering the generating tube potential to 55 kV from 60 kV, contrast could be maintained while preserving a moderate dose reduction, for some filter materials. In particular, for copper filtration, absorbed dose reduction of 10% was attainable without loss in contrast.

Using replacement instead of additional filtration shows no decrease in relative dose reduction for the same tube load. Use of a different image receptor did not significantly affect the results.

For fluoroscopy examinations using iodine or barium contrast media with a caesium iodide detector, the dosimetry results were very similar to those for radiography. For a high contrast object, contrast was minimally affected by the beam spectra, whereas for lower contrast studies the contrast depended on the precise spectral shape and the K-edge of the contrast media. Improved contrast could be obtained over a range of added filter materials and, for small tube loads, contrast was maintained close to reference level for virtually all filters.

Results were similar for both iodine and barium, though contrast improved over a wider range of tube loads for the latter case.

Copper was shown to be the optimal filter for dose reduction in neonates, with gadolinium or samarium filtration suitable for improving image contrast.

Chapter 7

Experimental Techniques

7.1 Introduction

Experimental work was undertaken for two reasons. The first of these was to verify the results obtained from the Monte Carlo simulations. This was necessary as, however well designed and tested the code, there was always the possibility that an approximation in the processes modelled, or a hidden bug, might bias the results obtained. The second reason was to establish that the theoretical results could be carried through to a clinical environment. This was important as, in practice, parameters are rarely as well defined or as continuously variable as they can be for a theoretical simulation (*eg* only discrete mAs values may be available, acceptible background densities are likely to be assessed visually rather than numerically *etc*) and the true geometry is likely to be more complex than that modelled.

To address each of the above, different types of experimental measurement were carried out. The first set were designed to match the computer simulations, in order to verify the code and the results obtained from it. These measurements were carried out in the departmental X-ray laboratory, irradiating simple slab phantoms corresponding as closely as possible those modelled in the Monte Carlo code. A second set of measurements were then performed to assess the application of results to clinical practice. This latter stage of the work was carried out in a local radiology department, with a high throughput of paediatric patients. Two types of clinical measurements were carried out; one simulating plain film radiography on a mobile X-ray set; the other simulating fluoroscopic procedures in the paediatric screening room. The former examination was selected as being representative of the most common X-ray procedure for neonates on a special care nursery and, therefore, an important category of examination for optimisation. Fluoroscopic procedures were included since they give a much higher dose per examination then simple radiography. All irradiations made in the clinical environment were performed on a neonatal anthropomorphic child phantom, and the close

cooperation of the senior paediatric radiographer was obtained in establishing suitable experimental parameters.

Dose measurements for all experimental work were made using thermoluminescent dosimeters and contrast was assessed from film density measurements. Sensitometric techniques were used to characterise the film response. Image quality was also judged subjectively, by experienced staff, from radiographs and the visual display unit (VDU) of the fluoroscopy equipment. These techniques are outlined in detail below, as are the experimental procedures.

7.2 TLD dosimetry

Thermoluminescent dosimeters (TLD) have been widely used and recommended for making measurements of patient dose from diagnostic radiology (IPSM, 1988; IPSM, 1992). The most usual form of TLD used is lithium fluoride, doped with magnesium and titanium. This has the advantage of near tissue equivalence in its radiation response, relative insensitivity to light and a low fading rate (Chandra *et al*, 1982). The problems identified in Chapter 2, regarding the use of TLD for paediatric dose measurement, did not affect their use in these experiments as there was no necessity to use low doses. Two types of TLD were used for this work, both supplied by Harshaw and read out using Harshaw readers which employ hot nitrogen gas heating with a closed loop feedback system producing linearly ramped temperatures (Moscovitch *et al*, 1990).

For the laboratory measurements, using the slab phantom, Harshaw 'X-Rad' dosemeters were used. These consist of 3mm by 3mm chips of lithium fluoride type TLD-700 (99.93% Li-7; 0.07% Li-6) doped with magnesium and titanium, hermetically bonded to a kapton substrate. These dosemeters were individually calibrated, and read out using a Harshaw 6600 reader with a heat cycle consisting of a heating rate of 15°C sec^{-1} upto 300°C, with an acquire time of 20s. These dosemeters have been widely investigated for use in patient dosimetry (Broadhead, 1997), showing reproducibility to within 3% and a minimum detectable dose of the order of 0.16 mGy. The energy response of the dosemeters was shown to be constant to within 7% for diagnostic X-ray beams from 60 to 100 kV. Before each use, the dosemeters

were annealed by putting them through the usual read cycle, as was recommended by Broadhead, then packaged in small plastic pouches for protection. The TLDs were read out approximately 24 hours after irradiation, at which time the rate of fading is low. For each experiment, ten dosemeters were retained to assess the background dose, which was then subtracted from each measured dose.

For the dosimetry with the anthropomorphic phantom, Harshaw TLD 100 chips were used. These consist of 3 mm by 3 mm lithium fluoride, 1 mm thick. They were oven annealed (1 hour at 400°C and 16 hours at 80°C), as recommended by Harshaw, before use and packed in small plastic sachets which were then either placed on the phantom surface or rolled and inserted into the holes inside the phantom, for assessment of organ doses. The dosemeters were read out on a Harshaw 5500 machine, also with a heat cycle consisting of a heating rate of 15°C sec^{-1} upto 300°C, with an acquire time of 20s, and the chips were individually calibrated, as before. The reproducibility of these chips has been shown to be 3.5%, with a detection limit of 0.05 mGy. Energy response was constant to within 5% for diagnostic spectra from 60 to 100 kV (Broadhead, 1997). As for the former set of measurements, ten chips were retained to assess the background dose for each experiment.

7.3 Image quality measurements

Definitions of contrast have been discussed earlier in Chapter 4. For radiographs and spot films, contrast is most easily expressed simply as a difference in optical density between adjacent areas of film. Optical densities were measured using a Parry digital transmission densitometer DT1505, for which the stated accuracy is 1% of reading ± 0.01D. Fog levels, as determined from an unexposed portion of the film, were subtracted from all readings.

7.3.1 Sensitometry

Sensitometry is the study of the quantitative relationship between exposure and optical density. It may be carried out in terms of either light or X-ray sensitometry, using time or intensity scale exposures. In light sensitometry a strip of film is exposed to a series of different light intensities, at a wavelength appropriate for the film used, in the form of narrow

steps. For X-ray sensitometry using time scale exposure, successive exposures are given on adjacent areas of a photographic layer by using a constant exposure rate at increasing times of exposure. Intensity scale exposure for X-rays consists of taking increasing exposures on strips of film at a given time, usually by changing the source-film distance. After processing the film or films and correcting measured densities for background fog levels (deduced from a processed unexposed film) a plot of film density against the logarithm of relative exposure gives the characteristic curve which demonstrates the reponse of the film.

Prior to commencing the initial laboratory measurements, both light and X-ray sensitometry was carried out on the film to be used in the experiments. The former used an X-Rite 383 light beam sensitometer on the 'green' setting, *ie* emitting light at the green end of the spectrum as do the screen phosphors used, and the X-ray sensitometry was carried out by moving a piece of lead stepwise across the film as a series of exposures was made on the X-ray set, at fixed settings. All films produced during the laboratory measurements were also exposed to the light beam sensitometer prior to processing, firstly as a check on the film quality and the processing - so that the effect of temporal variations in these parameters could be excluded - and secondly so that the radiographic contrast could be related to the exposure contrast. The latter bore a more direct relationship to the absorbed energy contrast in the screens, as determined from the Monte Carlo code. The exposure contrast, calculated from the sensitometric curve is given by the formula

$$C = \frac{10^{0.15sn_1} - 10^{0.15sn_2}}{10^{0.15sn_1}} \qquad (7.1)$$

where sn_1 and sn_2 refer to the sensitometric step numbers corresponding to the densities beside and behind the contrast detail respectively.

7.4 Patient phantoms

7.4.1 Tissue equivalent slabs

For the experimental verification of the Monte Carlo results, slabs of the tissue equivalent material (MS20, SB5 and LN100) simulated in the code were used, from RMI. These

materials form part of a series of epoxy resin based tissue substitutes, described by White *et al* (1977) that were formulated from an analytical procedure using basic interaction data (White, 1977). For MS20, a muscle substitute, the mass attenuation and energy absorption coefficients are given as within 3% of that for actual muscle across the diagnostic energy range. A muscle equivalent material was selected for soft tissue simulation, in preference to one simulating adipose tissue since for children, particularly very young children, muscle is the predominant soft tissue component (White *et al*, 1991). For the hard bone substitute, SB5, the mass attenuation and energy absorption coefficients are accurate to within 2%. The lung equivalent material is manufactured from epoxy resin expanded using foam (White *et al*, 1986). The amount of foam added for this series of materials affects the density, thus lung at different stages of inflation can be simulated. LN100 is the material simulating fully inflated lung tissue. This was considered the most appropriate as chest radiography is normally carried out on inspiration. The mass attenuation and energy absorption coefficients for LN100 are within 3% of those for the simulated tissue across the diagnostic energy range.

The tissue equivalent slabs, all 50 × 50 cm, were obtained in thicknesses of 0.5 (for SB5 only), 1.0, 2.0 and 5.0 cm. At the centre of some of the slabs a small disc of material was removed, of diameter 1.5cm. Small disks of the different materials were cut to fit the holes made, so that a number of different patient thicknesses could be simulated with either bone or lung detail in soft tissue, or bone detail in lung. This is illustrated in figure 7.1 for a 1 cm thick detail in 5 cm tissue. The available slab dimensions were such that a range of total thicknesses could be obtained.

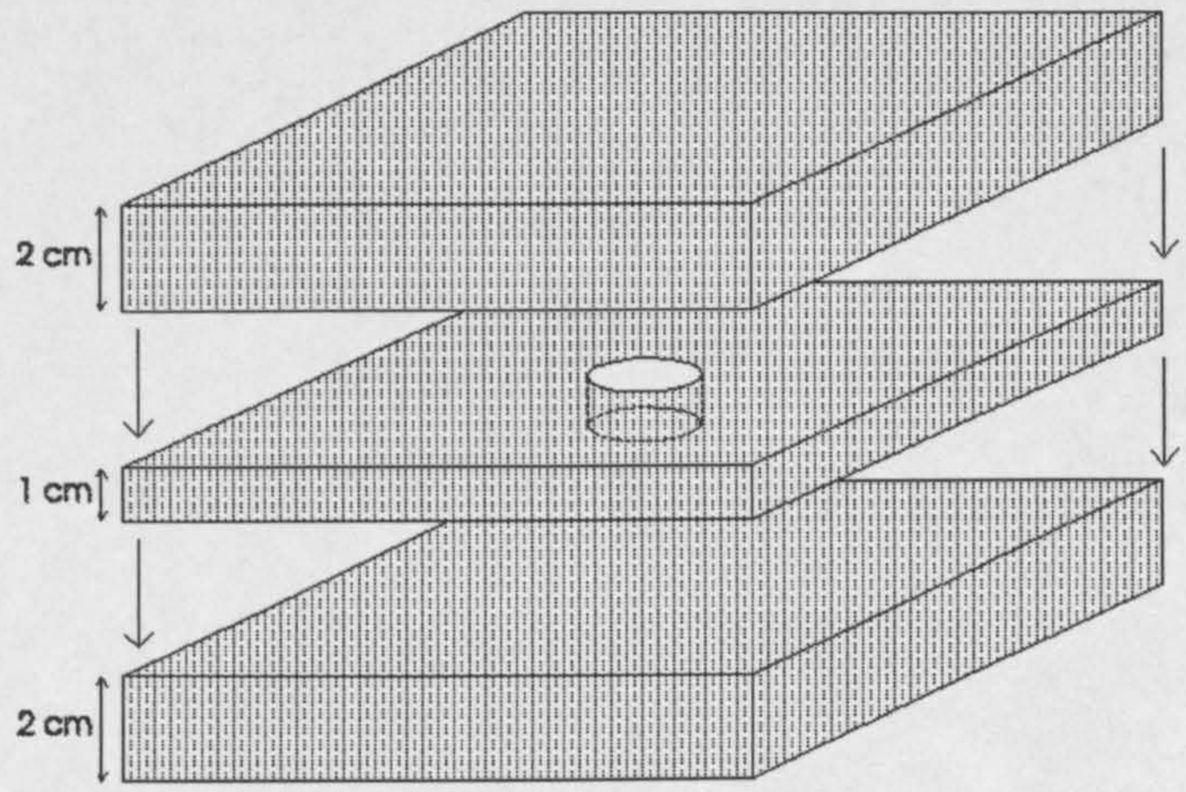

Figure 7.1 : Exploded view of tissue equivalent phantom

Using these slabs, geometries were obtained that were equivalent to those simulated in the Monte Carlo study, the only difference between being that for the computer simulation the slabs were assumed to be semi-infinite. Provided that, during the experimental work, the incident field-size was well within the area of the slab, this approximation should not significantly affect the results.

7.4.2 Anthropomorphic phantoms

An anthropomorphic phantom, representing a newborn infant was used for the second section of the experimental work. This was one (AHP-0) of a series of paediatric phantoms obtained from Latvian Medical Academy (Varchenya *et al*, 1993). The phantoms are illustrated in figure 7.2.

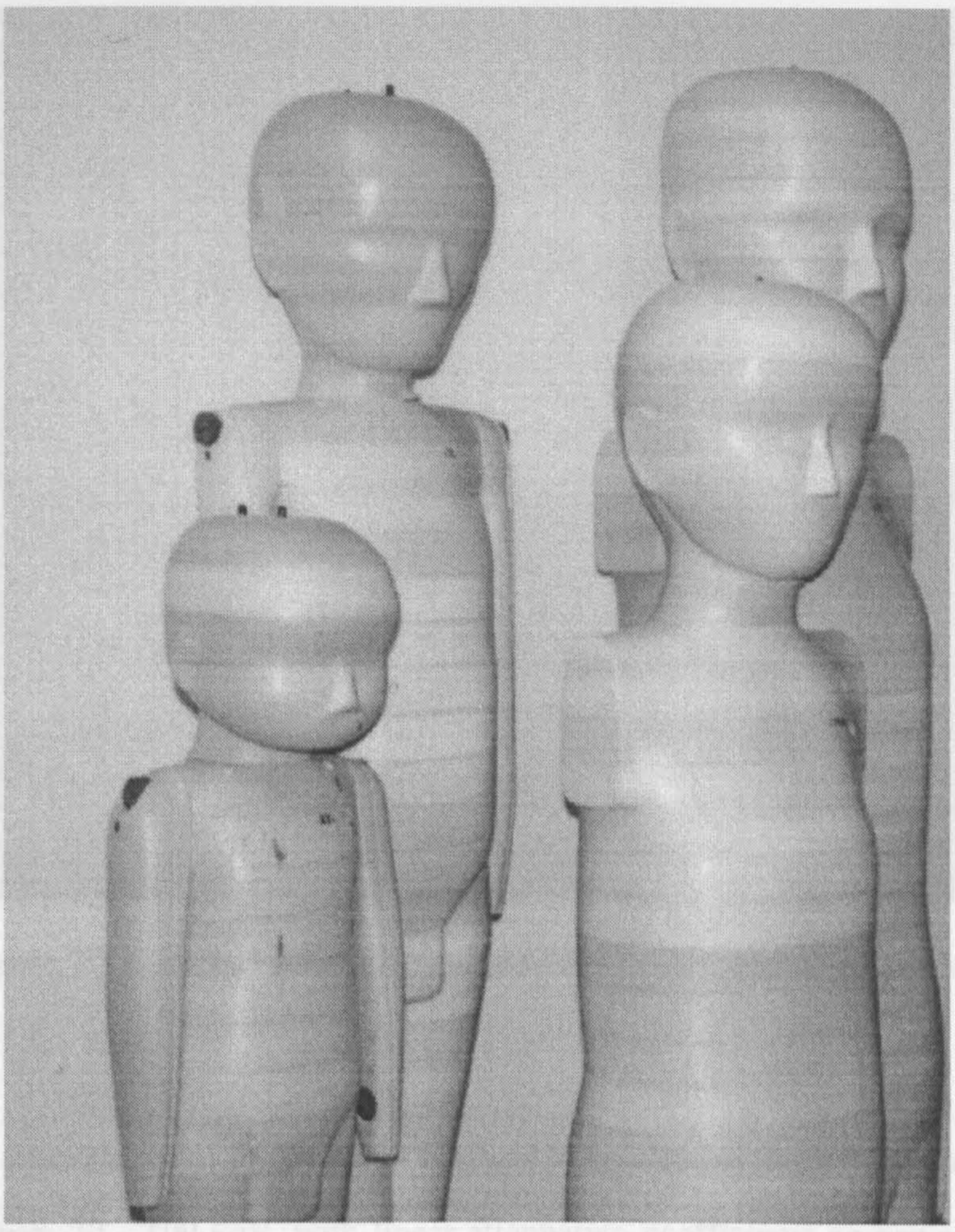

Figure 7.2 : Paediatric anthropomorphic phantoms

The composition of the phantom was P2D-MBT tissue equivalent material (density 1050 kgm^{-3}) with a plastic skeleton (density 1400 kgm^{-3}) and plastic lung (450 kgm^{-3}). It comprises 20 slices, with separate detachable arms. A total of 134 holes are contained within the phantom, for location of thermoluminescent dosimeters, and details of the relationship between the internal organs and the different hole numbers were provided with the phantom. The construction of the phantom slices is exhibited below in Figure 7.3

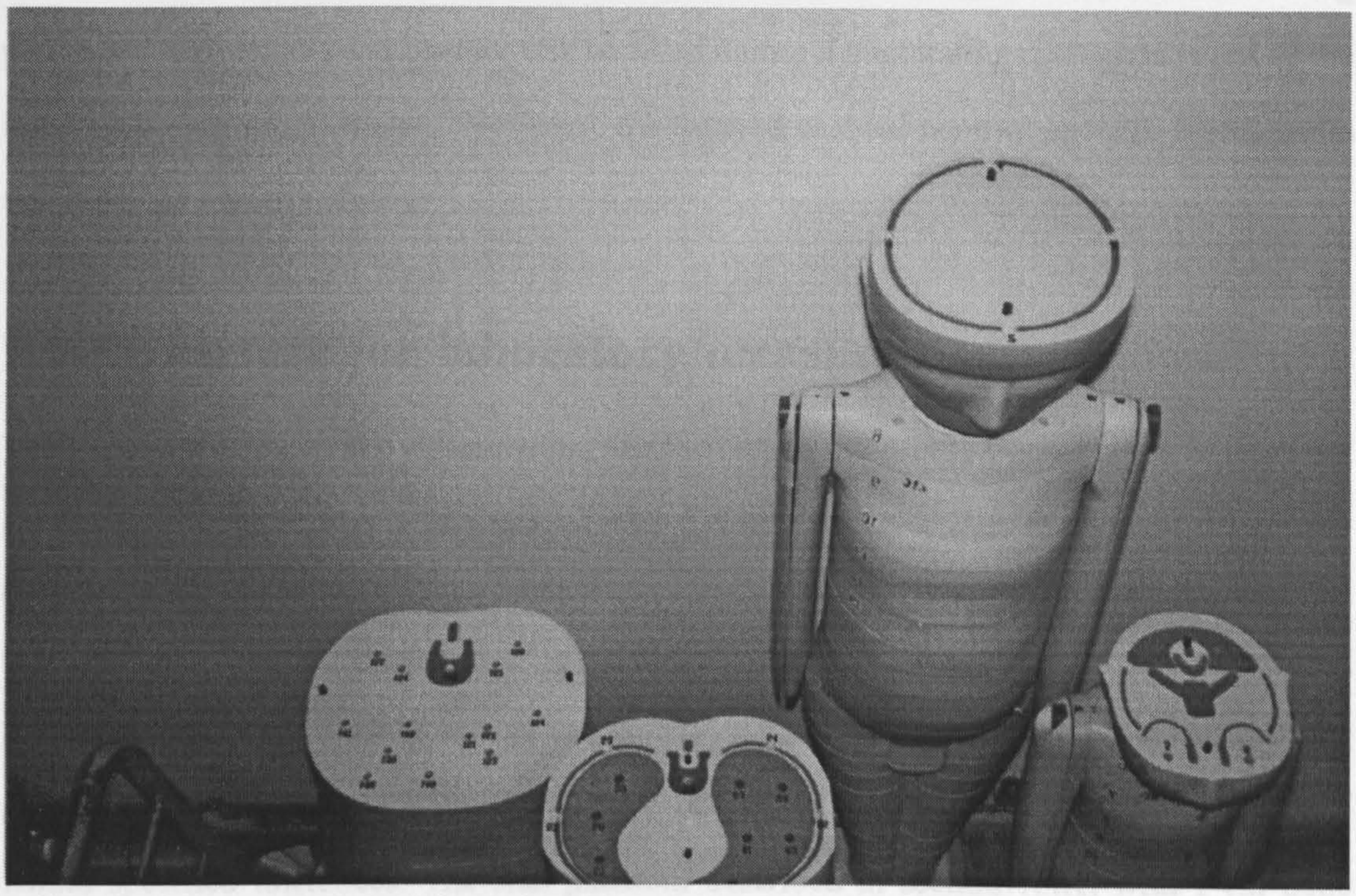

Figure 7.3 : Internal construction of paediatric anthropomorphic phantoms

The radiation equivalence of the phantom is stated to be close to that of the simulated tissues for energies from 20 - 100 keV, with linear attenuation coefficients agreeing to within 4% for all tissue types. Local measurements, however, have shown that at all tube potentials the phantoms significantly overestimate the attenuation, compared to water (Broadhead, 1998). However, this is unlikely to cause a problem for comparative dosimetry measurements.

Although radiographs of the phantom enabled direct assessment of bone/soft tissue contrast, it was necessary to introduce artificial contrast media for simulation of fluoroscopic examinations, which commonly use either iodine or barium based contrast agent. To achieve this, an extra phantom slice was constructed, from a 2 cm thick slab of MS20, to fit between slices 12 and 13 (around the abdomen of the phantom). At the centre of this slice, a 1.5 cm diameter hole was cut, and several small plastic vials manufactured to fit this hole. These could then be filled with the different contrast agents and placed in the additional phantom slice, which was then fitted into the rest of the phantom. Of necessity, this was only a rough approximation to an actual contrast examination as, in practice, the thickness and contours

taken up by the contrast within the body will vary hugely according to the examination being performed; *eg* urethers and bladder will be filled during a micturating cystogram, parts of the intestine during an enema *etc*. However, the method enabled contrast specific optimisation studies to be performed.

7.5 Procedure for laboratory measurements

The geometry used for the experimental verification of the Monte Carlo results is shown in figure 7.4 The X-ray unit comprised a Picker Vector 70 generator with a Picker X-ray tube attached to a Picker Cosmos tube stand. The nominal tube filtration was 2.5 mm Al, and with the DAP meter ionisation chamber attached the total filtration was 3 mm Al equivalence. Routine quality assurance is carried out on this tube and generator, and this showed that measured tube potentials were within ±2 kV of that set and that all other parameters were within specified tolerances. The slab phantom described in section 7.4.1, with 1 cm bone inset in 5 cm soft tissue, was set up on the floor with the tube head at its highest position, so as to obtain the maximum possible focus-skin distance (FSD). This was to alleviate one of the main practical problems encountered, namely the difficulty in obtaining sufficiently small values of mAs for the desired film density (of around 1.0). The phantom was placed directly on an Agfa Geveart screen containing Kodak Regular film. This configuration matches that of the computer simulations, and is representative of clinical practice for neonatal radiography. Tape was used to mark the position of the screen and phantom on the floor, and the position of the tube head, so that the geometry could be reproduced for each series of measurements.

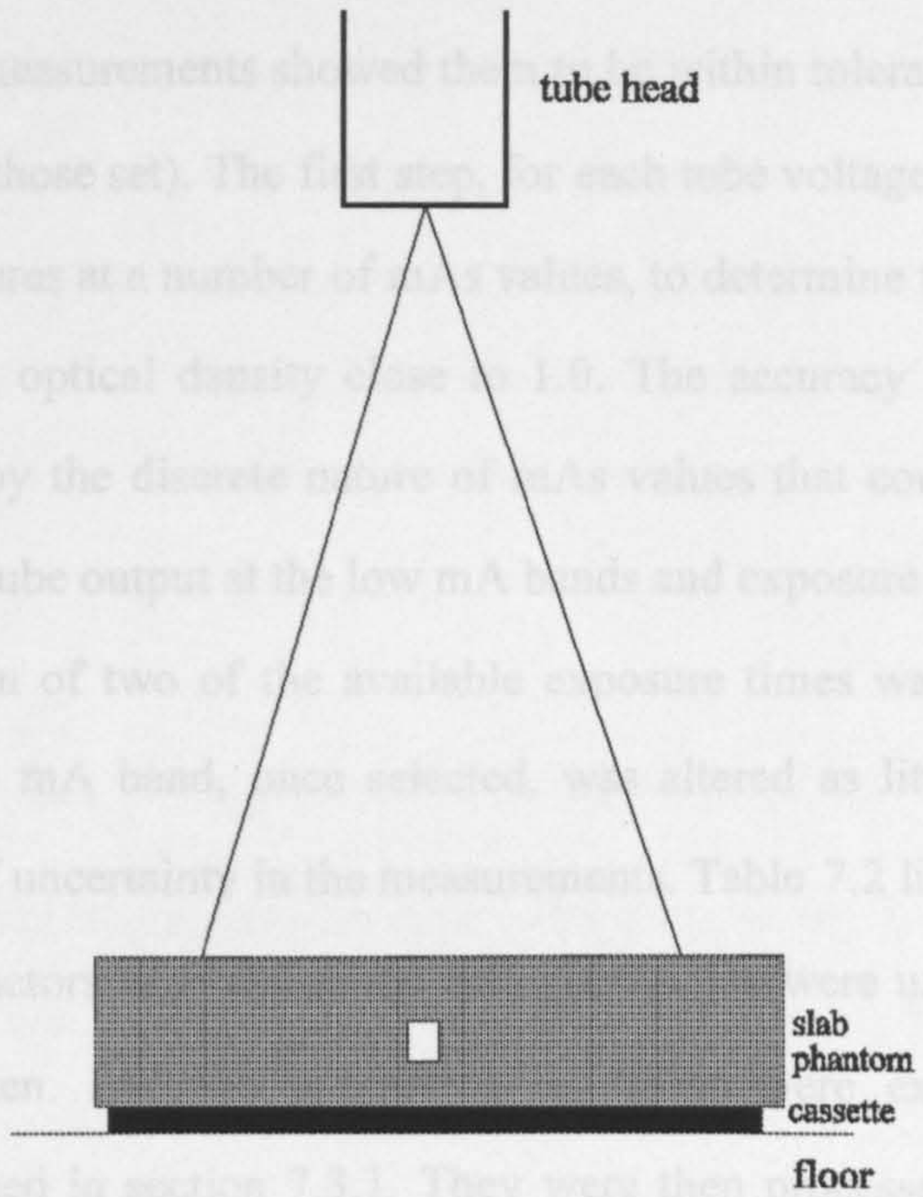

Figure 7.4 : Laboratory irradiation geometry

A number of filters were available for study, as listed in table 7.1.

0.1 mm copper	(Cu)
0.2 mm copper	(Cu)
0.1 mm erbium	(Er)
0.1 mm samarium	(Sm)
0.1 mm tin	(Sn)
0.1 mm gadolinium	(Gd)

Table 7.1 : Filters used in experimental measurements

The filters were obtained from Goodfellows and each was in the form of a 5 cm square sheet held within a slide mount for convenience and protection. The stated purity of the metals, on dispatch from the supplier, was greater than 99%, but they had been stored within the department for a number of years.

All measurements were compared to reference exposure conditions of 60 kV with no additional filtration. For each filter under investigation, measurements were carried out at

both 60 kV and 55 kV. Tube voltages on the set were checked as part of routine QA, and the most recent set of measurements showed them to be within tolerance (*ie* measured values were within ± 2 kV of those set). The first step, for each tube voltage and filter combination, was to carry out exposures at a number of mAs values, to determine the exposure parameters required to achieve an optical density close to 1.0. The accuracy to which this could be achieved was limited by the discrete nature of mAs values that could be selected, and the lack of stability of the tube output at the low mA bands and exposure times required. In some instances a combination of two of the available exposure times was necessary to obtain a suitable exposure. The mA band, once selected, was altered as little as possible so as to minimize one source of uncertainty in the measurements. Table 7.2 lists these experimentally determined exposure factors with which the radiographs that were used for comparing filter performance were taken. Prior to processing, all films were exposed with an X-Rite sensitometer as described in section 7.3.1. They were then processed using an Agfa Curix Compact daylight processor on which regular QA checks are performed.

		Filter						
		Al only	0.1mm Cu	0.2mm Cu	0.1mm Er	0.1mm Sm	0.1mm Sn	0.1mm Gd
mAs	@ 60 kV	3.0	5.0	7.2	8.0	8.4	14.2	9.0
	@ 55 kV	-	9.0	13.4	13.4	12.9	21.2	13.4

Figure 7.2 : Exposure factors used to produce test radiographs

Although ideally dosimetry would have been carried out concurrently with the film exposures, the radiation dose from a single exposure was too low for accurate TLD dosimetry. It was therefore necessary to use larger mAs values (simulating multiple exposures) when making the dosimetry measurements, than those used when exposing the film. As a result, the dosimetry measurements for each filter were made directly after obtaining the radiographs. Doses were measured at several points on and within the phantom using the X-rad dosemeters described in section 7.2. Doses were measured at four levels within the phantom; on both entrance and exit surfaces of the slab, and at 2 cm and 3cm depth (*ie* between slabs). Six dosemeters were used at each location, placed near the centre of the phantom without overlapping the area of bone detail. For all measurements of both

dose and contrast a large area ionization chamber (20X5-60, 60cc chamber; Radcal Inc.) was placed at a marked position on the surface of the phantom, inside the beam area but not covering the area of contrast material. The ion chamber readings were used to normalize the dose results to the exposure level corresponding to that used when taking the radiograph. This methodology was used as inconsistent results were obtained when extrapolating doses according to mAs values, as tube output was not linear in this region of the low mA/low exposure bands being operated.

7.6 Procedure for hospital measurements

Two sets of experimental measurements were carried out at the Royal Victoria Infirmary, Newcastle Upon Tyne, for plain film radiography and fluoroscopy respectively. These were carried out using the newborn anthropomorphic phantom. 134 TLD were used inside the phantom, for assessment of internal organ doses, and a total of 22 dosemeters were placed on the surface of the phantom, for the assessment of skin dose and entrance surface dose. Organ doses were calculated and also the effective dose, using the organ weighting factors given by the ICRP (ICRP 60, 1991). The calculation of effective dose provided a dose quantity for comparative purposes only, as the field sizes and positioning used for the experiments did not correspond to any particular type of examination.

7.6.1 Plain film radiography

In the first experiment, the phantom was radiographed on an MX4 mobile, similar to that used on the special care baby unit (SCBU), using an Ultravist screen-film system (a lanthanum based screen), which is the screen-film combination routinely used in the department. The phantom lay directly on the film casette, placed on a trolley and the initial radiographs were taken without any additional filtration at 60 kV, with the paediatric radiographer advising on the technique factors to be used (6 mAs). Further radiographs were taken with additional filters of 0.1 mm copper and then 0.1 mm dysprosium, both at 56 kVp (the nearest available setting to 55 kV). Available mAs settings were in discrete steps of 3 mAs, so it was not possible to match the background film densities exactly. Acceptable exposures were obtained using 12 mAs for the copper filter and 18 mAs for the dysprosium

filter. For the dosimetry measurements, doses were integrated over 20 exposures. The experimental geometry is shown figure 7.5. The field-size used was 22 cm × 18 cm, with a focus-skin distance (FSD) of 80 cm The tube was centred over the abdomen, and the extent of the beam area - as indicated by the light beam diaphragm- noted, to aid reproducibility. Contrast measurements were made from the radiographs obtained, using the lowest lumbar vertabrae as the area of interest and the surrounding soft tissue as background.

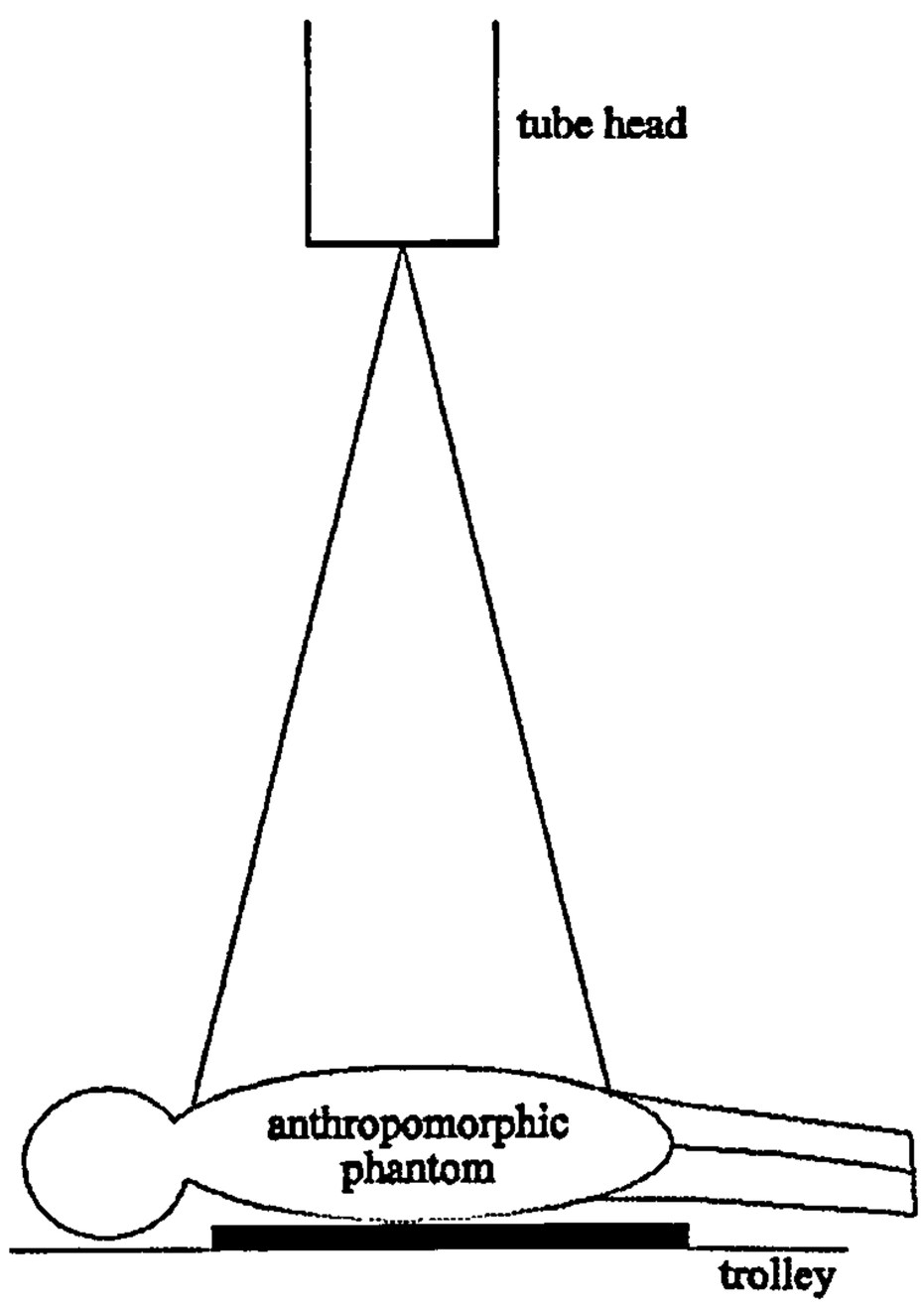

Figure 7.5 : Geometry of irradiations on MX4

7.6.2 Fluoroscopy

Fluoroscopy measurements were carried out in the Paediatric screening room. The equipment used was a Shimadzu 3 phase 12 peak generator HD1SOB - 30 with a Circlex tube, a Shimadzu image amplifier and Philips 100mm camera. The undercouch tube was not easily accessible for mounting additional filtration on the tube head, as is customary, so 0.1 mm copper filtration was introduced into the beam by means of a 50 × 50 cm sheet, placed on the couch directly beneath the phantom. The geometry is illustrated in figure 7.6.

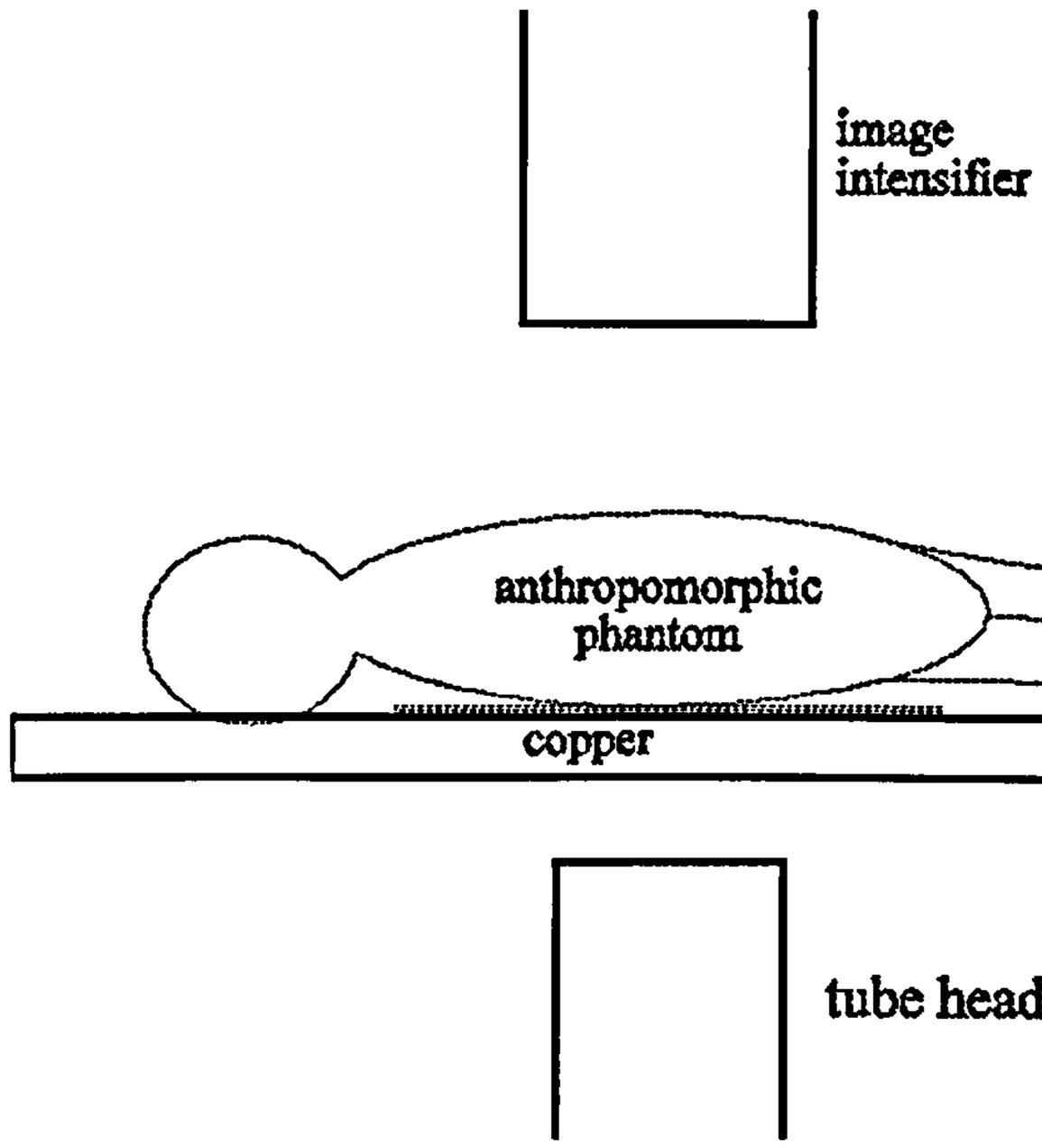

Figure 7.6 : Geometry for experimental measurements in paediatric screening room

The newborn anthropomorphic phantom was used, with an additional slice containing a cylinder of Isopaque Cysto, an iodine based contrast media used for neonatal cystograms, as previously described. The paediatric radiographer assisted in the preliminary trial of exposure factors for the experiment, to ensure that those chosen were clinically representative. Fluoroscopic screening in this room is normally carried out under manual control of technique factors. The technique factors used were 60kV and 0.5 mA, and these factors were unchanged with the copper filter in place as no adverse effect on image quality, as judged by the radiographer, was observed when viewing the image on the visual display unit. 100mm spot films are normally taken under AEC, with fixed tube voltage and current and this resulted in a slight increase in exposure time (from 8 to 9 ms) for films taken with the copper filter in place (at 60 kV and 150 mA).

For the dosimetry measurements, the phantom was screened for 5 minutes with the tube static and centred over the abdomen. The phantom was loaded with TLD as for the previous experiment, and the dose area product reading was also recorded. A single spot film was

taken at the end of the period of fluoroscopy in order to make objective measurements of contrast using the area of contrast media and the surrounding tissue.

7.7 Accuracy of measurements

There are many factors influencing the level of uncertainties in the experimental results. Assessment of the uncertainties in TLD measurements has been discussed in the National Protocol for patient dose measurements (IPSM, 1992). As, for this work, no calibration of the TLD was carried out, the dose is given by

$$D = X - B \tag{7.2}$$

where X and B are the mean measured and background counts respectively. The standard error in D, S_D is given simply by the quadrature sum of the individual standard errors.

$$\frac{S_D}{D} = \frac{\left[S_X^2 + \frac{S_B^2}{n_B}\right]^{1/2}}{(X - B)} \tag{7.3}$$

The standard deviation of X is used, in preference to the standard error, since it is the uncertainty associated with a single measurement, not the mean of a series of measurements, that is required (IPSM, 1992). The total random uncertainty for individual TLD measurements, at the 95% confidence limit is thus

$$U_D = 2\frac{\left[S_X^2 + \frac{S_B^2}{n_B}\right]^{1/2}}{(X - B)} \tag{7.4}$$

where S_X is the standard deviation of counts from a series of identical doses to the same TLD, S_B the standard deviation in the background and n_b the number of TLD used to assess the background. Non-random uncertainties are more difficult to quantify and may arise from the energy response of the dosemeters, non-linearity with dose, fading of the TLD signal and temporal variations in the TLD reader. For the TLD system used here, the non-random uncertainty has been shown to be less than 10% (Broadhead, 1997). Uncertainties in

calculated organ doses and in effective dose are greater than these, and depend on the size of the organ, the number of TLD used to assess the dose and the uncertainties in the organ weighting factors.

For density assessments, the uncertainty in each individual density measurement is 1% of the reading, but the main source of uncertainty in the contrast measurements arises from fluctuations in density, within a uniformly irradiated area of the film. These were assessed by making a series of density readings around each point of interest, and calculating the standard deviation of these. As

$$C = D_1 - D_2 \qquad (7.5)$$

The standard error in the calculated contrast is also given by the quadrature sum of the individual standard errors, and the overall uncertainty at the 95% confidence level by

$$U_C = 2 \frac{\left[\frac{S_{D_1}^{\ 2}}{n_{D_1}} + \frac{S_{D_2}^{\ 2}}{n_{D_2}} \right]^{1/2}}{D_1 - D_2} \qquad (7.6)$$

where D_1 and D_2 are the adjacent mean values of optical density for the two areas of interest, n_{D1} and n_{D2} are the number of measurements of each density and S_{D1} and S_{D2} are the standard deviations in the readings.

If absolute measurements of the dose and image quality parameters were required, other factors such as uncertainty in calibration of the TLD, the tissue equivalence of the phantoms *etc* would also have to be assessed, but for comparative measurements these have little importance as they affect all the measurement in the same way. Uncertainties arising from inaccurate repositioning between experiments, or variations in tube parameters could influence the result, but these have been minimized as far as possible.

7.8 Summary of chapter

In this chapter, the reasons for carrying out the different types of experimental measurements have been explained, and the techniques used for assessing dose and image quality described. These involved TLD dosimetry and contrast measurements both directly from film densities and using sensitometric techniques. The phantoms used in making the measurements were also described, and consisted of simple slab phantoms for the laboratory work and an anthropomorphic newborn phantom for the hospital based measurements. The various irradiation geometries used have been illustrated, and the experimental procedures outlined. The methods used for calculating the uncertainties in the measured quantities have also been presented.

Chapter 8

Results of Experimental Verification

8.1 Introduction

The results of the experimental measurements used to verify the Monte Carlo code are presented in this chapter. The first section gives the numerical derivation of the measurement uncertainties, for both dose and contrast measurements. The results from the laboratory measurements are then presented and compared with the theoretical predictions, in terms of both absolute values and the ratios of each quantity relative to baseline values. The results of the two types of clinical measurements are then given, and the factors affecting these discussed.

8.2 Uncertainties in measurements

The various sources of uncertainty in the experimental measurements have been discussed in the previous chapter. The total random uncertainty at 95% confidence level for individual TLD measurements was assessed for each set of results, according to equation 7.4, from the background TLD readings. The results are summarised in Table 8.1 below for the maximum and minimum values of X (TLD reading) found in each set of data, where the symbols are as given in section 7.7. *MX4* refers to film-screen radiography on the hospital MX4 mobile X-ray set, and *fluoro* to measurements made in the paediatric fluoroscopic room. The figures in the table demonstrate that when X is much greater than B the measurement uncertainty arises almost entirely from the reproducibility of the TLD signal, S_X.

Measurement set	S_X	S_B	n_B	X	B	U_D
0.1 mm copper	3%	4.3	10	253.7 1746	35.5	7.1% 6.1%
0.2 mm copper	3%	5.8	10	224.8 874.1	24.1	7.0% 6.2%
0.1 mm erbium	3%	6.7	10	193.8 968.7	27.7	7.3% 6.2%
0.1 mm samarium	3%	5.1	10	276.1 1280	27.4	6.6% 6.1%
0.1 mm tin	3%	7.2	10	192.3 1053	24.6	7.4% 6.2%
0.1 mm gadolinium	3%	4.2	8	285.1 1033	22.5	6.6% 6.1%
MX4 - no added filtration	3.5%	0.008	17	0.095 4.969	0.062	23.3% 7.1%
MX4 - with copper /dysprosium	3.5%	0.006	10	0.088 2.042	0.056	22.6% 7.2%
Fluoro - with/ without copper	3.5%	0.008	10	0.077 32.86	0.044	22.4% 7.0%

Table 8.1 : Uncertainties in TLD measurements

For the laboratory measurements, all uncertainties are around 6-7% of the dose value. The uncertainty arising from repositioning between experiments was assessed to be less than 1%, so the combined uncertainty was thus taken to be ± 7% for all laboratory dose measurements. For the hospital measurements, uncertainties range from around 7% for superficial organs within the beam area to over 20% for organs well outside the beam. For the clinical measurements, uncertainties also arise from the calculation of individual organ doses from the TLD measurements. These were assessed to be 20% for small organs such as the thyroid or ovaries where only 1 or 2 TLD were used to calculate the dose, 10% for larger organs, and 10% for distributed organs such as bone marrow dose. Uncertainties due to repositioning between experiments are also large for organs on the periphery of the beam, as dose drops sharply at the beam edge. Such uncertainties were judged to be in the order of 20% whereas repositioning uncertainties for other organs were close to zero. The combined uncertainties, for the clinical measurements, were obtained by summing the various components in

	small organs	large organs
beam centre	22%	14%
beam periphery	30%	25%
outside beam	28%	22%

Table 8.2 : Uncertainties for different sized organs at various beam positions.

quadrature and values used for different organ types are listed in Table 8.2. The uncertainty in calculated contrast for each radiograph is similarly given in Table 8.3 where the symbols are as defined in equation 7.5.

Meas. Set	S_{D1}	S_{D2}	n_{D1}	n_{D2}	D_1	D_2	U_C
0.1mm Cu	0.01	0.01	10	10	1.00	0.52	1.9%
0.2mm Cu	0.01	0.01	10	10	0.98	0.51	1.9%
0.1mm Er	0.01	0.01	10	10	0.99	0.50	1.8%
0.1mm Sm	0.01	0.01	10	10	1.07	0.46	1.5%
0.1mm Sn	0.01	0.01	10	10	0.92	0.42	1.8%
0.1mm Gd	0.01	0.01	10	10	0.98	0.42	1.6%
MX4-Al(pelvis)	0.02	0.05	5	5	1.59	1.42	28.3%
MX4-Al(spine)	0.09	0.05	5	5	1.78	1.31	19.6%
MX4-Cu(pelvis)	0.03	0.07	5	5	0.78	0.57	32.4%
MX4-Cu(spine)	0.06	0.07	5	5	1.00	0.58	19.6%
MX4-Dy(pelvis)	0.02	0.04	5	5	0.70	0.53	23.6%
MX4-Dy(spine)	0.07	0.03	5	5	0.72	0.39	0.66%
Fluoro - Al	0.02	0.004	5	5	0.27	0.01	8.2%
Fluoro - Cu	0.02	0.00	5	5	0.13	0.00	15.5%

Table 8.3 : Uncertainties in calculated contrast

For the laboratory measurements, fog levels on the various films were consistent to within ±0.01. Sensitometric measurements showed consistency in processing to within 1% across the range of exposure levels. Slight repositioning errors did not have an effect on the calculation of contrast, so that combined uncertainties at 95% confidence level were as listed in

Table 8.3 above. The uncertainty in contrast measurements on the laboratory film are low as there are only two, clearly defined areas on the film corresponding to the uniform tissue and contrast detail in the slab phantom. The contrast measurements made on the hospital films have a much greater level of uncertainty as the use of the anthropomorphic phantom resulted in large fluctuations of density over a small area, making repeatable density measurements difficult.

8.2 Laboratory measurements

Measurements of entrance dose, depth dose and film contrast were made, as described in Chapter 6 for a number of different beam filters, using the 5 cm tissue phantom containing 1 cm bone. The exposure factors used to acquire radiographs with a background density close to 1.0, as found experimentally, are listed in Table 8.4. for each filter, along with the actual background density obtained. As measurements corresponding to different filters were made on different days, baseline measurements, without additional filtration, were made on each occasion. The exposure factors used for these baseline radiographs were 60 kVp and 3 mAs.

Filter	baseline	filter @ 60 kV		filter @ 55 kV	
	bkgd density	mAs	bkgd density	mAs	bkgd density
0.1mm copper	0.98	5.0	0.99	9.0	1.00
0.2mm copper	1.02	7.2	0.98	13.4	0.97
0.1mm erbium	1.02	8.0	0.99	13.7	1.06
0.1mm samarium	1.05	8.4	1.07	12.9	1.06
0.1mm tin	0.90	14.2	0.92	21.2	0.90
0.1mm gadolinium	1.03	9.0	0.98	13.4	1.01

Table 8.4 : Exposure factors used for laboratory measurements (uncertainty in all density measurements ± 0.01)

Each of the above exposure factors was determined after experimenting with different mAs values to obtain the optimum film density, which is inevitably limited by the discrete nature

of the available tube current and exposure time settings. It can be seen from Table 8.4 that it was not possible to achieve identical film densities for the different combinations of tube voltage and filter, but the radiographs were adequate for use in making comparisons of film contrast. It is also apparent from the table that, although the same technique factors were set each time for the baseline radiographs, the background film density was not consistent. Possible reasons for this are fluctuations in the film quality, processing changes, or drift in the generator parameters over time. Routine QA checks on the set show that although tube output is generally consistent, and the measured tube voltages remain within ± 2 kV of the nominal values, the exposure timer performs erratically at the short exposure times corresponding to those used for these measurements. Prior to the start of the experimental work, the exposure timer error at a nominal setting of 30 ms was 18%, with a more recent measurement giving a 6% error. As all results have been considered in terms of the ratio of each quantity of interest for the test conditions relative to baseline values, the effect of such variation in equipment performance has been accounted for.

8.2.1 Contrast measurements

Film contrast for each radiograph was calculated as the difference in film density behind and beside the area of bone detail, the latter being the background density. These measured values of film contrast are given in Table 8.5, together with the corresponding values predicted from Monte Carlo simulations. The predicted contrast for baseline filtration of 3mm aluminium only is 0.423 ± 0.003.

filter	experimental results (± 0.01)			Monte Carlo results	
	baseline	@ 60 kV	@ 55 kV	@ 60 kV	@ 55 kV
0.1mm copper	0.48	0.42	0.48	0.375±0.004	0.438±0.005
0.2mm copper	0.55	0.47	0.52	0.339±0.004	0.371±0.005
0.1mm erbium	0.60	0.49	0.57	0.353±0.004	0.391±0.005
0.1mm samarium	0.62	0.61	0.66	0.413±0.005	0.448±0.005
0.1mm tin	0.57	0.50	0.52	0.366±0.007	0.425±0.010
0.1mm gadolinium	0.60	0.56	0.61	0.405±0.007	0.432±0.005

Table 8.5 : Measured and predicted values of film contrast

It can be seen that although experimental contrast values are all greater than those predicted, the relative values (*ie* values with additional filtration compared to those without) are consistent, as will be illustrated in Table 8.7, which gives the ratios of contrast values for each filter relative to the appropriate baseline value. One source of difference between the measured and predicted values is that the calculated contrasts are primary contrast values, derived from energy absorption in the screen. For these contrast values to relate accurately to differences in film density requires both measurement points to lie on the linear portion of the characteristic curve for the film. To investigate the extent to which this criteria affects the results, the sensitometric measurements made on each film processed were used in a separate derivation of contrast, based on film exposure, rather than film density as described in Chapter 7. These contrast values are given in Table 8.6.

filter	baseline	filter @ 60 kV	filter @ 55 kV
0.1mm copper	0.425	0.362	0.415
0.2mm copper	0.472	0.394	0.415
0.1mm erbium	0.472	0.404	0.463
0.1mm samarium	0.499	0.444	0.516
0.1mm tin	0.516	0.415	0.463
0.1mm gadolinium	0.481	0.454	0.499

Table 8.6 : Contrast values derived using sensitometric techniques (all ±5%)

For the first row of data in the table, that relating to added filtration of 0.1 mm copper, contrast values derived in this way show excellent agreement with those predicted. The contrast values derived in this way are all less than those measured directly from the film, but the relative changes for each different filter are not significantly affected by the calculation technique. This is illustrated in Table 8.7 which summarises the contrast ratios with and without additional filtration for the two measurement techniques and the predicted values.

	ratios of contrast for filter with respect to baseline					
	@ 60 kV			@ 55 kV		
	direct (± 0.01)	sensitom. (± 0.06)	predicted (± 0.02)	direct (± 0.01)	sensitom. (± 0.07)	predicted (± 0.02)
0.1mm Cu	0.88	0.85	0.89	1.00	0.98	1.04
0.2mm Cu	0.80	0.83	0.80	0.88	0.88	0.88
0.1mm Er	0.82	0.86	0.83	0.95	0.98	0.92
0.1mm Sm	0.98	0.91	0.98	1.06	1.03	1.06
0.1mm Sn	0.88	0.80	0.85	0.91	0.90	1.00
0.1mm Gd	0.93	0.94	0.96	1.02	1.04	1.02

Table 8.7 : Measured and predicted ratios of contrast for each irradiation condition with respect to baseline

The three sets of derived contrast ratios are in good agreement, within the stated uncertainties. This indicates that the Monte Carlo code gives good prediction of contrast changes, though absolute contrast values are less reliable. This is due to the large number of factors affecting them, such as the film, processor and variations in X-ray generator performance. It can be seen from Tables 8.4 and 8.5 that the best agreement between measured and calculated values is for the first set of measurements (those carried out with 0.1mm copper filtration) and that subsequent baseline measurements - made with identical technique settings - show a variation in contrast, with an overall increase observed over the period during which measurements were carried out. To assess the influence of changes in film or processing, the sensitometric curves for the various films were plotted , as shown in Figure 8.8, along with the date of measurement.

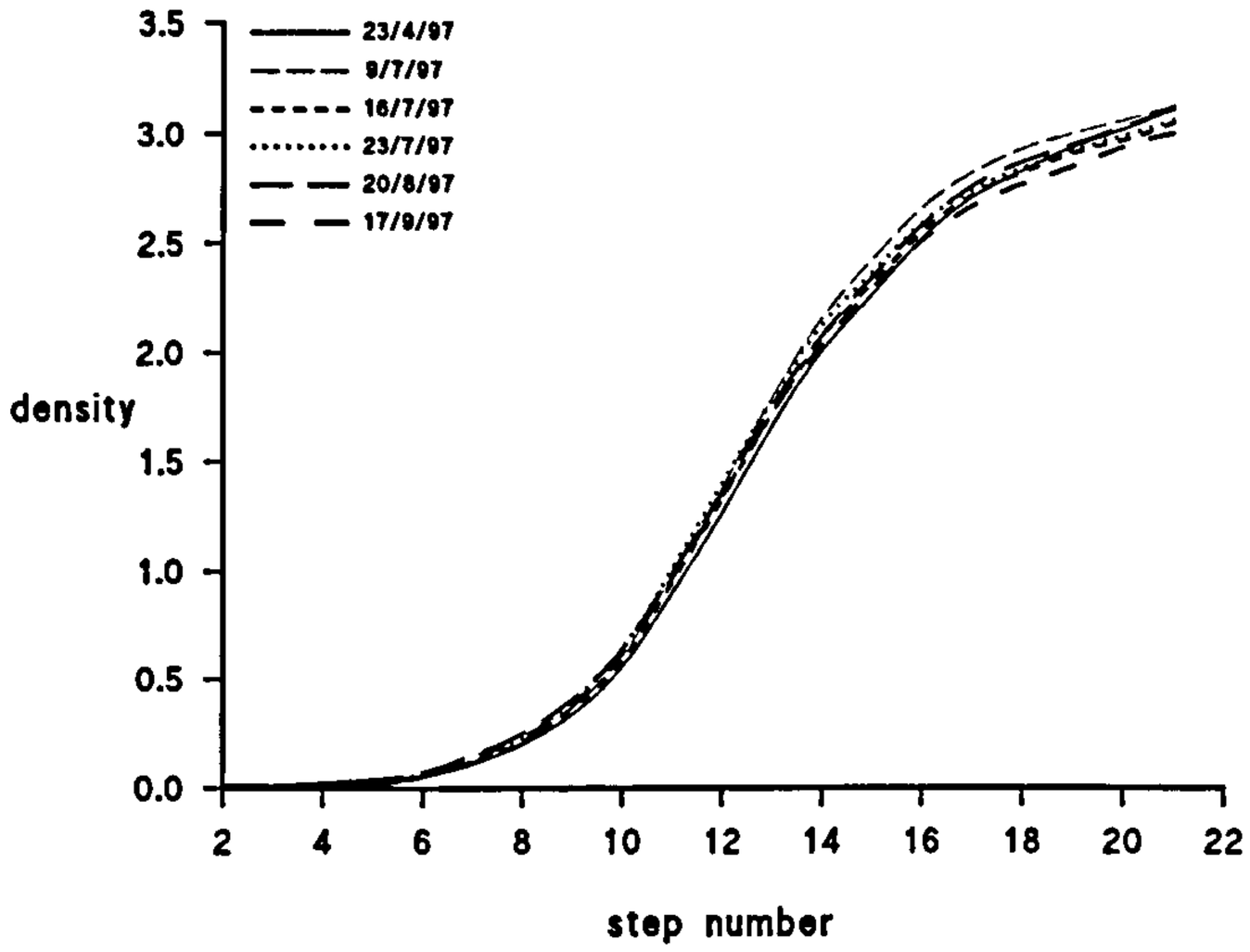

Figure 8.8 : Variation in sensitometric curve over time

Although slight changes in the shape of the characteriatic curve are apparent, they are within the expected day to day variations. In addition, there is no link to the time of irradiation and processing, or to the contrast values obtained. The differences between the curves also occur mainly at film densities greater than those used for the contrast measurements made. In the light of these comments, film response was deduced to be an unlikely cause of the fluctuations in contrast on different dates. These were most likely caused by fluctuations in the X-ray generator operating characteristics. Although of interest, they do not affect the experimental results, as it was the comparative readings from the same day that were being used to validate the Monte Carlo results.

8.2.2 Dosimetry measurements

Entrance dose was calculated as the mean dose measured by the six TLD at the surface of the slab phantom. The mid-body dose was calculated as the average of doses from the six TLD placed at 2 cm depth and the six TLD placed at 3 cm depth, and this quantity was compared to Monte Carlo calculated values of absorbed energy as both give a more representative assessment of patient dose than a simple entrance dose value, although they

can not be expected to be numerically equal as mid body dose will only be a very rough approximation to absorbed dose throughout the body. Exit dose values were also measured, using six TLD at the exit surface of the phantom. For each filter, measurements were carried out at both 60 and 55 kV with mAs values of 400 (for no additional filtration) or 1000 (with additional filtration), and results were then normalised to conditions of equal background density as described in section 7.5. The normalised dose values are presented in Table 8.8. It should be noted that the results for different measurement sets (*ie* different rows of the table) do not necessarily relate numerically to one another, as two different dosemeters were used during the course of the study and calibration factors have not been applied to the results. The object of the measurements was to compare results for a given filter with the corresponding baseline measurement (made in the same day with the same dosemeter) *ie* numbers along a single row.

filter	baseline			filter @ 60 kV			filter @ 55 kV		
	top	mid	exit	top	mid	exit	top	mid	exit
0.1mm Cu	31.3	18.2	5.6	19.9	15.5	5.7	25.3	18.9	7.8
0.2mm Cu	5.10	2.94	1.49	2.95	2.33	1.31	4.08	2.90	1.52
0.1mm Er	5.16	3.17	1.42	3.42	2.55	1.54	4.18	2.73	1.57
0.1mm Sm	5.43	2.99	1.42	5.03	3.32	1.64	5.73	3.60	1.82
0.1mm Sn	5.09	3.17	1.45	4.81	2.93	1.51	6.49	3.41	1.47
0.1mm Gd	3.84	2.21	1.14	2.26	1.61	0.79	3.42	2.21	1.09

Table 8.8 : Measured relative dose values at different depths : all values have uncertainty ± 7%

It can be seen from Table 8.8 that exit doses within each measurement set, *ie* along a single row, are very similar, as would be expected for conditions of equal background density. The more obvious differences are mirrored by differences in the background density of the test radiographs concerned, as given in Table 8.4 *eg* for 0.1 mm gadolinium filtration, the radiograph carried out at 60 kV had a background density of 0.98, compared to 1.03 at baseline.

The results were compared with those predicted by the Monte Carlo calculations by looking at the ratios of each dose quantity with and without the additional filter. These values are

given in Table 8.9 for entrance dose, mid slab dose and absorbed energy. The uncertainty in each experimental dose ratio, to within 95% confidence limits is ±10%. The uncertainty in the predicted ratios are 2.8% for entrance dose and 0.1% for absorbed energy.

filter	@ 60kV				@ 55kV			
	experiment		predicted		experiment		predicted	
	ent.dose (±10%)	mid dose (±10%)	ent.dose (±2.8%)	abs.en. (±0.1%)	ent.dose (±10%)	mid dose (±10%)	ent.dose (±2.8%)	abs.en. (±0.1%)
0.1mm Cu	0.64	0.85	0.72	0.84	0.81	1.04	0.89	0.96
0.2mm Cu	0.58	0.79	0.60	0.77	0.80	0.99	0.72	0.89
0.1mm Er	0.66	0.80	0.73	0.82	0.81	0.86	0.77	0.93
0.1mm Sm	0.93	1.11	0.84	1.03	1.06	1.20	0.96	1.09
0.1mm Sn	0.94	0.92	0.88	1.18	1.28	1.08	1.16	1.45
0.1mm Gd	0.67	0.83	0.72	0.88	0.89	1.00	0.89	1.02

Table 8.9 : Comparison of measured and predicted ratios of dose with and without filter

It can be seen from the figures in the table that the measured and predicted dose ratios agree to within the quoted uncertainties in all but two of the twenty-four data pairs. There does not appear to be any bias in the results, as the observed dose ratios are sometimes greater and sometimes smaller than those predicted. The only discrepancies are for absorbed energy reduction with the tin filter, for which measured values are less than those predicted by 22% and 25% at 60 kV and 55 kV respectively. This is explained by the fact that the experimental measurements are for mid body dose (*ie* at a depth of 2 cm) rather than total energy absorbed in the body. For most of the beam spectra involved in the experiments, the ratio of two such depth doses (with and without the additional filter) is very close to the ratio of energy imparted, but with tin filtration the beam spectrum has a sharp peak just under 30 keV, and photons of this energy will be absorbed within a short distance in the phantom tissue, thus contributing to the absorbed energy (as calculated by Monte Carlo) but not to the measured mid-body dose. The experimentally determined dose values are thus less than those predicted.

8.2.3 Tube loading

A comparison of predicted and measured tube loading, using the convention that this is proportional to the product of kV and mAs was initially made from consideration of the mAs values required for radiographs of equal background density. As the mA and exposure time settings on the X-ray set were shown to be inaccurate at the low levels used here (as discussed in section 7.5) relative output was also calculated from the ion chamber readings used for dose normalisation. Both derivations of tube load are given in Table 8.10, together with that predicted by the Monte Carlo calculations from a consideration of both the relative number of particle histories required for equal background density, and the tube voltage used in the simulations.

filter	relative tube load at 60 kV			relative tube load at 55 kV		
	from mAs	from ion chamber	from Monte Carlo	from mAs	from ion chamber	from Monte Carlo
0.1mm Cu	1.7	1.5	1.6	2.3	2.4	2.5
0.2mm Cu	2.4	2.0	2.4	4.1	3.5	3.9
0.1mm Er	2.7	2.2	2.2	4.1	3.2	3.4
0.1mm Sm	2.8	2.4	2.2	3.9	3.0	3.1
0.1mm Sn	4.7	3.4	2.9	6.5	5.1	4.7
0.1mm Gd	3.0	1.7	2.0	4.1	2.9	2.9

Table 8.10 : Comparison of measured and predicted tube loads. Uncertainties are ±10% for calculations for ion chamber readings and ±1% for Monte Carlo readings.

Agreement between measured and predicted tube loads is good for those calculated from the ion chamber measurements, but more variable when considering the mAs values alone, as was expected due to the known mAs problem. Results are in better agreement at 60 kV than at 55 kV, which may be due to the more complex method of calculating the tube load for the lower tube voltage. At 60 kV, a simple ratio of the number of photon histories required for equal background density could be used to determine relative mAs. For simulations using a 55 kV beam spectra, the relative number of photons produced for the two input spectra were calculated using the spectra generation program described earlier. The results for 0.1 mm tin

filtration show the greatest discrepancy between measured and predicted tube loads. although this is less than 10%.

8.3 Hospital measurements using plain film radiography

The second set of experimental measurements were carried out as described in section 7.6, using the neonatal anthropomorphic phantom and irradiating with a mobile X-ray set in a hospital radiology department. The measurements were designed to extrapolate the theoretical results to a clinical setting, and test the predicted effects of two specific filters (0.1 mm copper and 0.1 mm dysprosium) on dose and contrast.

8.3.1 Dosimetry measurements

Table 8.11 presents the measured values of entrance dose, absorbed dose to a selection of organs and effective dose calculated according to ICRP 60 for the three irradiation conditions; Baseline conditions of 60 kVp with no additional filtration, 56 kVp with 0.1mm copper filtration added and 56 kVp with 0.1mm dysprosium added. For the baseline measurements, mAs was selected according to advice from the paediatric radiographer. With the additional filtration in place, values of mAs were selected to give films subjectively assessed to be of similar density to the original, again by the paediatric radiographer. Values of effective dose are the average of male and female values.

	Dose (mGy) / Effective Dose (mSv)		
	Baseline	0.1mm Cu @ 56 kV	0.1mm Dy @ 56 kV
entrance dose	4.76 ± 0.33	1.93 ± 0.14	1.34 ± 0.09
thyroid	3.01 ± 0.90	1.10 ± 0.33	0.97 ± 0.29
lungs	1.47 ± 0.21	0.86 ± 0.12	0.68 ± 0.10
stomach	2.25 ± 0.32	1.23 ± 0.17	0.98 ± 0.14
kidneys	0.79 ± 0.11	0.39 ± 0.05	0.33 ± 0.05
ovaries	1.28 ± 0.28	0.63 ± 0.14	0.53 ± 0.12
testes	3.63 ± 1.09	1.64 ± 0.49	1.17 ± 0.35
breasts	3.95 ± 0.55	1.56 ± 0.22	1.28 ± 0.18
bone marrow	1.13 ± 0.20	0.55 ± 0.10	0.51 ± 0.09
skin	1.75 ± 0.32	0.73 ± 0.13	0.47 ± 0.08
colon	0.95 ± 0.13	0.43 ± 0.06	0.40 ± 0.06
effective dose	1.95 ± 0.39	0.93 ± 0.19	0.75 ± 0.15

Table 8.11 : Dosimetric measurements for the different irradiation conditions

The results for the different organs are also presented graphically in Figure 8.3.

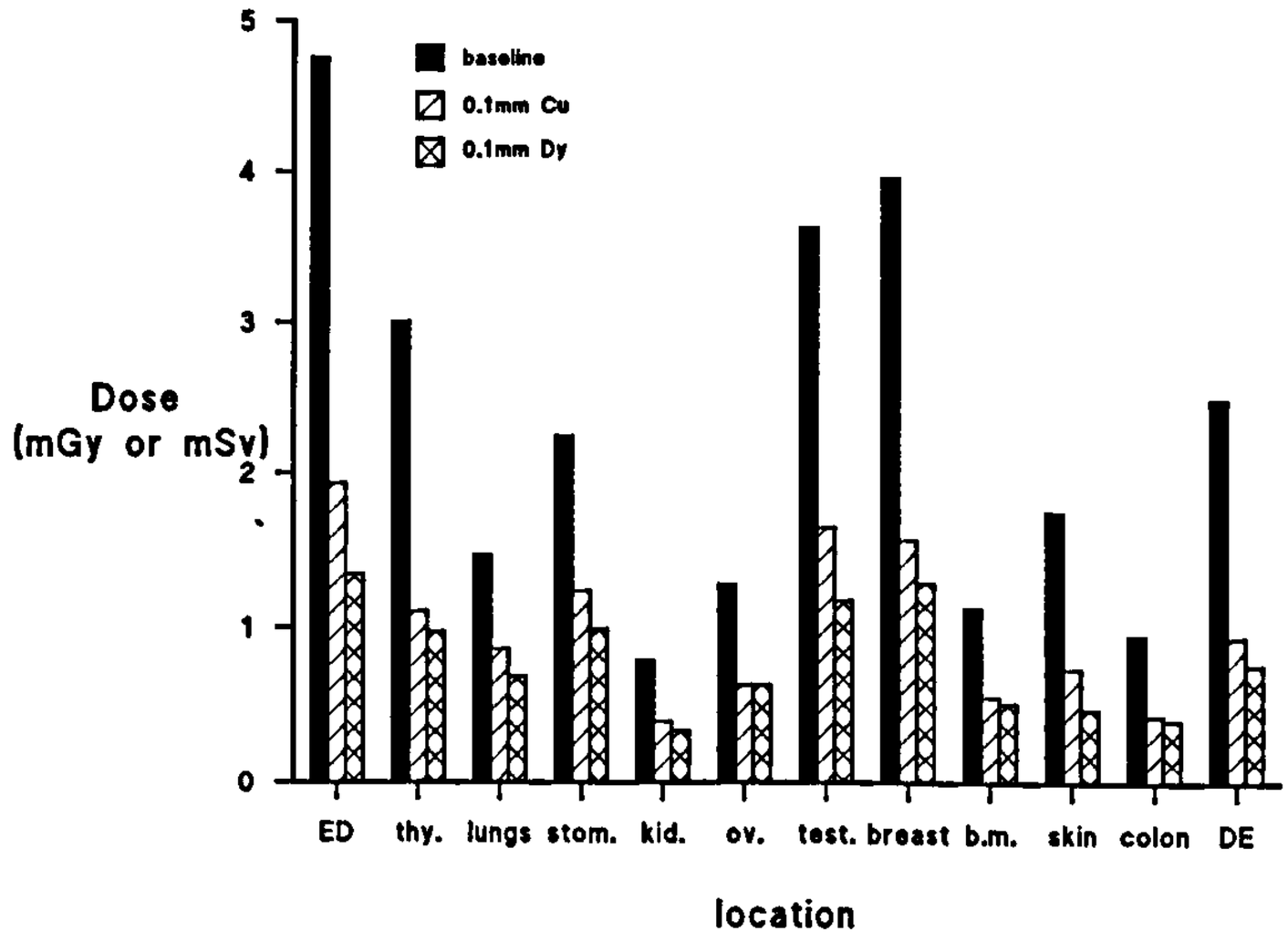

Figure 8.3 : Organ dose variation for different irradiation conditions

For the copper filter, it can be seen that entrance dose and doses to superficial organs, such as thyroid, breasts, testes and also the skin, are reduced by a factor of around 2.5. Dose to deeper organs, such as ovaries or kidneys, and dispersed organs such as bone marrow, is reduced by a factor closer to 2. For the dysprosium irradiation, entrance dose is reduced by a factor of 3.5, superficial organ dose by a factor of 3, and other organs by a factor of around 2 - 2.5. Values of effective dose have been calculated for interest, and for comparison of the dose reduction obtained with the different filters for these particular irradiation conditions. They have not, however been used as a major parameter of interest for two reasons:

- As discussed earlier, effective dose is not an appropriate risk estimator for children
- Values of effective dose are highly dependant on the beam size and positioning which, for the measurements performed here did not correspond to those for any particular examination. Measurements would have to be performed for a variety of beam sizes and positions for values of relative effective dose to be used meaningfully.

Dose reduction has instead been expressed for different types of organ, *eg* superficial organs within the beam area, superficial organs outside the beam area, small mid plane organs, dispersed organs *etc* to give a more general description of the effect of the additional filtration on dose. Greater dose reduction was observed for the dysprosium filter than for the copper filter. This may in part be explained by a consideration of the tube loads involved. For the copper filter, 12 mAs was used, a relative tube load of 1.9, and for the dysprosium filter 18 mAs, giving a relative tube load of 2.8 - each compared to radiographs without additional filtration at 60 kV and 6 mAs. The greater tube load would be expected to give greater dose reduction, as illustrated by the Monte Carlo results previously obtained. Background film densities were somewhat lighter for both additional filters, as mAs could only be set in discrete steps of 3 mAs. This biases the results toward lower doses, although this is a reflection of what would occur in clinical practice using this equipment.

The results were compared to those predicted from the Monte Carlo calculations and, in the case of the copper filtration, those obtained from laboratory measurements using the slab phantom. The ratios of dose values with and without the filter are given for each case in Table 8.12.

	dose reduction for Cu filter			dose reduction for Dy filter	
	phantom	slab	Monte Carlo	phantom	Monte Carlo
entrance dose	0.41 ± 0.04	0.81 ± 0.08	0.89 ± 0.02	0.28 ± 0.03	0.78 ±0.02
absorbed energy	-	-	0.96 ±0.001	-	0.90 ±0.001
mid slab dose	-	1.04 ± 0.10	-	-	-
ovaries	0.49 ± 0.15	-	-	0.41 ± 0.13	-
effective dose	0.37 ± 0.10	-	-	0.30 ± 0.08	-

Table 8.12 : Comparison of measured and predicted ratios of dose quantities with and without each filter for copper (Cu) and dysprosium (Dy)

The differences between measured and predicted dose reduction appear large, but should be considered in the light of the constraints on technique factor selection that were mentioned above. The mAs values used for the experimental measurements were 6 for the baseline measurements, 12 for the copper measurements and 18 for the dysprosium measurements. These factors were selected to give the 'best' images possible *ie* the best approximation to the background film density considered optimal by the paediatric radiographer. As the next selection either way was ± 3 mAs, it is possible that the optimal background density might have hypothetically been obtainable at 5 mAs for the baseline radiograph and 13 mAs for the radiograph made with copper filtration. This slight change in mAs values would change the entrance dose ratio for the copper filter to 0.53 from 0.41 - a 30% difference. The discrepancies observed between measured and predicted dose ratios highlight one of the problems in many theoretical optimisation studies where parameters, such as background density are constrained in a way that exceeds normal clinical practice. Such theoretical studies may then considerably underestimate the dose reductions which may be obtained. This is particularly the case for examinations such as plain film radiography of infants, especially on older equipment, where there is often difficulty in obtaining low enough exposures, and a lighter film may well be preferred if obtainable. The range of acceptable density levels is highly operator dependant and will usually be fairly broad.

Other factors that gave rise to differences between the theoretical simulation results and those obtained in the experiment were differences between the simulated slab phantom and the anthropomorphic phantom used here and differences between the theoretical and experimental beam spectra. The latter arise from the different tube voltage used experimentally (56 kV was the closest option to the 55 kV simulated), and the lower tube filtration (2.5 mm Al compared to 3 mm Al). Each of these will tend to increase the dose reduction attainable through additional filtration, and so contributes to the lower experimental dose ratios observed in Table 8.12.

8.3.2 Contrast measurements

The radiographs taken of the neonatal phantom included almost the entire trunk, and film density readings were taken at a number of locations including the spine, pelvic bone, and soft tissue surrounding these areas. From these measurements two contrast specifications were calculated; lumbar vertabrae against surrounding tissue, and pelvic bone against surrounding tissue. These contrast values are given in Table 8.13 for the different irradiation conditions,with uncertainties derived according to values given in Table 8.3.

	Baseline	0.1mm Cu @ 56 kV	0.1mm Dy @ 56 kV
contrast of pelvis	0.17 ± 0.05	0.21 ± 0.03	0.17 ± 0.02
contrast of spine	0.47 ± 0.10	0.42 ± 0.04	0.33 ± 0.02
bone/soft tissue contrast in lab	0.48 ± 0.01	0.48 ± 0.01	-
predicted bone/soft tissue contrast	0.42 ± 0.01	0.44 ± 0.01	0.40 ± 0.01

Table 8.13 : Measured contrast from radiographs of anthropomorphic phantom

For pelvic bone contrast, relative contrast values are the same as predicted, within experimental uncertainties, although the absolute values are lower. This corresponds to the smaller thickness of bone in the area of pelvis measured compared to that simulated. For the spine a slight loss of contrast was observed experimentally with the dysprosium filter, although this lies only just outside experimental uncertainties. Considering the differences in

phantom, X-ray spectra and relative background densities the agreement between theory and experiment is very good.

8.4 Hospital measurements using fluoroscopy

The second set of hospital measurements was carried out in the paediatric screening room, as described in section 7.6.2. Dosimetry results for irradiation of the neonatal phantom using five minutes fluoroscopy and a single spot film are presented in Table 8.14, which gives entrance dose, organ dose and effective dose values for irradiation with and without the copper filter. The technique factors used were 60 kV and 0.5 mA for fluoroscopy and 60 kV, 150 mA for the spot films. The exposure times for the spot films were 8ms without the copper and 9ms with the copper filter in place. For these technique factors, the relative tube load with each filter is 1.001, as the slight increase in exposure time for the spot film is negligible compared to the fluoroscopy time.

	Dose (mGy) / Effective Dose (mSv)		
	Baseline	0.1mm Cu @ 60 kV	Dose ratio
entrance dose	32.7 ± 2.3	17.6 ± 1.3	0.54 ± 0.05
thyroid	0.23 ± 0.06	0.12 ± 0.03	0.52 ± 0.21
lungs	1.98 ± 0.50	0.74 ± 0.19	0.34 ± 0.12
stomach	6.30 ± 0.88	3.43 ± 0.48	0.54 ± 0.04
kidneys	20.60 ± 2.88	12.00 ± 1.68	0.58 ± 0.11
ovaries	8.68 ± 1.91	5.58 ± 1.23	0.64 ± 0.20
testes	0.47 ± 0.14	0.29 ± 0.09	0.62 ± 0.26
breasts	0.35 ± 0.05	0.20 ± 0.03	0.57 ± 0.11
bone marrow	2.89 ± 0.52	1.59 ± 0.29	0.55 ± 0.14
skin	4.26 ± 0.77	3.40 ± 0.61	0.80 ± 0.20
colon	7.53 ± 1.05	5.08 ± 0.71	0.67 ± 0.13
effective dose	4.26 ± 0.89	2.54 ± 0.53	0.60 ± 0.18
DAP	211 ± 2	207 ± 2	0.98 ± 0.03

Table 8.14 : Dosimetry measurements for fluoroscopy of phantom

These results may be compared with those predicted from the Monte Carlo simulations which give entrance dose ratios of 0.74 ±0.02 and absorbed energy ratios of 0.83 ±0.02. These values are somewhat higher than those found experimentally. However, the simulated results were obtained for equal background density, with a relative tube load of 1.5 for irradiations performed with the copper, whereas the experimental results were performed at equal tube load. If the theoretical results are extrapolated to equal tube load (by dividing by 1.5) to correspond to the experimental conditions, dose ratios of 0.49 ±0.01 and 0.55 ± 3×10^{-4} are obtained for entrance dose and absorbed energy respectively. The measured and predicted entrance dose ratios would then be the same, to within the quoted uncertainties. The experimental absorbed dose ratios for mid-plane organs such as the stomach or ovaries would be close to that predicted theoretically for values of absorbed energy.

Other points to be noted from Table 8.14 are, firstly, that the DAP values recorded during the experimental measurements are not significantly different from each other. This is as expected, as the additional filtration is situated further down the imaging chain than the DAP meter, and technique factors were not significantly changed for the measurements made with the copper filtration. It is also apparent that the dose to the lungs was reduced by a greater amount than the entrance dose, which would contradict theoretical analysis. However, the lungs cover a large area that was partially within and partially outside the direct beam. The uncertainties associated with this dose measurement are thus large, and the apparent discrepancy would arise from a small shift (around 0.5 cm) in the position of the beam. This could easily have occurred, as for fluoroscopy there is no light beam diaphragm to check beam position prior to irradiation, and the phantom had to be moved between measurements to change the TLD.

Image contrast was assessed visually by the radiographer during fluoroscopy, and judged to be adequate without changing the exposure factors after addition of the copper filtration. Density measurements behind and beside the region of contrast on the spot films were used for objective assessment of contrast, and the values obtained are listed in Table 8.15 together with values predicted from Monte Carlo calculations.

	experimental measurements	predicted values
contrast with aluminium only	0.25 ± 0.02	0.414 ± 0.003
contrast with copper filter	0.16 ± 0.02	0.417 ± 0.004
contrast ratio	0.64 ± 0.11	1.007 ± 0.012

Table 8.15 : Measured and predicted contrast for fluoroscopic examination

Although the Monte Carlo predictions are for unchanged contrast with the copper filter in place, the experimental results show a reduced contrast for the latter case. This is due to the combined effect of the lower background density for the copper irradiation and the high contrast of the iodine and can be illustrated using Figure 8.4 which shows a typical film characteristic curve, plotting density against the log of the exposure to the film.

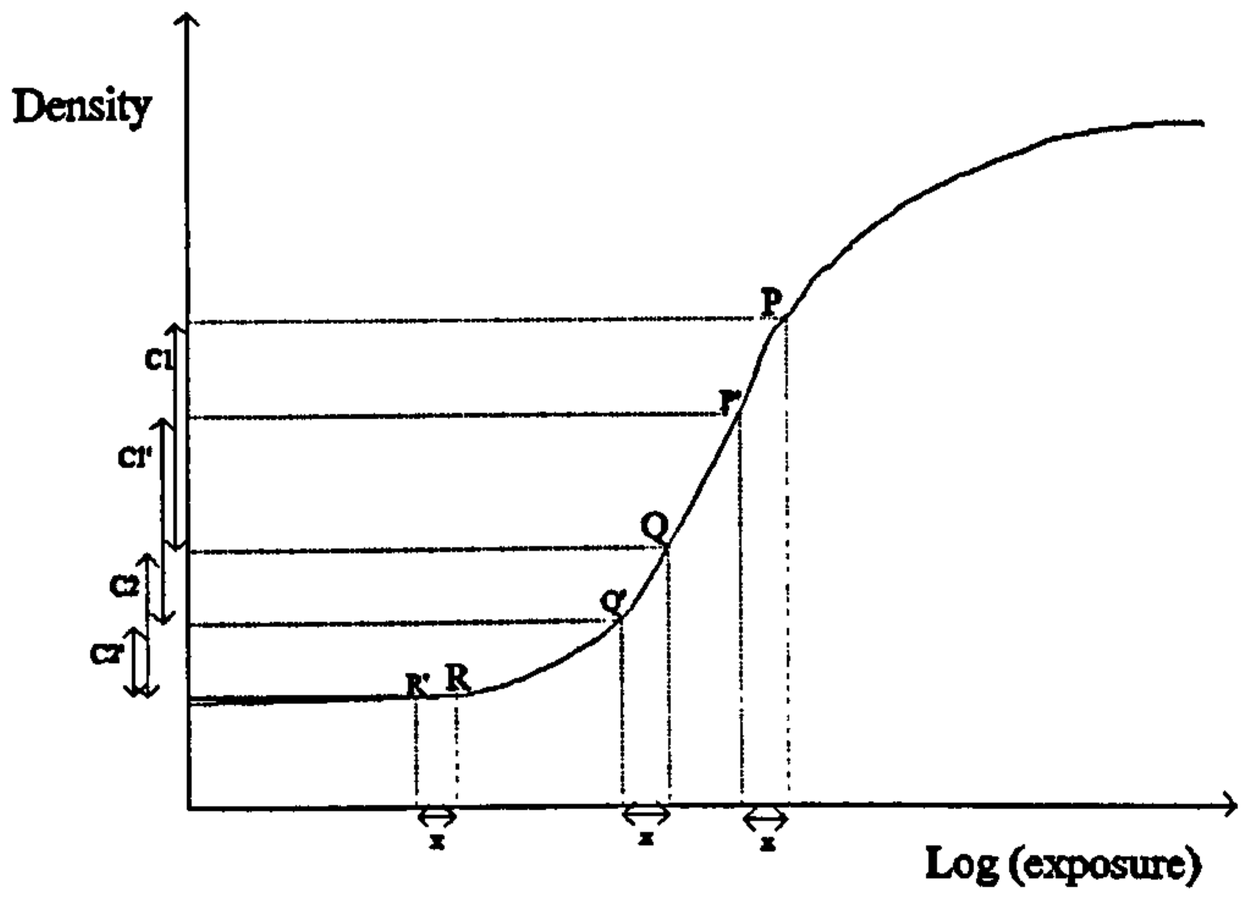

Figure 8.4 : Sensitometric curve showing how film contrast may be affected by the background exposure level

If the three points on the graph P, Q and R represent three points on a film, the contrast between two sets of points (P,Q and Q,R) are given by the density differences between them (C1 and C2). If the exposure to the whole film is reduced by a constant factor, all the points will be shifted along the x-axis by a constant amount - as a multiplication of E corresponds to an addition to log(E). The new film densities at the 3 points will then be represented by P', Q' and R', and the new contrast values by C1' and C2'. It can be seen that when both measurement points lie on the linear portion of the characteristic curve (*eg* P & Q), the film contrast is not affected by a change in exposure (C1 and C1' are approximately equal).

However, when one of the points lies in the low density 'toe' region of the curve (*eg* Q) the lower exposure leads to a reduced contrast as in this region density varies only slightly with exposure (C2' is less than C2). For the experimental measurements here, the density behind the contrast media was measured as zero above fog level for irradiation with the copper filter, and so lies in this 'toe' region of the characteristic curve. This results in the observed reduced contrast for the copper irradiation, for which the background film density was 0.133 ± 0.023 compared to the irradiation without the copper (background density 0.266 ± 0.023).

Despite the numerical differences in measured contrast, the mass thickness of iodine used was great enough for differences between irradiations with and without copper to be subjectively undiscernible with the imaging equipment being used. This highlights two points:

- The clinically required contrast or information content is of more importance in an optimisation study than numerically equal contrast/information content.
- There is little gain in pursuing slight modifications in image quality using beam spectral shaping if the imaging performance is limited by the equipment itself.

8.5 Conclusions from experimental verification

The results from the laboratory irradiations of tissue equivalent slabs validate the Monte Carlo predictions of both dose and contrast variation for different combinations of tube voltage and tube filtration. Absolute values of film contrast are not so well predicted, though this is of less relevance to the comparative study being carried out. In particular, the predicted dose saving characteristics of additional copper filtration, with maintained contrast at reduced tube voltage, were reproducible experimentally.

The measurements made in the hospital radiology department indicate that the predicted dose savings can be achieved in a clinical setting. Predictions of contrast changes are also shown to be valid under clinical conditions. Practical constraints, such as lack of flexibility in exposure settings may results in more variable dose savings than those predicted, and this is an important consideration when extrapolating theoretical results to a hospital environment.

The importance of the influence of other parts of the imaging chain *ie* image intensifier and camera, on achievable contrast and thus maximum dose savings was illustrated. The influence of a limited range of technique factor settings on the optimisation process was also highlighted.

The benefit of additional copper filtration for fluoroscopic examination of infants was confirmed.

Chapter 9

Clinical Trial of Additional Filtration

9.1 Introduction

The motivation for carrying out the investigation into the use of additional tube filtration was to find ways of improving dose optimisation in clinical practice. It was therefore important to consider the implementation of any suggested improved filtration combination in a clinical setting, to assess its practicality on a routine basis and assess changes in dose and image quality for a cohort of patients. The results obtained theoretically, and from experimental measurements would be of little practical value if they did not lead to benefit for the patients.

As fluoroscopic procedures account for higher doses than simple film screen examinations, a paediatric screening room was selected for the clinical trial. This was the same room in which experimental measurements had been undertaken, so the anticipated benefit to the patient had been well established (Chapter 8). Filtration of 0.1 mm copper was used for the trial as it had been shown to give the greatest dose saving, while maintaining contrast, for the patient sizes and tube potential range studied. Copper is also a relatively inexpensive material and is non-toxic - an important consideration for an impermanent filter, particularly in a children's room.

The practicalities of using additional filtration and the design of the trial are described below, followed by details of the techniques used for assessing the impact of the filter on both dose and image quality. The preliminary results of the trial are then described, including discussion of the practicalities of the filter's use. Discussion of the implications and conclusions drawn from the trial are presented at the end of the chapter.

9.2 Use of filter

A Shimadzu HD1SOB-30 X-ray set was used for the trial. This had a sealed undercouch tube which was inaccessible without engineering intervention. Constraints within the department meant that the room was regularly used for a range of adult fluoroscopic work in addition to paediatric fluoroscopy. For these reasons, additional filtration could neither be attached and removed by radiographic staff as required, nor permanently installed. A solution to this practical problem was to use a large area sheet of copper, placed directly beneath the patient. The 0.1 mm thick copper sheet used for experimental measurements in the room was laminated with a double layer of plastic for protection and used as a removable filter in this way.

9.2.1 Simulation of trial geometry

The geometrical configuration used in the trial was slightly different from that used in the Monte Carlo simulations described earlier, in Chapter 5, as the original geometry simulated overcouch irradiation with additional filtration attached to the tube head. A small number of further simulations were carried out to confirm that the results were not significantly affected by the change in geometry. The new simulation geometry is shown in Figure 9.1.

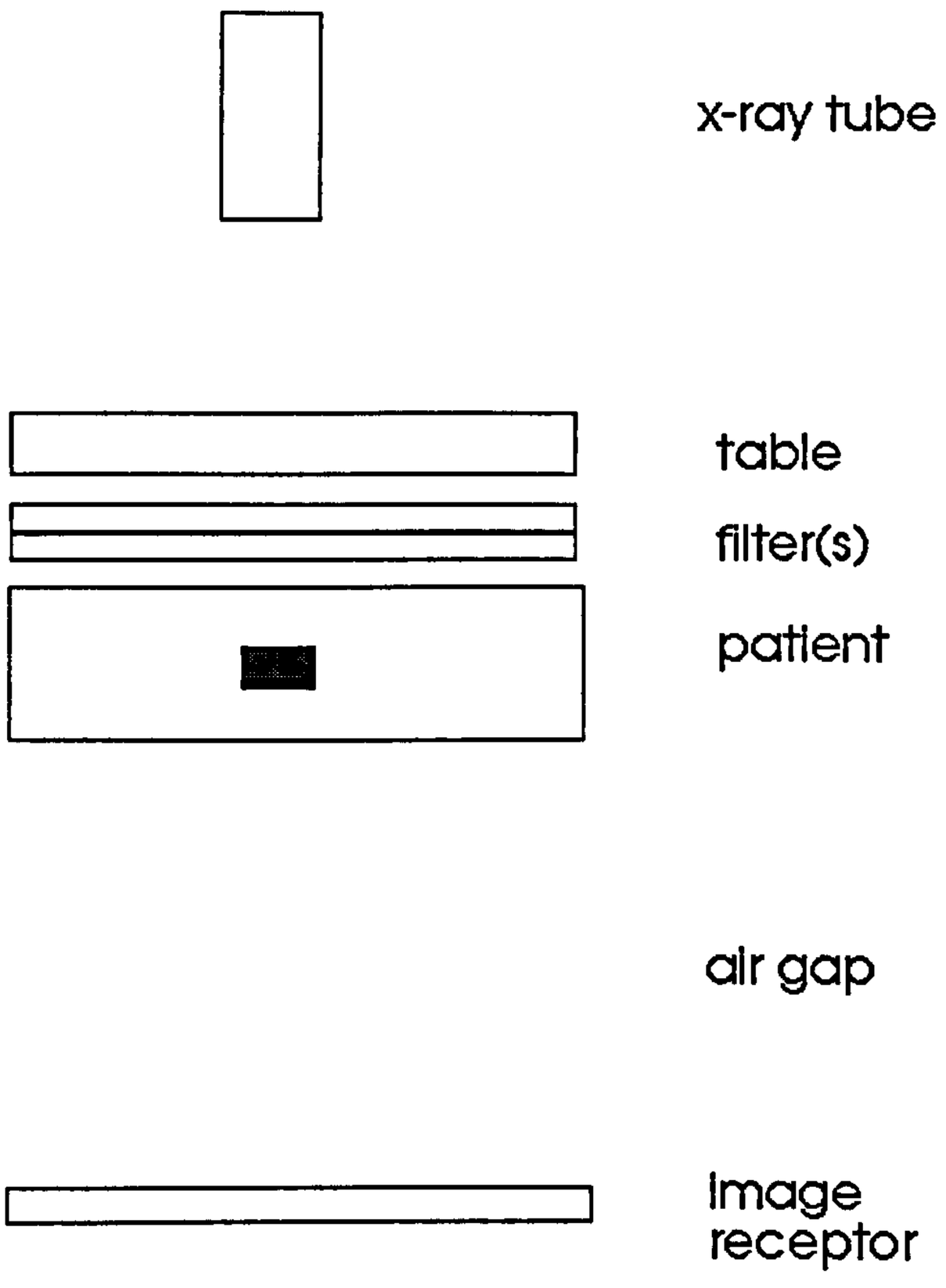

Figure 9.1 : Geometry used in Monte Carlo simulations of clinical trial.

In this geometry, the additional filtration is in direct contact with the entrance surface of the patient phantom, with an air gap between the phantom and image receptor, to simulate undercouch fluoroscopy of an infant lying on a sheet of filtration. The phantom used in the simulations was 1 cm iodine in 5 cm soft tissue and the tube voltage was 60 kV. The following additional filters were simulated.

- no additional filtration (3 mm aluminium only)
- 0.1 mm copper
- 0.1 mm copper + 0.1 mm aluminium.

The last of these was included to investigate whether additional aluminium filtration was required after the copper to absorb low energy K-fluorescence, as has been suggested (Jennings, 1988).

The results from these simulations are summarised in Table 9.1 where the ratios of each calculated quantity for simulations with and without additional filtration are presented. The results obtained for the original simulation geometry are also included for comparison.

	original geometry (0.1 mm Cu)	trial geometry (0.1 mm Cu)	trial geometry (0.1mm Cu +0.1mm Al)
Entrance dose ratio	0.69	0.74	0.74
Absorbed dose ratio	0.80	0.84	0.84
Contrast ratio	0.99	0.99	1.00

Table 9.1 : Results of Monte Carlo simulations of trial geometry: Ratios of dose and contrast (with additional filtration / without additional filtration).

The results show that the use of extra aluminium beyind the copper filter is not required, as it makes no difference to the entrance dose to the patient. The K-fluorescence from copper is of such a low energy (8.98 keV) that it is almost totally absorbed in the filter. In practice, there is also a thin layer of plastic coating and the patient clothing present to attenuate the extreme low energy end of the filtered spectrum. The copper sheet was thus used without the additional aluminium sheet throughout the trial. The results for the trial geometry show a small loss in dose reduction, compared to those obtained for the original geometry. This is due to the additional filtration of the couch on which the patient is lying as this 'hardens' the reference beam, and makes the effect of additional filtration slightly less pronounced. The benefit to the patient from the increased filtration, however, is still apparent.

9.3 Design of the Trial

The aims of the clinical trial were as follows:

- to assess the change in radiation dose to patients resulting from use of a 0.1 mm copper filter
- to assess the effect of the filter on image quality
- to assess the practicality and acceptibility of routine use of the filter.

Ethical approval for the trial was obtained from Newcastle and North Tyneside Health Authority and formal consent from the chief executive of the Royal Victoria Infirmary,

where the measurements were to be carried out, was also obtained. The parental information and consent forms that were designed and used are given in Appendix D.

Participants in the trial were infants from birth up to the age of 1 year, presenting for any type of fluoroscopic procedure. This age range was selected for the following reasons:

- simulation and experimental verification was carried out for neonatal sizes and, while results may be easily extrapolated to slightly larger patients, they cannot be assumed to apply to all paediatric age ranges.
- the size of the copper sheet (50 × 50 cm) limited the range of patient sizes that could be positioned accurately on the filter, particularly as young patients are frequently difficult to immobilise.

All children who were within the defined age band were included in the study, provided that parental consent was obtained. This excluded some in-patients whose parents were not available to give consent prior to the examination. Dosimetry data had been routinely collected in the room for several years, so this data was available for making comparisons of doses with and without the filter in place. A 'control' group of patients was thus established, comprising all children in the specified age-group who underwent radiological examination in the room during the 6 months preceeding the trial. Infants excluded from the trial solely due to lack of parental consent were also included in this control group. The full trial was designed to include measurements on 100 patients.

The following procedure was used for examinations with the filter:

- The purpose and nature of the trial were explained to the parents of the child by the radiographer, and they were given the patient information sheet and consent form to sign for the child's inclusion in the trial.
- Prior to commencing the examination, the copper filter was placed beneath the child.
- The examination was performed in exactly the same way as usual. Fluoroscopic technique factors were selected manually, according to normal practice. Any spot films required were taken using automatic exposure control - also according to normal practice.

- Dosimetry data was collected in the routine manner, as described in section 3.3 using a laptop computer connected to a DAP meter. A note regarding use of the copper was entered in the comments field during data entry for the examination.
- In the unlikely event of any overcouch radiographs being required (using the ceiling tube) the radiographer was instructed to remove the copper filter prior to taking the radiograph.
- The filter was to be removed immediately if, at any time during the examination, any dissatisfaction was felt by radiologist, radiographer, or adult accompanying the child, regarding image quality, patient comfort or ease of use.
- Any observations or remarks pertaining to use of the copper for the examination were written on the consent form. The forms were then all retained for future reference.

The dosimetry data obtained with the filter in place was compared with data obtained for patients in the control group. Spot films from closely matched patients, examined with and without the filter were used in a blind trial of image quality.

9.4 Dosimetry

Routine dose-area product measurements were already made on the fluoroscopic X-ray set used in the trial, with data logged on a laptop computer as described in Chapter 3. This practice continued throughout the trial of the copper filter. As the DAP meter was fixed to the tube head, below the additional filtration on which patients were lying, the presence of the filter would not be expected to affect the recorded DAP values, unless its use required changes in technique factors (kV and mA) from the values which would otherwise have been set. The DAP value at the patient entrance surface, however, will change as the filter attenuates the x-ray beam. The ratio of entrance doses with and without the x-ray beam is given by

$$\frac{ESD_{filt}}{ESD_0} = f \times \frac{DAP_{filt}}{DAP_0}$$

where ESD_{filt} and ESD_0 are the entrance surface dose values with and without the filter in

place respectively, and DAP_{filt} and DAP_0 are the corresponding values for recorded dose-area product values. The factor *f* incorporates the dose reduction arising directly from the attenuation of the copper filter, and the DAP ratio incorporates any effects from changes in technique factors (tube voltage, tube current or exposure/screening time). The equation assumes that field size remains constant, which is valid when considering the same examination performed with and without the filter.

The factor *f* was determined from the experimental measurements described in Chapter 8, and was taken to be 0.5 (Table 8.14). This factor is strictly valid only for the tube potential used during the measurement (60 kV both with and without the additional filter), as a change in tube voltage would change the attenuation of the copper. The magnitude of this effect is small, as the simulation results showed that the absorbed energy with the copper filter relative to reference conditions was the same at 70 kV as at 60 kV.

To describe the patient dose more completely, the measurements made with the anthropomorphic phantom were also employed to derive normalised organ dose factors, both with and without the copper filter present. These factors are calculated from the results presented in Table 8.14, and have been assessed for different groups of organs *ie* superficial organs inside and outside the beam area, deep organs inside and outside the beam area, large organs partially within the beam area, and dispersed organs (such as red bone marrow) located throughout the body. These normalised organ dose factors are listed in Table 9.2. Dose factors for specific named organs were not derived individually, as these depend crucially on beam size and position, and hence on the type and complexity of examination being performed. The more general dose factors allow assessment of patient dose under a wider range of examination conditions.

Organ Type	organ dose /entrance surface dose (mSv mGy^{-1})	
	without added filtration	with 0.1mm copper
I superficial organ within beam	0.6	0.7
II deep organ within beam	0.2	0.3
III organs outside beam	0.01	0.01
IV partially irradiated organ	0.05 - 0.2	0.05 - 0.2
V dispersed organ	0.1	0.1

Table 9.2 : Organ dose conversion factors

The use of these general organ dose coefficients has been compared with the use of effective dose coefficients derived from individual organ doses calculated using Monte Carlo techniques (Hart *et al*, 1996). Table 9.3 lists the organs included in the calculation of effective dose, and the category into which each falls (using the classification system described above) for urinary bladder examination, AP projection - using the field size and position described by Hart *et al* (1996). The organ factors given in Table 9.2 have then been used to derive effective dose factors both with and without additiional copper filtration for comparison with those published. It can be seen that the effective dose values calculated from the categorised organ dose factors used here are within 30% of values calculated from individual organ dose calculations. These published effective dose values have compared to previous factors published in Germany and are quoted as showing *reasonable agreement to within 30%* (Hart *et al*, 1996), with differences being ascribed to differences in organ positioning in the different phantoms. The fact that the discrepancies between alternative conventional calculations of effective dose conversion factors are similar to those between the conventional method and the organ categorisation used here, justifies the use of the latter method of dose assessment. It also corroborates the view that the use of the effective dose concept is inappropriate in paediatric radiology.

	Organ category (urinary bladder AP)	organ dose factors (from Table 9.2) mSv mGy^{-1}	
		60 kV, 3mm Al	60 kV, 3mm Al + 0.1mm Cu
lungs	III	0.01	0.01
stomach	III	0.01	0.01
liver	III	0.01	0.01
oesophagus	III	0.01	0.01
bone marrow	V	0.10	0.10
skin	V	0.10	0.10
gonads (M/F)	I/II	0.6/0.2	0.7/0.3
colon	II	0.20	0.30
bladder	II	0.20	0.30
thyroid	III	0.01	0.01
breast	III	0.01	0.01
bone	V	0.10	0.10
adrenals	III	0.01	0.01
brain	III	0.01	0.01
u.large intestine	IV	0.15	0.15
sm.intestine	II	0.20	0.30
kidney	III	0.01	0.01
muscle	V	0.10	0.10
pancreas	III	0.01	0.01
spleen	III	0.01	0.01
thymus	III	0.01	0.01
uterus	II	0.20	0.30
remainder total		0.71	0.91
Effective Dose factor		0.14	0.17
Effective Dose factor (Hart *et al*)		0.21	0.24

Table 9.3 : Comparison of effective dose factors derived using the analysis given here with published data (Hart *et al*, 1996)

9.5 Assessment of Image Quality

The quality of images obtained during the trial, both on the screen and 100mm spot films was assessed continually in terms of clinical acceptability, by the radiologists and radiographers working in the room. Any comments regarding the quality of the images were noted on the relevant consent form and staff were instructed to remove the filter if there was any doubt concerning the acceptibility of the images. A more formal assessment of image quality was also performed, using some of the 100mm spot films obtained. Comparison of films obtained with and without the filter present required careful selection of pairs of patients matching one another as closely as possible. The following criteria were used for matching patients, in priority order:

(1) examination type

(2) similar weight

(3) radiologist performing the examination

It would have been more desirable to match both weight and equivalent diameter, but little height information was collected for the infants examined in this room, due to practical difficulties, so values of equivalent diameter were not always available.

A total of nine pairs of patient examinations were identified, and the appropriate spot films retrieved from the patient files. All spot films taken in the department are stored by laminating those for each examination in a single sheet, so the entire set of films was used for the image quality assessment in each case. The patient information was masked and each sheet of films labelled, with those taken with and without the filter randomly assigned either A or B. A simple questionnaire was drawn up, asking the following questions for each pair of image sets:

(1) Which set of images do you prefer
(strongly A, slightly A, no preference, slightly B, strongly B) ?

(2) Are the images of satisfactory diagnostic quality (neither, A only, B only, both) ?

A copy of the questionnaire is given in Appendix D. It was completed by five members of staff (two paediatric radiographers, two paediatric radiologists and one physicist) and the results analysed. The radiographers and radiologists work routinely in the trial department

and the physicist is responsible for intensifier QA in the region but had no direct involvment in either the department or the project.

9.6 Results

Analysis of the results has been carried out, for a total of 34 patients examined during the first 5 months of the trial. The details of this patient group are given below in Table 9.4.

Examination Type	Num of patients	Mean age (months)	Mean weight (kg)
Barium meal	1	1	4.00
Barium meal & swallow	5	5	3.27
Barium Swallow	3	4	5.46
Cystogram	18	5	6.25
Cystometrogram	2	5	6.50
Intussuception air reduction	1	4	7.60
Loopogram	3	4	1.95
Water soluble swallow	1	12	7.30

Table 9.4 : Patients examined with copper filter

Details of the control group of patients *ie* those in the same age range undergoing fluoroscopic examination within the previous six months without use of the copper filter, are given in Table 9.5. The mean age and weights for each group have been presented in the tables to aid the interpretation of the dosimetry results.

Examination Type	Num of patients	Mean age (months)	Mean weight (kg)
Barium meal	18	8	6.81
Barium meal & swallow	30	8	.6.78
Barium Swallow	3	6	9.71
Cystogram	93	7	7.03
Cystometrogram	7	6	9.74
Intussuception air reduction	2	5	8.17
Loopogram	9	8	7.91
Water soluble swallow	2	2	3.95

Table 9.5 : Control group of patients

9.6.1 Dosimetry Results

The results of the routine dose assessments have been analysed by grouping them according to the various examination types listed in Tables 9.4 and 9.5. Values of mean DAP, screening time, and DAP normalised to unit screening time are presented in Table 9.6 below.

Exam.	Results with copper filter			Results from control group		
	DAP ($mGycm^{-2}$)	scr.time (s)	DAP/ time	DAP ($mGycm^{-2}$)	scr.time (s)	DAP /time
Ba.M.	598.5	240	2.49	680.0	135	5.64
Ba.M.&S.	609.2	176	3.37	678.7	125	7.29
Ba.S.	951.7	136	7.10	590.7	130	4.12
Cyst.	209.5	56	4.86	414.4	91	6.23
Cystomet.	155.5	87	1.77	197.6	96	3.35
Intus.	598.5	120	4.99	1360.1	210	5.44
Loop.	342.4	140	2.86	354.7	131	2.84
WS.S.	514.8	24	21.45	624.1	150	3.47

Table 9.6 : Dosimetry results from clinical trial

For most categories of examination, numbers of patients are too small to claim any statistical significance in the results. However, it can be seen from Table 9.6 that both DAP and normalised DAP values are mostly lower for examinations performed with the filter than for those without. The only examination for which the DAP is higher with the copper is barium swallow for which there are only 3 patients in each group. Normalised DAP is also higher for water soluble swallow, for which the single examination performed with copper was carried out with a very short screening time. The results indicate that use of the filter did not result in greatly increased technique factors. Screening times are also similar or lower with the filter in place.

For the cystogram examination the number of patients included in the trial was sufficient for statistical tests to be performed to investigate whether the normalised DAP results are significantly different when using the copper filter *ie* to demonstrate that the sample of DAP values for cystograms performed with the copper filter is taken from the same distribution as the sample of DAP values for cystograms performed without the filter. The common tests of significance apply only to *normal* distributions, whereas the normalised DAP distribution is skewed with a high dose tail, as shown in Figure 9.2 (i). However, it forms what is known as a log normal distribution as the log(DAP) values can be shown to be approximately normal, as illustrated in Figure 9.2 (ii) for both the trial and the control group data.

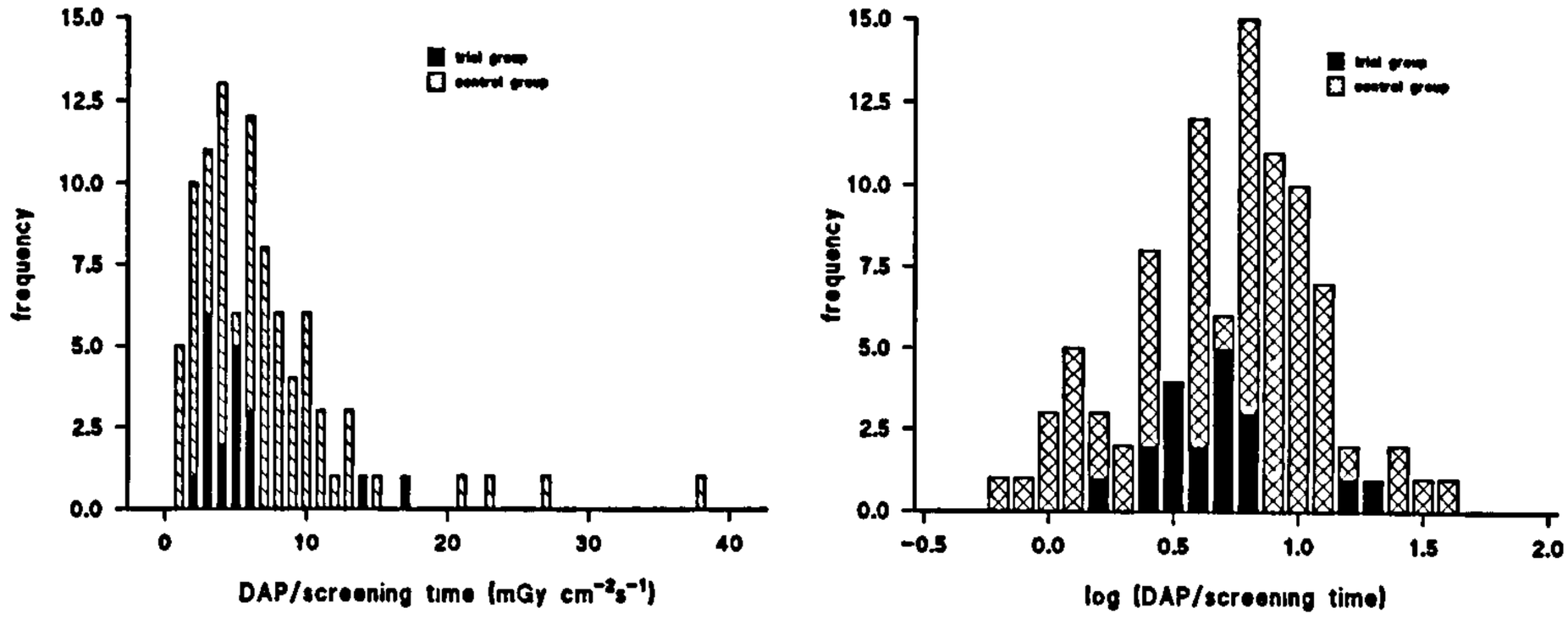

Figure 9.2 : Distribution of (i) DAP and (ii) log(DAP) for cystograms in the trial and control groups of patients

The usual method of demonstrating that two sample distributions are taken from the same population is to set the null hypothesis that *there is no difference between the two estimates of the population mean, ie* between the two sample means. As the two samples are reasonably large, the two sample *z* test may be used. The test statistic *z* is computed as the difference between the means divided by the standard error of the difference.

$$z = \frac{(\overline{x_1} - \overline{x_2})}{\sqrt{\frac{s_1^2}{n_1} + \frac{s_2^2}{n_2}}}$$

$\overline{x}_1$ and $\overline{x}_2$ are the means of the log(DAP) samples, s_1 and s_2 the standard deviation of the samples and n_1 and n_2 the number of measurements in the sample. Under the null hypothesis, *z* is distributed approximately as a Normal distribution with mean zero and standard deviation 1. For the log(DAP) data presented here, the parameter values are:

trial group	$x_1 = 0.599$	$s_1 = 0.259$	$n_1 = 18$
control group	$x_2 = 0.652$	$s_2 = 0.365$	$n_2 = 93$

which gives $z = 0.726$. The corresponding p value is 0.465. This is the probability of obtaining the given difference in means if the null hypothesis was true. Common practice is to require $p < 0.05$ in order to reject the null hypothesis. The large value of p leads to the conclusion that there is no significant difference between the two sample means, and DAP values (as measured at the tube head) are not significantly different with the copper filter in place than without the filter.

If then it is assumed that DAP values are not affected by use of the filter, the patient dose saving may be derived directly from the conversion factors listed earlier in Table 9.2. These show an entrance surface dose reduction of 0.5 and reduction of 0.6 and 0.75 for superficial and deep organs respectively within the beam area. This represents a large dose saving to the patient. The reduction in the associated risk to the patient will depend on the size and positioning of the beam, and the weighting factors used for organ radiosensitivity. Using the above factors would lead to a reduction in radiation risk of at least 25%.

9.6.2 Assessment of Image Quality

Throughout the trial, there were no adverse comments made on the standard of image quality, and at no time was it felt necessary to remove the filter in order to proceed with an examination. The results of the subjective assessment of image quality are summarised in Table 9.7 below.

	number of times each preference specified					number of image sets of diagnostic quality	
	strongly with Cu	slightly with Cu	no preference	slightly without Cu	strongly without Cu	with Cu	without Cu
radiologists	1	1	9	7	0	18	18
radiographers	1	6	3	8	0	18	16
physicist	1	0	3	5	0	-	-
total	3	7	15	20	0	36	34

Table 9.7 : Results of image quality assessment

From the Table it may be seen that, although the images taken without the copper came out as being 'slightly preferred' in the majority of cases, none were 'strongly preferred' and, more importantly, none of them were considered diagnostically unacceptable.

Of the comments made on the image sets, one of the radiographers noted that the edge of the copper could be seen on two of the film sheets, where the filter had slipped relative to the patient during the examination. It was also noted that two of the image sets were overexposed - one to the extent of being of unacceptable diagnostic quality to both radiographers. Both of these overexposed sets were from examinations performed without the copper. Interestingly, the 'unacceptable' set of images was actually preferred by one of the radiologists.

The results of the questionnaire, along with the experience of staff throughout the trial demonstrated that, with respect to its effect on image quality, the filter would be acceptable for use on a routine basis.

9.7 Practical Considerations

An important factor in determining whether the filter would be suitable for routine use in the paediatric fluoroscopy room, was whether any practical difficulties were experienced during the trial. Discussion with the staff involved yielded the following points:

- The time taken in placing the filter prior to the examination did not cause any disruption to work in the room.
- After 6 months use, there was no significant physical deterioration of the filter from handling, contamination or any other cause.
- There had been no indication that use of the filter caused any discomfort to the patient.
- The size of the filter (50 × 50 cm) meant that some difficulty was experienced in keeping some of the children, particularly the larger patients, over it throughout the entire examination.

The final point listed here was the only negative feature to emerge from the trial. To assess whether the possible slippage of the copper during an examination was a serious enough

drawback to restrict its routine use, required consideration of the consequences involved. As automatic exposure control is not used during fluoroscopy, there was no danger that a sudden loss of the copper filtration could cause changes in exposure factors that might have an adverse effect on either dose or image quality. If tube voltage or current were habitually being set higher when performing an examination with the copper, the unexpected removal of the copper from the field could cause overexposure to the patient. As, however, technique factors were not significantly changed as a result of the trial, this would not be a problem. Thus, inadvertent movement of the filter would negate the dose reduction anticipated but would not increase the patient dose. At worst it might be expected to provide a slight distraction to the staff viewing the image on the screen, but no adverse comments were made to this effect. A larger sheet of copper would ease these positioning problems, but would be more cumbersome to handle, besides being difficult to obtain and prepare for use.

From a practical point of view, the filter was thus judged to be acceptable for use with infants within the age range of the trial patients. It was felt though that, as expected, the filter would not be suitable for use with older children. Even if they could be immobilised sufficiently over the copper sheet, the usual practice during cystograms of taking post-micturition exposures erect for children old enough to stand would require procedural changes to prevent the filter from falling.

9.8 Discussions and conclusions

One important consideration that has been highlighted during the trial is the issue of *acceptable* versus *best* image quality. This has been discussed theoretically in Chapter 4, and the results of the image quality assessment carried out as part of this clinical trial confirm that a much greater dose reduction may be achieved when considering acceptability rather than equality of images. This was evidenced by the difference between the theoretical change in dose with use of the filter (26% reduction in entrance dose), which was based on constant energy absorption in the phosphor, and that achieved in practice, which was considerably larger (50% reduction in entrance dose). It has also been shown that, for subjective assessment of images, the decision on what constitutes *best* may be very dependant on the

viewer, thus indicating that considerable latitude in image parameters may be permissable in many circumstances.

In conclusion, the clinical trial of a 0.1 mm copper filter for use in fluoroscopy examinations of infants has been successfully initiated in a paediatric fluorocopy room in a large general hospital. The practical difficulties of attaching an additional filter to a non-dedicated undercouch tube were successfully addressed by lying the infants on a copper sheet.

The results obtained during the clinical trial have been influenced to a marked degree by the manual control of technique factors that was employed by the radiographic staff. If an AEC device were used, it would almost certainly increase the exposure factors used with the copper in place, to maintain the brightness at the phosphor. This would result in higher DAP values for examinations performed with the filter and thus reduce the dose saving provided. However, the DAP values would need to increase by as much as 30% in order to obscure the absorbed dose reduction, and by a factor of 2 before the entrance dose reduction is no longer observed. In practice, general AEC performance is so poor for children, as discussed in Chapter 4, that its use is uncommon for paediatric fluoroscopy examinations.

The initial results of the trial showed that the filter was found to give substantial reductions in patient dose. Entrance surface doses were reduced by 50%, superficial organ doses by 40% and deep organ doses by 25%. The reduction in risk was more variable, depending on the specifics of each individual examination, but was estimated to be in the order of at least 25%.

Use of the filter did not significantly affect image quality, and made no impact on the diagnostic results of the examination. The only practical difficulty experienced lay in keeping some of the older children over the filter throughout the examination, but this was not felt to be a insuperable problem. These results lead to the conclusion that the copper filter would be suitable for routine use during fluoroscopic examination of infants in the paediatric screening room.

Chapter 10

Application to Other Patient Categories and Suggestions for Further Work

10.1 Introduction

The preceeding chapters have presented an optimisation strategy for paediatric radiology, comprising dosimetry techniques, theoretical simulations, experimental verification and clinical implementation. This strategy has been applied in detail to the optimisation of radiation dose for neonates for both bone radiography and fluoroscopic examination using iodine or barium contrast agents. Theoretical simulations were performed for a wide range of filter materials and thicknesses, and the effect of changes in tube voltage, varying screen phosphor and the use of replacement or additional filtration were studied. Results have been analysed in terms of beam spectra, and the findings verified experimentally.

In this chapter, the applicability of the optimisation strategy to other situations will be considered, in the light of the results already obtained. In particular, the effect of variations in patient size will be addressed, as this is a fundamental issue in paediatric radiology, and also the effect of different tissue types. Each of these will be discussed in terms of the beam spectra and the transmission properties of the phantom, in a similar way to the analysis presented in Chapter 6. This enables some general predictions to be made regarding the effect of size and tissue type on results. The results of a small number of further Monte Carlo simulations, for a range of sizes and two pairs of contrasting tissues, were used to test these predictions, and these are also presented. There were two reasons for carrying out such simulations:

- to make a preliminary assessment of how the results may be extended to other age groups and tissue types
- to identify the most promising areas for further study

At the end of the chapter, suggestions for the focus of further work are given, both for Monte Carlo study and experimental verification. Suggestions are also made for advancing some of the general concepts utilised in paediatric dose optimisation.

The specific phantom sizes and compositions considered for application of the techniques were:

- bone detail in 10 cm soft tissue
- iodine in 10 cm soft tissue
- barium in 15 cm soft tissue
- lung detail in 5 cm soft tissue
- bone detail in 5 cm lung tissue.

The first of these represents bone radiography on a child of around 1 year of age, and the contrast media studies represent a water soluble contrast examination, also on a 1 year old, and a barium examination on a child of around 5 years. The selection of examination types covers a range of examination categories and includes examinations that are frequently performed for the relevant age group. The last two phantom specifications in the list above involve lung tissue, firstly as contrast tissue then as background, as this is the only major tissue type (affecting radiological examination) that has not been incorporated into the initial optimisation study. The effect of lung tissue in the phantom has important implications for the optimisation of radiographic examination of the chest.

The uncertainties for values calculated in the Monte Carlo simulations are given in Table 10.1. They have been derived according to equation 5.1, as before.

	abs.energy	ent.dose	bkgd	contrast
bone in 10cm soft tissue	±0.04%	±2.4%	±0.2%	±10-20%
iodine in 10cm soft tissue	±0.11%	±6.0%	±0.4%	±6-10%
barium in 15cm soft tissue	±0.09%	±4.5%	±0.4%	±14-27%
bone in 5cm lung	±0.04%	±8.2%	±0.2%	±1-3%
lung in 5cm soft tissue	±0.19%	±4.9%	±0.3%	±9-25%

Table 10.1 : Uncertainties in Monte Carlo calculations

The results of the simulations are presented in a similar format to that used previously (Chapter 6), with trends in dose and contrast plotted against tube load for different filter materials, for comparison with the trends predicted from a consideration of the beam spectra.

10.2 Effect of patient size on optimisation study

Paediatric patients have sizes ranging from that of a premature neonate to that of a young adult, and the effects of beam filtration on contrast and the dose to a patient of a particular size cannot simply be extrapolated to a different size. The size of the patient's body will affect the amount of energy absorbed in it, and since it filters the beam spectrum it also affects the contrast achievable. Tube voltage will also need to increase with increasing patient size, to achieve the necessary exposure level at the image receptor.

10.2.1 Dose

The effect of varying patient thickness on absorbed dose can be considered in terms of the absorption spectra of different phantom thicknesses. Figure 10.1, shows absorption spectra for the 5 cm phantom at 60 kV and for the 10 cm and 15 cm phantoms at 70 kV.

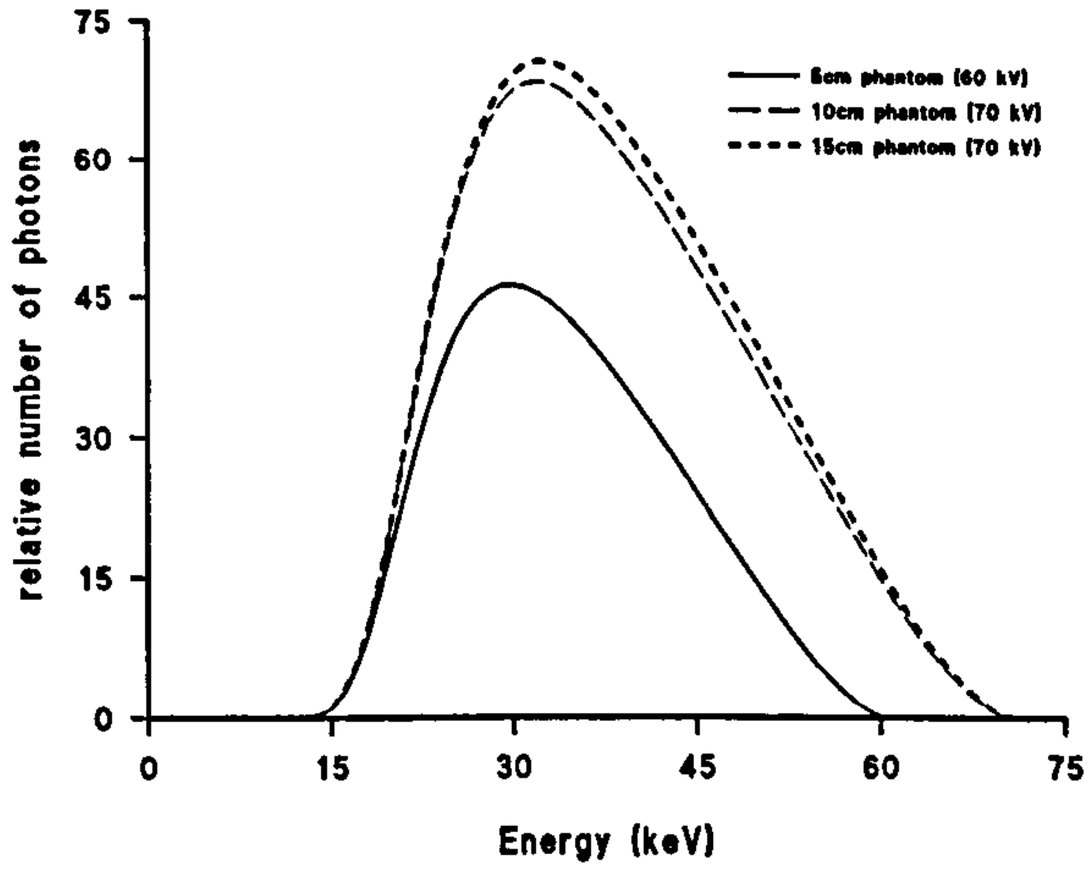

Figure 10.1 : Absorption spectra in different size phantoms

It is apparent from the Figure that there is only a slight change in the normalised beam spectra for the different sized phantoms, with the absorption peak shifting to higher energies

with increasing size. The effect of filtration on dose to the larger phantoms may be predicted from consideration of the filtered 70 kV beam spectra, and those for several different filters are given in Figure 10.2.

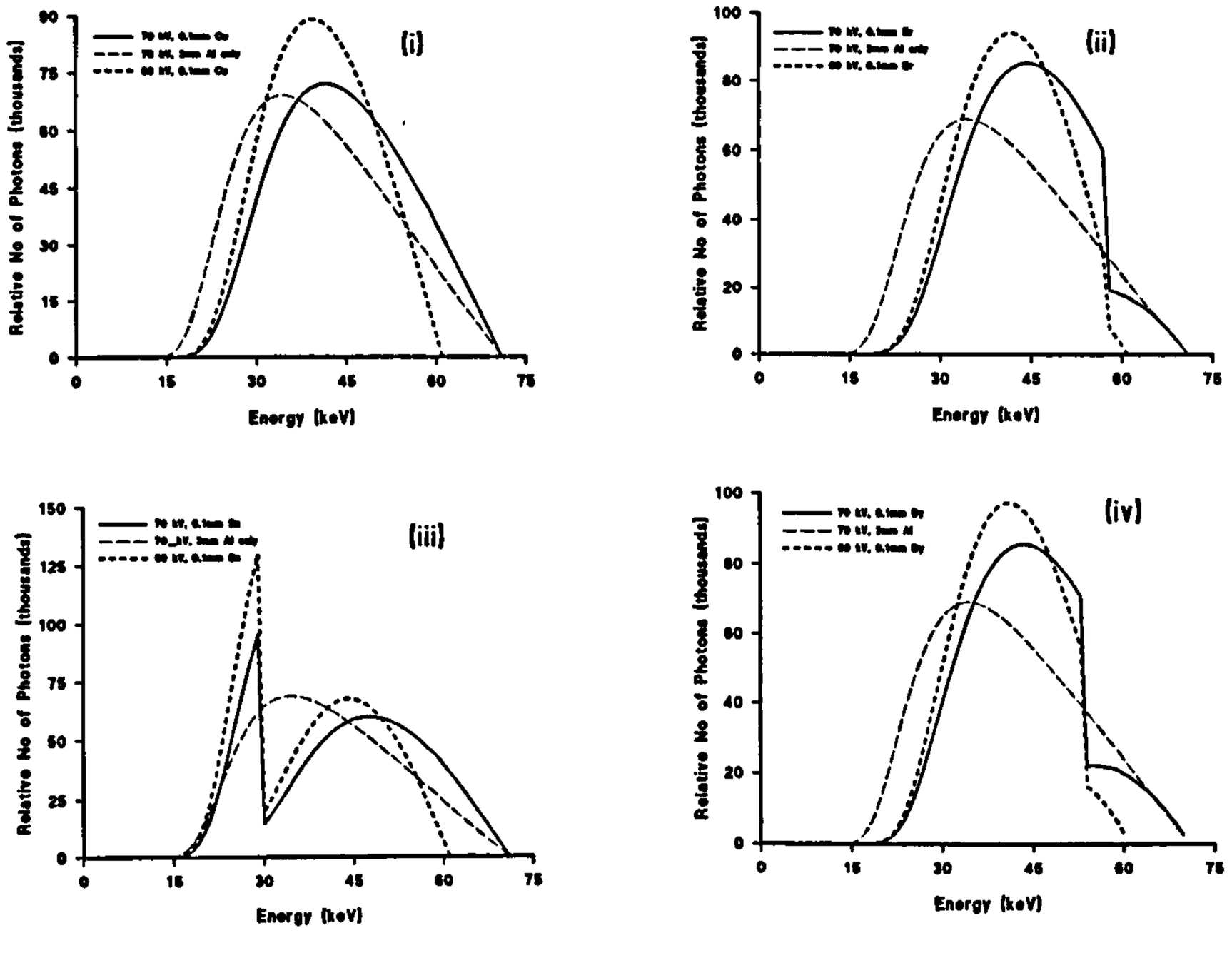

Figure 10.2 : Spectra for 60 kV and 70 kV beams filtered by (i) copper (ii) erbium (iii) tin and (iv) samarium : reference spectrum 70 kV, 3 mm aluminium

Analysis of the earlier results for the 5 cm phantom (Chapter 6) demonstrated that the K-edge of tin coincided with the absorption peak in the phantom and resulted in increased dose with tin filtration. The shift in absorption peak energy with phantom size (Figure 10.2ii) actually crosses over the tin K-edge, so that the adverse dose effects of tin can be expected to decrease for thicker phantoms. For other filters, where the K-edge lies towards the edge of the absorption peak, previous results showed that the dose reduction properties of filters depended critically on the mean beam energy (Section 6.2.3). Figure 10.2 shows that, at 70 kV, K-edge filters such as erbium attenuate a greater proportion of the high energy part of the spectrum than at 60 kV, as the K-energy is further below the maximum beam energy. For this reason, the mean beam energy of the K-edge filtered beams will be relatively lower, compared to a copper filtered beam, than at 60 kV and the relative absorbed dose reduction obtained with copper could be expected to increase. This effect of raising the tube voltage

is likely to be more significant to the behaviour of the K-edge filters than the change in phantom thickness itself, since the change in beam spectra (Figure 10.2) is greater than the change in phantom absorption spectra (Figure 10.1). Dose variation can be expected to be independent of the composition of the contrast detail simulated, and the independence of dose reduction with image receptor that was shown earlier in Section 6.2.4 is likely to hold.

To test these predictions, Monte Carlo simulations were carried out for 1 cm bone in 10 cm soft tissue with 6 different filter materials, and the variation in each dose quantity with tube load is shown in Figure 10.3. The data points and error bars are included on the graph. The error bars for absorbed energy values are of the same magnitude as the data points themselves. Simulations were also carried out for 10 cm tissue with iodine contrast and 15 cm tissue with barium contrast, each with a caesium iodide detector. These results are given in Figures 10.4 and10.5.

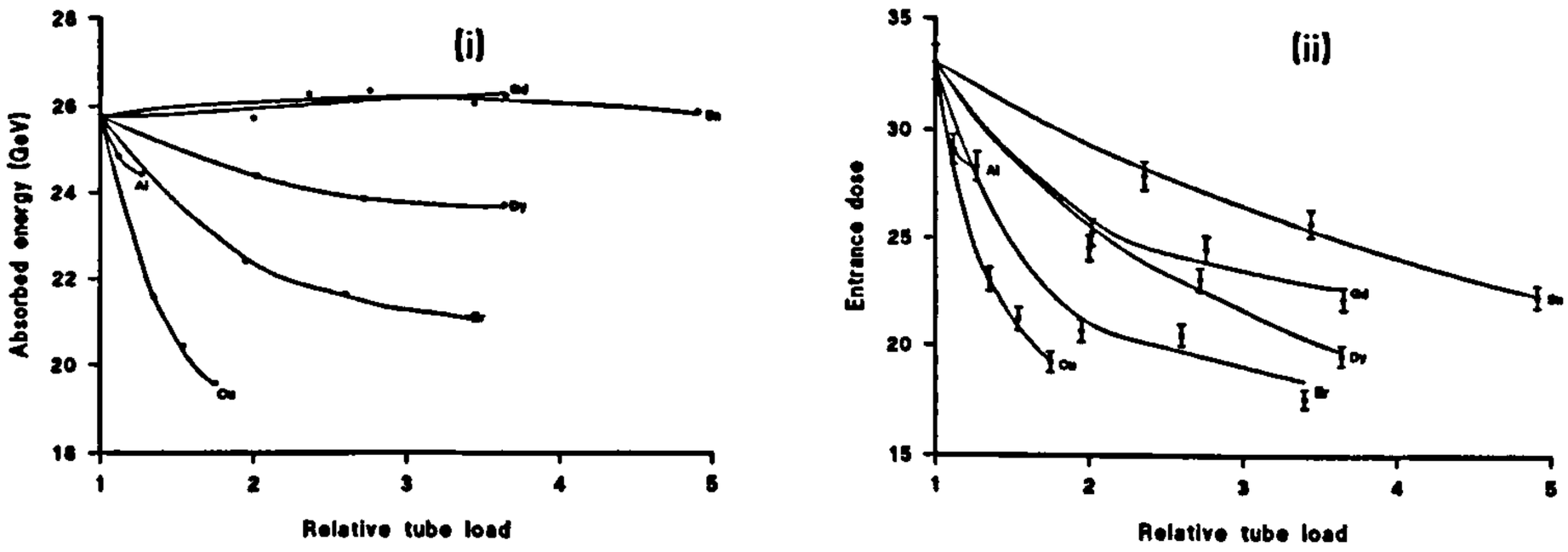

Figure 10.3 : Variation in (i) absorbed energy and (ii) entrance dose for 1cm bone in 10cm soft tissue

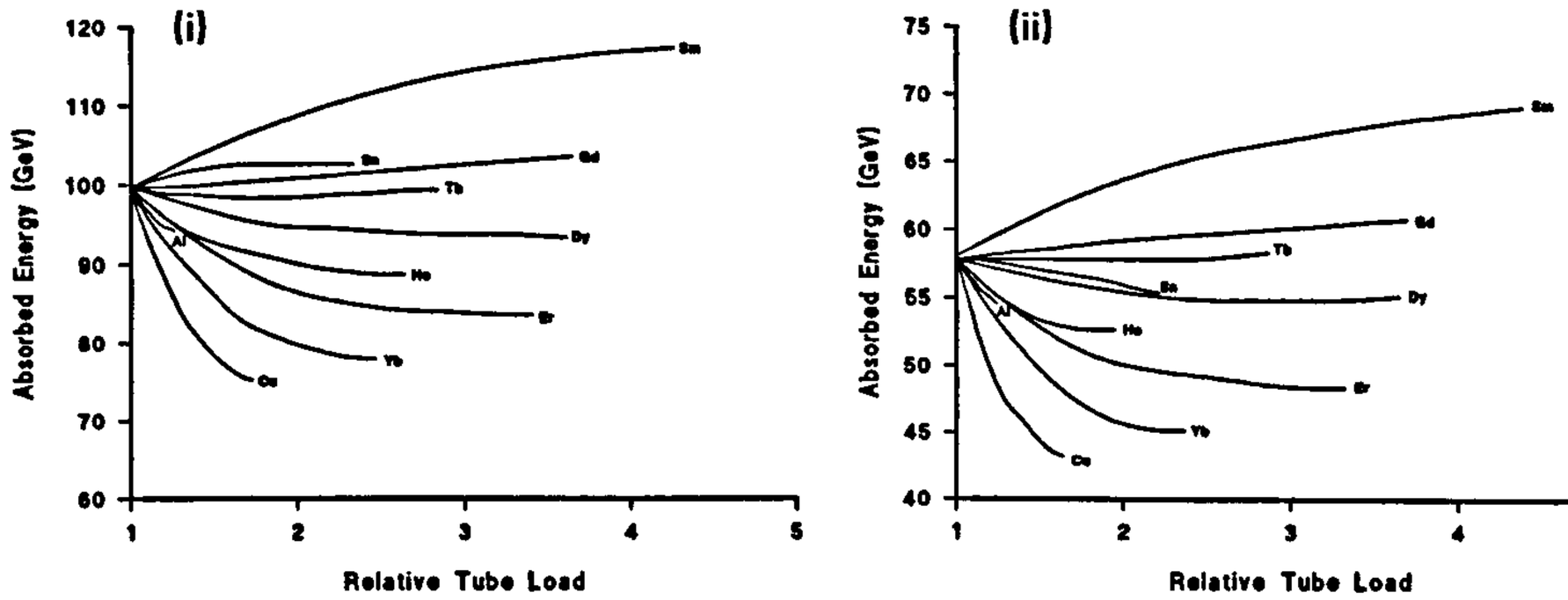

Figure 10.4 : Variation in absorbed energy with tube load for (i) 10 cm phantom and (ii) 15 cm phantom

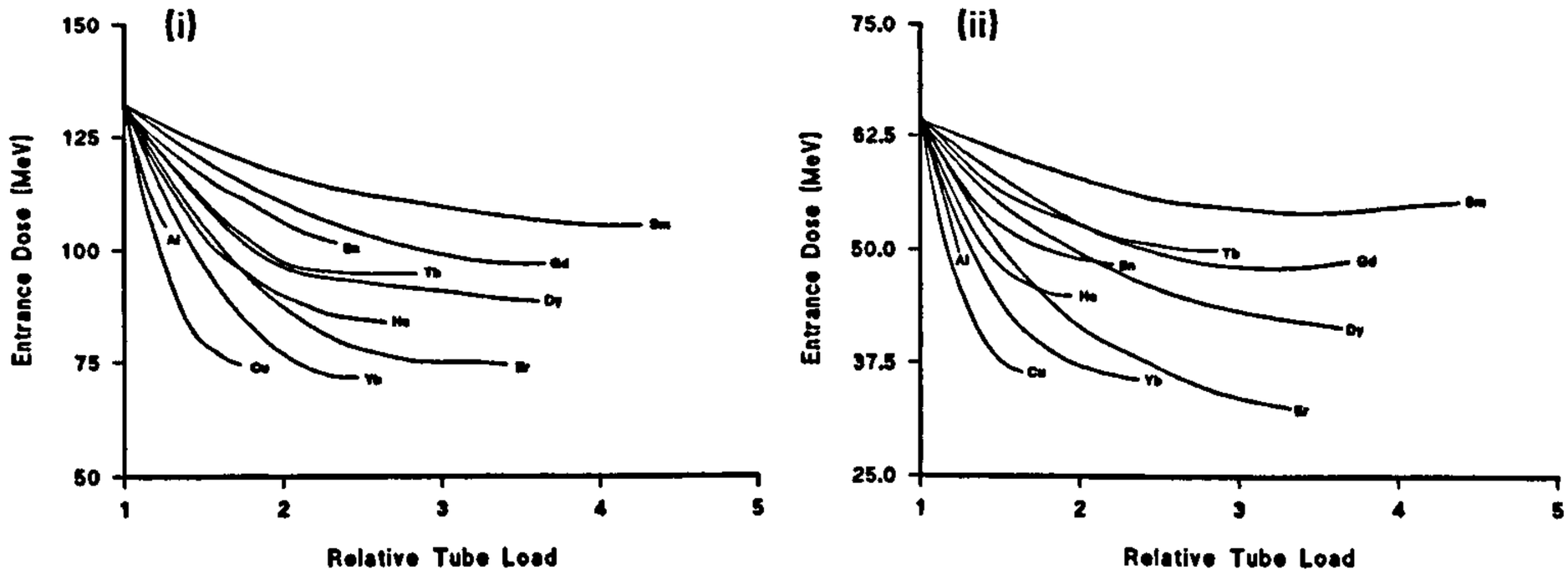

Figure 10.5 : Variation in entrance dose with tube load for (i) 10cm phantom and (ii) 15 cm phantom

The variation of both dose quantities in the 10 cm phantom is very similar for the simulations of both bone (Figure 10.3) and iodine (Figures 10.4 and 10.5), as was predicted above. Dose variation for the 15 cm phantom is also very similar to that of the 10 cm phantom. The main difference is that both of the curves for tin (*ie* entrance dose and absorbed dose variation) show a greater rate of decrease for the larger phantom, sufficient to shift their position relative to the other curves. Out of the filter materials simulated, copper exhibits the greatest amount of dose reduction, for both phantom thicknesses. Samarium shows increasing dose with tube load and gadolinium and terbium give fairly flat curves.

When dose results are compared to those presented in chapter 6 for the 5 cm phantom (Figure 6.3) several differences are apparent for the two larger sizes:

- Tin shows increasing dose reduction with increasing phantom thickness
- Samarium shows increasing dose with tube load instead of the virtually flat curve exhibited previously for the 5 cm phantom
- the curves for gadolinium and terbium show little change in dose with tube load
- the remaining K-edge materials also exhibit slightly less dose reduction compared to that for the 5cm phantom, although the curves for copper and aluminium are very similar.

To illustrate the trends itemised above, the Z-dependance for relative absorbed energy is shown in figure 10.6 for the three different phantom sizes. All data are for a tube load of 1.5, relative to the appropriate reference conditions (60 kV, 3 mm Al for the 5 cm phantom and 70 kV, 3 mm Al for the 10 cm and 15 cm phantoms).

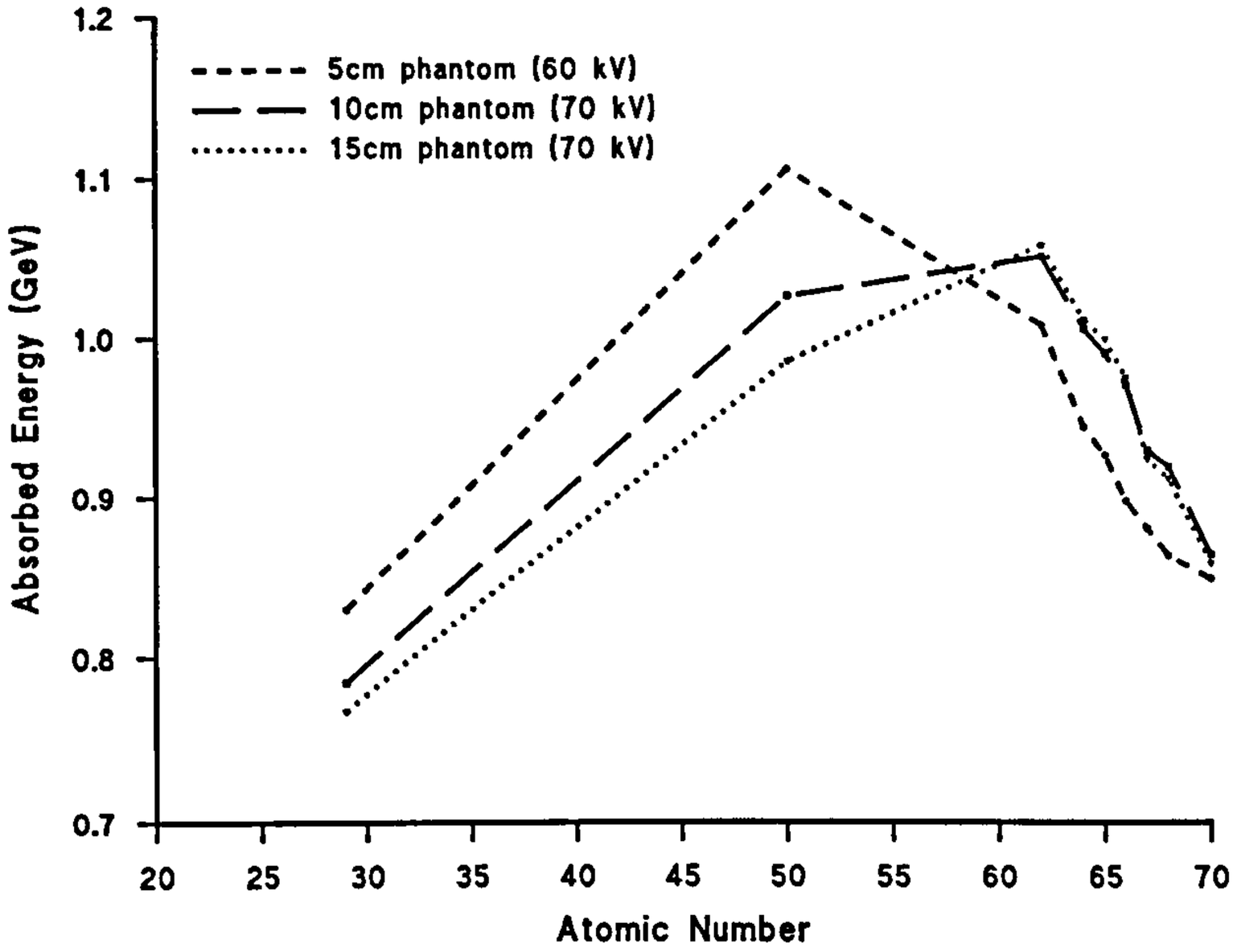

Figure 10.6 : Z dependence of relative absorbed energy for different phantom sizes

As predicted above, the benefit of copper over K-edge filters increases with phantom thickness. The properties of the tin filter are most effected by the phantom change, as predicted from the position of the K-edge. It is interesting to note that for the K-edge filters curves are virtually identical for the two larger phantom sizes. Both of these sets of simulations were carried out at the 70 kV. The dose reduction properties of the K-edge filters are significantly greater for the 5cm phantom originally studied, using a 60 kV beam. However, the copper has a greater effect on dose at the higher kV. This confirms that for the K-edge materials in particular, the kV used is likely to affect the results more than the actual patient thickness.

10.2.2 Contrast

The effect of phantom thickness on contrast can be predicted from consideration of the signal spectrum for each phantom, where signal spectra are derived as explained in section 6.2.3.

Signal spectra for 1 cm bone in 10 cm tissue, and 100 mg cm^{-2} iodine in 10 cm soft tissue are given in Figure 10.7.

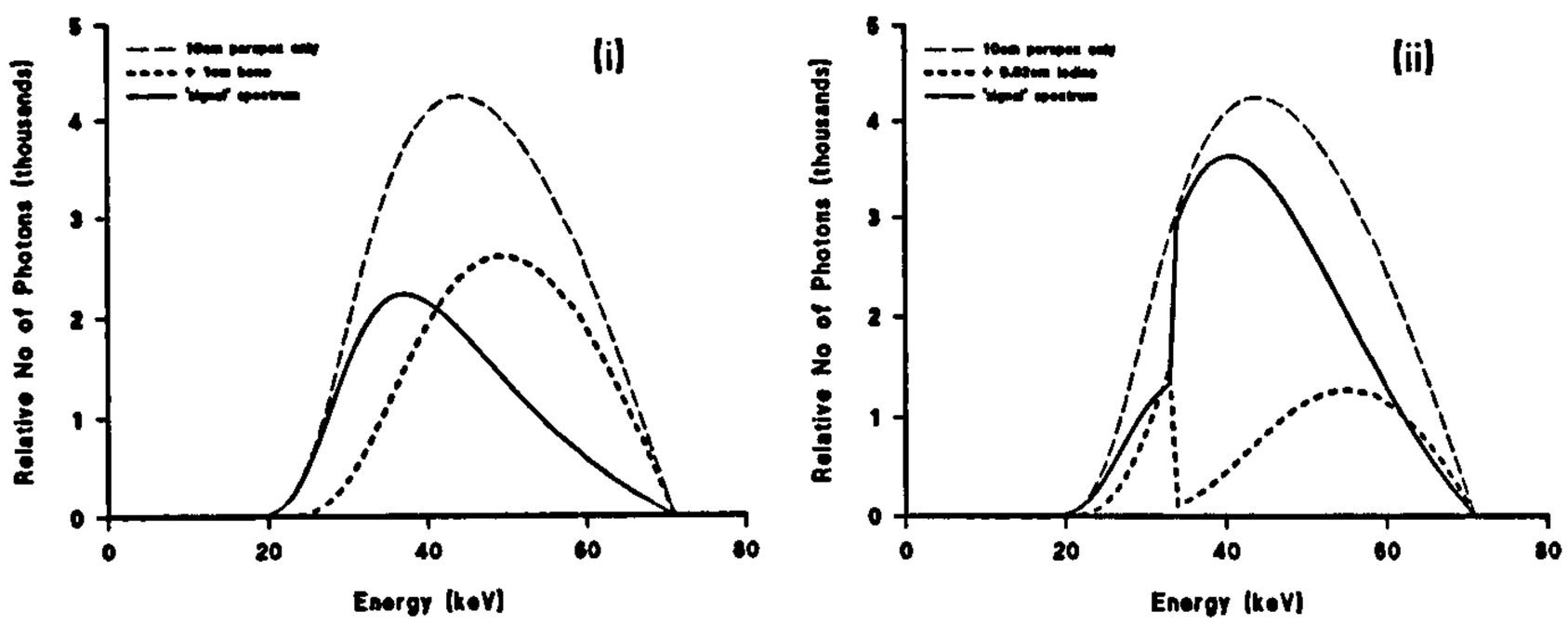

Figure 10.7 : Signal spectra for 10 cm tissue with (i) 1cm bone and (ii) 100 mg cm^{-2} iodine

The effect of the various beam filters on contrast may be assessed from a consideration of the beam spectra shown in Figure 10.2 and the signal spectra of Figure 10.7. From these it can be seen that, for the spectra plotted, all filter materials would be expected to give decreasing contrast, with the possible exception of tin where the K-edge peak occurs within the signal spectrum. Since the signal spectrum peaks at a slightly higher energy than the reference spectrum (70 kV, 3 mm Al) it is probable that very small amounts of additional filtration would give an increase in contrast. For iodine, the signal spectrum is very similar to that for the 60 kV beam (Figure 6.24) as the peak is fixed above the K-edge. The peak is slightly broader for the 70 kV beam and this, together with the slighly harder (relative to 60 kV) filtered beam spectra, should make contrast variation for the 10 cm phantom follow similar trends to those for the neonate.

To assess the predicted contrast results, the results of Monte Carlo simulations carried out for 1 cm bone in 10 cm soft tissue are given in figure 10.8. These show variation in contrast with tube load for 6 different filters.

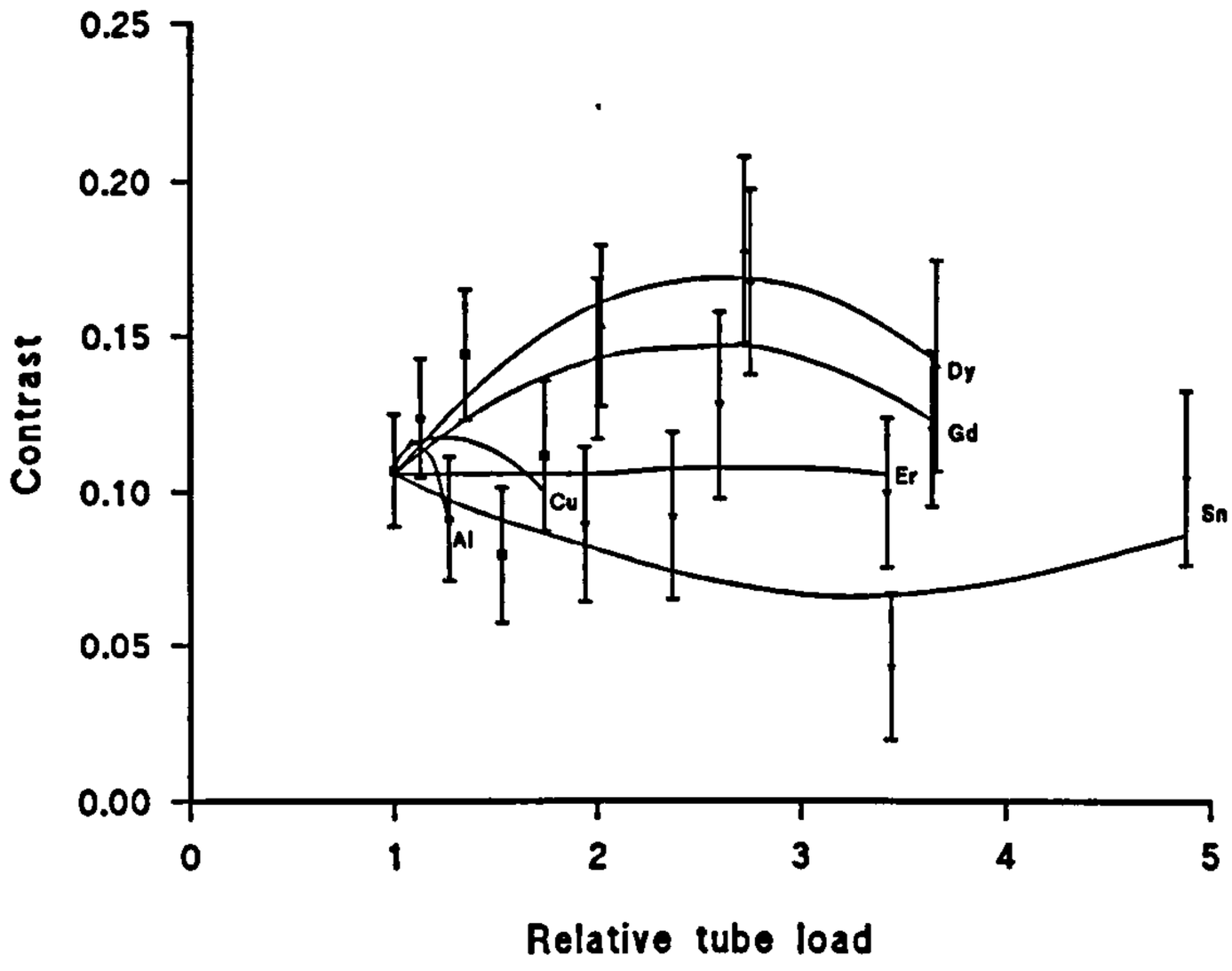

Figure 10.8 : Variation in contrast with tube load for 1cm bone in 10cm tissue

The large uncertainties in the data for the contrast graphs mean that there can be little confidence in the exact shape of the curves drawn. The indications are, however, that contrast initially increases with added filtration, although to a greater extent than was predicted above. This highlights an area where further work would be of particular merit.

10.3 Effect of varying tissue type

Variations in the composition of the phantom background and contrast tissues, although less influential than patient size, will still affect the results of an optimisation study. The composition of the main body of the phantom will affect the absorbed energy and entrance dose, and changes in either of the contrasting tissues will obviously alter the behaviour of contrast with additional filtration. The effect on dose and contrast of substituting lung equivalent material into the phantom has been considered.

10.3.1 Dose

The absorption spectra for 5 cm lung tissue is shown in Figure 10.9. This was generated by assuming the same composition as soft tissue with a decreased density so is, in effect,

equivalent to a smaller thickness of soft tissue. The absorption spectra for 5 cm soft tissue is shown for comparison.

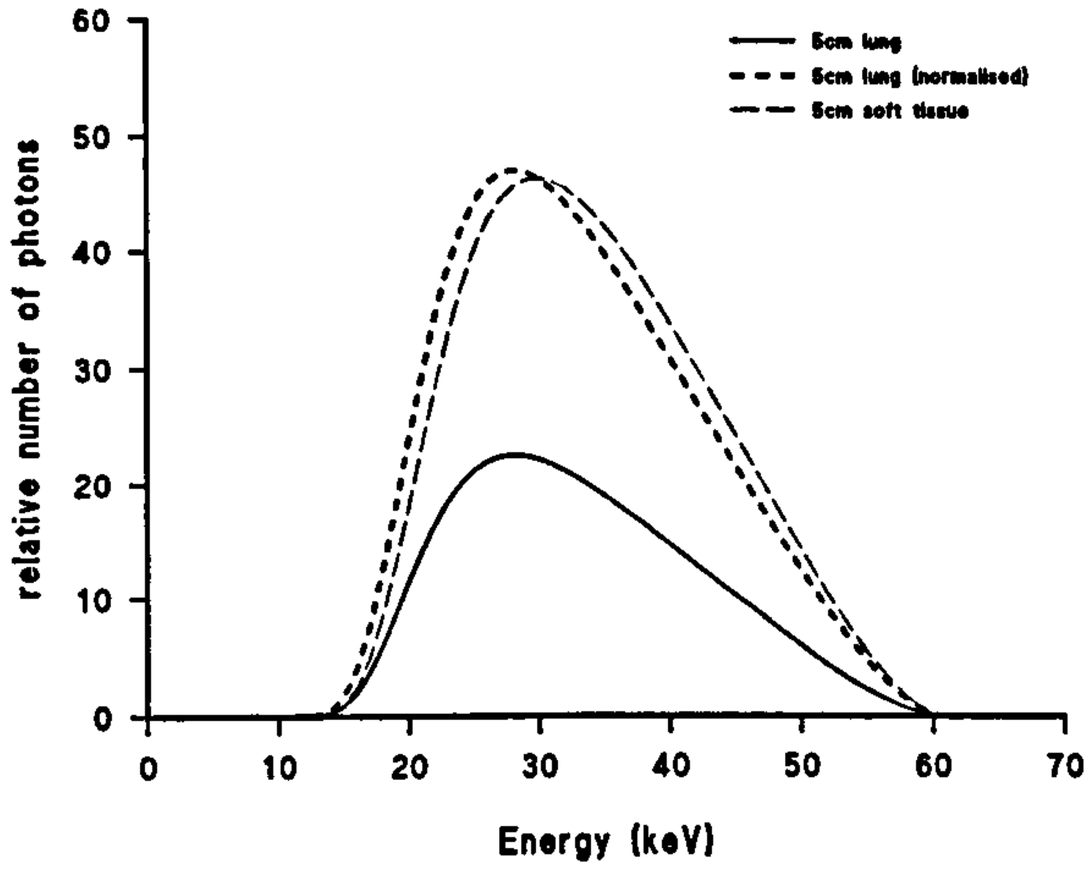

Figure 10.9 : Absorption spectra for 5cm lung equivalent material and 5cm soft tissue

Figure 10.9 shows the similarity between the absorption spectra for the two phantom materials. That for lung peaks at a slightly lower energy than that for soft tissue, corresponding more closely to the K-edge of tin. It would thus be expected that tin filtration might give even greater dose increases with tube load in lung than those observed for soft tissue. For other filter materials, the small difference in beam spectra is unlikely to affect the dose trends.

Monte Carlo simulations were carried out for 5 cm lung, containing 1 cm bone detail, at 60 kV with a lanthanum screen. Figure 10.10 shows the variation in dose quantities with tube load for these conditions.

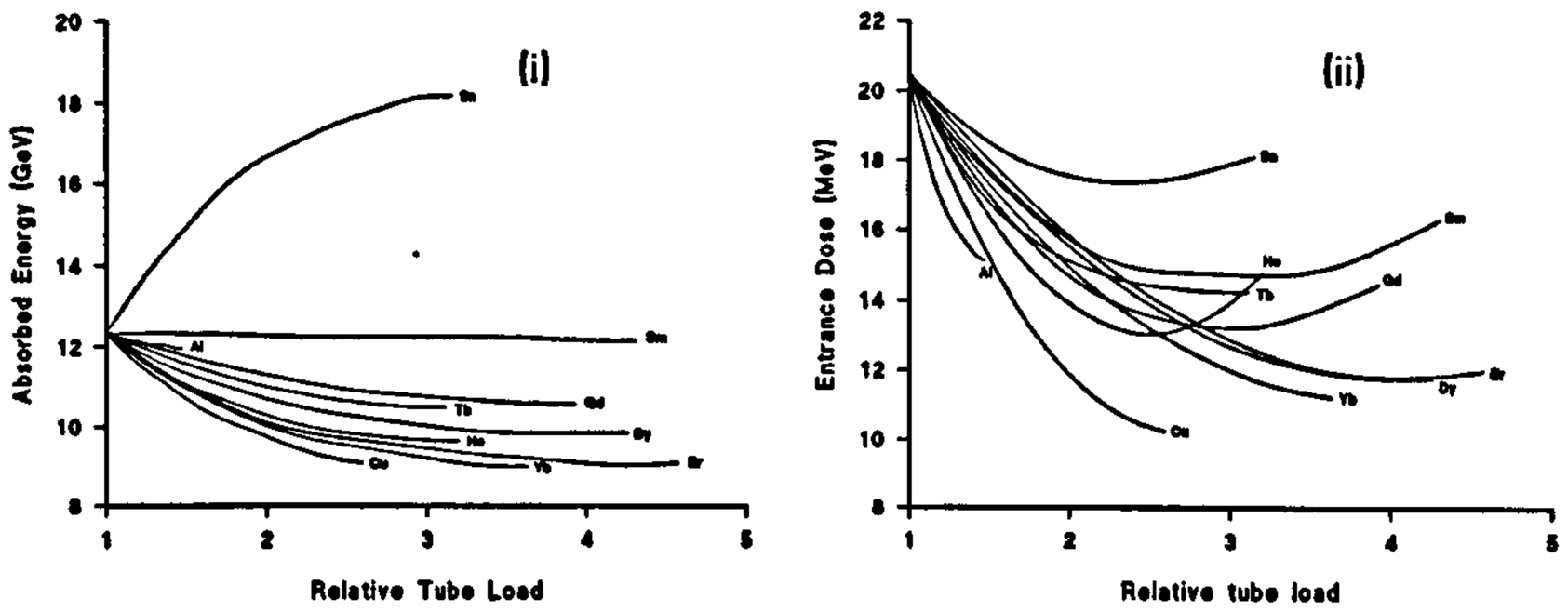

Figure 10.10 : Variation in (i) absorbed energy and (ii) entrance dose for 1cm bone in 5cm lung tissue

The graphs for absorbed energy show the familiar shapes, with tin giving increasing dose with tube load, samarium a fairly flat response and the remaining curves showing decreasing dose with tube load. Although the curves for bone in lung appear closer together than those previously shown for bone in soft tissue (Figure 6.3), the percentage dose reduction is actually approximately the same as for soft tissue (around 75% at a tube load of 2.0), but the dose increase with the tin filter is much greater (around 145% at a tube load of 3, compared to 124% for soft tissue) - as was predicted from consideration of the absorption and beam spectra. The curves for entrance dose variation, however, show different characteristics to those observed previously, as several of the curves show dose starting to increase at high tube loads. The uncertainties on the data points are high, and this apparent effect may not be genuine, particularly as no corresponding effect is seen for the absorbed energy curves.

10.3.2 Contrast

The contrast of bone in lung may be interpreted in terms of the signal spectrum, given in figure 10.11.

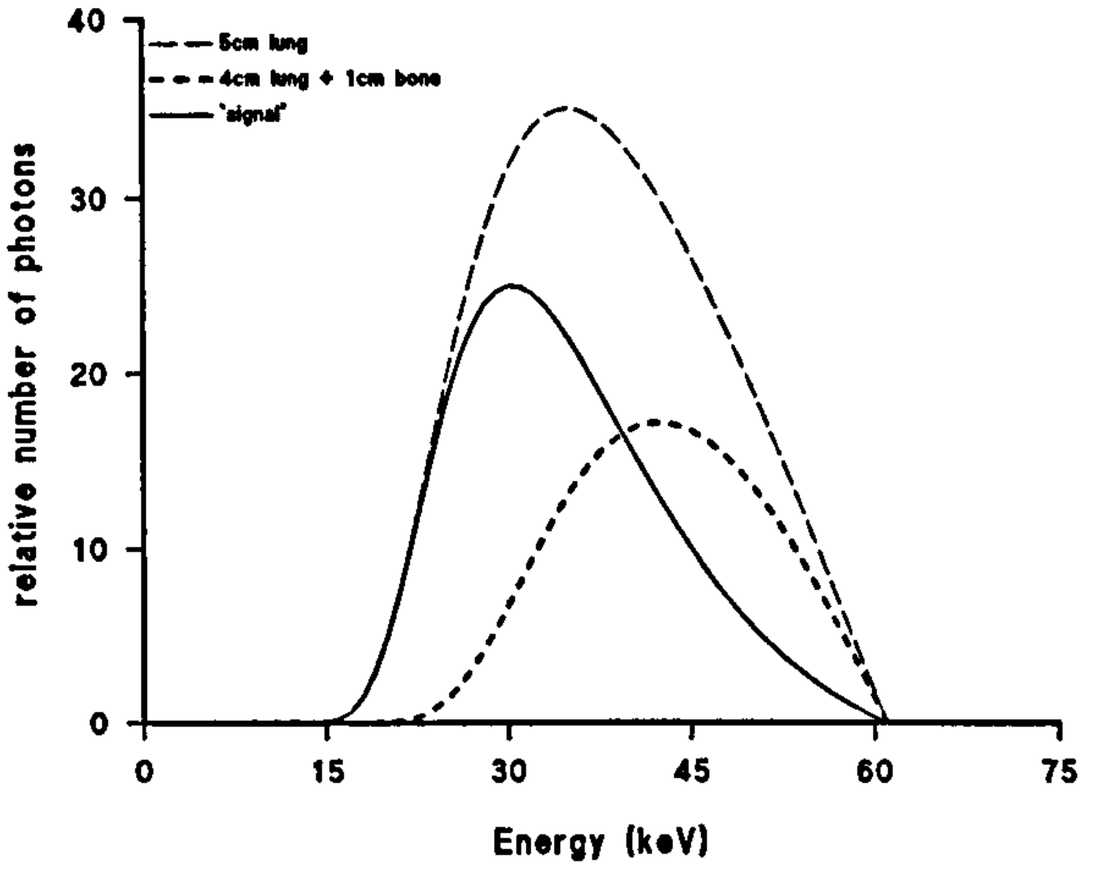

Figure 10.11 : Signal spectrum for 1cm bone in 5cm lung tissue

The signal spectrum exhibits a low energy peak, at a slightly lower energy than that for bone in soft tissue, so that any additional filtration (which will increase mean beam energy) would be expected to reduce contrast more than for the simulation of bone in soft tissue. Even tin is likely to reduce contrast as the signal spectrum peaks below the tin K-edge. The corresponding curves for lung in soft tissue are shown in Figure 10.12.

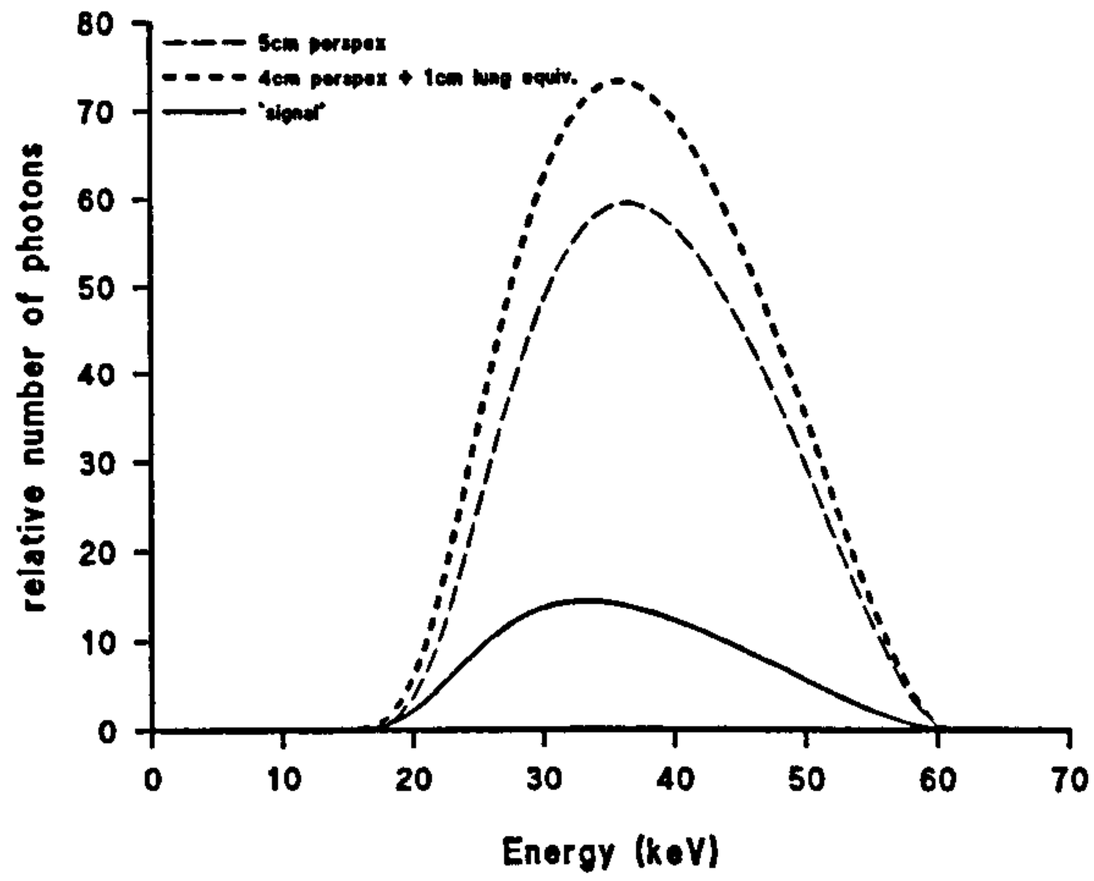

Figure 10.12 : Signal spectrum for 1cm lung in 5cm soft tissue

For lung in soft tissue, the signal spectrum exhibits a broader peak than that for bone in lung. This means that, although the larger amounts of filtration will reduce contrast, the situation for small amounts of additional filtration is likely to be more complex. Figure 10.13 shows the signal spectrum superimposed on a number of filtered beam spectra for a 60 kV beam (taken from Chapter 6). From this it can be seen that additional aluminium filtration should increase contrast, as the filtered spectra shown in Figure 10.13(i) give increasing overlap with the signal spectrum. The same is true for samarium filtration, although the effect is less marked and tails off for increasing filter thicknesses. For the remaining filters, the beam hardening should decrease contrast, as there is less overlap between filtered and signal spectra than for the reference spectrum.

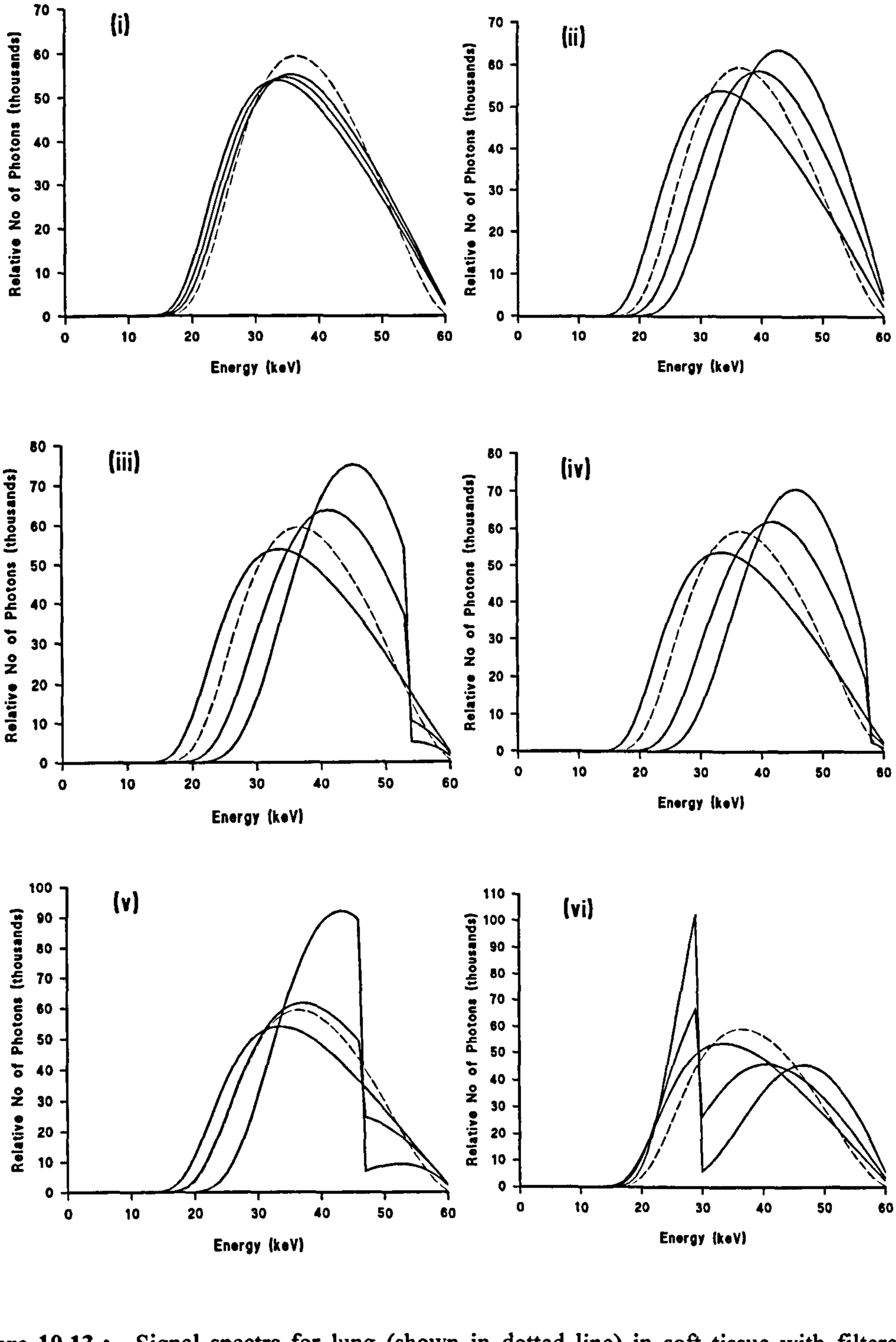

Figure 10.13 : Signal spectra for lung (shown in dotted line) in soft tissue with filtered beam spectra for (i) aluminium (ii) copper (iii) dysprosium (iv) erbium (iv) samarium and (vi) tin. The reference spectrum (70 kV, 3 mm Al) is also plotted.

The variation in contrast with tube load, as determined by Monte Carlo simulation is shown in Figure 10.14 for 1 cm bone detail in 5 cm lung tissue and Figure 10.15 for 1 cm lung

detail in 5 cm soft tissue. The former shows that, as predicted above, contrast is reduced for bone in lung for all added filtration. The curves for lung in soft tissue show an increase in contrast with tube load for aluminium, and an initial incease for samarium. Tin filtration gives a slight drop in contrast and the other curves lie close together, giving a contrast reduction of around 10% at a tube load of 2. These results confirm the predictions given above, in spite of the relatively large uncertainties in the data points.

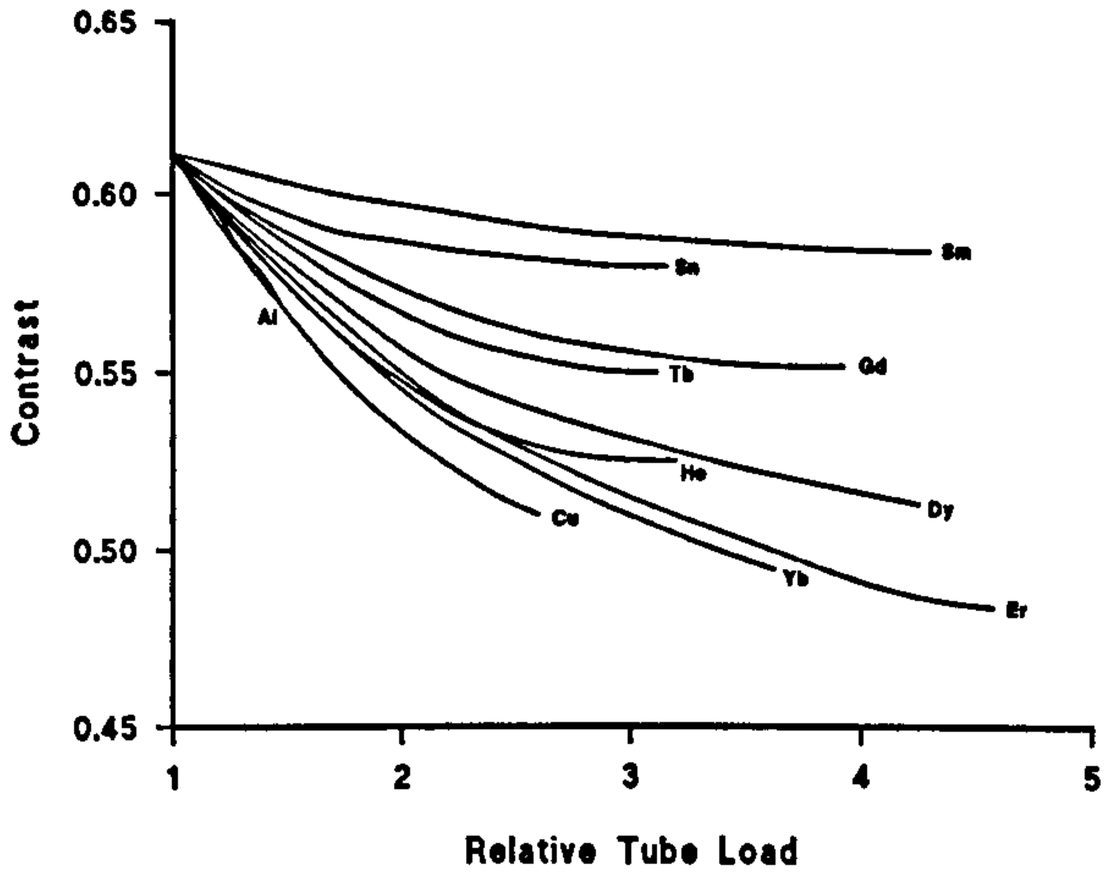

Figure 10.14 : Variation of contrast with tube load for 1cm bone in 5cm lung tissue

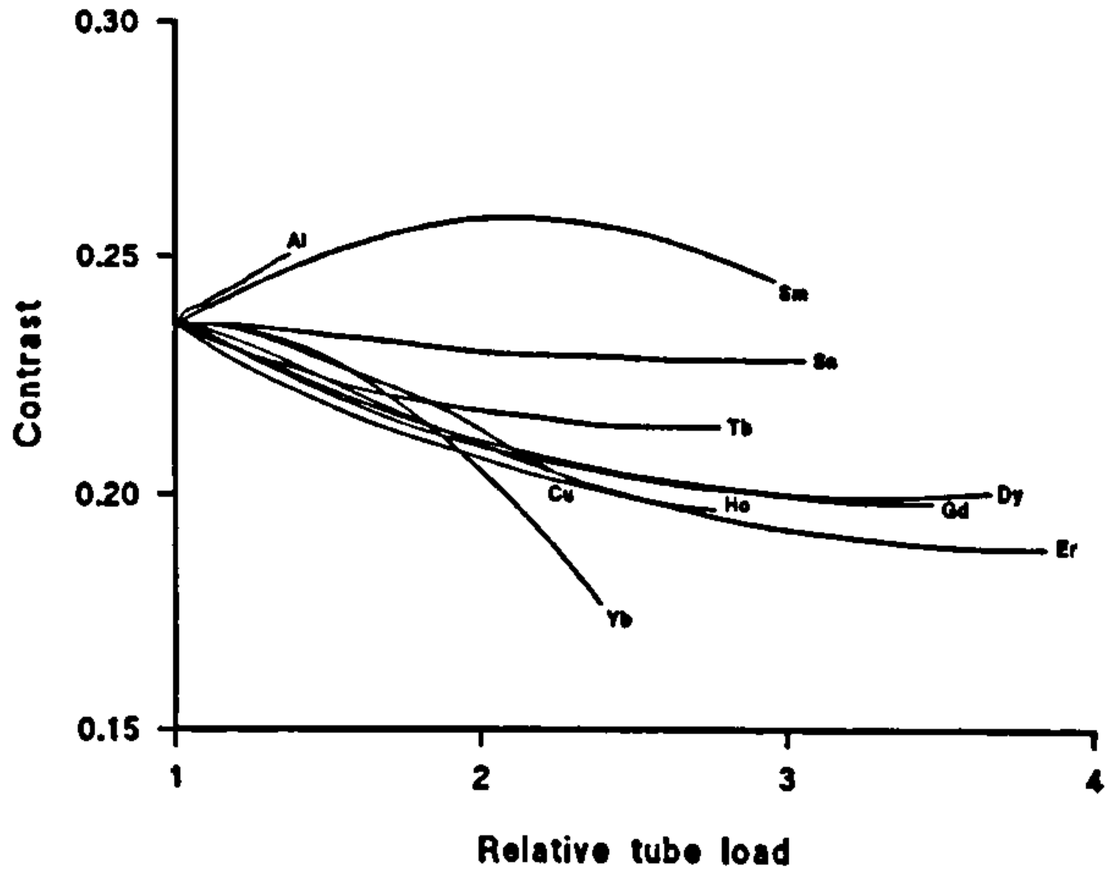

Figure 10.15 : Contrast variation for 1cm lung in 5cm soft tissue

It is interesting to note that the situation simulated here is effectively the contrast between different thicknesses of the same material, as the composition of the lung and soft tissue substitutes is virtually identical, apart from the density. This may thus be comparable to circumstances where the required information from an image concerns fluctuation in tissue density, rather than different tissue types.

10.4 Summary of predictions for other patient categories

Spectral analysis and test simulations carried out for larger phantom thicknesses suggest that the results obtained for the neonatal phantom may broadly apply to older children. The general shape of dose and contrast variation curves will be similar to those obtained for the neonatal phantom. However, it is likely that for added tin and copper filtration the relative dose reduction will increase with patient thickness, for the values of tube potential used here, and for k-edge filters be reduced. The behaviour of the K-edge filters may depend more on the tube potential used than on the actual phantom thickness.

Consideration of the inclusion of lung substitute material in the phantom indicates that the results obtained earlier for bone in soft tissue may be applied also to radiography in the chest region. The pattern of dose reduction is likely to be similar, except for the tin filter which is predicted to give even bigger doses with increasing tube load when imaging the lungs. Contrast is likely to decreases more, at equivalent tube loads, for bone in lung than for bone in soft tissue. For lung in soft tissue, contrast may increase slightly for small amounts of added aluminium or samarium.

10.5 Suggestions for further work

The large number of variable parameters for these simulations mean that the possibilities for extending the theoretical analysis are extensive. However, a number of specific areas worthy of further study may be highlighted. These can be categorised into theoretical simulations, experimental and clinical measurements, and general dosimetry concerns

10.5.1 Monte Carlo simulations

The recommended next stage in the computer simulation work would be to look in detail at the effect of varying tube potential on the test results described here for the larger phantom sizes. The two specific questions to be addressed are:

- For radiography, can a reduction in tube potential, in conjunction with added filtration, maintain image contrast and significant dose reduction, as was suggested for the neonatal work.
- Does a more careful selection of tube potential affect the performance of the K-edge filters, with respect to either dose or image quality, for the thicker phantoms.

An assessment of contrast variation for fluoroscopy work with contrast media is also required, and a general extension of all results to very low contrast imaging, representing specific clinical situations would be a valuable area of study. The latter would require additional variance reduction techniques, or lengthy computational times to obtain statistically significant results.

10.5.2 Experimental work

Laboratory measurements with the slab phantoms are recommended to verify the results described in this chapter *ie* for thicker phantoms and also for lung equivalent material. The potential for a thin filter of gadolinium or samarium to be used as a contrast enhancing filter for fluoroscopic examination of neonates should be investigated in a clinical setting. A general use filter for older patients, most probably copper as suggested by initial results, should also be investigated clinically. The practical problems anticipated with its use also need to be addressed.

Any simulations carried out for low contrast situations would also need to be verified experimentally. This would entail substantial practical difficulties using the current laboratory facilities, and would probably require use of a more modern, high power, steady output X-ray generator in order to achieve measurable and consistent results.

10.5.3 General dosimetry considerations

Two aspects of general paediatric dosimetry are recommended for further work. These are firstly an investigation of how field size varies with patient size for different fluoroscopic and radiographic examinations. This would involve collecting and analysing patient and examination data. Secondly the question of a suitable risk related quantity, or quantities, for paediatric radiology needs to be addressed. This could possibly involve considering absorbed dose or energy imparted to different 'compartments' of the body, as an intermediary between the total energy imparted concept, which can be easily applied to a specific patient examination but does not allow for different tissue sensitivities, and effective dose which includes organ sensitivities but is virtually impossible to assess accurately for a specific patient examination. Identification and incorporation of realistic organ risk factors for paediatrics would also need to be included in this project.

Chapter 11

Summary and Conclusions

11.1 Paediatric patient dosimetry

The collection and analysis of good quality paediatric dose data is a prerequisite to any dose optimisation stategy. As shown in Chapter 3, the current literature demonstrates that, although results of a number of paediatric dosimetry surveys have been published in recent years, the amount of data available is small. This is particularly a problem when the wide range of patient sizes is considered. There has been no consistent approach to dealing with variations in patient size when analyzing and comparing dosimetry data. The routine collection of dosimetry data has been made possible by a semi-automated system, utilising a laptop computer connected to a DAP meter. This enabled large quantities of paediatric dose-area product data to be collected from a number of hospitals, which could then be reported back to each department to complete the dose audit chain. The results showed considerable variation between centres, highlighting the potential for optimisation of doses. A method of correcting dosimetry data for patient size, within each of the 5 agebands defined by the CEC, was developed and shown to reduce variability in DAP due to size. The size correction method utilises the concept of equivalent diameter, and the exponential attenuation of X-ray energy within the patient.

The choice of dose descriptor for paediatric dosimetry is complicated by the need to balance the desirability for a quantity related to radiation risk with the need for ease of assessment and applicability to any given patient examination. The currently popular concept of effective dose is inappropriate for paediatric dosimetry as the risk factors from which it is derived are not applicable to paediatric patients. In addition, although data is available for calculating effective dose from directly measurable quantities such as entrance dose or DAP, these data will only apply to examinations for which parameters such as field size and position correspond exactly to those used in their derivation. For fluoroscopic procedures, this constraint will rarely be satisfied, and the calculation of effective dose for a specific patient examination will involve large uncertainties.

11.2 Results from theoretical simulation

Monte Carlo code has been developed, and verified experimentally, to investigate the effect of added filtration on patient dose and image contrast for a range of conditions, primarily for neonates. The main results can be summarised as follows :

- Additional copper filtration exhibited the greatest dose reduction for equal tube load.
- For radiography of bone in soft tissue, a reduction in tube voltage in conjunction with small amounts of additional filtration could be used to maintain contrast and reduce both entrance dose and absorbed energy. The theoretical absorbed dose reduction is of the order of 10% for equal contrast.
- For fluoroscopy using iodine or barium contrast agents, contrast was not markedly affected by small amounts of additional filtration, enabling significant dose reduction to be achieved - of the order of 40% reduction in entrance dose and 15% reduction in absorbed energy.
- A thin filter of samarium or gadolinium was found to give enhance contrast without increasing patient dose, for imaging of iodine or barium.
- The choice of image receptor did not have a significant effect in determining values of dose or image quality.
- The use of replacement filtration was demonstrated to offer no advantage over additional filtration.
- Experimental verification of the Monte Carlo predictions gave good agreement for values of absorbed dose, entrance dose, contrast and tube load, to within the calculation and measurement uncertainties.

11.3 Clinical Implementation

An extensive theoretical study alone is of no practical benefit to patients. Consideration of how theoretical results may be implemented in clinical practice is an essential stage of an optimisation strategy. For this work, experimental measurements were carried out in a clinical environment, and these yielded a number of important points concerning the application of optimisation techniques, which may be summarised as follows:

- Parameters that may be constrained to remain constant in a theoretical simulation are unlikely to remain rigidly so during clinical practice. *Eg* background density may

fluctuate quite considerably within an acceptable range and, for paediatric exposures will often be limited by the discrete nature of exposure factor settings.

- Acceptable contrast is usually more relevant than equal contrast, particularly as the latter is hard to judge subjectively. This may depend on the nature of the examination involved.
- Image quality may also be limited by the X-ray equipment being used, particularly for older image intensifier systems, where small changes in primary contrast may not be discernible due to degradation along the imaging chain.

A 0.1mm copper filter was used in a clinical trial, for fluoroscopic examination of infants, and resulted in dose reduction of 50% for entrance dose and 25-40% for organ doses, without significant loss of image qualiy. The practical problems associated with using the filter were overcome by lying the children on a large copper sheet.

11.4 Optimisation

The optimisation of paediatric patient dose with image quality is not a subject that should be over simplified, as it is affected by a large number of factors as discussed in Chapter 4. While generalisations, such as the CEC image quality criteria may be a useful 'first step', the specific requirements and complications of individual patient examinations need to be addressed. In order to achieve this, the underlying principles and effects of varying parameters on one another need to be understood, and related to the clinical situation. Diverse factors such as the type of equipment available, whether or not the equipment is dedicated to paediatric use and the compliance of patients need to be considered, as well as the information required from the examination being performed. The practical implications of any optimisation strategy, such as cost and acceptability to overworked staff are also important. The success of optimisation procedures can only be assessed when reliable methods of assessing patient doses are in place.

The work presented here has addressed the most important of these issues by, firstly, developing a strategy of paediatric dose measurement. Secondly, an optimisation strategy has been developed incorporating theoretical simulation, experimental verification and clinical implementation. The specific optimisation technique of beam filtering has been studied in detail, through both simulation and experiment, from an approach of studying trends in different parameters rather than applying a number of constraints in an attempt to find an absolute ranking of filter materials.

The extrapolation to clinical use has been achieved for a particular category of radiological examination, namely fluoroscopy in infants, and consideration has been given as to how the techniques and results might be applied to other paediatric age groups and examination categories. A number of suggestions have been made regarding future progression of the work, based on the success of the strategies that have been developed. The methodologies described here may also be applied to the optimisation of both computed tomography and computer radiography, which are increasingly becoming the techniques of the future. Such scientifically based, yet practical strategies, for both dosimetry and optimisation are required for the continued reduction of radiation dose in paediatric radiology.

Appendix A

Results of dose survey

Hospital ID	Mean screening times (s)					
	Cystogram	Ba Swal.	Ba Meal	Ba Enema	Ba Fol.Thr.	Ba Meal&Swal
A2	101		146			
B1	53	56	84		120	
C1	35	59	82			82
C2	63	161				118
D		66	116			
E	114	28	145			
F1		288	191	126	158	126
G			78			
H		130	96			120
I	47	133	85			
J1	6		240			
K1		96				
K2	92	214	234		210	98
L2	81	119	72			138
M1	154	185	175	97		168
N1			48	10		
N2	66	36	80			
O1			11	75		
O2	34	54	67			
P1	87	93	276	84	31	126
R	100	12	20	108		

Table A.1 : Screening time data for neonates

Hospital ID	Mean numbers of radiographs (R) and spot/DSI films (S)											
	Cystogram		Ba Swal.		Ba Meal		Ba Enema		Ba Fol.Thr.		Ba Meal&Swal	
	R	S	R	S	R	S	R	S	R	S	R	S
A2	1	5			7	11						
B1		4	3	5	1	3						
C1		20		3		14						5
C2				3								3
D		5		4	1	6						
E		4		4		4						
F1			1	14	1	6	1	8	1	7		4
G					13							
H				6	3	16						7
I		2		10		2						
J1		7				11						
K1												
K2		6		7		15				10		6
L2		7		9		9				12		9
M1		14		6	1	8	3	3				7
N1						4		15				
N2		16		14		6						
O1		6	2	13		8		6				
O2			1									
P1		6		5		13	3	3		2		6
R		3		6		5		6				

Table A.2 : Numbers of radiographs and spot films for neonates

Hospital ID	Mean Tube Potential (kV)					
	Cystogram	Ba Swal.	Ba Meal	Ba Enema	Ba Fol.Thr.	Ba Meal&Swal
A2	63		50			
B1	62	72	77		90	
C1	63	62	50			60
C2	60	62				60
D	69	55	57			
E	68	62	90			
F1		60	69	90	60	60
G			81			
H		70	50			60
I	65	88	71			
J1	60		70			
K1		70				
K2	60	62	60		50	60
L2	59	59	58	52		58
M1	65	61	68	93		50
N1			80	60		
N2	60	78	75			
O1	62	90	68	65		
O2	59	50	62			
P1	58	60	60	90	70	90
R	64	62	68	70		

Table A.3 : Tube voltage data for neonates

Hospital ID	Mean Size Corrected Energy Imparted (mJ)					
	Cystogram	Ba Swal.	Ba Meal	Ba Enema	Ba Fol.Thr.	Ba Meal&Swal
A2	9.43		11.96			
B1	4.02	4.14	40.22			
C1	7.03	3.30	4.80			3.87
C2	2.51	8.19				8.80
D	1.21	1.29	3.39			
E	8.49	5.34	9.06			
F1		5.31	7.07	38.22		2.14
G			97.94			
H		5.49	1.13			4.90
I	2.01	8.02	5.70			
J1	0.86		27.02			
K1		5.00				
K2	9.35	9.11	25.65			5.54
L2	3.07	4.13	7.77	11.22		3.48
M1	12.93	15.05	17.20	19.71		9.30
N1			1.80	0.90		
N2	0.29	2.93	2.32			
O1	0.54	1.41	1.97	0.78		
O2	0.43	0.46	0.94			
P1	3.28	3.17	5.87	12.34		32.58
R	2.77	1.70	2.51	7.89		

Table A.4 : Energy imparted data for neonates

Hospital ID	Mean screening times (s)				
	Cystogram	Ba Swal.	Ba Meal	Ba Enema	Ba Meal&Swal
A1	65				144
A2	72		19		198
B1	82	121	113		63
C1	43	37	105		26
C2	81	109	78		91
D	74	59	56	258	150
E	75		52	286	
F1	134	95	101	219	104
H	136	292	254	408	
I	64	128	124	156	108
J1	41	77	120		60
J2	68		78		
K1		252			
K2	126	167	222		199
L2	43	40	82	6	179
M1	88	139	132	217	132
N1	45	168			
N2	83	79	125		
O1	1	2	19	4	
O2	36	96	66		
P1	88	86	7		
Q1		6	122		
R	17	2	14		78
S				114	

Table A.5 : Screening time data for infants

Hospital ID	Mean numbers of radiographs (R) and spot/DSI films (S)									
	Cystogram		Ba Swal.		Ba Meal		Ba Enema		Ba Meal&Swal	
	R	S	R	S	R	S	R	S	R	S
A1	1	3							9	
A2	2	6				6				
B1		2		7	2	4				4
C1		10		5		16				7
C2		7		4						
D		4		4		6		5		5
E		5				9		1		
F1		7		17		6		8		5
H		8		12		9		7		
I		1		6		5		4		6
J1		5		20		10				7
J2		8								
K1				4						
K2		6		7		5				7
L2		6		7		9	1	7		9
M1	1	7	1	4		5		3	1	4
N1		3						6		
N2		5		4		6				
O1		6		6		8		6		5
O2		1		29						
P1		3		10		8				
Q1						8				
R	1	5		3		4				5
S							4	6		5

Table A.6 : Numbers of radiographs and spot films for infants

Hospital ID	Mean Tube Potential (kV)				
	Cystogram	Ba Swal.	Ba Meal	Ba Enema	Ba Meal&Swal
A1	60				90
A2	53		80		50
B1	72	73	80		80
C1	61	64	67		64
C2	56	56	60		60
D	57	67	66	60	60
E	75		90	70	
F1	63	62	62	75	67
H	62	67	70	70	
I	65	72	76	74	80
J1	67	62	60		60
J2	60		60		
K1		70			
K2	70	58	60		62
L2	60	62	61	60	60
M1	57	64	73	73	58
N1	72			50	
N2	66	72	67		
O1	65	70	70	68	77
O2	60	70	63		
P1	62	62	67		
Q1		60	70		
R	62	70	68		70
S				70	

Table A.7 : Tube voltage data for infants

Hospital ID	Mean Size Corrected Energy Imparted (mJ)				
	Cystogram	Ba Swal.	Ba Meal	Ba Enema	Ba Meal&Swal
A1	1.87				4.95
A2	5.48		2.16		16.19
B1	6.84	9.85	13.39		6.56
C1	4.99	5.94	14.34		4.83
C2	5.25	11.89	6.02		7.55
D	2.70	8.61	3.94	6.42	3.14
E	22.09		22.25	37.24	
F1	6.53	3.92	5.26	21.74	5.81
H	4.83	19.12	10.16	41.11	
I	4.53	11.29	12.81	128.58	14.20
J1	6.64	6.11	7.02		4.86
J2	15.00		2.17		
K1		508.2			
K2	14.80	12.89	10.94		11.45
L2	3.96	6.83	6.55	8.51	5.00
M1	8.83	26.78	18.6	29.05	12.53
N1	1.50			3.37	
N2	4.11	4.41	7.01		
O1	1.06	1.46	3.10	1.41	2.54
O2	0.68	1.66	1.43		
P1	5.12	6.48	10.66		
Q1		0.13	12.14		
R	2.76		4.33	2.06	1.68
S				43.14	

Table A.8 : Energy imparted data for infants

Hospital ID	Mean screening times (s)					
	Cystogram	Ba Swal.	Ba Meal	Ba Enema	Ba Fol.Thr.	Ba Meal&Swal
A1	48					
A2	159	82	104	342		
B1	69	95	89			
B2				240		54
C1	74	72	88	222		171
C2	46	91		62	30	106
D	76	37	100			
E			194	244		
F1	185	78	76	147	60	
G			210			
H	137	186	132	222	42	285
I	90	128	108	221	71	124
J1	42	42		600		120
J2	90					192
K1		588				
K2	102	152	330			132
L2	62	76	86	60		120
M1	162	196	118	104		
N1	51				24	
N2	61	67	86	142	96	84
O1	12	13	29	4	17	90
O2	41	83	71			
P1	98	97	134	186	97	67
Q1				126		
R	41		34			
S		54				
T			60			

Table A.9 : Screening time data for 1-5 year olds

Hospital ID	Mean numbers of radiographs (rads) and spot/DSI films (films)											
	Cystogram		Ba Swal.		Ba Meal		Ba Enema		Ba Fol.Thr.		Ba Meal&Swal	
	R	S	R	S	R	S	R	S	R	S	R	S
A1	2											
A2		10		9		9	4	13				
B1		3		5		5						4
B2							8	12				
C1		10		4		17						12
C2		1		8				4		3		4
D		3		7		7						
E						12	5	2				
F1		6		8		7		7		1		
F2							2					
G					8	10						
H		8		8		5				3		8
I		1		14		3		5		4		6
J1		6		30				20				30
J2		2										17
K1												
K2		4		4		9						6
L2		7		9		9		7		2		9
M1	1	6		12		4	1	2				
N1		2										
N2		3		1		4	1	7		9		5
O1		6		17		8		5		6		4
O2		1				5						
P1		3		5		8		8		6		4
Q							2	8				
R		4				7						
T					1	2						

Table A.10 : Numbers of radiographs and spot films for 1-5 year olds

Hospital ID	Mean Tube Potential (kV)					
	Cystogram	Ba Swal.	Ba Meal	Ba Enema	Ba Fol.Thr.	Ba Meal&Swal
A2	62	90	62	90		
B1	68	73	78			90
B2				90		70
C1	62	60	72	83	50	63
C2	63	60		63		
D	62	90	68			
E			90	94		
F1	65	62	65	71	60	
F2				90		
G			85			
H	68	65	77	60	70	65
I	66	66	73	75		67
J1	63	70		70		60
J2	60					70
K1		70				
K2	60	61	60			60
L2	64	66	67	68	62	68
M1	62	72	90	77		
N1	61				50	
N2	65	65	74	83	90	70
O1	67	67	69	60	70	77
O2	60	60	63			
P1	64	64	66	60	76	72
Q				95		
R	64		79			
S		50				
T			50			

Table A.11 : Tube voltage data for 1-5 year olds

Hospital ID	Mean Size Corrected Energy Imparted (mJ)					
	Cystogram	Ba Swal.	Ba Meal	Ba Enema	Ba Fol.Thr.	Ba Meal&Swal
A2	27.34	19.89	13.35	260.58		
B1	8.26	12.05	10.59			29.29
B2				73.27		
C1	11.29	0.87	11.35	32.3		22.00
C2	7.62	16.02		27.79	12.79	20.31
D	8.42	5.33		6.82		
E			17.88	64.16		
F1	14.29	4.40	7.64	12.14	10.58	
F2				3.95		
G			375.41			
H	12.64	37.68	17.40	10.49	6.89	25.61
I	9.29	24.55	19.69	37.77	12.46	17.10
J1	12.98	5.99		54.98		7.76
J2	8.42					9.94
K1		41.97				
K2	12.53	10.12		30.23		14.88
L2	9.07	14.25	13.06	23.47	3.93	11.49
M1	31.65	44.28	26.04	29.80		
N1	3.95				1.30	
N2	3.27	2.59	4.58	19.47	34.75	1.85
O1	2.48	3.08	5.08	1.49	1.85	21.43
O2	1.61	3.37	2.40			
P1	9.03	9.02	16.05	22.47	20.33	11.45
Q1				235.58		
R	4.26		8.92			
S		1.77				
T			0.30			

Table A.12 : Energy imparted data for 1-5 year olds

Hospital ID	Mean screening times (s)					
	Cystogram	Ba Swal.	Ba Meal	Ba Enema	Ba Fol.Thr.	Ba Meal&Swal
A2	507		134			348
B1	97	108	136			
C1	168	102	226	170	90	
C2	80	116		66	75	92
D	122	84				
E			160			
F1	154	77	120	80	108	
G				132		
H	100	141	182		114	102
I	90	73	116	42	83	128
J1	78	150		40		
J2	84					
K2	77	176	84	168		116
L2	58	93	69	147	57	146
M1	88	88	177	180		96
N1	48	78				
N2	129	100	136		78	
O1	27		56	109	75	
O2	40		81			
P1	103	66	141	98	57	162
Q1		44	113		132	90
R	19		37			
S						
U			132			

Table A.13 : Screening time data for 6-10 year olds

Hospital ID	Mean numbers of radiographs (rads) and spot/DSI films (films)											
	Cystogram		Ba Swal.		Ba Meal		Ba Enema		Ba Fol.Thr.		Ba Meal&Swal	
	R	S	R	S	R	S	R	S	R	S	R	S
A2		25				5					13	5
B1	1	4		8	4	5						
C1		2		2		33	1	60				
C2		1		3				5		2		5
D		8		6								
E					4	9						
F1		6		14		20	2	3		9		
G							5	7				
H		8		4		10				4		9
I		1		14		5		7		3		12
J1		7		12				10				
J2		77										
K2		4		7		10		6				11
L2		7		10		10		10	3	4		10
M1		5	1	11		6	2	8				
N1		3		9								
N2		4		7		8			4	4		
O1		7				8	1	7		7		
O2		4				6						
P1		3		8		9	1	7		4		26
Q1				11		7						
R		5				5						5
S												
U					10							

Table A.14 : Numbers of radiographs and spot films for 6-10 year olds

Hospital ID	Mean Tube Potential (kV)					
	Cystogram	Ba Swal.	Ba Meal	Ba Enema	Ba Fol.Thr.	Ba Meal&Swal
A2	60		70			70
B1	83	70	79			
C1	67	65	70	75	70	
C2	63	62		70	65	62
D	66	60				
E			90			
F1	69	75	70	78	70	
G				86		
H	70	70	67		70	70
I	69	82	73	70	75	68
J1	75	60		75		
J2	60					
K2	60	60	60	60		77
L2	72	71	78	84	90	80
M1	77	100	60	95		60
N1	70	90				
N2	72	76	72		90	
O1	66		72	78	72	
O2	62		62			
P1	65	70	73	83	67	70
Q1		60	60			
R	63		74			70
S					60	
U			60			

Table A.15 : Tube voltage data for 6-10 year olds

Hospital ID	Mean Size Corrected Energy Imparted (mJ)					
	Cystogram	Ba Swal.	Ba Meal	Ba Enema	Ba Fol.Thr.	Ba Meal&Swal
A2	106.53		46.88			79.49
B1	17.30	21.61	20.16			
C1	27.17	13.91	48.18	54.50	10.28	
C2	24.74	33.79		27.39	26.06	25.01
D	13.38	10.12				
E			18.01			
F1	26.35	7.22	12.03	107.19	10.90	
G				221.33		
H	8.56	19.82	23.33		23.45	25.52
I	15.55	20.79	27.42	32.42	27.04	35.11
J1	13.56	10.82		12.49		
J2	7.25					
K2	13.74	18.38	67.89	24.91		30.31
L2	15.51	11.49	22.78	65.93	7.23	21.36
M1	25.53	134.58	42.34	112.69		37.87
N1	46.05	17.31				
N2	9.20	45.77	12.94		4.62	
O1	4.25		13.20	15.46	10.15	
O2	9.25		4.51			
P1	19.24	14.50	46.10	50.62	12.05	39.74
Q1		5.39	23.01			11.95
R	4.77		6.68			
S					23.21	
U			38.37			

Table A.16 : Energy imparted data for 6-10 year olds

Hospital ID	Mean screening times (s)					
	Cystogram	Ba Swal.	Ba Meal	Ba Enema	Ba Fol.Thr.	Ba Meal&Swal
A1						168
A2	423			92	53	126
B1	72	57	48			54
C1	102	96	92			54
C2	84	105	146		63	
D		96	109			
E			121			
F1	115		62	117	60	
G		89		102		
H		194	105			204
I	98	85	159	112	58	75
J1					115	
K1		302	246			
K2	102	120	108		266	285
L1	54					
L2	42	76	36	185	208	117
M1	114	63	90	516	36	135
N1			96			
N2	30	60		100	84	66
O1	66	41	68	50	110	22
O2	42	66	112	42	59	
P1	80	90	156	218	97	108
Q		107	124			
R	34	49	62			78
S		108			80	

Table A.17 : Screening time data for 11-16 year olds

Hospital ID	Mean numbers of radiographs (R) and spot/DSI films (S)											
	Cystogram		Ba Swal.		Ba Meal		Ba Enema		Ba Fol.Thr.		Ba Meal&Swal	
	R	S	R	S	R	S	R	S	R	S	R	S
A1										1		6
A2		12					10		2			
B1		2		8		7						6
C1		2		34		16						
C2		1		8		16				2		7
D				11		10						7
E						7						
F1		6				6	3	5	1	8		
G				18			8					
H				12		10						10
I		1		12		10	2	7		3		7
J1									3	11		
K1				7		7						
K2		5		38		14				11	2	6
L1		6										
L2		7		13		12	5	8		7		15
M1				6		4		5		1	4	11
N1						8						
N2				4		8	4	6	2	1	2	4
O1		7		14		10	1	5		6		3
O2		2				1	2	7				
P1		4		9	1	7	2	5	1	5		8
Q1				8		10						
R		3		5		5						8
S				10					1	4		

Table A.18 : Numbers of radiographs and spot films for 11-16 year olds

Hospital ID	Mean Tube Potential (kV)					
	Cystogram	Ba Swal.	Ba Meal	Ba Enema	Ba Fol.Thr.	Ba Meal&Swal
A1					90	
A2	70		70	70	70	
B1	90	90				90
C1	70	70	72			50
C2	70	65	70		75	80
D		90	68			70
E			90			
F1	70		65	80	80	
G		70		90		
H		70	70			65
I	69	82	94	88	81	70
J1					75	
K1		77	70			
K2	70	67	90		90	
L1	90					
L2	76	80	81	86	100	88
M1	60	80	60	60	70	83
N1			80			
N2	70	80	73	100	80	
O1	69	72	70	73	70	60
O2	60	60	65	90	62	90
P1	74	66	77	90	70	90
Q1		72	71			
R	68	66	79			90
S		70			70	60

Table A.19 : Tube voltage data for 11-16 year olds

Hospital ID	Mean Size Corrected Energy Imparted (mJ)					
	Cystogram	Ba Swal.	Ba Meal	Ba Enema	Ba Fol.Thr.	Ba Meal&Swal
A1					1.59	18.41
A2	208.43			137.85	9.82	
B1	8.97	20.06	20.75			23.61
C1	5.13	20.55	35.01			12.26
C2	36.32	52.95	73.27		28.24	
D		50.34	43.46			16.86
E			134.08			
F1	28.07		16.11	77.35	21.72	
G		13.45		138.04		
H		54.95	39.06			67.14
I	29.85	26.71	75.48	87.88	35.25	50.36
J1					75.77	
K1		60.41	43.56			
K2	73.93	54.26	131.21		213.56	
L1	17.64					218.19
L2	38.84	31.11	50.13	165.25	84.69	40.80
M1	75.95	40.55	78.24	163.83	27.71	67.95
N1			39.49			
N2	2.09	7.31	25.77	72.15	38.11	19.24
O1	13.78	9.22	12.93	13.48	43.35	2.64
O2	1.25	8.00	11.76	13.16	11.30	
P1	45.38	44.69	43.23	172.33	38.06	66.04
Q1		43.76	58.59			
R	18.76	13.90	15.45			22.17
S					39.66	

Table A.20 : Energy imparted data for 11-16 year olds

Appendix B

Usercode Listing

```
%L
%E
!INDENT M 4;"INDENT MORTRAN LISTING BY 4 PER LEVEL"
!INDENT F 2;"INDENT FORTRAN OUTPUT BY 2 PER LEVEL"
"*****************************************************************
*********"
"                                                                 "
"                  ******************                           "
"                  *                  *                           "
"                  *  PEDSIM1.MOR     *                           "
"                  *                  *                           "
"                  ******************                           "
"                                                                 "
" This code is used to simulate paediatric x-ray examinations, using  "
" a simple body phantom, k-edge filtration, diverging beam geometry,  "
" and an input kV spectrum. Quantities measured include  the energy   "
" absorption in the phantom and energy absorbed in a screen phosphor. "
" Particle splitting is used as a means of variance reduction, and K- "
" edge photons are tracked in the filter and phosphor.               "
"                                                                   "
"*****************************************************************
*********"

"_____________________________________________________________"
"STEP 1:  USER-OVERRIDE-OF-EGS4-MACROS                          "
"_____________________________________________________________"
REPLACE {$MXMED} WITH {20}   "20 media in the problem(default 10)  "
REPLACE {$MXREG} WITH {20}   " 20 geometric regions (default 2000)  "
REPLACE {$MXSTACK} WITH {5000}"maximum number of particles on stack    "
REPLACE {$MXPLNS} WITH {8}  "maximum number of planes                  "
REPLACE {$MXELEMS} WITH {3} "maximum number of elements in one medium
"

"** Random Number Generator **"
REPLACE {;COMIN/RANDOM/;} WITH {;COMMON/RANDOM/IXX;}
PI = 3.141592654;
REPLACE {$RANDOMSET#;} WITH
{IXX=IXX*663608941;{P1}=0.5 + IXX*0.23283064E-09;}

OPEN(1,'INPUT.DAT', STATUS='OLD');
$UINPUT(1) IXX; (I9);

"** Parameters for diverging beam **"
$UINPUT(1) ANGLE; (F6.4); "          ANGLE SET BY USER"
```

```
ANGFACT=1-COS(ANGLE);

"MACRO TO DETERMINE DIRECTION OF INCIDENT PARTICLE"
REPLACE {$SELECT_DIRECTION;} WITH
{$RANDOMSET RANDIR1; $RANDOMSET RANDIR2;
COSTHE=1.0-RANDIR1*ANGFACT;
SINTHE=SQRT(1.0-COSTHE*COSTHE);
PHI = RANDIR2*2*PI;
COSPHI = COS(PHI);
SINPHI = SIN(PHI);
UIN = SINTHE*COSPHI;
VIN = SINTHE*SINPHI;
WIN = COSTHE;}

"** Parameters for input energy spectrum **"
REPLACE {$KV} WITH {70}     "kVp of spectrum used                    "

"DEFINE A COMMON FOR SPECTRUM GENERATING & PARTICLE
SPLITTING
VARIABLES"
REPLACE {;COMIN/USER/;} WITH

{;COMMON/USER/IENERGY,IRAWDATA($KV),ISUMDATA($KV),EBINA($KV),
SPECTRUM($KV),RANDX,IRSPLT($MXREG),LSPLT,NSPLT;}

"RANDOM ENERGY SELECTION FROM SPECTRUM"
REPLACE {$SELECT_ENERGY;} WITH {$RANDOMSET RANDX; IENERGY=1;
WHILE (RANDX > SPECTRUM(IENERGY)) [IENERGY=IENERGY+1];
EIN=IENERGY/1000.0; EBINA(IENERGY)=EBINA(IENERGY)+1;}

"** Parameters for particle splitting  **"

"TRANSFER OF PROPERTIES TO SPLIT PARTICLES"
REPLACE {$PARTICLE-SPLITTING;} WITH
  {;IF(LSPLT.NE.0) [WT(NP)=WT(NP)/LSPLT;  DO ISPLT=1,NSPLT [
    $TRANSFER PROPERTIES TO (NP+ISPLT) FROM (NP);
    U(NP+ISPLT)=U(NP);  V(NP+ISPLT)=V(NP);  W(NP+ISPLT)=W(NP);
    E(NP+ISPLT)=E(NP);  IQ(NP+ISPLT)=IQ(NP);]  NP=NP+NSPLT;]}

"** Parameters for K-edge fluorescence **"
REPLACE {;COMIN/EDGE/;} WITH

{;COMMON/EDGE/IEDGFL($MXREG,$MXELEMS),ELEM($MXMED,2,$MXELEMS),


$LGN(EKALPH,EKBETA,BKR1,BKR2,PROP,CUMPROP,EKBIND($MXMED,$MXEL
E
    MS));}

    "NOTE 1: COMMON/EDGE/ IS A NON-EGS4 COMMON THAT IS DEFINED
HERE IN
    "
```

```
"      ORDER TO BE ABLE TO INCLUDE IT IN 'COMIN/..../' BELOW.    "
    "NOTE 2: THE K-EDGE FLUORESCENT TRANSPORT OPTION IS
CONTROLLED BY
    "
    "      A FLAG (FOR EACH 'REGION') CALLED IEDGFL.  IEDGFL MUST    "
    "      BE SET TO ZERO FOR ALL REGIONS, AND THEN REDEFINED TO
"
    "      NON-ZERO FOR THOSE 'K-EDGE TRANSPORT' REGIONS, PRIOR TO
"
    "      CALLING THE USER-DEFINED SUBROUTINE EDGSET.          "
    "                                                  "

    "** Parameters for ten-region geometry **"
    REPLACE {;COMIN/GEOM/;} WITH
    {;COMMON/GEOM/TFILT,FSD,TBODY,TGAP,TPHOS,
                              TCONT,RCONT,DCONT;}
    NREG=$MXREG;
    NMED=$MXMED;
    NPLAN=$MXPLNS;
    NCYL=1;

    "** Parameters for scoring **"
    REPLACE {;COMIN/SCORE/;} WITH


{;COMMON/SCORE/ENABS,ENENT,ENSCON,ENSBAK,RADIN2,RADOUT2,RCONT
2,
MXNP;}

;COMIN/BOUNDS,CYLDTA,EDGE,GEOM,MEDIA,MISC/;
;COMIN/PHOTIN,PLADTA,RANDOM,SCORE,STACK,THRESH,USER/;
"  THE ABOVE EXPANDS INTO A SERIES OF COMMON STATEMENTS"

"-------------------------------------------------------------"
"STEP 2 PRE-HATCH-CALL-INITIALIZATION                          "
"-------------------------------------------------------------"
$TYPE MEDARR(24,$MXMED) /$S'AIR',21*' ',$S'PERSPEX',17*' ',
$S'MS20',20*' ',$S'SB5',21*' ',$S'LN10_00',17*' ',$S'LN10_100',16*' ',
$S'CAWO4',19*' ',$S'GD2O2S',18*' ',$S'CSI',21*' ',$S'LAOBR',19*' ',
$S'AL',22*' ',$S'BA',22*' ',$S'CU',22*' ',$S'ER',22*' ',$S'FE',22*' ',
$S'GD',22*' ',$S'I',23*' ',$S'NB',22*' ',$S'PB',22*' ',$S'DY',22*' '/;
"                        PLACE MEDIA NAMES IN AN ARRAY"
"                        $S IS A MORTRAN MACRO TO EXPAND STRINGS"
"                        $TYPE IS INTEGER(F4) OR CHARACTER*4(F77)"
DO J=1,NMED[
DO I=1,24[MEDIA(I,J)=MEDARR(I,J);]]
"THIS IS TO AVOID A DATA STATEMENT FOR A VARIABLE IN COMMON"
"DUNIT DEFAULTS TO 1, I.E. WE WORK IN CM"

$UINPUT(1) IFILT,DUMP,IPHAN,DUMP,ICONT,DUMP,IPHOS,DUMP,IGAP;
 (4(I2,I1),I2);
```

```
/MED(1),MED(7)/=0;"          REGIONS 1 & 7 ARE VACUUM"
MED(2)=IFILT;"               REGION 2 IS FILTER MATERIAL"
/MED(8),MED(9),MED(4)/=IPHAN;" REGIONS 8,9 & 4 ARE PHANTOM
MATERIAL"
MED(10)=ICONT;"              REGION 10 IS CONTRAST MEDIA"
MED(6)=IPHOS;"               REGION 6 IS PHOSPHOR MATRIAL"
MED(3)=1;"                   REGION 3 IS AIR"
MED(5)=IGAP;"                REGION 5 IS AIR OR PERSPEX"

/ECUT(2),ECUT(4),ECUT(6),ECUT(8),ECUT(9),ECUT(10)/=0.70;
"   TERMINATE ELECTRON HISTORIES AT 0.70 MEV IN ALL MEDIA"
    /PCUT(2),PCUT(4),PCUT(6),PCUT(8),PCUT(9),PCUT(10)/=0.01;
    "   TERMINATE   PHOTON HISTORIES AT 0.01 MEV IN ALL MEDIA"

    DO I=1,NMED[
    IRAYLR(I)=1; "   TURN ON RAYLEIGH SCATTERING IN ALL MEDIA
"
    DO J=1,$MXELEMS[
    IEDGFL(I,J)=0;]" TURN OFF K-EDGE FLAG FOR ALL ELEMENTS IN ALL
MEDIA    "
            ]
    IRAYLR(1)=0; IRAYLR(7)=0; "TURN OFF RAYLEIGH OPTION FOR VACUUM
    REGNS"

     "ENTER ATOMIC NUMBER OF ELEMENT TO ENABLE FLUORESCENCE"
    $UINPUT(1) IEDGFL(2,1),DUMP,IEDGFL(2,2),DUMP,IEDGFL(2,3);
     (2(I2,I1),I2);
    $UINPUT(1) IEDGFL(6,1),DUMP,IEDGFL(6,2),DUMP,IEDGFL(6,3);
     (2(I2,I1),I2);

    " NOTE:  A SPECIAL VERSION OF SUBROUTINE PHOTO MUST BE
INCLUDED   "
    "       WITH THIS USER CODE WHEN IEDGFL-VALUE(S)  ARE NON-ZERO.
"

    %E
    "-------------------------------------------------------------"
    "STEP 3   HATCH-CALL                                          "
    "-------------------------------------------------------------"
    ;OUTPUT;('1 START SIMULATION'//
    ' CALL HATCH TO GET CROSS-SECTION DATA'/);
    CALL HATCH;"    PICK UP CROSS SECTION DATA FOR W"
    "           DATA FILE MUST BE ASSIGNED TO UNIT 12"

    ;OUTPUT AE(1)-0.511, AP(1);
    ('0KNOCK-ON ELECTRONS CAN BE CREATED AND ANY ELECTRON
FOLLOWED
    DOWN TO'
    /T40,F8.3,' MeV KINETIC ENERGY'/
    '   BREM PHOTONS CAN BE CREATED AND ANY PHOTON FOLLOWED
DOWN TO
        '
```

```
/T40,F8.3,' MeV ');"NOTE, AE VALUES CAN OVER-RIDE ECUT VALUES"

"SET UP K-EDGE PARAMETERS NEEDED BY SUBROUTINE PHOTO"

"first enter symbols of each element in fluorescence media  "
$TYPE ELEM;
$TYPE ELEMARR1(2,$MXELEMS) /$S'CA',$S'W ',$S'O '/;
DO J=1,$MXELEMS [
  DO I=1,2 [ELEM(4,I,J)=ELEMARR1(I,J);]]

"enter relative proportion of each element, and its binding energy"
"default is 1 element with binding energy EBINDA                  "
DO I=1,NMED [PROP(I,1)=1; EKBIND(I,1)=EBINDA(I);
  IF($MXELEMS.GT.1) [DO J=2,$MXELEMS [PROP(I,J)=0;
    EKBIND(I,J)=0.0;]]]
PROP(7,1)=0.1666667; PROP(7,2)=0.1666667; PROP(7,3)=0.6666666;
EKBIND(7,1)=0.00404; EKBIND(7,2)=0.06951; EKBIND(7,3)=0.00053;
PROP(8,1)=0.831;     PROP(8,2)=0.0845;    PROP(8,3)=0.0845;
EKBIND(8,1)=0.05023; EKBIND(8,2)=0.00053; EKBIND(8,3)=0.00247;
PROP(9,1)=0.512;     PROP(9,2)=0.488;
EKBIND(9,1)=0.03596; EKBIND(9,2)=0.03316;
PROP(10,1)=0.592;    PROP(10,2)=0.068;    PROP(10,3)=0.34;
EKBIND(10,1)=0.03893;EKBIND(10,2)=0.00053;EKBIND(10,3)=0.01348;

"calculate cumulative proportions  "
DO I=1,NMED [CUMPROP(I,1)=PROP(I,1);
  IF($MXELEMS.GT.1) [DO J=2,$MXELEMS [
    CUMPROP(I,J)=CUMPROP(I,J-1)+PROP(I,J);]]
  IF(CUMPROP(I,$MXELEMS).NE.1) [
    OUTPUT I; (' INCORRECT PROPORTIONS GIVEN FOR MEDIA ',I3);]]

CALL EDGSET;

"-------------------------------------------------------------"
"STEP 4  INITIALIZATION-FOR-HOWFAR                                "
"-------------------------------------------------------------"
"PARTICLE SPLITTING PARAMETERS"
$UINPUT(1) LSPLT; (I3);
"0 FOR NO SPLITTING, ELSE EQUALS NUMBER OF SPLITS"
NSPLT = 0;
IF(LSPLT.NE.0) ["DO ONLY IF SPLITTING TURNED ON"
NSPLT=LSPLT-1;]
DO IRL=1,$MXREG [IRSPLT(IRL)=0];
"SPLITTING TURNED ON IN REGIONS 3, 5 & 10"
IRSPLT(5) = 1;

"TFILT;   THICKNESS OF FILTER"
"FSD      FOCUS-SKIN-DISTANCE"
"TBODY    BODY THICKNESS      "
"TGAP     DISTANCE FROM LOWER BODY SURFACE TO SCREEN "
"TPHOS    PHOSPHOR THICKNESS "
"TCONT    LENGTH OF CONTRAST CYLINDER                 "
```

```
    "RCONT    RADIUS OF CONTRAST CYLINDER                    "
    "DCONT    DEPTH OF CONTRAST CYLINDER                     "

    $UINPUT(1)
TFILT,DUMP,FSD,DUMP,TBODY,DUMP,TGAP,DUMP,TPHOS,DUMP,
    TCONT,DUMP,RCONT,DUMP,DCONT; (7(F7.4,I1),F7.4);

    "PLANE DEFINITION - ALL PERPENDICULAR TO Z AXIS"
    DO J=1,8 [
      PCOORD(1,J)=0.0; PCOORD(2,J)=0.0;
      PNORM(1,J)=0.0;  PNORM(2,J)=0.0;    PNORM(3,J)=1.0;]
    PCOORD(3,1)=0.0;   PCOORD(3,2)=TFILT; PCOORD(3,3)=FSD;
    PCOORD(3,4)=PCOORD(3,3)+TBODY; PCOORD(3,5)=PCOORD(3,4)+TGAP;
    PCOORD(3,6)=PCOORD(3,5)+TPHOS;
    PCOORD(3,7)=FSD+DCONT;         PCOORD(3,8)=PCOORD(3,7)+TCONT;
    CYRAD2(1)=RCONT*RCONT;

    "-------------------------------------------------------------"
    "STEP 5  INITIALIZATION-FOR-AUSGAB                                "
    "-------------------------------------------------------------"
    MXNP = 0;
    ENABS  = 0;"         ZERO ABSORBED ENERGY COUNTERS       "
    ENENT  = 0;
    ENSCON = 0;
    $UINPUT(1) ENSBAK; (I5);
    RADIN  = 1.02*RCONT*(FSD+TBODY+TGAP)/(FSD+DCONT);
    RADOUT = 0.98*(FSD+TBODY+TGAP)*TAN(ANGLE);
    RADIN2 = RADIN * RADIN;
    RADOUT2= RADOUT*RADOUT;
    RCONT2 = RCONT * RCONT;

    "-------------------------------------------------------------"
    "STEP 6   DETERMINATION-OF-INICIDENT-PARTICLE-PARAMETERS
"
    "-------------------------------------------------------------"
    "DEFINE INITIAL VARIABLES FOR HIGH ENERGY BEAM OF e- NORMALLY
    INCIDENT"
    "ON THE SLAB"
    IQIN=0;"                INCIDENT CHARGE - PHOTONS"
    /XIN,YIN,ZIN/=0.0;"     INCIDENT AT ORIGIN"
    IRIN=2;"                STARTS IN REGION 2"
    WTIN=1.0;"              WEIGHT = 1 SINCE NO VARIANCE REDUCTION USED"

    "-------------------------------------------------------------"
    "STEP 6B   INITIALISATION FOR SELECTION FROM ENERGY SELECTION
"
    "-------------------------------------------------------------"

    "INITIALISATION OF ARRAY ELEMENTS TO ZERO "
    DO I=1,$KV[
    IRAWDATA(I)=0; ISUMDATA(I)=0; SPECTRUM(I)=0;]
```

```
    "KV SPECTRUM DATA (GENERATED BY BIRCH-MARSHALL PROGRAM)
READ IN"
    "IRAWDATA ARRAY CONTAINS NUMBERS OF PHOTONS AT EACH
ENERGY     "
    "SUMDATA ARRAY CONTAINS CUMULATIVE TOTALS OF PHOTONS
"
    OPEN (2, 'ESPEC.DAT', STATUS='OLD');
    READ (2,:formlab:) IRAWDATA(1);
    ISUMDATA(1) = IRAWDATA(1);
    DO I=2,$KV[
    READ (2, :formlab:) IRAWDATA(I);
    ISUMDATA(I) = IRAWDATA(I) + ISUMDATA(I-1);]
    :formlab: FORMAT(F30.6);

    "SPECTRUM ARRAY CONTAINS DATA NORMALISED TO A TOTAL OF 1
PHOTON"
    FACTOR = ISUMDATA($KV);
    DO I=1,$KV[
    SPECTRUM(I) = ISUMDATA(I)/FACTOR;]

    "INPUT FILE CLOSED"
    CLOSE (2);

    "-------------------------------------------------------"
    "STEP 7   SHOWER-CALL                                   "
    "-------------------------------------------------------"
    $UINPUT(1) NCASE; (I9);  "INITIATE THE SHOWER NCASE TIMES"

    DO I=1,NCASE[ $SELECT_DIRECTION; $SELECT_ENERGY;
    CALL SHOWER(IQIN,EIN,XIN,YIN,ZIN,UIN,VIN,WIN,IRIN,WTIN);
    OUTPUT I, MXNP; (I8,'   ',I8); ]

    "-------------------------------------------------------"
    "STEP 8   OUTPUT-OF-RESULTS                             "
    "-------------------------------------------------------"
    OUTPUT ENABS,ENSCON,ENSBAK; ('0 ABSORBED ENERGY IS ',E10.4/,
    '0 SCREEN DETAIL IS ',E10.4/,'0 SCREEN BACKGROUND IS ',E10.4);

    OPEN(3,'RESULTS');

    CONT = 1 - (ENSCON/RCONT2)/(ENSBAK/(RADOUT2-RADIN2));
    $UOUTPUT(3) ENABS,ENSCON,ENSBAK,CONT; (' ABSORBED ENERGY =
    ',E10.4/,
    ' CONT EXP = ',E10.4/,'BKGD EXP = ',E10.4/,'CONTRAST = ',E10.4);

    CLOSE(1);
    CLOSE(3);

    STOP;END;  "END MAIN ROUTINE"

"   **************************************************
"
```

```
"    ************************************************************
"
"************************************************************************
********"
"                                                                      "
SUBROUTINE HOWFAR;
"                                                                      "
"************************************************************************
********"
COMIN/CYLDTA,PLADTA,STACK,EPCONT,GEOM,USER/;
    IRL = IR(NP);
    IF (IRSPLT(IRL).EQ.1.AND.IRL.NE.IROLD.AND.IQ(NP).EQ.0.AND.W(NP).GE.0)[
      $PARTICLE-SPLITTING;]

    IF(IR(NP) = 7) [IDISC=1;
                "TERMINATE THIS HISTORY: IT IS BEYOND THE PHOSPHOR"]

    ELSEIF(IR(NP) = 1) [IDISC=1;
                "TERMINATE THIS HISTORY: IT IS REFLECTED TOWARDS
SOURCE"]

    ELSEIF(IR(NP) = 2) [$PLAN2P(2,3,1,1,1,-1);
                    "INSIDE FILTER "]

    ELSEIF(IR(NP) = 3) [$PLAN2P(3,8,1,2,2,-1);
                    "BETWEEN FILTER & BODY"]

ELSEIF(IR(NP) = 8) [$PLANE1(7,1,IHIT,TPLN);
                  IF (IHIT=1)[
                    $FINVAL(TPLN,XF,YF,ZF);
                    IF ((XF*XF + YF*YF).GE.CYRAD2(1))
                      [IRNXT=4;] ELSE [IRNXT=10;]
                    $CHGTR(TPLN,IRNXT);
                          ]
                  ELSEIF (IHIT=0)[
                    $PLANE1(3,-1,IHIT,TPLN);
                    IF (IHIT=1)[ $CHGTR(TPLN,3);]
                              ]
    " IN BODY "  ]

ELSEIF(IR(NP) = 10) [$CYLNDR(1,1,IHIT,TCYL);
                    IF (IHIT=1)[ $CHGTR(TCYL,4);]
                    $PLAN2P(8,9,1,7,8,-1);
                  "IN CONTRAST CYLINDER"]

ELSEIF(IR(NP) = 4) [$CYLNDR(1,0,IHIT,TCYL);
                   IF (IHIT=1)[ $CHGTR(TCYL,10);]
                   $PLAN2P(8,9,1,7,8,-1);
                  "IN BODY "]

ELSEIF(IR(NP) = 9) [$PLANE1(4,1,IHIT,TPLN);
```

```
                IF (IHIT=1)[ $CHGTR(TPLN,5);]
                ELSEIF (IHIT=0)[
                  $PLANE1(8,-1,IHIT,TPLN);
                  IF (IHIT=1)[
                    $FINVAL(TPLN,XF,YF,ZF);
                    IF ((XF*XF + YF*YF).GE.CYRAD2(1))
                      [IRNXT=4;] ELSE [IRNXT=10;]
                    $CHGTR(TPLN,IRNXT);
                           ]
                             ]
" IN BODY "  ]

ELSEIF(IR(NP) = 5) [$PLAN2P(5,6,1,4,9,-1);
                    "BETWEEN BODY & PHOSPHOR"]

ELSEIF(IR(NP) = 6) [$PLAN2P(6,7,1,5,5,-1);
                    "INSIDE PHOSPHOR"]

RETURN;
END;   "END OF SUBROUTINE HOWFAR"

"*****************************************************************
*******"

SUBROUTINE AUSGAB(IARG);

"*****************************************************************
*******"
"                                                               "
"  In this AUSGAB routine we find the energy absorbed in regions 4,  "
"  8 & 9 (ie the body)  and also the energy absorbed in the screen   "
"  both behind and beside the contrast detail.                      "
"                                                               "
"*****************************************************************
*******"

COMIN/EPCONT,GEOM,SCORE,STACK/; " WE USE EDEP FROM EPCONT    "
                               "       RCONT FROM GEOM     "
                               "     ENSCORE FROM  SCORE   "
                               "IR(NP) & IARG FROM STACK   "
IF (NP.GE.MXNP) [MXNP = NP;]
IF (IARG.LE.4) [
IF (IR(NP).EQ.8)[
  ENABS=ENABS+EDEP*WT(NP);
  IF ((Z(NP).LE.FSD+1.0).AND.(X(NP)*X(NP)+Y(NP)*Y(NP).LE.1.0))
    [ENENT=ENENT+EDEP*WT(NP);]
                ]
ELSEIF ((IR(NP).EQ.4).OR.(IR(NP).EQ.9))[
      ENABS=ENABS+EDEP*WT(NP);          ]
ELSEIF (IR(NP)=6)[
    IF (X(NP)*X(NP)+Y(NP)*Y(NP).LE.RCONT2) [
      ENSCON=ENSCON+EDEP*WT(NP);          ]
```

```
        ELSEIF (X(NP)*X(NP)+Y(NP)*Y(NP).LE.RADOUT2).AND.
(X(NP)*X(NP)+Y(NP)*Y(NP).GE.RADIN2)[
         ENSBAK=ENSBAK+EDEP*WT(NP);]
                    ]
                ]

RETURN;END;"END OF AUSGAB"

"*****************************************************************
*****"
SUBROUTINE EDGSET;

"*****************************************************************
*****"
" The flag IEDGFL(IR) contains the atomic number of the medium for "
" each region (IR), or it contains zero in order to disable K-edge "
" fluorescence for that region.  The cross sections and energies   "
" are from:  E. Storm and H. I. Israel, At. Data and Nucl. Data    "
"            Tables 7 (1970) 565.                                 "
" K-edge fluorescent yields are from:  Lederer et al, Table of the "
"                                      Isotopes (6th Edition).     "
"*****************************************************************
*****"
;COMIN/EDGE,MEDIA,PHOTIN,MISC/;
DIMENSION EALF(100),EBET(100),OMEG(92),PHOTOK(100),PKA(100);
"-------------------------------------------------------------"
"Average photon energies (EALF) (L -> K electron transitions).     "
"                (Table 5 of Storm and Israel)                     "
DATA EALF/0.   , 0.   , 0.054, 0.109, 0.184, 0.297, 0.393, 0.524,
          0.675, 0.849, 1.041, 1.255, 1.487, 1.739, 2.014, 2.307,
          2.622, 2.957, 3.312, 3.690, 4.088, 4.508, 4.949, 5.411,
          5.895, 6.400, 6.925, 7.472, 8.041, 8.631, 9.243, 9.876,
         10.532,11.210,11.907,12.630,13.375,14.142,14.933,15.746,
         16.584,17.443,18.327,19.235,20.167,21.122,22.103,23.108,
         24.138,25.192,26.272,27.378,28.510,29.667,30.851,32.062,
         33.297,34.564,35.858,37.179,38.528,39.906,41.313,42.750,
         44.218,45.714,47.242,48.801,50.392,52.014,53.670,55.356,
         57.078,58.832,60.620,62.443,64.303,66.200,68.133,70.103,
         72.113,74.159,76.246,78.378,80.547,82.757,85.018,87.321,
         89.662,92.050,94.491,96.977,99.516,102.10,104.74,107.44,
         110.20,113.03,115.93,118.89/;
"-------------------------------------------------------------"
"Average photon energies (EBET) (M -> K electron transitions).     "
"                (Table 5 of Storm and Israel)                     "
DATA EBET/0.   , 0.   , 0.   , 0.   , 0.   , 0.   , 0.   , 0.   ,
          0.   , 0.   , 0.   , 0.   , 0.   , 1.838, 2.142, 2.468,
          2.817, 3.191, 3.589, 4.012, 4.459, 4.931, 5.427, 5.947,
          6.492, 7.059, 7.649, 8.265, 8.907, 9.572,10.263,10.983,
         11.730,12.503,13.300,14.126,14.980,15.859,16.767,17.700,
         18.661,19.648,20.785,21.705,22.778,23.878,25.008,26.166,
         27.354,28.573,29.821,31.103,32.414,33.757,35.131,36.535,
```

```
     37.966,39.431,40.930,42.460,44.024,45.622,47.253,48.918,
     50.618,52.352,54.123,55.930,57.772,59.652,61.572,63.531,
     65.529,67.564,69.642,71.759,73.919,76.121,78.367,80.656,
     82.991,85.370,87.796,90.273,92.794,95.365,97.989,100.66,
     103.39,106.17,109.01,111.90,114.85,117.86,120.93,124.08,
     127.29,130.58,133.96,137.41/;
"-------------------------------------------------------------"
"Fluorescent yields (OMEG) (probability to get fluorescent photon  "
" per K-shell vacancy. (Table III.IV from Bambynek et al)        "
DATA OMEG/0.    ,0.    ,0.    ,0.    ,0.    ,0.    ,0.    ,0.    ,
          0.    ,0.    ,0.    ,0.    ,0.0357,0.0470,0.0604,0.0761,
          0.0942,0.115 ,0.138 ,0.163 ,0.190 ,0.219 ,0.250 ,0.282 ,
          0.314 ,0.347 ,0.381 ,0.414 ,0.445 ,0.479 ,0.510 ,0.540 ,
          0.567 ,0.596 ,0.622 ,0.646 ,0.669 ,0.691 ,0.711 ,0.730 ,
          0.748 ,0.764 ,0.779 ,0.793 ,0.807 ,0.819 ,0.830 ,0.840 ,
          0.850 ,0.859 ,0.867 ,0.875 ,0.882 ,0.889 ,0.895 ,0.901 ,
     0.906 ,0.911 ,0.915 ,0.920 ,0.924 ,0.928 ,0.931 ,0.934 ,
     0.937 ,0.940 ,0.943 ,0.945 ,0.948 ,0.950 ,0.952 ,0.954 ,
     0.956 ,0.957 ,0.959 ,0.961 ,0.962 ,0.963 ,0.964 ,0.966 ,
     0.000 ,0.968 ,0.000 ,0.000 ,0.000 ,0.000 ,0.000 ,0.000 ,
     0.000 ,0.000 ,0.000 ,0.976/;
"-------------------------------------------------------------"
"Probability for the removal of a K-electron by PE effect (PHOTOK) "
" =(K-shell PE cross section)/(total PE cross section).          "
"                  (Table 8 of Storm and Israel)                "
DATA PHOTOK/1.   ,1.   ,1.   ,1.   ,1.   ,1.   ,1.   ,1.   ,
          1.   ,1.   ,0.928,0.922,0.916,0.911,0.907,0.903,
          0.900,0.896,0.893,0.890,0.888,0.885,0.883,0.880,
          0.878,0.876,0.874,0.872,0.871,0.870,0.869,0.867,
          0.866,0.864,0.863,0.861,0.859,0.858,0.856,0.855,
          0.853,0.852,0.850,0.848,0.846,0.844,0.843,0.841,
          0.840,0.839,0.837,0.836,0.835,0.833,0.832,0.830,
          0.828,0.827,0.825,0.824,0.823,0.821,0.820,0.818,
          0.817,0.815,0.814,0.813,0.812,0.811,0.809,0.807,
          0.805,0.803,0.801,0.800,0.798,0.796,0.794,0.792,
          0.790,0.788,0.786,0.784,0.782,0.780,0.778,0.776,
          0.774,0.772,0.770,0.767,0.764,0.762,0.759,0.756,
          0.753,0.751,0.749,0.746/;
"-------------------------------------------------------------"
"Relative probability of a K-alpha photon emission (PKA)        "
" =(K-alpha intensity)/(K-alpha intensity + K-beta intensity).  "
"                  (Table 6 of Storm and Israel)                "
DATA PKA/1.   ,1.   ,1.   ,1.   ,1.   ,1.   ,1.   ,1.   ,
          1.   ,1.   ,1.   ,1.   ,1.   ,1.   ,1.   ,0.955 ,
          0.940 ,0.924 ,0.914 ,0.904 ,0.901 ,0.898 ,0.8965,0.895 ,
          0.894 ,0.893 ,0.8925,0.892 ,0.891 ,0.890 ,0.8875,0.885 ,
          0.8825,0.880 ,0.878 ,0.876 ,0.874 ,0.872 ,0.8685,0.867 ,
          0.865 ,0.863 ,0.861 ,0.859 ,0.8575,0.856 ,0.8545,0.853 ,
          0.852 ,0.851 ,0.8495,0.848 ,0.847 ,0.846 ,0.845 ,0.844 ,
          0.843 ,0.842 ,0.841 ,0.840 ,0.839 ,0.838 ,0.8365,0.835 ,
          0.8345,0.834 ,0.833 ,0.832 ,0.8315,0.831 ,0.830 ,0.829 ,
          0.828 ,0.827 ,0.8265,0.826 ,0.8255,0.825 ,0.8245,0.824 ,
```

```
      0.823 ,0.822 ,0.8215,0.821 ,0.8205,0.820 ,0.819 ,0.818 ,
      0.8175,0.817 ,0.8165,0.816 ,0.815 ,0.814 ,0.8135,0.813 ,
      0.8125,0.812 ,0.811 ,0.810/;
"-------------------------------------------------------------"
" The following are in COMMON/EDGE/ (see macro definition):    "
"-------------------------------------------------------------"
" EKALPH is the energy of the K-alpha X-ray.                   "
" EKBETA is the energy of the K-beta X-ray.                    "
" BKR1   is the probability for a K-shell emission times the   "
"        probability for a fluorescent photon emission due to an "
"        electron transition from the X -> K shell.           "
" BKR2   is BKR1 times the probability that the fluorescent photon "
"        is due to an electron transition from the L -> K shell.  "
"-------------------------------------------------------------"
" EBINDA is the energy of the K-edge (in COMMON/PHOTIN/).      "
"-------------------------------------------------------------"
OUTPUT ; (' OUTPUT FROM SUBROUTINE EDGSET:'/
        ' REGION MEDIUM NAME                ',
' AV. K-EDGE    EKALPH    EKBETA      BKR1      BKR2'/);

DO JJ=1,$MXREG [DO KK=1,$MXELEMS [IZ=IEDGFL(JJ,KK); IMED=MED(JJ);
  IF IMED.GT.0. [
    IF IZ.GT.0  [
      BKR1(IMED,KK)=OMEG(IZ)*PHOTOK(IZ);
      BKR2(IMED,KK)=BKR1(IMED,KK)*PKA(IZ);
      EKALPH(IMED,KK)=EALF(IZ)*1.E-3;
      EKBETA(IMED,KK)=EBET(IZ)*1.E-3;
      OUTPUT JJ,(MEDIA(I,IMED),I=1,24),KK,(ELEM(IMED,I,KK),I=1,2),
      EBINDA(IMED),EKALPH(IMED,KK),EKBETA(IMED,KK),
      BKR1(IMED,KK),BKR2(IMED,KK);
        (1X,I3,1X,24A1,1X,I3,1X,2A1,1X,1P5E10.2);
      ]
    ELSE [
      OUTPUT JJ,(MEDIA(I,IMED),I=1,24),KK,(ELEM(IMED,I,KK),I=1,2);
      (1X,I3,1X,24A1,1X,I3,1X,2A1,' -- K-EDGE FLUORESCENCE OPTION',
      ' NOT ENABLED FOR THIS REGION --');
      ]]
  ELSE [OUTPUT JJ,IMED; (2(1X,I6),' VACUUM');]]]

RETURN;
"END OF SUBROUTINE EDGSET"  END;
"*************************************************************
*****"
"                              STANFORD LINEAR ACCELERATOR CENTER"
SUBROUTINE PHOTO;
"                              K-EDGE VERSION --  3 JUN 1984/1330"
"*************************************************************
*****"
"******* SPECIAL VERSION FOR TREATING K-EDGE FLUORESCENCE
*********"
"*************************************************************
```

```
*****"
" Programmers:  W. R. Nelson and T. M. Jenkins (SLAC)          "
"*************************************************************
*****"
" This is a special K-edge version of an EGS4 subroutine that is  "
" patterned after a method developed in 1978 by A. Clark (LBL)    "
" with the help of W. R. Nelson (SLAC).  It requires subroutine   "
" EDGSET (or equivalent for setting up the branching ratios and   "
" fluorescent photon energies.                                    "
"*************************************************************
*****"

;COMIN/DEBUG,EDGE,EPCONT,MEDIA,PHOTIN,SCORE,STACK,UPHIOT,USEFUL/
;
    $ENERGY PRECISION PEIG;
    COMIN/RANDOM/;  "LOCATED HERE TO AVOID FORTRAN 77 DIAGNOSTIC"

    PEIG=E(NP);

    $RANDOMSET RANDK;  "DETERMINE WHICH TYPE OF ATOM HAS BEEN
HIT  "
    NN=1;
    WHILE (RANDK.GT.CUMPROP(MEDIUM,NN)) [NN=NN+1];
    NUMEL=NN;

    IF(E(NP).LE.EKBIND(MEDIUM,NUMEL))  [EDEP=PEIG; IBLOBE=1;]
    ELSE [
     IF(IEDGFL(IR(NP),NUMEL).NE.0)  [
      $RANDOMSET BR;
      IF(BR.GT.BKR1(MEDIUM,NUMEL)) [ENEW=0.0;]
      ELSE [ICOUNT=ICOUNT + 1;
        IF (BR.LE.BKR2(MEDIUM,NUMEL)) [ENEW=EKALPH(MEDIUM,NUMEL);]
        ELSE [ENEW=EKBETA(MEDIUM,NUMEL);]]]
     ELSE [ENEW=0.0;]
     EDEP=EKBIND(MEDIUM,NUMEL)-ENEW;
     E(NP)=EDEP;
     IBLOBE=0;  "FLAG INDICATING 'NOT' BELOW BINDING ENERGY"

"END OF 'K-EDGE P.E. IS POSSIBLE' LOOP"]

$AUSCALL($PHOTXAUS);

IF(IBLOBE.EQ.1) [E(NP)=PZERO;]
ELSE [IQ(NP)=-1; "PHOTOELECTRON (ALWAYS SET UP)"
  E(NP)=PEIG-EKBIND(MEDIUM,NUMEL)+PRM;
  IF(IEDGFL(IR(NP),NUMEL).NE.0)  ["SET UP FLUORESCENT PHOTON"
  IF(BR.GT.BKR1(MEDIUM,NUMEL)) [RETURN;]
  "HOWEVER, K-EDGE NOT CHOSEN ABOVE"
    NP=NP+1;
    E(NP)=ENEW;
    IQ(NP)=0;
```

```
    "PHOTON COMES OFF ISOTROPICALLY"
    $RANDOMSET RNISO;
    COSTHE=2.0*RNISO-1.0;
    SINTHE=SQRT(1.0-COSTHE*COSTHE);
    U(NP)=0.0; V(NP)=0.0; W(NP)=1.0; "MAKES THINGS EASIER IN UPHI"
    CALL UPHI(2,1);
    $TRANSFER PROPERTIES TO (NP) FROM (NP-1);
  "END OF FLUORESCENT PHOTON SET UP"]
"END OF 'SET UP PARTICLE(S)' LOOP"]

RETURN;
"END OF SUBROUTINE PHOTO" END;

%E
```

Appendix C

Introduction to MORTRAN

MORTRAN is a structured language, implemented as a set of macros which are used by the macro processor to translate the language into FORTRAN. Extensions to the language may be made at any time with user-defined macros. The language exhibits the following features:

- Free-field (column boundaries may be ignored).
- Alphanumeric labels of arbitrary length.
- Comments inserted anywhere in the text.
- Nested block structure.
- Conditional statements which may be nested.
- Loops which test for termination at the beginning or end or both or neither.
- EXIT any loop.
- NEXT of any loop.
- Multiple assignment statements.
- Conditional compilation.
- Program listing features include automatic printing of nesting level and automatic indentation according to nesting level.
- Abbreviations for simple input/ouput statements.
- Interspersion of FORTRAN text with MORTRAN text.

The coding rules that apply may be summarized as :

- Terminate statements with a semicolon (;).
- Enclose comments in quotation marks (").
- Enclose labels in colons (:).
- Enclose character strings in apostrophes (').
- Blanks may be inserted freely except in labels, character strings and user defined macros.

C.1 Structure of code

Any valid FORTRAN statement becomes a valid MORTRAN statement when any continuation marks have been deleted and the statement is terminated by a semicolon. A sequence of MORTRAN statements (S_1, S_2, S_3 *etc*) may be enclosed in square brackets ([S_1; S_2; S_3;] to give a **block**. Such blocks may be nested to any level. In the descriptions below, an arbitrary block is indicated by [...].

Conditional statements may take the following forms, where *e*, *f*, and *g* are any logical expressions.

IF *e* [...]

IF *e* [...] ELSE [...]

IF *e* [...] ELSEIF *f* [...] ELSEIF *g* [...] ELSE [...]

Loops may be expressed with the logical condition *e* tested at either the beginning or end of the loop:

WHILE *e* [...]

LOOP [...] WHILE *e* ;

Tests may also be made at both ends of the loop:

WHILE *e* [...] UNTIL *f* ;

WHILE *e* [...] WHILE *f* ;

UNTIL *e* [...] WHILE *f* ;

UNTIL *e* [...] UNTIL *f* ;

Control variables may also be used in loops, in the following formats:

FOR *v* = *e* TO *f* BY *g* [...]

FOR *v* = *e* BY *g* TO *f* [...]

FOR *v* = *e* TO *f* [...]

The other types of loop that may be written are:

DO *I* = *J*, *K*, *N* [...]

and LOOP [...] REPEAT

to escape from this last loop requires use of the EXIT statement or

IF (*e*) EXIT;

C.2 Other Features

The value of some expression or variable may be assigned to several variables in a single statement by writing

/p, q, r....z/ = e

where *p, q, r....z* are variables and *e* is an expression, which is assigned to each variable in turn.

Whenever input or output is to the standard FORTRAN input or output units, the following input/output (i-o) abbreviations may be used.

INPUT i-o list; (format list);

OUTPUT i-o list; (format list);

Relational operators may be expressed in the usual FORTRAN notation, or may be denoted by

<, <=, =<, =, ~=, =>, >=, >

and logical operators by

& (AND), ¦ (OR), and ~ (NOT)

Macro definitions are written in the form

REPLACE {*pattern*} WITH {*replacement*}

The *pattern* may contain up to 9 formal parameters, each of which represents a variable lenght character string, and is denoted by the symbol #. The *replacement* may contain an arbitrary number of occurrences of formal parameters of the form $\{P_i\}$ (i=1,2,...9). During expansion of the macro, each formal parameter $\{P_i\}$ of the replacement part is replaced by the i-th actual parameter. An example of such a macro is:

REPLACE {*PLUS #;*} WITH {*{P1}={P1}+1;*}

This macro would match, for example, the program text

PLUS A(I,J,K);

and expand it to

A(I,J,K)= A(I,J,K)+1;

A number of 'processor control directives' are available in MORTRAN, and these may be either column-one-restricted-directive which each begin with a "%" in column 1 and for which only 1 per line is recognized, and free-form directives which may be unlimited and appear anywhere on a line. The latter begin with an exclamation mark and end with a semicolon.

C.3 Further Reading

The above summary gives an outline of the main features of MORTRAN programming, to aid in the understanding of the usercode given in Appendix B, for a reader familiar with FORTRAN. A more in depth analysis of the MORTRAN programming language is given in the SLAC-265 manual (Nelson *et al*, 1985).

Appendix D

Clinical trial documents

Trial of New Radiographic Technique for Paediatrics

INFORMATION SHEET FOR PARENTS

Recent European guidelines on diagnostic radiographic imaging in paediatrics recommend that additional copper filtration be used for performing x-ray examinations of children. This removes some low energy components of the x-ray beam, and should result in a lower radiation dose to the patient.

The use of such an additional filter is to be investigated for a trial period at the Royal Victoria Infirmary, for fluoroscopic examinations of children up to 1 year old. This will involve placing a laminated sheet of copper under the child for the duration of the examination. No other changes in normal procedure will be involved, and no extra radiation exposure will be given. It is anticipated that use of the copper sheet will reduce the radiation dose received by the child during the examination. Radiation doses are already routinely monitored in the room in which the trial is to take place and this will continue, to assess the effect of the additional filter.

The copper filter may be removed at any time during the examination should the clinical or radiographic staff experience any disatisfaction with the procedure, or should you wish it for any reason.

You may decline for your child to participate in this trial, or withdraw at any time, without giving a reason and without incurring displeasure or penalty.

The radiographer giving this form to you will be happy to answer any queries or provide further information that you might require. In the event of any problem or further query arising, please contact either Ms Claire-Louise Chapple or Dr Keith Faulkner at the Regional Medical Physics Department, Newcastle General Hospital (Tel. 0191 273 8811 x22400).

Trial of New Radiographic Technique for Paediatrics

CONSENT FORM FOR PARENTS

I ..... have read the accompanying information sheet, and consent for ..... to be included in the trial of use of additional copper filtration during x-ray examination.

signed ..... (parent/guardian) date .....

witnessed by .....

Trial of Additional Copper Filtration in Rm 11
Image Quality Assessment

Image Set	Which set of images do you prefer?					Are the images of satisfactory diagnostic quality?			
1	strongly prefer A	slightly prefer A	no preference	slightly prefer B	strongly prefer B	neither	A only	B only	both

comments :

2	strongly prefer A	slightly prefer A	no preference	slightly prefer B	strongly prefer B	neither	A only	B only	both

comments :

3	strongly prefer A	slightly prefer A	no preference	slightly prefer B	strongly prefer B	neither	A only	B only	both

comments :

4	strongly prefer A	slightly prefer A	no preference	slightly prefer B	strongly prefer B	neither	A only	B only	both

comments :

5	strongly prefer A	slightly prefer A	no preference	slightly prefer B	strongly prefer B	neither	A only	B only	both

comments :

6	strongly prefer A	slightly prefer A	no preference	slightly prefer B	strongly prefer B	neither	A only	B only	both

comments :

7	strongly prefer A	slightly prefer A	no preference	slightly prefer B	strongly prefer B	neither	A only	B only	both

comments :

8	strongly prefer A	slightly prefer A	no preference	slightly prefer B	strongly prefer B	neither	A only	B only	both

comments :

9	strongly prefer A	slightly prefer A	no preference	slightly prefer B	strongly prefer B	neither	A only	B only	both

comments :

Name..... (optional) radiologist / radiographer / physicist

References

ADRIAN, 1959, 1960, 1966. Interim, second & final reports of Adrian Committee on radiological hazards to patients, (HMSO, London).

ALMEN A. & MATTSSON S., 1995. The radiation dose to children from X-ray examinations of the pelvis and the urinary tract. *British Journal of Radiology*, 68(810) :604-13.

ALMEN A. & NILSSON M., 1996. Simple methods for the estimation of dose distributions, organ doses and energy imparted in paediatric radiology. *Physics in Medicine and Biology*, 41 :1093-1105.

ALM CARLSSON G., CARLSSON CA. & PERSLIDEN J., 1984. Energy imparted to the patient in diagnostic radiology: calculation of conversion factors for determining the energy imparted from measurements of the air collision kerma integrated over beam area. *Physics in Medicine and Biology*, 29(11) :1329-1341.

ANDREO P., 1991. Monte Carlo Techniques in medical radiation physics. *Physics in Medicine and Biology*, 36(7) :861-920.

ATKINS HL., FAIRCHILD RG., ROBERTSON JS. & GREENBERG D., 1975. Effect of absorption edge filters on diagnostic x-ray spectra. *Radiology*, 115 :431-437.

BERGER MJ. & SELTZER SM., 1964. *Tables of energy losses and ranges of electrons and positrons.* National Aeronautics and Space Administration Report Number NASA-SP-3012.

BERGER MJ. & SELTZER SM., 1968. *Electron and photon transport programs* I Introduction and notes on program DATAPAC 4; II Notes on program ETRAN-15. Rep. NBS 9836 and 9837 (Gaithesburg, NBS).

BEWLEY DK., LAWS JW. & MYDDLETON CJ., 1957. Maternal and foetal radiation dosage during obstetric radiographic examinations. *British Journal of Radiology*, 30 :286-290.

BIELAJEW, AF., HIRAYAMA H., NELSON WR. & ROGERS DWO., 1994. *History, overview and recent improvements of EGS4.* National Research Council of Canada Report NRCC-PIRS-0436.

BIRCH R. & MARSHALL M., 1978. Computation of Bremsstrahlung X-ray spectra and comparison with spectra measured with a Ge(Li) detector. *Physics in Medicine and Biology*, 24(3) :303-317.

BIRCH R., MARSHALL M. & ARDRAN GM., 1979. *Catalogue of spectral data for diagnostic x-rays.* The Hospital Physicists Association Scientific Report Series 30 (HPA, London).

BISSONNETTE J-P. & SCHREINER J., 1991. A comparison of semiempirical models for generating tungsten target x-ray spectra. *Medical Physics*, 19(3) :579-582.

BROADHEAD DA., FAULKNER K., RAWLINGS DJ. & CHAPPLE C-L., 1997. Automated thermoluminescent dosimetry for simple radiographic procedures. *Journal of Radiation Protection*, 17(1) :17-24.

BROADHEAD DA, 1998. Private communiation.

BURTON EM., KIRKS DR., STRIFE JL., HENRY GC. & KEREIAKES JG., 1988. Evaluation of a low dose neonatal chest radiographic system. *American Journal of Radiology*, 151 :999-1002.

CARLSSON GA., CARLSSON CA. & PERSLIDEN J., 1984. Energy imparted to the patient in diagnostic radiology: calculation of conversion factors for determining the energy imparted from measurement of the air collision kerma integrated over beam area. *Physics in Medicine and Biology*, 29(11) :1329-1341.

CARRIER R. & BÉÏQUE R., 1992. Analagous filters for beam shaping in diagnostic radiology. *Physics in Medicine and Biology*, 37(6) :1313-1320.

CHAN H-P. & DOI K., 1983. Energy and angular dependence of x-ray absorption and its effect on

radiographic response in screen-film systems. *Physics in Medicine and Biology*, 28(5) :565-579.

CHAN H-P. & DOI K., 1984. Radiation dose in diagnostic radiology: Monte Carlo simulation studies. *Medical Physics*, 11 :480-491.

CHANDRA B., LAKSHMANAN AR. & BHATT RC., 1982. Photon energy dependence of various TL peaks in LiF (TLD-100). *Int. J. Appl. Radiat.*, 33 : 1399-1402.

CHAPPLE, C.-L., FAULKNER, K. and HARRISON, R.M., 1990. An investigation into the performance of an automated quality assurance and dosimetry system in diagnostic radiology. *The British Journal of Radiology*, 63, 635-640.

CHAPPLE C-L., FAULKNER K., LEE RJ. & HUNTER EW., 1992. Results of a survey to paediatric patients undergoing common radiological examinations. *British Journal of Radiology*, 65 :225-231.

CHAPPLE C-L., FAULKNER K., LEE RJ. & HUNTER EW., 1993. Results of a survey to paediatric patients undergoing less common radiological procedures involving fluoroscopy. *British Journal of Radiology*, 66 :823-827.

CHAPPLE C-L., FAULKNER K. & HUNTER EW., 1994. Energy imparted to neontes in a special care baby unit. *British Journal of Radiology*, 67 :366-370.

CHAPPLE C-L., BROADHEAD D. & FAULKNER K., 1995. A phantom based method for deriving typical patient doses from measurements of dose-area product on populations of patients. *British Journal of Radiology*, 68 :1083-1086.

CHEN CS., DOI K., VYBORNY C., CHAN H-P. & HOLJE G., 1980. Monte Carlo simulation studies of detectors used in the measurement of diagnostic x-ray spectra. *Medical Physics*, 7(6) :627-635.

CHIN S., COLE TJ., PREECE MA. & RONA K., 1996. Growth charts for ethnic populations in the UK. *The Lancet*, 347 839-840.

CLAYTON CG., FARMER FT. & WARRICK MB., 1957. Radiation doses to the foetal and maternal gonads in obstetric radiography during late pregnancy. *British Journal of Radiology* 30 :291.

CLEVELAND RH., CONSTANTINOU C., BLICKMAN JG., JARAMILLO D. & WEBSTER E., 1992. Voiding cystourethrography in children: Value of digital fluoroscopy in reducing radiation dose. *American Journal of Radiology*, 152 :137-142.

COLE TJ., 1994. Do growth charts need a facelift? *British Medical Journal*, 308 :641-642.

COLLEGE OF RADIOGRAPHERS, 1990. *Guidelines for the introduction of a quality assurance programme in a diagnostic imaging department*, (CoR, London).

COMMISION OF THE EUROPEAN COMMUNITIES, 1996. *European guidelines on quality criteria for diagnostic radiographic images*. Edited by Carmichael JHE, Maccia C, Moores BM, Oestmann JW, Schibilla H, Teunen D, Van Tiggelen R & Wall B. EUR 16260 (Office for Official Publications of the European Communities, Luxemburg).

COMMISION OF THE EUROPEAN COMMUNITIES, 1996. *European guidelines on quality criteria for diagnostic radiographic images in paediatrics*. Edited by Kohn MM., Moores BM., Schibilla H., Schneider K., Stender HSt., Stieve FE., Teunen D. & Wall B. EUR 16261EN, (Office for Official Publications of the European Communities, Luxemburg).

CONTENTO G., MALISAN MR., PADOVANI R., MACCIA C., WALL BF. & SHRIMPTON PC., 1988. A comparison of diagnostic radiology practice and patient exposure in Britain, France and Italy. *British Journal of Radiology*, 61 :143-152.

CRANAGE RW., HOWARD CJ. & WELSH AD., 1992. Dose reduction by the use of erbium filtration in a general radiographic room. *British Journal of Radiology*, 65 :232-237.

CRISTY M., 1980. *Mathematical phantoms representing children of various ages for use in estimates of internal dose*. U.S. Nuclear Regulatory Commission Rep. NUREG/CR-1159 (also Oak Ridge National Laboratory Rep. ORNL/NUREG/TM-367).

DANCE DR., 1990. Monte Carlo calculation of conversion factors for the estimation of mean glandular dose. *Physics in Medicine and Biology*, 35 :1211-1219.

DREXLER G., WILLIAMS G. & ZANKL M., 1985. The meaning and the principle of determination of the effective dose equivalent in Radiation Protection. *Radiation Protection Dosimetry*, 12(2) :95-100.

FAULKNER, K., BARRY, J.L. and SMALLEY, P., 1989. Radiation dose to neonates on a Special Care Baby Unit. *The British Journal of Radiology*, 62, 230-233.

FENDEL H., SCHNEIDER K., KOHN MM. & BAKOWSKI C., 1989. Specific principles for optimization of image quality and patient exposure in paediatric radiology. *British Institute of Radiology Report 20* :91-101.

FLEAY RF., FOX RA., SPRAGUE PL. & ADAMS JP., 1984. Dose reduction in pediatric radiology using rare earth filtration. *Paediatric Radiology*, 14 :332-334.

FLEAY RF., 1980. Energy band selection in radiology by K-absorption edge filtration. *Australasian Radiology*, 24 :323-327.

FLETCHER, E.W.L., BAUM, J.D. and DRAPER, G., 1986. The risk of diagnostic radiation of the newborn. *The British Journal of Radiology*, 59, 165-170.

FRANCOIS P., BEURTHERET A., DUTREIX A. & DE VATHAIRE F., 1988. A mathematical child phantom for the calculation of dose to the organs at risk. *Medical Physics*, 15(3) :328-333.

FREEMAN JV., COLE TJ., CHINN S., JONES PRM., WHITE EM. & PREECE MA., 1990. Cross-sectional stature and weight reference curves for the UK. *Arch. Dis. Child.*, 73 :117-124.

FURLONGER BJ., 1982. High kV filtered beam technique for demonstrating bronchial situs. *Radiography*, 48(574) :197-219.

GAGNE RM., QUINN PW. & JENNINGS RJ., 1994. Comparison of beam hardening and K-edge filters for imaging barium and iodine during fluoroscopy. *Medical Physics*, 2(1) :107-121.

GIBBS SJ., 1989. Influence of organs in the ICRPs remainder on effective dose equivalent computed for diagnostic radiation exposures. *Health Physics*, 56(4) :515-520.

GOLIKOV VY. & NIKITIN VV., 1989. Estimation of the mean organ doses and the effective dose equivalent from RANDO phantom measurements. *Health Physics*, 56(1) :111-115.

GONZÁLEZ L., VÁNÓ E. & RUIZ MJ., 1995. Radiation doses to paediatric patients undergoing micturating cystourethrography examinations and potential reduction by radiation protection optimization. *British Journal of Radiology*, 68(807):291-5.

GROSSWENDT B., 1988. Photon Monte Carlo transport in radiation protection. *Monte Carlo transport of electrons and photons*. Edited by Jenkins TM., Nelson WR. & Rindi A. (Plenum, New York) :503-522.

GUSTAFSSON M. & MORTENSSON W., 1983. Radiation exposure and estimate of late effects of chest roentgen examinations in children. *Acta Radiologica Diagnosis* 24 :309-314.

HANSSON B., FINNBOGASON T., SCHUWERT P. & PERSLIDEN J., 1997. Added copper filtration in digital paediatric double-contrast colon examinations: effects on radiation dose and image quality. *European Radiology*, 7(7):1117-22.

HARRISON RM., CLAYTON CB., DAY MJ., OWEN MB. & YORK MF., 1983. Survey of doses to patients in five common diagnostic examinations. *British Journal of Radiology*, 56 :383-395.

HART D., JONES DG. & WALL BF., 1996. *Coefficients for estimating effective doses from paediatric x-ray examinations*. National Radiological Protection Board Report NRPB-R279, (HMSO, London).

HART, D & WALL BF, 1994. Estimation of effective dose from dose-area product measurements for barium meals and enemas, *British Journal of Radiology*, 67 :485-489. ??

HART D., HILLIER MC., SHRIMPTON PC. & BUNGAY D., 1996. *Doses to patients from medical x-ray examinations in the UK - 1995 review*. National Radiological Protection Board Report NRPB-R289 (HMSO).

HEGGIE JCP., 1990. A survey of doses to patients in a large public hospital resulting from plain film radiographic procedures. *Australasian Physical and Engineering Sciences in Medicine*, 13(2) :71-80.

HEGGIE JCP., 1992. The usefulness of K-edge filters in automatic brightness controlled fluoroscopy and digital subtraction angiography. *Australasian Physical & Engineering Sciences in Medicine*, 15(1) :9-14.

HERMAM MW., MAK HK. & LACHMAN RS., 1987. Radiation exposure reduction by use of Kevlar cassettes in the neonatal nursery. *American Journal of Radiology*, 148 :969-972.

HIRNING CR., 1992. Detection and determination limits for thermoluminescence dosimetry. *Health Physics*, 62(3) :223-227.

HUBBELL JH., 1982. Photon mass attenuation and energy absorption coefficients from 1 keV to 20 MeV. *International Journal of Applied Radiation and Isotopes*, 33 :1269-1290.

HUDA W. & SANDISON GA., 1984. Estimation of mean organ doses in diagnostic radiology from rando phantom measurements. *Health Physics*, 47(3) :463-467.

HUDA W. & GKANATSIOS NA., 1997. Effective dose and energy imparted in diagnostic radiology. *Medical Physics*, 24(8):1311-6.

HUDA W. & BISSESSUR K., 1990. Effective dose equivalents, H_E in diagnostic radiology. *Medical Physics*, 17(6) :998-1003.

HUGHES JS. & O'RIORDAN MC., 1993. *Radiation exposure of the UK population: 1993 Review*. National Radiological Protection Board Report R263, (HMSO, London).

INSTITUTE OF PHYSICAL SCIENCES IN MEDICINE, NATIONAL RADIOLOGICAL PROTECTION BOARD AND COLLEGE OF RADIOGRAPHERS, 1992. *National Protocol for Patient Dose Measurements in Diagnostic Radiology*, (NRPB, Chilton).

INTERNATIONAL COMMISSION ON RADIOLOGICAL PROTECTION, 1975. *Report of the task group on Reference Man*, ICRP Publication 23 (Pergamon Press, Oxford).

INTERNATIONAL COMMISSION ON RADIOLOGICAL PROTECTION,1991. 1990 *Recommendations of the International Commission on Radiological Protection*. ICRP Publication 60 (Pergammon Press, Oxford).
Ionising Radiation Regulations 1985. (HMSO, London).

JANGLAND L. & AXELSSON B., 1990. Niobium filters for dose reduction in pediatric radiology. *Acta Radiologica*, 31(5) :540-541.

JENNINGS RJ., 1988. A method for comparing beam hardening filter materials for diagnostic radiology. *Medical Physics*, 15(4) :588-599.

JOHNSON MA. & BURGESS AE., 1981. Clinical use of a gadolinium filter in pediatric radiology. *Paediatric Radiology*, 10 :229-232.

JOHNSON DW. & GOETZ WA., 1986. Patient exposure trends in medical and dental radiography. *Health Physics*, 50 :107:116.

JONES, D.G. and Wall, B.F., 1985. *Organ doses from medical X-ray examinations calculated using Monte Carlo techniques*. National Radiological Protection Board Report, NRPB-R186 (HMSO, London).

JOSEPH PM., BERDON WE., BAKER DH., SLOVIS TL. & HALLER JO., 1976. Upper airway obstruction in infants and small children. *Radiology*, 121 :143-148.

KARLSSON A., SCHUWERT P. & MORTENSSON W., 1994. Radiation exposure to children in diagnosing and at hydrostatic reduction of intussusception. *Acta Radiologica* 35(3):296-9.

KLEIN O. & NISHINA Y., 1929. Über die streuung von strahlung durch freie electrinen nach der neuen relativistischen quantum dynamic von Dirac. *Z. für Physic*, 52 :853.

KOCH HW. & MOTZ JW., 1959. Bremsstrahlung cross-section formulas and related data. *Rev. Mod. Phy.* 31 :920.

KOEDOODER K. & VENEMA HW., 1986. Filter materials for dose reduction in screen-film radiography. *Physics in Medicine and Biology*, 31(6) :585-600.

KOHN ML., GOOCH AW. & KELLER WS., 1988. Filters for radiation reduction: a comparison. *Radiology*, 167 :255-257.

KYRIOU JC., FITZGERALD M., PETTETT A., COOK JV. & PABLOT SM., 1996. A comparison of doses and techniques between specialist and non-specialist centres in the diagnostic X-ray imaging of children. *British Journal of Radiology*, 69 :437-450.

LE HERON JC., 1992. Estimation of effective dose to the patient during medical x-ray examinations from measurements of dose-area product. *Physics in Medicine and Biology*, 37(11) :2117-2126.

LEVETT J, 1990. Use of K-edge filters in pediatric radiology. MSc Thesis, University of Aberdeen.

LINDSKOUG BA., 1989. Has the patient got anything to do with it? *British Institute of Radiology Report 20* :193-195.

LINDSKOUG BA, 1992. The Reference Man in diagnostic radiology dosimetry. *British Journal of Radiology*, 65(773):431-7.

LINDSKOUG BA., 1992. Exposure parameters in pediatric radiology. *British Journal of Radiology*, 65 :431-437.

McCALL RC., McINTYRE RD. & TURNBULL WG., 1978. Improvement of linear accelerator depth dose curves. *Medical Physics* 5, 518-524.

McDONALD S., MARTIN CJ., DARRAGH CL. & GRAHAM DT., 1996. Dose-area product measurements in paediatric radiography. *British Journal of Radiology*, 69 :318-325.

McPARLAND BJ., GORKA W., LEE R., LEWALL DB. & OMOJOLA MF., 1996. Radiology in the neonatal intensive care unit: dose reduction and image quality. *British Journal of Radiology*, 69(826):929-37.

MAILLIE D., SEGAL A. & LEMKIN J., 1982. Effect of patient size on doses received by patients in diagnostic radiology. *Health Physics*, 42(5) :665-670.

MARTIN CJ, FARQUHAR B, STOCKDALE, E and MacDONALD, S, 1994. A study of the relationship between patient dose and size in paediatric radiology. *British Journal of Radiology*, 67 :864-871.

MARSHALL NW., FAULKNER K. & WARREN H., 1996. Measured scattered x-ray energy spectra for simulated irradiation geometries in diagnostic radiology. *Medical Physics*, 23(7) :1271-1276.

MESSEL H. & CRAWFORD DF., 1970. *Electron-photon shower distribution function*. (Pergamon Press, Oxford).

METZGER R., RICARDSON R. & VAN RIPER K., 1993. A Monte Carlo model for retrospective analysis

of shield design in a diagnostic x-ray room. *Health Physics*, 65(2) :164-171.

MOSCOVITCH M., SZALANCZY A., BRUML WW., VELBECK KJ. & TAWIL RA., 1990. A TLD system based on gas heating with linear time-temperature profile. *Radiation Protection Dosimetry*, 34(1/4) :361-364.

MUIRHEAD CR., COX R., STATHER SW., MacGibbon BM., EDMONDS AA. & MAYLOCK RGE., 1993. Estimates of late radiation risks to the UK population. National Radiological Protection Report NRPB 4 (4).

NAGEL HD., 1989. Comparison of performance characteristics of conventional and K-edge filters in general diagnostic radiology. *Physics in Medicine and Biology*, 34 :1269.

NEITZEL U., KOSANETZKY J. & HARDING G., 1985. Coherent scatter in radiographic imaging: a Monte Carlo simulation study. *Physics in Medicine and Biology*, 30(12) :1289-1296.

NELSON WR., HIRAYAMA H. & ROGERS DWO., 1985. *The EGS4 code system*. Stanford Linear Accelerator Center Report SLAC-265, (National Technical Information Service, Virginia USA).

NELSON WR. & JENKINS TM., 1988. *Writing SUBROUTINE HOWFAR for EGS4*. Stanford Linear Accelerator Centre Report SLAC TN-87-4, (National Technical Information Service, Virginia USA).

NICHOLSON RA., THORNTON A. & AKPAN M., 1995. Radiation dose reduction in paediatric fluoroscopy using added filtration. *British Journal of Radiology*, 68(807):296-300.

NICKOLOFF EL. & BERMAN HL., 1993. Factors affecting X-ray spectra. *Radiographics*, 13 :1337-1348.

NATIONAL RADIOLOGICAL PROTECTION BOARD & ROYAL COLLEGE of RADIOGRAPHERS, 1990. *Patient dose reduction in diagnostic radiology*. Documents of the NRPB, 1, 3 (HMSO, London).

OOSTERKAMP WJ., 1963. Monochromatic x-rays for medical fluoroscopy and radiography? *Medicamundi* 7(3) :68-77.

PATROCINIO HJ., BISSONNETTE J-P., BUSSIÈRE MR. & SCHREINER LJ., 1996. Limiting values of backscatter factors for low-energy x-ray beams. *Physics in Medicine and Biology*, 41 :239-253.

PERSLIDEN, J and SANDBORG, M, 1993. Conversion factors between energy imparted to the patient and air collision kerma integrated over beam area in paediatric radiology, *Acta Radiol.*, 34, 92-98.

PERSLIDEN J., 1986. Application of the Monte Carlo method to diagnostic radiology. Linköping University Medical Dissertations No 220. (Linköping, Sweden).

PERSLIDEN J., PETTERSSON HB. & FALTH-MAGNUSSON K., 1996. Radiation dose at small intestinal biopsies in children: results of a national study. *Acta Paediatrica*, 85(9):1042-6.

PETOUSSI N., ZANKL M., STIEVE FE. & DREXLER G., 1989. Patient organ doses for proposed technical parameters and their variations. *British Institute of Radiology Report 20* :246-249.

RAINBOW AJ. & COCKSHOTT WP., 1989. Patient dose measurements & Quality Assurance - 13 year regional survey. *British Institute of Radiology Report 20* :177-180.

REGANO LJ. & SUTTON RA., 1992. Radiation dose reduction in diagnostic x-ray procedures. *Physics in Medicine and Biology*, 37(9):1773-88.

ROBINSON A. & DELLAGRAMMATICAS HD., 1983. Radiation doses to neonates requiring intensive care. *British Journal of Radiology*, 56 :397-400.

ROGERS DWO. & BIELAJEW AF., 1984. *Use of EGS for Monte Carlo calculations in medical physics*. National Research Council of Canada, Report PXNR-2692.

ROGERS DWO. & BIELAJEW AF., 1990. Monte Carlo techniques of electron and photon transport for

radiation dosimetry. In *The Dosimetry of Ionizing Radiation*, Vol III, Chapter 5, (Academic Press).

ROSENSTEIN, H., BECK, T.J. and WARNER, G.G., 1979. *Handbook of selected organ doses for projections common in paediatric radiology*. US Department of Health, Education and Welfare, Publication (FDA) 79-8079 (Rockville, Maryland).

RUIZ MJ., GONZALEZ L., VANO E. & MARTINEZ A., 1991. Measurement of radiation doses in the most frequent simple examinations in paediatric radiology and its dependence on patient age. *British Journal of Radiology*, 64(766):929-33.

SANDBORG M., CARLSSON CA. & ALM CARLSSON G., 1989. Choice of optimal energy spectra in diagnostic radiology: an analysis based on calculated signal-to-noise ratios in clinical, partially absorbing detectors. *British Institure of Radiology Report 20* :141.

SANDBORG M., CARLSSON CA. & ALM CARLSSON G., 1994. Shaping X-ray spectra with filters in X-ray diagnostics. *Medical and Biological Engineering and Computing*, 32 :384-390.

SANDBORG M., DANCE DR., CARLSSON GA., & PERSLIDEN J., 1993. Monte Carlo study of grid performance in diagnostic radiology: factors which affect the selection of tube potential and grid ratio. *British Journal of Radiology*, 66(792):1164-76.

SANDBORG M., 1989. Erbium filter in diagnostic radiology: calculations of contrast and patient mean absorbed dose. *British Institure of Radiology Report 20* :169-171.

SANDBORG M., DANCE DR., CARLSSON GA., & PERSLIDEN J., 1994. Monte Carlo study of grid performance in diagnostic radiology: task dependent optimization for screen-film imaging. *British Journal of Radiology*, 67 :76-85.

SANDBORG M., DANCE DR., PERSLIDEN J. & CARLSSON GA., 1994. A Monte Carlo program for the calculation of contrast, noise and absorbed dose in diagnostic radiology. *Computer Methods and Programs in Biomedicine*, 42 :167-180.

SANDBORG M., CHRISTOFFERSSON J-O., ALM CARLSSON G., ALMÉN T. & DANCE DR., 1995. The physical performance of different contrast agents: calculations using a Monte Carlo model of the imaging chain. *Physics in medicine and Biology*, 40 :1209:1224.

SCHUELER BA., JULSRUD PR., GRAY JE., STEARS JG. & WU KY, 1994. Radiation exposure and efficacy of exposure-reduction techniques during cardiac catheterization in children. *American Journal of Roentgenology* 162(1):173-7.

SHRIMPTON PC., JONES DG. & WALL BF., 1988. The influence of tube filtration and potential on patient dose during x-ray examinations. *Physics in Medicine and Biology*, 33(10) :1205-1212.

SHRIMPTON, P.C., WALL, B.F., JONES, D.G. and FISHER, E.S., 1984. The measurement of energy imparted to patients during diagnostic X-ray examinations using the Diamentor exposure-area-productmeter. *Physics in Medicine and Biology*, 29, 10, 1199-1208.

SHRIMPTON PC., 1985. Energy imparted as a measure of radiological hazard to patients from x-ray examinations. *Med. Biol. Eng. Comput.* 23 Supplement Part 2 :1135-1136.

SHRIMPTON PC., WALL BF., JONES DG., FISHER ES., HILLIER MC. & KENDALL GM., 1986. *A national survey of doses to patients undergoing a selection of routine x-ray examinations in English hospitals*. National Radiological Protection Board Report NRPB-R200, (HMSO, London).

SCHULTZ FW., GELEIJNS J. & ZOETELIEF J., 1994. Calculation of dose conversion factors for posterior-anterior chest radiography of adults with a relatively high-energy x-ray spectrum. *British Journal of Radiology*, 67 :775-785.

SIMPKIN DJ., 1980. Shielding requirements for constant-potential diagnostic x-ray beams determined by a Monte Carlo calculation. *Health Physics* 56(2) :151-164.

SIMPKIN DJ. & MACKIE TR., 1990. Monte Carlo determination of the beta dose kernal in water. *Medical Physics* 17 :178-187.

SMATHERS RL., ALFORD BA., MESSENGER J., AGARWAL SK. & TAYLOR TS., 1984. Radiation dose reduction in the neonatal intensive care unit: Comparison of three gadolinium oxysulfide screen-film combinations. *Investigative Radiology*, 19 :578-582.

SMITH, W.L., GRESHAM, E., BERG, R., HOBSON, L., FRANKEN, E.A. and SMITH, J.A., 1979. A practical method for monitoring diagnostic radiation dosage in the newborn nursery. *Radiology*, 132, 189-191.

SÖDERBERG J. & PERSLIDEN J., 1996. Comparison of heterogeneous child phantoms with paediatric patients. *Radiation Protection Dosimetry*, 67 :257-261.

STATHER, J.W., MUIRHEAD, C.R., EDWARDS, A.A., HAMSON, J.D., LLOYD, D.C. and WOOD, N.R., 1988. *Health effects developed from the 1988 UNSCEAR report*. National Radiological Protection Board Report, NRPB-R226 (HMSO, London).

STERN SH., DENNIS MJ., WILLIAMS G. & ROSENSTEIN M., 1995. Simulation of the upper gastrointestinal fluoroscopy examination for calculation of absorbed dose in tissue. *Health Physics*, 69(3) :391-395.

STORM E. & ISRAEL HI., 1970. Photon cross-sections from 1 keV to 100 MeV for elements Z=1 to Z=100. *Atomic Data and Nuclear Data Tables*, 7 :565.

TAPIOVAARA MJ. & SANDBORG M., 1995. Evaluation of image quality in fluoroscopy by measurements and Monte Carlo calculations. *Physics in Medicine and Biology*, 40 :589-607.

THOMPSON WL., 1979. *MCNP - A general Monte Carlo code for neutron and photon transport, a summary*. Rep. LA-7396-M (NM:ASL, Los Alamos).

TUCKER DM., BARNES GT & CHAKRABORTY DP., 1991. Semiempirical model for generating tungsten target X-ray spectra. *Medical Physics*, 18(2) :211-217.

VAÑÓ E., OLIETE S., GONZÁLEZ L., GUIBELALDE E. & VELASCO A., 1995. Image quality and dose in lumbar spine examinations: results of a 5 year quality control programme following the European quality criteria trial. *British Journal of Radiology*, 68 :1332-1335.

VARCHENYA V., GUBATOVA D., SIDORIN V. & KALNITSKY S., 1993. Children's heterogeneous phantoms and their application in Roentgenology. *Radiation Protection Dosimetry*, 49(1/3) :77-78.

VEIT R. & ZANKL M., 1993. Variation of organ doses in paediatric radiology due to patient diameter, calculated with phantoms of varying voxel size. *Radiation Protection Dosimetry*, 49(1/3) :353-356.

VENEMA HW., 1979. X-ray absorption, speed and luminescent efficiency of rare earth and other intensifying screens. *Radiology*, 130 :765-771.

VILLIGRAN JE., HOBBS BB. & TAYLOR KW., 1978. Reduction of patient exposure by use of heavy elements as radiation filters in diagnostic radiology. *Radiology*, 127 :249-254.

VOGEL F., 1992. Risk calculations for hereditary effects of ionizing radiation in humans. *Human Genetics*, 89 :127-146.

VYBORNY CJ., METZ CE., DOI K. & ROSSMANN K., 1977. Screen/film system speed: its dependence on x-ray energy. *Radiology*, 125 :811-816.

VYBORNY CJ., METZ CE. & DOI K., 1980. Relative efficiencies of energy to photographic density conversions in typical screen/film systems. *Radiology*, 136 :465-471.

VYBORNY CJ., METZ CE. & DOI K., 1980. Large area contrast prediction in screen-film systems. SPIE Vol 233 *Application of Optical Instrumentation in Medicine* VIII :30-36.

WALL BF. & SHRIMPTON PC., 1989. Patient exposure criteria. *British Institute of Radiology Report 20* :239-241.

WANG Y., McARDLE GH., FEIG SA., KARASICK S., KOOLPE HA., MAPP E., RAO VM., STEINER RM. & WECHSLER RJ., 1984. Clinical application of yttrium filters for exposure reduction. *Radiographics*, 4(3) :479-505.

WERNER A. & ISDALE JM., 1986. Radiation hazards in a pediatric intensive care unit. *Paediatric Radiology* 16 :275-277.

WESENBERG, R.L., ROSSI, R.P. and HENDEE, W.R., 1977. Radiation exposure in radiographic examinations of the newborn. *Radiology*, 122, 499-504.

WESENBERG RL., AMUNDSON GM., MUELLER DL. & COUPLAND SG., 1987. Ultra low dose routine pediatric radiography utilizing a rare earth filter. *Journal of the Canadian association of Radiology*, 38 :158-164.

WHITE DR., WIDDOWSON EM., WOODARD HQ. & DICKERSON WT., 1991. The composition of body tissues (II) Fetus to young adult. *British Journal of Radiology*, 64 :149-159.

WHITE DR., MARTIN RJ. & DARLISON R., 1977. Epoxy resin based tissue substitutes. *British Journal of Radiology*, 50 :814-821.

WHITE DR., CONSTANTINOU C. & MARTIN RJ., 1986. Foamed epoxy resin based lung substitutes. *British Journal of Radiology*, 59 :787-790.

WHITE DR., 1977. Formulation of tissue substitute materials using basic interaction data. *Physics in Medicine and Biology*, 22(5) :889-899.

WORLD HEALTH ORGANISATION, 1986. *A rational approach to radiographic investigations.* (WHO Technical Report 689, Geneva).

WORLD HEALTH ORGANISATION, 1987. *Rational use of diagnostic imaging in paediatrics.* (WHO Technical Report 757, Geneva).

WRAITH CM., MARTIN CJ., STOCKDALE EJ. McDONALD S. & FARQUHAR B., 1995. An investigation into techniques for reducing doses from neo-natal radiographic examinations. *British Journal of Radiology*, 68(814):1074-82.

WU JR., HUANG TY., WU DK., HSU PC., and WENG PS., 1991. Radiation exposure of pediatric patients and physicians during cardiac catheterization and balloon pulmonary valvuloplasty. *American Journal of Cardiology*, 68(2):221-5.

YAMAGUCHI C., YAMAMOTO T., TERADA H. & AKISADA M., 1983. Effect of tungsten absorption edge filter on diagnostic x-ray spectra, image quality and absorbed dose to the patient. *Physics in Medicine and Biology*, 28 :223-232.

ZANKL M., PETOUSSI N., VEIT R., DREXLER G. & FENDEL H., 1989. Organ doses for a child in diagnostic radiology: comparison of a realistic and a MIRD-type phantom. *British Institute of Radiology Report 20* :196-198.